A Theory of Isobaric Analog Resonances*

NAFTALI AUERBACH† ‡, JÖRG HÜFNER§, A. K. KERMAN†, C. M. SHAKIN||

Laboratory for Nuclear Science and Department of Physics, Massachusetts Institute of Technology, Cambridge, Massachusetts 02139

A theory of analog resonances is reviewed which makes use of projection operators. The Hilbert space is divided into three parts: a continuum or open-channel space, an analog-state space, and a compound space. The phenomena are discussed in terms of the dynamical coupling of these spaces. The parameterization of the T matrix is discussed in detail, and equations are presented for various cross sections. The commutator $[H, T_-]$, where T_- is the isospin-lowering operator, plays an important role in the theory, and the various terms which contribute to this commutator are discussed. The energy splitting of the isospin multiplet, i.e., the Coulomb displacement energy, is discussed in detail. The importance of the analog resonance phenomena for the extraction of spectroscopic information is stressed, and it is shown how such information may be obtained. Various processes which contribute to the escape amplitude of the analog state are classified, and some numerical estimates are given. For several regions of the Periodic Table, graphs are presented for the various theoretical escape amplitudes, continuum energy shifts, asymmetry phases, and optical phase shifts, etc. Spectroscopic factors are calculated and compared with those obtained in other experiments.

CONTENTS

* This work is supported in part through funds provided by the Atomic Energy Commission under Contract AT(30-1-2098).

† Part of this work was performed while these authors were at the State University of New York at Stony Brook, Stony Brook, New York 11790.

‡ Present Address: Department of Physics and Astronomy, Tel-Aviv University, Tel-Aviv, Israel.

§ Present Address: Physik Institut der Universität, 78 Freiburg (Breisgau), Germany.

|| Present Address: Department of Physics, Case Western Reserve University, Cleveland, Ohio 44106.

1. INTRODUCTION

The recent application of the isospin concept in nuclear physics is a remarkable example of a common occurrence in physics; often some of the older ideas that seemed to have exhausted all of their applicability and context come back to life with more variety and deeper meaning.

When introduced in the thirties by Heisenberg [He32] and then developed by Wigner [Wi37], the concept of isospin seemed useful only for light nuclei. It was believed that as soon as the number of protons was increased considerably, the Coulomb interaction would break the isospin symmetry and there would be no physical correspondence between the actual nuclear states and the representations of the SU_2 group in isospin space. This was mainly thought to be the case because the increase in the Coulomb splitting of the isospin multiplet with Z would eventually place members of the multiplet at such high excitation energies that they would actually be in the continuum and not yield any observable consequences.

The discovery of isobaric analog *resonances* in the charge-exchange (p, n) reaction by Anderson *et al.* [An61; 62a,b] and the observation of the same resonances in elastic proton scattering by Fox *et al.* [Fo64], led to a "renaissance" of the isospin concept in nuclear physics. It was realized that members of the multiplet in the continuum were identifiable [An61, 62a,b], and theoretical discussion was generated [La62a–d; Ro65a]. The resonances being observed in the system $(Z+1, N-1)$ were interpreted as the second member, with quantum numbers $(T, T-1)$, of a $(2T+1)$ multiplet. The first member of the multiplet, with quantum numbers (T, T), is a low-lying bound state of the neighboring nucleus (Z, N); this nucleus is termed the *parent* nucleus and its states the parent states.

If there were no isospin-violating forces, the analog state[1] would be degenerate with the parent as well as the other members of the multiplet. Only those parts of the Hamiltonian which do not commute with the generators of rotations in isospin space, T, will cause the breaking of the multiplet. The most important of these forces, the Coulomb interaction between the protons, shifts the analog state upward in energy and into the continuum. The analog state is imbedded in a vast spectrum of states of lower isospin; however, the long-range nature of the Coulomb force causes the coupling to the neighboring states to be weak. Therefore the presence of the analog state is able to affect scattering phenomena only over a narrow energy range. It is then observed as a narrow resonance in cross sections with intermediate energy resolution. (Indeed, this phenomena provides an excellent example for the theory of intermediate structure [Fe67]).

A large number of resonance experiments have been performed since the early discovery, because it was soon realized that the analog resonances provide a powerful tool for studying the properties of the parent states. The partial widths deduced from elastic proton scattering provide information about the relationship between the parent state and the target ground state. This type of information is not unique to the isobaric analog studies. Similar information may be obtained from various transfer experiments such as (d, p), (d, t), (α, t) etc. A unique and outstanding advantage of the isobaric analog experiments is the possibility of studying the relationship between the parent states and the *excited* states of the target. Once the resonance is excited (say by scattering of protons or by charge exchange) it may decay to the low-lying target excited states. By observing these decays and determining their partial widths, parentage information is obtained.

The aim of this work is to review the *phenomenon* of the isobaric analog resonance in one consistent, self-

[1] See Sec. 2.1 for a precise definition of the analog state.

contained theoretical framework. We will not try to review all of the theoretical work [La62a–d; Ro65a; Ma66c; We66; Ma67; Me67; We67a,b; Bu68; Me68; Ma69a; Ta69; Bu70; Fa71]. However, we have attempted to discuss and calculate all of the parameters which characterize the resonance. Our description is based on a unified theory [Fe58,62] of nuclear reactions. The specific features associated with isobaric analog resonances were given in [Pi67; Ke68]. In the present review we demonstrate how these methods can be expanded to provide a complete description of the phenomenon. We show which essential physical quantities enter into the calculation of each of the resonance parameters and how the spectroscopic information may be extracted. In carrying out this program we discuss a significant portion of the data. However, a review of the experiments is beyond the scope of this work.

The literature dealing with analog resonances and related physical phenomena is very extensive. Many of the theoretical results obtained in this work have been derived by other authors using different reaction theories. The reader who wishes to obtain an overview of the various theories that have been employed will do well to consult the theoretical references listed above as well as the three books listed below:

1. *Isobaric Spin in Nuclear Physics*, edited by J. D. Fox and D. Robson, (Academic, New York, 1966).
2. *Nuclear Isospin*, edited by J. D. Anderson, S. D. Bloom, J. Cerny, and W. W. True (Academic, New York, 1969).
3. *Isospin in Nuclear Physics*, edited by D. H. Wilkinson (North-Holland Publ. Co., Amsterdam, 1969).

The first two of these books represent conference summaries. The third is particularly valuable in that it contains a series of review articles that treat subjects that we have only touched upon, and which also discuss the phenomena using reaction theories other than that used here.

The advantage of the approach used here is the natural separation of the problems associated with the bound state structure of the parent and target states from the problems of the reaction theory. This separation allows us to make use of the empirical information obtained from optical model and coupled channel studies. It also allows us to unambiguously incorporate various models for the structure of the bound states.

In Sec. 2 we begin by defining the analog states in terms of the parent state and the isospin-lowering operator. We then go on to define the orthogonal open-channel (continuum) space by making use of projection operators. The rest of the Hilbert space is termed the compound space. It contains all of the very complicated states giving rise to compound-nucleus statistical effects as well as some simple modes which are not conveniently included in the open channel space. Having all the complicated modes in one subspace facilitates the introduction of statistical assumptions.

Although the definition of the "open-channel space" is not unique, this feature is more of an advantage than a disadvantage. The flexibility in defining the open-channel space allows one to choose the channels in a way dictated by the actual physical situation. Channels may be pulled out from the open-channel space and put into the compound space and vice versa, depending on whether these channels have some particular physical interest. Whether a certain degree of freedom is in the channel space or included in the compound space does not change the final result provided no approximations are made in the calculation of the quantities involved. The reaction theory formalism is also generalized to include direct channel coupling of any number of channels.

Using this formal structure we derive the resonance expressions for appropriately energy averaged scattering amplitudes. This allows us to define the resonance parameters in terms of specific matrix elements. Indeed, it is seen that all important couplings of the analog state to the channel or compound spaces are given in terms of the commutator of the Hamiltonian with the total isospin lowering operator.

Expressions are also given for the cross sections. In addition, there is some discussion of the statistical treatment of the compound space and the introduction of the "doorway" concept.

Section 3 contains a discussion of all of the contributions to the commutator $[H, T_-]$. In addition to the important contribution of the Coulomb interaction between the protons, we also include *nuclear* isospin violations and various magnetic effects.

In Sec. 4 we introduce some of the notation and techniques by discussing the calculation of the simple matrix element which determines the norm of the analog state. This leads to a preliminary discussion of isospin violations in the parent nucleus.

We go on in Sec. 5 with a discussion of the magnitude of the energy splitting of the multiplet, which is defined as the displacement energy. We give formulas accurate enough to estimate the effects of all of the terms discussed in Sec. 3. This leads to an assessment of our ability to use information about the displacement energy to determine the neutron distribution.

The important escape amplitudes, which determine the partial widths, are defined and discussed in Sec. 6. The expression of the analog state in terms of the parent allows us to discuss "escapes from the parent" in terms of a charge-changing "interaction" defined by the commutator. This simplifies the discussion because the parent is one of the primary objects of spectroscopic attention.

The escapes are classified in terms of the complexity of the process involved. The simplest process is the direct escape of a *neutron* in the parent into the *proton* continuum. This escape is mediated by the charge-

changing Coulomb interaction mentioned above, averaged over the protons in the parent. This is a single-particle field which leads to a simple integral defining an elementary single-particle escape amplitude. The complete amplitude may be expressed in terms of this amplitude multiplied by spectroscopic factors, plus amplitudes for more complex processes. These include rearrangement effects which are not expressible in terms of a single-particle field, channel coupling effects, and escapes which proceed via the compound nucleus. Estimates of all of these effects (including the smaller isospin violating terms of Sec. 3) are given. In general the complex processes are very small, so that experimental determination of partial widths can lead to spectroscopic information.

Section 6 ends with a discussion of forbidden escape amplitudes using all of the same methods as above.

A discussion of the physics associated with the total width of the resonance is presented in Sec. 7. As usual this carries along with it the concept of an energy shift. In general, the contributions arise from both the coupling to the compound modes as well as from continuum coupling. The compound terms can be estimated using a doorway approach, including the anti-analog and the giant-monopole modes. The particular separation of compound and continuum effects is strongly influenced by the treatment of the channel coupling. (This coupling might lead to a giant-monopole resonance in proton scattering.)

Finally, in Sec. 8, we present sample calculations of all of the resonance parameters, for various regions of the periodic table. Comparison with the experimental partial widths for several closed-shell regions is carried out to show how the theory can be used for extracting spectroscopic information. Where it is possible, we also make comparison with transfer experiments.

2. PROJECTION OPERATORS AND A REACTION THEORY FOR ANALOG RESONANCES

In this chapter we wish to review and expand upon the theory of analog resonances as formulated in [Pi67]. Central to the approach presented there is a division of the complete Hilbert space of the scattering problem into three orthogonal subspaces. The projection operators for these spaces are denoted by P, A, and q. On occasion we will refer to these spaces as the *continuum space*, the *analog space*, and the *compound-nucleus space*, respectively. The complete state vector of the problem is written in the projection operator formalism as

$$|\Psi\rangle = P|\Psi\rangle + A|\Psi\rangle + q|\Psi\rangle. \tag{2.1}$$

The projection operators will be defined below.

2.1 The Analog States

In the study of analog resonances via a projection-operator formalism, certain special features arise which affect the precise definition of the continuum space. Therefore it is advantageous to define the analog space before specifying the continuum space in detail.

Following [Pi67], the *analog states* with $Z+1$ protons and $N-1$ neutrons are defined as follows. We consider states of the parent nucleus with Z protons and N neutrons, and denote these states as $|\pi_i\rangle$. These states are the actual eigenstates of the total Hamiltonian, i.e.,

$$H|\pi_i\rangle = E_i|\pi_i\rangle. \tag{2.2}$$

The analog states are then

$$\begin{aligned}|A_i\rangle &= T_-|\pi_i\rangle/\langle\pi_i|T_+T_-|\pi_i\rangle^{1/2}\\ &= T_-|\pi_i\rangle/(\mathrm{N}_i)^{1/2},\end{aligned} \tag{2.3}$$

where T_+, T_- are components of the total isospin operator.[2]

The analog states embedded in the continuum of H give rise to *analog resonances* through their coupling to the continuum and the compound nucleus modes. This point will be clarified in Sec. 2.3 where we discuss the T matrix for analog resonances.

We should point out that the states $|A_i\rangle$ have the same spacial character as the parent states. Unlike the parent states, the analog states are not eigenstates of H. The Hamiltonian would be diagonal in the space spanned by these states if isospin-violating terms were absent. In general, the states $|A_i\rangle$ are not mutually orthogonal. However, we are able to define the projection operator for the analog space as

$$A = \sum_{i,j} |A_i\rangle(\mathrm{n}^{-1})_{ij}\langle A_j|, \qquad \mathrm{n}_{ij} \equiv \langle A_i|A_j\rangle, \tag{2.4}$$

where the sum contains the analog states of interest.

Equation (2.3) provides a natural definition for the analog states.[3] We may list the various properties which follow from this choice:

(i) The definition is *model independent* as the parent $|\pi\rangle$ is an eigenfunction of H. This definition has the valuable feature of separating the structure problem for the parent state from the formulation of the reaction theory. After the development of the theory, various models for the parent state may be introduced and their consequences explored. Of course, the isospin operator T_- is independent of the description chosen for the parent state.

(ii) In the absence of isospin-violating terms in H, the analog states, as defined, are eigenfunctions of H, part of an isospin multiplet.

(iii) The matrix elements coupling the analog states

[2] The magnitude of the normalization factor, $\langle\pi_i|T_+T_-|\pi_i\rangle \equiv \mathrm{N}_i$, is $2T=N-Z$ if isospin is a good quantum number for the state $|\pi_i\rangle$, and is only slightly larger if isospin is violated weakly. See Sec. 4.

[3] The analog *states* are auxiliary quantities in the theory of isobaric analog resonances and are not directly observable. Therefore other definitions for these states are possible. The calculated T matrix for the isobaric analog *resonances* should be the same, independent of the definition chosen; however, the calculation required could be quite different if other definitions are made.

to the P and q spaces may be written in terms of the isospin-violating parts of H. This is of great advantage since this part of the Hamiltonian is small and well known (cf. Sec. 3). For example, let us consider the matrix elements of H taken between an analog state and a state Φ which is either in the continuum or in the compound nucleus space. This matrix element may be written

$$\langle\Phi \mid H \mid A\rangle = (1/\mathrm{N}^{1/2})\langle\Phi \mid V^{(-)} \mid \pi\rangle; \qquad V^{(-)} \equiv [H, T_-], \tag{2.5}$$

where the result follows from the fact that $\mid \pi\rangle$ is an eigenfunction of H and that the states of the P and q spaces are orthogonal to $\mid A\rangle$ by construction. In the following we will make extensive use of Eq. (2.5).

(iv) The main isospin violation arises from the two-body Coulomb force acting between protons, and therefore the coupling between the analog state and the P and q spaces is weak. Other sources of isospin violation are discussed in Sec. 3.

(v) Finally, it should be pointed out that we need not make the assumption that $\mid \pi\rangle$ has good isospin. The question of isospin purity of $\mid \pi\rangle$ is taken up in Secs. 4 and 5.

2.2 Wave Functions for the Continuum Space

Several definitions of the P space are possible and one has the option of choosing the definition most appropriate to the problem under consideration.

(i) For a study of elastic scattering, the P space may be defined as including only the elastic channel.

(ii) In the case that there are only a few open channels for the energies of interest, one may include all of these in the P space.

(iii) If many channels are open, it is possible to define the P space to include the elastic channel and those channels strongly coupled to it.

In general, it is desirable to avoid solving coupled equations in the description of the P-space propagation. This is possible if a DWBA treatment of the direct coupling between the various open channels provides a good approximation. The treatment of scattering from deformed nuclei where a perturbative approach to the coupling between the open channels is least adequate is a more difficult computational problem.[4] The numerical results which we will present in Sec. 8 are limited to analog resonance phenomena in spherical nuclei.

2.21 The Continuum Space

The detailed definition of the P-space projection operator is peripheral to our main interest. Therefore it has been relegated to Appendix I. It is useful, however, to summarize those results which are particularly relevant to the calculations reported here.

[4] However, use of the adiabatic approximation which neglects coriolis coupling can be used to partly simplify this problem [Ch57; Ke71].

In the Appendix we have defined a set of channel vectors $\mid r, c)$ describing a proton created at a *distance* r from a target state λ[5]:

$$\mid r, c) \equiv \mid r, [(l, \tfrac{1}{2})jI]\mathrm{JM}, \lambda\rangle = \sum_{m_j, M} C_{m_j M \mathrm{M}}{}^{iIJ} a^{\dagger}_{(l,1/2)jm_j}(r) \mid \lambda, IM\rangle. \tag{A1.7}$$

The angular momentum $(l\tfrac{1}{2})j$ of the particle is coupled to the angular momentum I of the target to form a total channel angular momentum, JM. The single label c then stands for the coupling scheme $\{[(l\tfrac{1}{2})jI]\mathrm{JM}, \lambda\}$. The set $\mid r, c)$ is not orthonormal and an orthonormal set $\mid r, c\rangle$ is introduced via an appropriate[6] transformation (Eq. A1.13).

In terms of the vectors $\mid r, c\rangle$, we may define the projection operator [Ke66],

$$\mathrm{P} = \sum_c \int_0^{\infty} \mid r, c\rangle r^2\, dr \langle r, c \mid. \tag{A1.15}$$

This projection operator does not define a space orthogonal to the analog space. However, it is useful for discussions of the optical model presented in the next section and in Appendix A1.2. The continuum projection operator P appropriate to the theory of analog resonances, will be discussed further in Sec. (2.23).

2.22 Coupled Optical Equations

It is useful at this point to discuss the projection operator treatment of the optical potential [Fe58; Fe62] (cf. Appendix A1.2).[7] One defines the operator $\mathrm{Q} = 1 - \mathrm{P}$. We may write the total wave function as $\mid \Psi\rangle = \mathrm{P} \mid \Psi\rangle + \mathrm{Q} \mid \Psi\rangle$, and the Schrödinger equation $H \mid \Psi\rangle = E \mid \Psi\rangle$ as two coupled equations

$$\begin{aligned}(E - H_{\mathrm{PP}})\mathrm{P} \mid \Psi\rangle &= H_{\mathrm{PQ}}\mathrm{Q} \mid \Psi\rangle,\\ (E - H_{\mathrm{QQ}})\mathrm{Q} \mid \Psi\rangle &= \mathrm{H}_{\mathrm{QP}}\mathrm{P} \mid \Psi\rangle.\end{aligned} \tag{A1.18}$$

By eliminating $\mathrm{Q} \mid \Psi\rangle$, an equation for $\mathrm{P} \mid \Psi\rangle$ may be written

$$[E - H_{\mathrm{PP}} - H_{\mathrm{PQ}}(E^{(+)} - H_{\mathrm{QQ}})^{-1} H_{\mathrm{QP}}]\mathrm{P} \mid \Psi\rangle = 0. \tag{A1.21}$$

The solution of (A1.21) will describe the full complication of the compound nucleus through the energy dependence in the propagator $(E^{(+)} - \mathrm{H}_{\mathrm{QQ}})^{-1}$. Nevertheless, we are able to define a single-particle amplitude,

[5] When using equations from the Appendix, we will always give the equation number as given there.

[6] Notice that the distinction is made by using round and angular brackets: $\mid r, c)$ and $\mid r, c\rangle$.

[7] This form is easily generalized to include any number of analog states, in which case there would be a sum of resonant terms in $T_{c'c}$ obtained from the analysis of the expression

$$T_{c'c} = T_{c'c}{}^{\mathrm{opt}} + \sum_{i,j} \langle \tilde{\Phi}_{c'}{}^{(-)} \mid \mathrm{H}_{PA} \mid A_i\rangle \langle A_i \mid (E^{(+)} - \mathrm{H}_{AA} - \mathrm{H}_{AP} G_P{}^{(+)} \mathrm{H}_{PA})^{-1} \mid A_j\rangle \langle A_j \mid \mathrm{H}_{AP} \mid \Phi_c{}^{(+)}\rangle.$$

$\Psi_{cc'}{}^{(+)}(r)$, through the relation

$$\langle r,c' \mid \Psi_c{}^{(+)}\rangle \equiv \Psi_{cc'}{}^{(+)}(r)$$

or

$$\mathrm{P} \mid \Psi_c{}^{(+)}\rangle = \sum_{c'} \int_0^\infty \mid r,c'\rangle \Psi_{cc'}{}^{(+)}(r) r^2\, dr. \quad \text{(A1.22)}$$

The subscripts refer to the boundary conditions for the equations determining $\Psi_{cc'}{}^{(+)}(r)$; the asymptotic form of this amplitude has incoming waves only in channel c, and outgoing waves in the other channels c' (including $c'=c$). With the definition

$$h_{cc'}(r,r') = \langle r, c \mid H_{\mathrm{PP}} + H_{\mathrm{PQ}}(E^{(+)} - H_{\mathrm{QQ}})^{-1} H_{\mathrm{QP}} \mid r', c'\rangle, \quad \text{(A1.23)}$$

we may reduce the Eqs. (A1,21) to a set of coupled equations for $\Psi_{cc'}{}^{(+)}(r)$

$$\sum_{c'} \int_0^\infty h_{c'',c'}(r,r') \Psi_{cc'}{}^{(+)}(r') r'^2\, dr' = E \Psi_{cc''}{}^{(+)}(r). \quad \text{(A1.25)}$$

The solution of Eq. (A1.25) describes many compound nucleus resonances. However, we are concerned here only with obtaining the energy averaged T matrix. As pointed out in Sec. 2.4 and the Appendix, the energy averaging procedure leads to a definition of the optical Hamiltonian in terms of an energy averaging parameter I. This prescription has been extensively discussed in [Fe67] and [Pi67], and we will not go into it here except to say that it corresponds to an average over the compound nuclear resonances with a Lorentzian weight factor. Thus from (A1.23) we are led to introduce

$$h_{cc'}{}^{\mathrm{OPT}}(r,r') = \langle r, c \mid H_{\mathrm{PP}} + H_{\mathrm{PQ}}(E - H_{\mathrm{QQ}} + iI/2)^{-1} H_{\mathrm{QP}} \mid r', c'\rangle, \quad \text{(A1.27)}$$

and an optical wave function $\psi_{cc'}{}^{(+)}(r)$ which is obtained from the solution of coupled optical equations

$$\sum_{c'} \int_0^\infty h_{c'',c'}{}^{\mathrm{OPT}}(r,r') \psi_{cc'}{}^{(+)}(r') r'^2\, dr = E \psi_{cc''}{}^{(+)}(r). \quad \text{(A1.28)}$$

In general, the optical Hamiltonian, h^{OPT}, is a nonlocal one-body operator which may couple the various channels of the P space. In the case that the P space contains only the elastic channel, we may obtain some information about h^{OPT} from the many phenomenological potentials (usually of the Saxon–Woods form) which reproduce the energy averaged elastic scattering T matrix [Pe62,63; Ro65b; Ho67b; Sa67; Be69].

In several cases, phenomenological optical Hamiltonians are also available which include channel coupling to collective states [Ta65; Gl68]. For the calculations reported here we have chosen $h_{cc'}{}^{\mathrm{OPT}}$ to be diagonal in the channel indices, that is, we neglect direct interactions. Therefore, we may discuss the simpler form,

$$\int_0^\infty h^{\mathrm{OPT}}(r, r') \psi_\alpha{}^{(+)}(r') r'^2\, dr' = E \psi_\alpha{}^{(+)}(r). \quad \text{(A1.29)}$$

Here α may denote the quantum numbers l, j, and E of the continuum wave function. The neglect of direct interaction is not a fundamental restriction and can be removed [Pi69]. At many points in our development we will write our formulas so that they are valid in the case this coupling is not neglected.

2.23 Orthogonality of the Continuum and Analog Spaces

We now return to the theory of analog resonances. The analog space has already been defined in Sec. 2.1. As discussed in detail in the Appendix, it is necessary to construct the continuum space projection operator P such that the P and A spaces are orthogonal. The orthogonality requirement arises from the fact that sometimes $\mid \pi\rangle$ contains a bound neutron coupled to a core. The corresponding analog state will then contain a component with a proton coupled to the core. This feature leads to a lack of orthogonality between the P and A spaces which is removed by the following procedure described in more detail in Appendix 1.

We define a new projection operator [see (A1.33)],

$$P = \mathrm{P} - \sum \mathrm{P} \mid A_i\rangle (\mathrm{p}^{-1})_{ij} \langle A_j \mid \mathrm{P}, \quad (2.6)$$

$$\mathrm{p}_{ij} = \langle A_i \mid \mathrm{P} \mid A_j\rangle, \quad (2.7)$$

so that the continuum space defined by the new projection operator P is orthogonal to the analog space.

We have also found it useful to introduce the bound functions

$$u_{A,c}(r) \equiv \langle r, c \mid A\rangle = \mathrm{N}^{-1/2} \langle r, c \mid T_- \mid \pi\rangle \quad \text{(A1.34)}$$

representing that part of $\mid A\rangle$ which is in the space $\mid r, c\rangle$. These functions as well as the solutions of Eq. (A1.28), $\psi_{cc'}{}^{(+)}(r)$, may be considered as column vectors whose components are labeled by channel indices. Introducing the Green's function $G_{cc'}{}^{(+)}(r,r')$ for $h_{cc'}{}^{\mathrm{OPT}}(r,r')$, we may write wave functions for the P space:

$$\varphi^{(+)}(r) = \psi^{(+)}(r) - \left(\int_0^\infty G^{(+)}(r,r') u_A(r') r'^2\, dr' \int_0^\infty u_A(r) \psi^{(+)}(r) r^2\, dr \Big/ \int_0^\infty \int_0^\infty r^2\, dr u_A(r) G^{(+)}(r,r') u_A(r') r'^2\, dr' \right), \quad (2.8)$$

Here $G^{(+)}$ is taken to be a matrix with respect to the channel indices and appropriate summations over channel labels are implied. The first subscript of $\psi_{cc'}{}^{(+)}(r)$ just gives information specifying the incoming channel and is not summed. Equation (2.8) implies immediately that

$$\int \varphi^{(+)}(r) u_A(r) r^2 \, dr = 0. \tag{2.9}$$

The function $\varphi^{(+)}(r)$ is actually the scattering solution of a *projected* optical Hamiltonian. Schematically, we have

$$h_P{}^{\mathrm{OPT}} = (1 - |u_A\rangle\langle u_A|) h^{\mathrm{OPT}} (1 - |u_A\rangle\langle u_A|), \tag{2.10}$$

where $|u_A\rangle$ is the normalized one-body state vector corresponding to $u_A(r)$. The one-body Green's function for $h_p{}^{\mathrm{OPT}}$ is related to $G^{(+)}$ by

$$G_P{}^{(+)} = G^{(+)} - G^{(+)} |u_A\rangle (\langle u_A | G^{(+)} | u_A\rangle)^{-1} \langle u_A | G^{(+)}. \tag{2.11}$$

Again in Eqs. (2.10)–(2.11), we have suppressed the coordinate variables as well as the summations over channel labels. Some elementary computational procedures for the construction of the functions $\varphi^{(+)}(r)$ are given in Appendix 1.3.

We wish to use the *one-body* scattering states just defined to construct *many-body* scattering states. This may be done by appropriately combining the wave functions $\varphi^{(+)}(r)$ of Eq. (2.8) with the channel vectors defined above. For example, consider the case with no channel coupling. The desired vectors are then

$$|\Phi_c{}^{(\pm)}\rangle = \int_0^\infty |r, c\rangle \varphi_c{}^{(\pm)}(r) r^2 \, dr. \tag{2.12}$$

In the simple case in which a target with $I=0$ is described in terms of a single Slater determinant for A particles and the P space contains only one channel, the coordinate representation of $|\Phi_c{}^{(\pm)}\rangle$, Eq. (2.12), is a Slater determinant of $(A+1)$ particles where the additional orbital is given by Eq. (2.8). In the case that direct interaction between the P-space channels is included, Eq. (2.12) is generalized to

$$|\Phi_c{}^{(\pm)}\rangle = \sum_{c'} \int_0^\infty |r, c'\rangle \varphi_{cc'}{}^{(\pm)}(r) r^2 \, dr, \tag{2.13}$$

where the boundary conditions are such that $\varphi_{cc'}{}^{(+)}(r)$ has incoming waves only in channel c, and outgoing waves in channels c' (including $c'=c$).

We remark again that the state vectors of Eqs. (2.12) or (2.13) do not span the *entire* P space. If we use the definition of Eq. (2.8) for φ, we do not include the state vector $\sum_c \int |r, c\rangle u_{A,c}(r) r^2 \, dr$. Its effect is of course partly included in the analog state $|A\rangle$. The remainder is usually discussed in connection with the compound space.

In the approach used here, where the effects of the analog state are treated explicitly, the *projected* optical Hamiltonian (2.10) should be used. The difference between the potential scattering obtained from $h_p{}^{\mathrm{OPT}}$ and h^{OPT} is small and is always taken into account. Finally, we note that for most calculations, in addition to choosing the optical Hamiltonian to be diagonal in the channels, it is taken to be local and channel independent. The actual phenomenological forms used will be discussed in later sections.

2.3 The T Matrix for Analog Resonances

Thus far, the continuum and analog spaces have been defined. Formally, the projection operator for the compound-nucleus space is therefore $q = 1 - P - A$. After the formal expressions for the T matrix are obtained and the physical quantities are identified, we will present a more detailed discussion of the q space.

2.31 Formal Derivation of the T Matrix

We have written the total wave function in terms of its projection onto the three orthogonal subspaces

$$|\Psi\rangle = P|\Psi\rangle + A|\Psi\rangle + q|\Psi\rangle. \tag{2.14}$$

Starting from the Schrödinger equation $H|\Psi\rangle = E|\Psi\rangle$, we use the projection operators to obtain the coupled equations,

$$\begin{aligned}
(E - H_{PP}) P|\Psi\rangle &= H_{PA} A|\Psi\rangle + H_{Pq} q|\Psi\rangle \\
(E - H_{qq}) q|\Psi\rangle &= H_{qA} A|\Psi\rangle + H_{qP} P|\Psi\rangle, \\
(E - H_{AA}) A|\Psi\rangle &= H_{Aq} q|\Psi\rangle + H_{AP} P|\psi\rangle,
\end{aligned} \tag{2.15}$$

where $H_{PP} = PHP$, $H_{Pq} = PHq$, etc. The theory for the energy-averaged scattering amplitude is most easily developed if a formal elimination of the q space is made. This procedure leads naturally to the definition of

$$\mathrm{H}(E) = H + H[q/(E - H_{qq})]H. \tag{2.16}$$

In terms of this *effective Hamiltonian* the equations become

$$\begin{aligned}
[E - \mathrm{H}_{PP}(E)] P|\Psi\rangle &= \mathrm{H}_{PA}(E) A|\Psi\rangle, \\
[E - \mathrm{H}_{AA}(E)] A|\Psi\rangle &= \mathrm{H}_{AP}(E) P|\Psi\rangle.
\end{aligned} \tag{2.17}$$

These equations give rise to rapidly fluctuating cross sections with many resonances due to the q space modes in H. Because we wish to obtain energy-averaged cross sections rather than discuss the fine structure of the analog resonances, we replace the variable E in Eq. (2.16) by $E + \frac{1}{2}(iI)$, which corresponds to an average over the resonance with a Lorentzian weight function as in Sec. (2.22).

The effective Hamiltonian appropriate to the calculation of the energy-averaged T matrix is then

$$\mathrm{H}[E + \tfrac{1}{2}(iI)] = H + H\{q/[E - H_{qq} + \tfrac{1}{2}(iI)]\}H. \tag{2.18}$$

The matrix elements of this operator in the P space lead us to the optical equations in Sec. (2.22).

We then derive the T matrix from the equations,

$$\{E-\mathrm{H}_{PP}[E+\tfrac{1}{2}(iI)]\}P\mid\Psi\rangle=\mathrm{H}_{PA}[E+\tfrac{1}{2}(iI)]A\mid\Psi\rangle,$$
$$\{E-\mathrm{H}_{AA}[E+\tfrac{1}{2}(iI)]\}A\mid\Psi\rangle=\mathrm{H}_{AP}[E+\tfrac{1}{2}(iI)]P\mid\Psi\rangle, \quad (2.19)$$

as follows.

We may write an integral equation for $P\mid\Psi\rangle$ using Eq. (2.19). If there are incoming waves in channel c, we have

$$P\mid\Psi_c^{(+)}\rangle=\mid\Phi_c^{(\pm)}\rangle + (E^{(+)}-\mathrm{H}_{PP})^{-1}\mathrm{H}_{PA}(E^{(+)}-\mathrm{H}_{AA})^{-1}\mathrm{H}_{AP}P\mid\Psi_c^{(+)}\rangle, \quad (2.20)$$

where $\mid\Phi_c^{(+)}\rangle$ is a solution of

$$(E-\mathrm{H}_{PP})\mid\Phi_c^{(+)}\rangle=0. \quad (2.21)$$

The formal solution of Eq. (2.20) is

$$P\mid\Psi_c^{(+)}\rangle=\mid\Phi_c^{(+)}\rangle+(E^{(+)}-\mathrm{H}_{PP})^{-1}\mathrm{H}_{PA} \times\{1/[E^{(+)}-\mathrm{H}_{AA}-\mathrm{H}_{AP}(E^{(+)}-\mathrm{H}_{PP})^{-1}\mathrm{H}_{PA}]\} \times\mathrm{H}_{AP}\mid\Phi_c^{(+)}\rangle. \quad (2.22)$$

The T matrix is readily found to be

$$T_{c'c}=T_{c'c}{}^{\mathrm{OPT}}+\langle\tilde{\Phi}_{c'}{}^{(-)}\mid\mathrm{H}_{PA} \times\{1/[E^{(+)}-\mathrm{H}_{AA}-\mathrm{H}_{AP}(E^{(+)}-\mathrm{H}_{PP})^{-1}\mathrm{H}_{PA}]\} \times\mathrm{H}_{AP}\mid\Phi_c^{(+)}\rangle, \quad (2.23)$$

where c and c' denote the various channels of the P-space and $T_{c'c}{}^{\mathrm{OPT}}$ is the T matrix for scattering due to H_{PP}.

In Eq. (2.23) the adjoint vector $\langle\tilde{\Phi}_{c'}{}^{(-)}\mid$ is defined by

$$\langle\tilde{\Phi}_{c'}{}^{(-)}\mid(\mathrm{H}_{PP}{}^{\dagger}-E)=0 \quad (2.24)$$

where $\mathrm{H}_{PP}{}^{\dagger}$ is the Hermitian conjugate of H_{PP}.

2.32 Definition of the Resonance Parameters

For a single analog resonance, the energy-averaged T-matrix, Eq. (2.23), takes the form

$$T_{c'c}=T_{c'c}{}^{\mathrm{OPT}}+\frac{\langle\tilde{\Phi}_{c'}{}^{(-)}\mid\mathrm{H}_{PA}\mid A\rangle\langle A\mid\mathrm{H}_{AP}\mid\Phi_c^{(+)}\rangle}{(E^{(+)}-\langle A\mid\mathrm{H}\mid A\rangle-\langle A\mid\mathrm{H}_{AP}\mathrm{G}_P{}^{(+)}\mathrm{H}_{PA}\mid A\rangle)}, \quad (2.25)$$

where we have defined the Green's function,

$$\mathrm{G}_P{}^{(+)}=1/[E^{(+)}-\mathrm{H}_{PP}(E+iI/2)]. \quad (2.26)$$

The second term of Eq. (2.25) represents the *analog resonance* part of the T-matrix, which we denote $T_{c'c}{}^{A}$.

The energy, E_R, of the analog resonance is given by

$$E_R=\mathrm{Re}\,[\langle A\mid\mathrm{H}_{AA}\mid A\rangle+\langle A\mid\mathrm{H}_{AP}\mathrm{G}_P{}^{(+)}(E_R)\mathrm{H}_{PA}\mid A\rangle] \quad (2.27)$$

and the total width, Γ, by

$$\Gamma=-2\,\mathrm{Im}\,[\langle A\mid\mathrm{H}_{AA}\mid A\rangle+\langle A\mid\mathrm{H}_{AP}\mathrm{G}_P{}^{(+)}(E_R)\mathrm{H}_{PA}\mid A\rangle]. \quad (2.28)$$

These quantities are discussed in Secs. 5 and 7.

Here we will consider the numerator of Eq. (2.25) and discuss the wave functions which appear in $\mid\Phi_c^{(+)}\rangle$ and $\langle\tilde{\Phi}_{c'}{}^{(-)}\mid$. We recall that we had written

$$\mid\Phi_c^{(+)}\rangle=\sum_{c'}\int_0^\infty\mid r,c'\rangle\varphi_{cc'}{}^{(+)}(r)r^2\,dr, \quad (2.13)$$

with the boundary condition that only channel c has incoming waves. It is useful to extract a phase factor from $\varphi_{cc'}{}^{(+)}(r)$ and define the functions $\varphi_{cc'}{}^{(0)}(r)$ by

$$\varphi_{cc'}{}^{(+)}(r)=\exp(i\delta_c-\eta_c)\varphi_{cc'}{}^{(0)}(r). \quad (2.29)$$

Here δ_c and η_c are the real and imaginary parts of the phase shift[8] in channel c such that

$$r\varphi_{cc}{}^{(0)}(r)\underset{r\to\infty}{\sim}(k/\pi E)^{1/2}\times\sin[kr-\tfrac{1}{2}(\pi l)-\eta\ln 2kr+\delta_c+i\eta_c]. \quad (2.30)$$

We also need the adjoint vector

$$\langle\tilde{\Phi}_c^{(-)}\mid=\sum_{c'}\int_0^\infty\tilde{\varphi}_{cc'}{}^{(-)*}(r)r^2\,dr\langle r,c'\mid, \quad (2.31)$$

and the relation

$$\tilde{\varphi}_{cc'}{}^{(-)*}(r)=\varphi_{cc'}{}^{(+)}(r). \quad (2.32)$$

We write

$$\langle A\mid\mathrm{H}_{AP}\mid\Phi_c^{(+)}\rangle=\exp(i\delta_c)\gamma_{A,c}, \quad (2.33)$$

where we have defined the complex *escape amplitude*,

$$\gamma_{A,c}=\exp(-\eta_c)\sum_{c'}\int_0^\infty\varphi_{cc'}{}^{(0)}(r)\mathrm{V}_{c'}{}^{A}(r)r^2\,dr. \quad (2.34)$$

In Eq. (2.34) we have introduced a complex *analog state form factor* for channel c by[9]

$$\mathrm{V}_c{}^{A}(r)=\langle A\mid\mathrm{H}_{AP}\mid r,c\rangle=\langle r,c\mid\mathrm{H}_{PA}\mid A\rangle. \quad (2.35)$$

The analog state form factor is complex because of the replacement of E by $E+iI/2$ in H. The escape amplitude is complex since both $\mathrm{V}_c{}^{A}(r)$ and $\varphi_{cc'}{}^{(0)}(r)$ are complex.

---

[8] Note that δ_c *includes* the Coulomb phase σ_l.

[9] The equality in Eq. (2.35) follows from the relation

$$\mathrm{H}^{\dagger}(E+iI/2)=\mathrm{H}(E-iI/2)$$

and the time reversal invariance of H.

Similarly, we define

$$\langle \tilde{\Phi}_c^{(-)} \mid \mathrm{H}_{PA} \mid A \rangle = \exp(i\delta_c)\gamma_{c,A}, \quad (2.36)$$

and easily derive the simple result

$$\gamma_{c,A} = \gamma_{A,c}. \quad (2.37)$$

In terms of the quantities just defined, the analog resonance part of the T matrix may be written

$$T_{c'c}{}^{A} = \exp(i\delta_{c'})\gamma_{A,c'}\gamma_{A,c}\exp(i\delta_c)/[E-E_R+\tfrac{1}{2}(i\Gamma)]. \quad (2.38)$$

As an example we may consider the elastic channel T matrix for a target with $I=0$. Denoting the elastic channel by $c=0$, and suppressing the indices (l,j), we have

$$T_{00}{}^{\mathrm{OPT}} = -\pi^{-1}\exp(i\delta-\eta)\sin(\delta+i\eta). \quad (2.39)$$

The analog resonance part of the T matrix is then

$$T_{00}{}^{A} = \frac{\exp(2i\delta)(\gamma_{A,0})^2}{E-E_R+i\Gamma/2} = \frac{\exp(2i\delta)}{2\pi}\frac{\exp(2i\phi_0)\Gamma_0}{E-E_R+i\Gamma/2}. \quad (2.40)$$

Equation (2.40) defines the *escape width* Γ_0 (which is real and positive), and the *asymmetry phase* ϕ_0, for the elastic channel. The phase ϕ_0 appears because the amplitude $\gamma_{A,0}$ is complex; it gives rise to asymmetries in the shape of the resonant cross section.

The energy averaged S matrix for this case is therefore

$$S = \exp(2i\delta)\left[\exp(-2\eta) - \frac{i\exp(2i\phi_0)\Gamma_0}{E-E_R+i\Gamma/2}\right], \quad (2.41)$$

which is the expression for this quantity presented in [Pi67].

More generally, we may define an escape width for channel c,

$$\exp(2i\phi_c)\Gamma_{A,c} = 2\pi(\gamma_{A,c})^2. \quad (2.42)$$

2.33 *Coordinate Space Equations for the Analog Resonance*

Equations (2.19) to (2.22) can be written in an alternate form if we use the channel vectors $\mid r, c\rangle$ introduced above. For simplicity we consider the case of only a single analog state $\mid A\rangle$. We define

$$\beta_c = \langle A \mid \Psi_c^{(+)}\rangle, \quad (2.43)$$

and

$$E_A = \langle A \mid \mathrm{H}_{AA}(E+iI/2) \mid A\rangle. \quad (2.44)$$

Using these definitions and Eqs. (2.10), (2.35), and (A1.22), we may write the coupled equations (2.19) as

$$E\Psi_{cc'}{}^{(+)}(r) - \sum_{c''}\int_0^\infty [h_P{}^{\mathrm{OPT}}(r,r')]_{c'c''}\Psi_{cc''}{}^{(+)}(r')r'^2dr' = \beta_c \mathrm{V}_{c'}{}^{A}(r), \quad (2.45)$$

$$(E-E_A)\beta_c = \sum_{c'}\int_0^\infty \mathrm{V}_{c'}{}^{A}(r)\Psi_{cc'}{}^{(+)}(r)r^2\,dr. \quad (2.46)$$

The solution for the function $\Psi_{cc'}{}^{(+)}(r)$ is then

$$\Psi_{cc'}{}^{(+)}(r) = \varphi_{cc'}{}^{(+)}(r) + \left(\sum_{c''}\int_0^\infty dr'(r'^2)[G_P{}^{(+)}(r,r')]_{c'c''}\mathrm{V}_{c''}{}^{A}(r')\gamma_{Ac}\exp(i\delta_c)\right) \times \left(E-E_A-\sum_{c'c''}\int_0^\infty\int_0^\infty dr(r^2)\mathrm{V}_{c'}{}^{A}(r)[G_P(r,r')]_{c'c''}\mathrm{V}_{c''}{}^{A}(r')r'^2\,dr'\right)^{-1} \quad (2.47)$$

which is the coordinate space form of Eq. (2.22). Here $\varphi_{cc'}{}^{(+)}(r)$ is the solution of the projected optical equation

$$E\varphi_{cc'}{}^{(+)}(r) - \sum_{c''}\int_0^\infty dr'(r'^2)[h_P{}^{\mathrm{OPT}}(r,r')]_{c'c''}\varphi_{cc''}{}^{(+)}(r') = 0 \quad (2.48)$$

with incoming waves only in channel c. The solution of this equation has been discussed in Sec. 2.23 [Eq. (2.8)]. The Green's function for the projected optical Hamiltonian, $G_P{}^{(+)}$, has been given in Eq. (2.11) in terms of the unprojected Green's function $G^{(+)}$.

Finally, we note that inspection of the asymptotic form of Eq. (2.47) will yield the T matrix whose formal expression is Eq. (2.23).

2.4 The Compound Nucleus Space and Statistical Assumptions

The q space contains a very large number of states, which in general are very complicated. One tries to make statistical assumptions concerning matrix elements involving these states.

In the theory presented in the previous sections, the q space appeared only in the effective Hamiltonian of Eq. (2.18), $\mathrm{H}=H+W$, with

$$W = \sum_q \{H \mid q\rangle\langle q \mid H/[E-E_q+\tfrac{1}{2}(iI)]\} \quad (2.49)$$

and $H_{qq} \mid q\rangle = E_q \mid q\rangle$. It is worth noting that H_{qq} has both a discrete and a continuous spectrum. The exact structure of this spectrum depends on the choice of the P space. Recall that the P space was defined in terms of

target states $|\lambda\rangle$. We denote the energies of these states by E_λ. For each of the states $|\lambda\rangle$ not included in the construction of the P space, H_{qq} has a continuum of solutions starting at E_λ. If for some energy, E, there are some open channels not in the P space, E is in the continuum of H_{qq}.

2.41 *The Optical Hamiltonian*

The operator W projected on the P space is part of the optical Hamiltonian. In general, a number of channels will be important and W_{PP} will have diagonal and nondiagonal matrix elements between these channels. The matrix elements of W taken with respect to the channel vectors $|r, c\rangle$ contribute to the optical potential:

$$W_{cc'}^{\mathrm{OPT}}(r, r') = \sum_q \frac{\langle r, c \mid H \mid q\rangle\langle q \mid H \mid r', c'\rangle}{[E-E_q+\frac{1}{2}(iI)]}. \quad (2.50)$$

Note that the operator $W_{cc'}^{\mathrm{OPT}}$ is nonlocal in general and contributes both to the real and imaginary parts of the coupled-channel optical potential. We do not attempt to calculate $W_{cc'}^{\mathrm{OPT}}$; rather, we *identify* the full operator $h_{cc'}^{\mathrm{OPT}}$ (of which $W_{cc'}^{\mathrm{OPT}}$ is a part) with the optical Hamiltonian *experimentally determined* from the elastic (and inelastic) scattering[10] away from the analog resonances. If the experimental results indicate that the optical Hamiltonian is approximately diagonal in the channels c and c', we will choose $h_{cc'}^{\mathrm{OPT}}$ appropriately. Otherwise, $h_{cc'}^{\mathrm{OPT}}$ describes the direct channel coupling.

Present experiments seem to be compatible with a *local* optical potential. It is clear from (2.50) that the optical potential is nonlocal in general. The real part of the optical potential is nonlocal due to the nonlocality of $W^{\mathrm{OPT}}(r, r')$, and also due to the proper treatment of exchange. The latter nonlocality may be more important than that due to $W^{\mathrm{OPT}}(r, r')$ which is expected to be small for r sufficiently different from r'. This follows if one uses a statistical argument in forming the sum in Eq. (2.50). Then only for $r=r'$, $c=c'$ will we completely avoid cancellation of the sum on q due to randomness of the matrix elements $\langle r, c \mid H \mid q\rangle$. For simplicity, one often chooses to use local optical potentials, but one must keep in mind that matrix elements involving the optical wave function *inside* the nucleus will depend somewhat on this choice [Pe62].

2.42 *Matrix Elements between the Analog State and the Compound States*

There are two types of matrix elements of W where coupling of the analog to the compound states occurs.

(i) The *compound mixing* denotes the matrix element

$$\langle A \mid W \mid A\rangle = \sum_q \langle A \mid H \mid q\rangle\langle q \mid H \mid A\rangle/[E-E_q+\tfrac{1}{2}(iI)]$$
$$\equiv \Delta^{\mathrm{COMP}}-\tfrac{1}{2}(i\Gamma^{\mathrm{COMP}}). \quad (2.51)$$

No assumptions of random sign can be made here, since the matrix elements $\langle A \mid H \mid q\rangle$ appear quadratically. The quantities Δ^{COMP} and Γ^{COMP} are then the shift and width due to coupling of the analog state to the compound nucleus modes.

(ii) The coupling of the analog state $|A\rangle$ with the continuum channels via $\{q\}$ appears in matrix elements of the type

$$\langle r, c \mid W \mid A\rangle$$
$$= \sum_q \langle r, c \mid H \mid q\rangle\langle q \mid H \mid A\rangle/[E-E_q+\tfrac{1}{2}(iI)]. \quad (2.52)$$

Such matrix elements are needed in the calculation of the escape amplitude [Eqs. (2.33–2.35)] as well as in the continuum shift (see Sec. 7). We might make the assumption that the matrix elements $\langle q \mid H \mid A\rangle$ have random signs for the set $\{q\}$ and are uncorrelated to the matrix elements $\langle r, c \mid H \mid q\rangle$. It follows that

$$\langle r, c \mid W \mid A\rangle \simeq 0. \quad (2.53)$$

To this approximation we may then replace H by H in all calculations.

One can make a crude estimate of the actual magnitude of the left side of Eq. (2.53) by considering a particular escape amplitude calculation. We calculate the absolute square of the term arising from the matrix element of W in (2.36). This leads to an expression which is a double sum on q. The randomness of the complicated compound-nucleus matrix elements then suggests that only the squared terms in the sum will not cancel, and we obtain

$$\delta\Gamma_{A,c}^{(2)} = \sum_q \{\langle A \mid H \mid q\rangle^2\Gamma_q/[(E-E_q)^2+\tfrac{1}{4}I^2]\}, \quad (2.54)$$

where

$$\Gamma_q = 2\pi \mid \gamma_{q,c} \mid^2, \quad (2.55)$$

with

$$\exp(i\delta_c)\gamma_{q,c} = \langle q \mid H \mid \Phi_c^{(+)}\rangle$$
$$\equiv \sum_{c'} \int_0^\infty \varphi_{cc'}^{(+)}(r)\,\langle r, c' \mid H \mid q\rangle r^2\,dr. \quad (2.56)$$

[10] By contrast, in the shell-model theory of nuclear reactions [Ma69a] statistical assumptions are made concerning the matrix elements between continuum states and the states q, e.g.,

$$\langle \sum_q V_{cq}V_{c'q}\rangle \propto \delta_{cc'}.$$

Also for matrix elements involving the analog state one assumes

$$\langle \sum_q V_{Aq}V_{qc}\rangle = 0.$$

Here, the brackets denote an ensemble average and $V_{qc}(V_{qA})$ the matrix elements between the compound states and the continuum (analog) states. The T matrix is not a quadratic function of the matrix elements V_{Aq} or V_{cq}. Ensemble averaging of the T matrix necessitates the evaluation of averages of terms of higher order in these matrix elements. The statistical assumptions made in this work are of a different nature, and we avoid some problems inherent in other approaches.

The quantities Γ_q are close to the actual compound nucleus widths of the states $|q\rangle$, except for the fact that $\varphi^{(+)}(r)$ does not come from exactly the correct optical potential (which should be real).

Apart from fluctuations in Γ_q this expression is really very close to Γ^{COMP} defined in (2.51). Thus we can see that

$$\delta\Gamma_{A,c}{}^{(2)} \simeq \bar{\Gamma}_q \Gamma^{\mathrm{COMP}}/I, \tag{2.57}$$

with $\bar{\Gamma}_q$ some average of the compound nucleus widths. In general the averaging interval I must be at least as large as Γ^{COMP}. The latter quantity seems to be one of the smaller contributions to the total analog resonance width. Therefore,

$$\delta\Gamma_{A,c}{}^{(2)} \lesssim \bar{\Gamma}_q, \tag{2.58}$$

is a small quantity. However there will be cases where even this small value cannot be ignored.

We have not looked at the interference term $\delta\Gamma_{A,c}{}^{(1)}$ between H and W which would arise in the evaluation of Eq. (2.42) because (2.53) indicates that this is zero. When we come to more specific models for the q space, the interference term will actually be the only important one. Here we can see that this term might be of the order of magnitude

$$\delta\Gamma_{A,c}{}^{(1)} = 2\cos\phi(\Gamma_{A,c}\delta\Gamma_{A,c}{}^{(2)})^{1/2}, \tag{2.59}$$

where $\cos\phi$ is random and varies from -1 to $+1$. Thus we find

$$\delta\Gamma_{A,c}{}^{(1)} \lesssim (\Gamma_{A,c}\bar{\Gamma}_q)^{1/2}. \tag{2.59a}$$

2.43 Doorway States

In some cases the assumption of random matrix elements is inadequate. There may be a few states in the q space that play an important role in the evaluation of W because they have significant couplings to the analog or the continuum spaces. Let us consider the matrix elements $\langle A|H|q\rangle$. As noted above these depend on the isospin-violating force, that is, predominantly on the long-range Coulomb potential. Therefore these matrix elements will be significant for those compound states $|q\rangle$ containing the same configurations as in $|A\rangle$. Most of these states $|q\rangle$ have dominant components with isospin quantum numbers one unit less than that of the analog state. States of this type which appear in a shell-model description of the analog-state structure have been termed "configuration states" in the literature [La62c]. Among these is the *antianalog state* which is known to have significant coupling to the analog state [see Sec. 6]. In addition to the configuration states, we may consider those states remaining in the q space which are describable as particles coupled to a vibration. Indeed, if one considers a multipole expansion of the isospin-violating force which affects the coupling between the A and q spaces, the configuration states will be important for the coupling via the monopole component, states including a collective dipole mode will be important for the dipole term of the multipole expansion, etc. We also note that the particle plus vibration states will be important for the escape matrix elements $\langle q|H|\Phi_c{}^{(+)}\rangle$ describing the transition from the q space to the continuum.

With these points in mind we may divide the q space into two parts:

Class I. The configuration states, particularly the antianalog. Also those collective modes (particle plus vibration) which are not removed to the P space.[11] We denote states of Class I by $|d\rangle$, and the corresponding projection operator as d. The states $|d\rangle$ may be thought of as a kind of "doorway" into the compound space from the A space.

Class II. States of more complex configurations. The projection operator for Class II is $q'=q-d$. By definition, the random-phase argument should be valid for the states of Class II, and the matrix elements $\langle q'|H|A\rangle$ should be small.

The coupling of the A and P spaces through the q space may be indicated as the Fig. (2.1a). On the assumption that the states $|d\rangle$ act as "doorway" states, this coupling may be described as in Fig. (2.1b) where the direct coupling between the A and q' spaces *and* between the P and q' spaces has been neglected. In order to make these considerations more precise, we use the projection operator relations given in [Pi67] to write

$$d[1/(E-H+\tfrac{1}{2}(iI))]d = d\{E-H_{dd}+\tfrac{1}{2}(iI)-H_{dq'}[E-H_{q'q'}+\tfrac{1}{2}(iI)]^{-1}H_{q'd}\}^{-1}d. \tag{2.60}$$

Finally, assuming that the doorways are not strongly

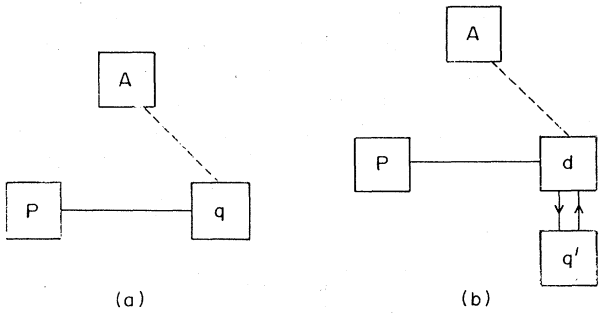

FIG. 2.1. The decay of the analog state into the continuum via the compound states. Figure 2(a) shows the general case, Eq. (2.52), the dashed line representing an isospin violating force, the solid one a nuclear force. Figure 2(b) depicts the doorway hypothesis, Eq. (2.63), where the coupling of the doorway states d to the remaining compound states q' mainly lead to a spreading width.

[11] For example, if a channel consisting of a neutron coupled to the analog of the target state is placed in the P space, one would have equations similar to those of Lane [La62d] describing the P-space scattering. This choice is not particularly suited to our microscopic theory, because part of the analog state is then in the P space.

coupled to each other through q', (which follows from a random-sign assumption for the matrix elements $\langle q' \mid H \mid d\rangle$), we may write Eq. (2.60) as

$$d[E-H+\tfrac{1}{2}(iI)]^{-1}d=\sum_d \mid d\rangle[E-E_d+\tfrac{1}{2}(i\Gamma_d)]^{-1}\langle d\mid, \tag{2.61}$$

with

$$E_d-\tfrac{1}{2}(i\Gamma_d)=\langle d\mid H\mid d\rangle + \sum_{q'}\{\langle d\mid H\mid q'\rangle\langle q'\mid H\mid d\rangle/[E-E_{q'}+\tfrac{1}{2}(iI)]\}, \tag{2.62}$$

so that (2.52) may be written

$$\langle r, c\mid W\mid A\rangle = \sum_d \{\langle r, c\mid H\mid d\rangle\langle d\mid H\mid A\rangle/[E-E_d+\tfrac{1}{2}(i\Gamma_d)]\}. \tag{2.63}$$

Similarly, the compound-mixing term Eq. (2.51) is, in this approximation,

$$\langle A\mid W\mid A\rangle \simeq \sum_d \{\langle A\mid H\mid d\rangle\langle d\mid H\mid A\rangle/[E-E_d+\tfrac{1}{2}(i\Gamma_d)]\}. \tag{2.64}$$

These equations are very similar to (2.52) except that we hope to make specific statements about the doorway matrix elements.

The role of the doorway states in the calculation of the various physical quantities will be taken up again in Secs. 6 and 7.

2.5 Average and Compound Nucleus Cross Sections

In this section we present some useful formulae for the average differential and polarization cross sections and discuss the compound nucleus cross section in the statistical approximation.

2.51 Average Cross Sections and Polarization

The differential and polarization cross sections for a transition from the target state λ angular momentum I, to the target state λ' angular momentum I' may be written in terms of the channel T matrix defined in Sec. 2.3. Thus [Ke61], we have

$$d\sigma_{\lambda\lambda'}/d\Omega=(4\pi^3/k_\lambda^2)[2(2I+1)]^{-1} \times\sum_{cc'c_1c_1'L} T_{cc'}{}^*\langle c'\mid\mid Y_L\mid\mid c_1'\rangle T_{c_1c_1'}\langle c\mid\mid Y_L\mid\mid c_1\rangle P_L(\theta) \tag{2.65}$$

and

$$P(\theta)\,d\sigma_{\lambda\lambda'}/d\Omega=(4\pi^3/k_\lambda^2)[(2I+1)]^{-1} \times\sum_{cc'c_1c_1'L} T_{cc'}{}^*\langle c'\mid\mid \mathbf{Y}_{L1L}\mid\mid c_1'\rangle T_{c_1c_1'}\langle c\mid\mid Y_L\mid\mid c_1\rangle \times\{i/[L(L+1)]^{1/2}\}P_L{}^{(1)}(\theta), \tag{2.66}$$

where $P_L(\theta)$ is the Legendre polynomial, and $P_L{}^{(1)}(\theta)$ is the associated Legendre polynomial. The reduced matrix elements are given in terms of our angular momentum coupling scheme [Eq. (A1.7)] as

$$\langle c\mid\mid Y_L\mid\mid c_1\rangle \equiv\langle(l\tfrac{1}{2})j(\lambda)IJ\mid\mid Y_L\mid\mid(l_1\tfrac{1}{2})j_1(\lambda_1)I_1J_1\rangle\delta_{II_1}\delta_{\lambda\lambda_1}, \tag{2.67}$$

$$=(-1)^{J_1-\frac{1}{2}+I+L} \times\left(\frac{(2J+1)(2J_1+1)(2j+1)(2j_1+1)(2L+1)}{4\pi}\right)^{1/2} \times\begin{Bmatrix} J & j & I\\ j_1 & J_1 & L\end{Bmatrix}\begin{pmatrix} j & L & j_1\\ \tfrac{1}{2} & 0 & -\tfrac{1}{2}\end{pmatrix}\tfrac{1}{2}[1+(-1)^{l+L+l_1}], \tag{2.68}$$

and

$$\langle c\mid\mid \mathbf{Y}_{L1L}\mid\mid c_1\rangle \equiv\langle(l\tfrac{1}{2})j(\lambda)IJ\mid\mid \mathbf{Y}_{L1L}\mid\mid(l\tfrac{1}{2})j_1(\lambda_1)I_1J_1\rangle\delta_{II_1}\delta_{\lambda\lambda_1}$$

$$=(2L+1)(-1)^{J_1-\frac{1}{2}+I+L+l} \times\left(\frac{6(2J+1)(2J_1+1)(2j+1)(2j_1+1)(2l+1)(2l_1+1)}{4\pi}\right)^{\frac{1}{2}} \times\begin{Bmatrix} l & \frac{1}{2} & j\\ l_1 & \frac{1}{2} & j_1\\ L & 1 & L\end{Bmatrix}\begin{Bmatrix} J & j & I\\ j_1 & J_1 & L\end{Bmatrix}\begin{pmatrix} l & L & l_1\\ 0 & 0 & 0\end{pmatrix} \tag{2.69}$$

The tensor operator in (2.66) and (2.69) is defined in general as (we use only $K=L$ here)

$$\mathbf{Y}_{L1K\mu}\equiv\sum_{m\nu}\langle L1K\mu\mid Lm1\nu\rangle Y_{Lm}(\theta,\varphi)\sigma_{1\nu}, \tag{2.70}$$

with

$$\sigma_{10}=\sigma_z \tag{2.71}$$

$$\sigma_{1\pm1}=\mp(\sigma_x\pm i\sigma_y)/\sqrt{2}, \tag{2.72}$$

in terms of the Pauli matrices.

When the T matrix is dominated by a single analog resonance with angular momentum J the expressions are simpler. Then we have

$$(d\sigma_{\lambda\lambda'}/d\Omega)_{\text{Res}}=(4\pi^3/k_\lambda^2)[2(2I+1)]^{-1} \times[(E-E_R)^2+\tfrac{1}{4}(\Gamma^2)]^{-1}\sum_L \Gamma_L{}^{\lambda'I'}(J)\Gamma_L{}^{\lambda I}(J)P_L(\theta), \tag{2.73}$$

where

$$\Gamma_L{}^{\lambda I}(J)=\sum_{ljl_1j_1}\exp(-i\delta_c)\gamma_{A,c}{}^*\langle c\mid\mid Y_L\mid\mid c_1\rangle\gamma_{A,c_1} \times\exp(i\delta_{c_1}) \tag{2.74}$$

depends on the resonance parameters of (2.33). The channels c, c_1 in the sum (2.74) all have the same values of (λIJ), and therefore are summed only on (lj) and (l_1j_1).

The polarization cross section has a similar form

$$P(\theta)\,d\sigma_{\lambda\lambda'}/d\Omega=4\pi^3/k_\lambda^2)\,(2I+1)^{-1}[(E-E_R)^2+\tfrac{1}{4}\Gamma^2]^{-1}\times\sum_L\Gamma_{L1L}^{\lambda I'}(J)\,\Gamma_L^{\lambda I}(J)[L(L+1)]^{-1/2}P_L^{(1)}(\theta),\tag{2.75}$$

with

$$\Gamma_{L1L}^{\lambda I}(J)=i\sum_{cc_1}\exp(-i\delta_c)\gamma_{A,c}{}^*\langle c\,||\,\mathbf{Y}_{L1L}\,||\,c_1\rangle\gamma_{A,c_1}\times\exp(i\delta_{c_1}).\tag{2.76}$$

Because of the symmetry relation

$$\langle c\,||\,\mathbf{Y}_{L\lambda K}\,||\,c_1\rangle=(-1)^{J-J_1+L+\lambda+K}\langle c_1\,||\,\mathbf{Y}_{L\lambda K}\,||\,c\rangle,\tag{2.77}$$

the quantities $\Gamma_L^{\lambda I}(J)$ and $\Gamma_{L1L}^{\lambda I}(J)$ are real.

Before making use of Eq. (2.65) in the case of elastic scattering, it is necessary to separate the T matrix into a Coulomb scattering part and a nuclear part. The analog resonance affects the elastic cross section mainly through the interference terms between the nuclear and Coulomb T matrices since the purely nuclear term is smaller. Thus we have

$$\frac{d\sigma}{d\Omega}=\left(\frac{d\sigma}{d\Omega}\right)_{\text{COUL}}+\left(\frac{d\sigma}{d\Omega}\right)_{\text{NUCL}}+\left(\frac{d\sigma}{d\Omega}\right)_{\text{INT}}.\tag{2.78}$$

The Coulomb term is given as usual by

$$(d\sigma/d\Omega)_{\text{COUL}}=|f_c|^2,\tag{2.79}$$

with

$$f_c(\theta)=(\eta/2k)[\sin(\theta/2)]^{-2}\exp\{2i\sigma_0-2i\eta\ln\sin(\theta/2)\},\tag{2.80}$$

where

$$\eta/2k=Ze^2/4E,\qquad E=\hbar^2k^2/2\mu,\tag{2.81}$$

and σ_0 is the $l=0$ Coulomb phase.

The interference term is given by

$$(d\sigma/d\Omega)_{\text{INT}}=2\,\text{Re}\,\{f_c{}^*A_0^{\lambda I}\},\tag{2.82}$$

where $A_0^{\lambda I}(\theta)$ is the spin independent part of the nuclear elastic scattering amplitude from state λI,

$$A_0^{\lambda I}(\theta)=(\pi/k)[2(2I+1)]^{-1}\sum_{ljJ}(2J+1)\,T_{cc}P_l(\theta).\tag{2.83}$$

We recall that c stands for $[(l\tfrac{1}{2})j(\lambda)IJ]$.

Finally, we write the interference term for the polarization cross section

$$[P(\theta)\,(d\sigma/d\Omega)]_{\text{INT}}=2\,\text{Re}\,\{f_c{}^*A_1^{\lambda I}\},\tag{2.84}$$

with

$$A_1^{\lambda I}(\theta)=(\pi/k)[i/2(2I+1)]\sum_{ljJ}(2J+1)\,T_{cc}(-1)^{l+j-\frac{1}{2}}\times\begin{Bmatrix}l & 1 & l\\ \frac{1}{2} & j & \frac{1}{2}\end{Bmatrix}[6(2l+1)/l(l+1)]^{1/2}P_l^{(1)}(\theta).\tag{2.85}$$

In both (2.83) and (2.85) it is understood that the nuclear amplitude includes the usual Coulomb phase factor $\exp(2i\sigma_l)$. If T_{cc} is dominated by a single analog resonance with angular momentum J the expressions (2.83) and (2.85) simplify accordingly.

2.52 The Compound Nucleus Part of the Cross Section

The derivation of the energy averaged T matrix has been the subject of the previous sections. Furthermore, the cross section associated with the energy averaged T matrix has been given in Eq. (2.65). Experiments performed with an energy resolution less than the width of the isobaric analog resonance yield the *energy-averaged cross section* which is not identical with the cross section[12] of Eq. (2.65). The difference originates from the fluctuations. Usually, one identifies the fluctuation part of the cross section with the compound nucleus cross section and derives it in a statistical model [Fe60]. There one introduces the transmission coefficients $P_c(E)$ associated with a channel c by[13]

$$P_c(E)=1-\sum_{c'}|S_{c,c'}(E)|^2,\tag{2.86}$$

where c stands for the quantum numbers $[(l\tfrac{1}{2})j(\lambda)IJ]$. The compound nucleus cross section for the target to go from state λI to state $\lambda' I'$ is then

$$(d\sigma_{\lambda\lambda'}/d\Omega)_{\text{CN}}=(\pi/k_\lambda^2)[2(2I+1)]^{-1}\sum_J[P_J(E)]^{-1}\times\sum_L P_{LJ}^{\lambda I}(E)\,P_{LJ}^{\lambda' I'}(E)\,P_L(\theta),\tag{2.87}$$

with

$$P_{LJ}^{\lambda I}(E)=\sum_{lj}P_c(E)\,\langle c\,||\,Y_L\,||\,c\rangle,\tag{2.88}$$

and

$$P_J(E)=\sum_{lj\lambda I}P_c(E),\tag{2.89}$$

where the sum on c in (2.89) runs over *all* open channels with fixed E and J.

Since the diagonal reduced matrix elements in (2.88) vanish for odd values of L, the compound nucleus cross section is symmetric around 90°. The compound nucleus polarization cross section vanishes identically because $\langle c\,||\,\mathbf{Y}_{L1L}\,||\,c\rangle\equiv 0$.

If we use the property

$$\langle(l\tfrac{1}{2})jIJ\,||\,Y_0\,||(l\tfrac{1}{2})jIJ\rangle=[(2J+1)/4\pi]^{1/2},$$

the total compound nucleus cross section becomes

$$\sigma_\lambda^{\text{CN}}\equiv\sum_{\lambda' I'}\int d\Omega\,(d\sigma_{\lambda\lambda'}/d\Omega)_{\text{CN}}=(\pi/k_\lambda^2)[2(2I+1)]^{-1}\sum_{ljJ}(2J+1)P_c(E).\tag{2.90}$$

[12] The interference terms (2.82–4) are correctly averaged except for the slow energy dependence of $f_c(\theta)$.

[13] The original discussion of the transmission coefficients did not include the consideration of direct channel coupling. In Eq. (2.86) we have extended the definition to include this feature. The "transmission coefficients" are to be interpreted as the probability for the formation of the compound nucleus.

If the neutron channels dominate the sum in Eq. (2.89), the total compound nucleus cross section is the cross section for the total p–n reaction.

For those channels, which are not directly coupled to the isobaric analog resonance either because of spin selection rules or because of a very small coupling matrix element, the transmission coefficients are calculated from an optical potential,

$$P_c^{\mathrm{OPT}}(E)=1-|\exp[2i(\delta_c+i\eta_c)]|^2$$
$$=1-\exp[-4\eta_c(E)], \qquad (2.91)$$

at the channel kinetic energy. All the optical transmission coefficients [Eq. (2.91)] will show a smooth energy behavior over the range of the isobaric analog resonance. Well below the Coulomb barrier the transmission coefficients for charged particles will be small compared to those for neutrons.

For those channels coupled significantly to the analog resonance the transmission coefficients are given by a resonant expression

$$P_c^A(E)=1$$
$$-|\exp(-2\eta_c)-\{i\Gamma_{A,c}\exp(2i\phi_c)/[E-E_R+\tfrac{1}{2}(i\Gamma)]\}|^2, \qquad (2.92)$$

$$=[1-\exp(-4\eta_c)]$$
$$\times\{[(E-E_R-\Delta_c)^2+B_c]/[(E-E_R)^2+\tfrac{1}{4}\Gamma^2]\}, \qquad (2.93)$$

where

$$\Delta_c=(\Gamma_{A,c}/2)(\sin 2\phi_c/\sinh 2\eta_c), \qquad (2.94)$$

and

$$B_c=(\Gamma_{A,c}^2/4\sinh^2 2\eta_c)$$
$$\times[\cos 2\phi_c+\exp(2\eta_c)+(\Gamma/\Gamma_{A,c})\sinh 2\eta_c]$$
$$\times[\cos 2\phi_c-\exp(2\eta_c)+(\Gamma/\Gamma_{A,c})\sinh 2\eta_c]. \qquad (2.95)$$

The resonant transmission coefficient has the following properties [Ro65a]:

(i) If E is not near E_R, we have $P_c^A(E)\sim P_c^{\mathrm{OPT}}(E)$.

(ii) There is a characteristic asymmetry with Δ_c positive.

(iii) Since $P_c^A(E)\geq 0$, we must have $B_c\geq 0$. As the first bracketed term of Eq. (2.95) is positive, we have the condition

$$\cos 2\phi_c\geq \exp(2\eta_c)-(\Gamma/\Gamma_{A,c})\sinh 2\eta_c. \qquad (2.96)$$

Because $\cos 2\phi_c\leq 1$, it follows that

$$\Gamma/\Gamma_{A,c}\geq[\exp(2\eta_c)-1]/\sinh 2\eta_c\geq 1. \qquad (2.97)$$

(iv) If the equality holds in Eq. (2.96), then $B_c=0$. In that case, $P_c^A(E_R+\Delta_c)$ vanishes.

(v) In the limit $\eta\to 0$ $\phi_c\to 0$ we see that $P_c^{\mathrm{OPT}}\to 0$ and

$$P_c^A(E)\to\Gamma_{A,c}(\Gamma-\Gamma_{A,c})/[(E-E_R)^2+\tfrac{1}{4}\Gamma^2] \qquad (2.98)$$

which has a maximum value of unity when $\Gamma=2\Gamma_{A,c}$.

For the scattering of protons in the neighborhood of the analog resonance, we may then neglect the proton transmission coefficients in all nonresonant channels. We expect an enhancement of the fluctuating part of the cross section in the neighborhood of the analog resonance, because of the resonant form of (2.93). At low energies, where the sum in (2.89) is not too large, this contribution may interfere seriously with a reliable extraction of the resonance parameters, since a knowledge of $d\sigma^{\mathrm{CN}}/d\Omega$ presupposes a knowledge of the resonance parameters of P_c^A in Eq. (2.92-3).

3. THE ISOSPIN-VIOLATING PARTS OF THE HAMILTONIAN

We have seen that the interesting quantities associated with isobaric analog resonances are given in terms of the isospin-violating parts of the Hamiltonian. It is possible to distinguish between isospin-violating forces which are directly related to the electromagnetic interaction and those effects which are less directly related, such as the p-n mass difference or the isospin-violating parts of the strong interaction. In the following we shall examine all of these effects.

3.1 Electromagnetic Interactions

The electromagnetic interactions are dominated by the Coulomb repulsion of the protons, but there are several other effects associated with the nucleon magnetic moments and the nucleon finite size.

3.11 The Coulomb Potential

The dominant part of the isospin-violating force is the well-known Coulomb potential

$$V_c=\tfrac{1}{4}\sum_{i>j}(e^2/|\mathbf{r}_i-\mathbf{r}_j|)(1-\tau_z^i)(1-\tau_z^j). \qquad (3.1)$$

This force is rather weak compared to the nuclear forces, has a long range, and is spin independent. The commutator,

$$V_c^{(-)}=[V_c,T_-]=\tfrac{1}{4}\sum_{i>j}(e^2/|\mathbf{r}_i-\mathbf{r}_j|)$$
$$\times[(1-\tau_z^i)\tau_-^j+(1-\tau_z^j)\tau_-^i], \qquad (3.2)$$

where $\tau_-=\tau_x-i\tau_y$, is a two-body force which changes a neutron–proton pair into a proton–proton pair.

3.12 The Finite-Size Effect

The Coulomb potential, Eq. (3.1), is derived for point charges. In order to incorporate the finite charge extension of the proton, we use a Coulomb potential modified at short distances. Basically, this modification may be deduced from electron–proton scattering experiments. The results of these experiments can be summarized in an *empirical* formula for the proton form factor [Go67]

$$G_p(q^2)=(1+\tfrac{1}{12}r_p^2q^2)^{-2}=1-\tfrac{1}{6}r_p^2q^2+(r_p^4q^4/48)+\cdots, \qquad (3.3)$$

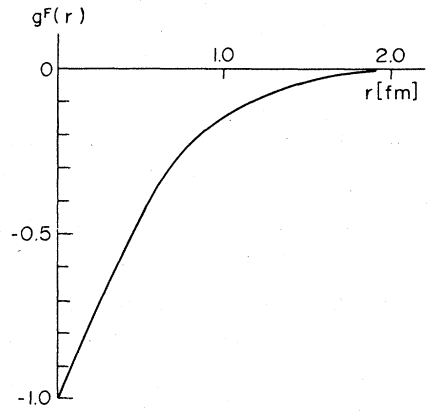

FIG. 3.1. The function $g^F(r)$ which provides the correction for finite proton size—see Eqs. (3.7) and (3.9).

where the root-mean-square radius has the value

$$r_p = 0.83f. \tag{3.4}$$

In the momentum representation, the Coulomb potential for point charges is given by

$$V(q) = (4\pi)^{-1}\int \exp\,(i\mathbf{q}\cdot\mathbf{r})\,(e^2/r)\,d^3r = e^2/q^2 \tag{3.5}$$

The modified Coulomb interaction, which includes the finite proton size for *both protons* is then

$$V_c^F(q) = G_p(q^2)\,(e^2/q^2)\,G_p(q^2) = (e^2/q^2) - (e^2 r_p^2/3) + \cdots. \tag{3.6}$$

In the coordinate representation we define a function $g^F(r)$, such that

$$V_c^F(r) = (e^2/r)[1 + g^F(r)]. \tag{3.7}$$

Using Eqs. (3.6) and (3.7) we find

$$g^F(r) = \frac{2}{\pi}\int_0^\infty dq\,\frac{\sin qr}{q}\,[G_p^2(q^2) - 1]. \tag{3.8}$$

The integral may be performed analytically to yield

$$g^F(x) = -e^{-x}[(48 + 33x + 9x^2 + x^3)/48], \tag{3.9}$$

where

$$x = (12)^{1/2}(r/r_p).$$

Since $g^F(x)$ is of short range compared to the size of the nuclear wave functions, we sometimes use the approximation

$$g^F(r) \simeq -(r_p^2/3)[\delta(r)/r]. \tag{3.10}$$

The actual function $g^F(r)$ is exhibited in Fig. 3.1.

3.13 *Vacuum Polarization*

To lowest order in the fine structure constant the vacuum polarization corresponds to a small spreading of the charge of the proton over a range of one-half the electron Compton wavelength. The virtual emission and absorption of an electron–positron pair gives rise to a repulsive potential $V_{\rm pol.}$ which has to be added to the Coulomb repulsion e^2/r of two protons. One finds [Fo54,55; Du57; He60],

$$V_{\rm pol} = (2\alpha/3\pi)\,I(r)\,(e^2/r),$$
$$\alpha = e^2/\hbar c \simeq 1/137, \tag{3.11}$$

with

$$I(r) = \int_1^\infty dx\,\exp\,(-2\kappa r x)[(1/x^2) + (1/2x^4)](x^2-1)^{1/2}. \tag{3.12}$$

The characteristic length which determines the range of $I(r)$ is the Compton wavelength of the electron divided by 2π, $\kappa^{-1} = \hbar/m_e c = 386.2f$. For values of $2\kappa r$ small compared to 1, the function $I(r)$ can be expanded to give

$$I(r) = [-\gamma + \tfrac{5}{6}] + |\ln(\kappa r)| + \tfrac{1}{8}(6\pi\kappa r) + O[(\kappa r)^2] + \cdots \qquad \kappa r \ll 1 \tag{3.13}$$

with Euler's constant $\gamma = 0.5772$. For two protons *inside* a nucleus, the expansion given in Eq. (3.13) is good. Equations (3.11–3.13) refer to point protons. By transforming Eq. (3.11) to momentum space and introducing the proton form factor as in Eq. (3.6) the singularity of $V_{\rm pol}$ at $r=0$ may be removed. Some numerical estimates of the contribution of the vacuum polarization to Coulomb displacement energies are given in Sec. 5.14. The electron–proton scattering experiments which are used to determine the proton form factor have a vacuum polarization correction [Ch 56]. In the analysis of these experiments one corrects for the vacuum polarization and certain other radiative diagrams *before* the nucleon form factor is extracted. Therefore, no double counting occurs if one takes into account both the vacuum polarization and the proton form factor in calculating Coulomb energies and escape amplitudes.

There is one effect on the vacuum polarization which has not been estimated but which we would like to point out here. This refers to the fact that the two-body polarization potential (3.11) is calculated in free space. In fact all the rest of the protons are present within nuclear distances so that the vacuum polarization takes place in the presence of the strong (Z) nuclear Coulomb field. This will distort the wave functions of the virtual electron–positron pairs and should affect the potential even at short distances.

3.14 *Relativistic Corrections and Magnetic Interaction*

To obtain the isospin-violating terms in the nuclear Hamiltonian which are of order $(v/c)^2$ we may consider the reduction of relativistic two-particle wave equations to this order [Sc50; Ba55]. Consider a collection of

nucleons with charges

$$e_i = e(1-\tau_z{}^i)/2 \tag{3.14}$$

and magnetic moments

$$\mu_i = \{\mu_0[(1-\tau_z{}^i)/2]+\mu_i{}'\}, \qquad \mu_0 = e\hbar/2Mc, \tag{3.15}$$

where $\mu_i{}'$ are the anomalous moments. We have,

$$\mu_i = \{\mu_n \tfrac{1}{2}(1+\tau_z{}^i)+\mu_p \tfrac{1}{2}(1-\tau_z{}^i)\}\mu_0, \tag{3.16}$$

where $\mu_n = -1.913$, and $\mu_p = 2.793$.

The total many-body Hamiltonian including the lowest-order relativistic corrections is derived to be[14]

$$H = \sum_i \left(\frac{p_i{}^2}{2M} - \frac{p_i{}^4}{8M^3c^2}\right) + \tfrac{1}{2}\sum_{ij}\frac{e_ie_j}{r_{ij}} + V^{\mathrm{NUCL}} + V^{\mathrm{MAG}}, \tag{3.17}$$

where V^{NUCL} contains the strong-interaction terms and V^{MAG} contains isospin-violating terms not considered previously. We have [Cl70]

$$V^{\mathrm{MAG}} = \tfrac{1}{2}\sum_{ij}\left\{-\frac{e_ie_j}{2M^2c^2}[\mathbf{p}_i\cdot\mathbf{r}_{ij}{}^{-1}\mathbf{p}_j + \mathbf{p}_i\cdot\mathbf{r}_{ij}(r_{ij}{}^3)^{-1}\mathbf{r}_{ij}\cdot\mathbf{p}_j] + \mu_i\mu_j\left[\frac{\boldsymbol{\sigma}_i\cdot\boldsymbol{\sigma}_j}{r_{ij}{}^3} - 3\frac{(\boldsymbol{\sigma}_i\cdot\mathbf{r}_{ij})(\boldsymbol{\sigma}_j\cdot\mathbf{r}_{ij})}{r_{ij}{}^5} - \tfrac{8}{3}\pi\boldsymbol{\sigma}_i\cdot\boldsymbol{\sigma}_j\delta(\mathbf{r}_{ij})\right]\right.$$

$$\left. + \pi\left[\frac{e_ie_j}{M^2c^2} - 4\left(\frac{e_j\mu_i}{2Mc} + \frac{e_i\mu_j}{2Mc}\right)\right]\delta(\mathbf{r}_{ij}) - \frac{2e_i}{Mc}\mu_j\boldsymbol{\sigma}_j\cdot\frac{(\mathbf{r}_{ij}\times\mathbf{p}_i)}{r_{ij}{}^3} - \frac{e_i}{Mc}\boldsymbol{\sigma}_j\cdot\frac{(\mathbf{r}_{ji}\times\mathbf{p}_j)}{r_{ij}{}^3}[2\mu_j - \mu_0\tfrac{1}{2}(1-\tau_z{}^j)]\right\} \tag{3.18}$$

with

$$\mathbf{r}_{ij} = \mathbf{r}_i - \mathbf{r}_j \quad \text{and} \quad r_{ij} = |\,\mathbf{r}_i - \mathbf{r}_j\,|.$$

Equation (3.18) contains five terms which we may discuss in order:

(i) The first term provides an additional (momentum-dependent) proton–proton interaction. If we estimate the effect of such a term in the Fermi-gas approximation, we see that the direct terms vanish. The exchange terms yield a small contribution to the displacement energies (Sec. 5) of the order $(Ze^2/R)\cdot(\lambda_p/R)^2$, where λ_p is the reduced Compton wavelength of the proton. This term is therefore of the order of 0.2% of the displacement energy.

(ii) The interaction between the magnetic moments is a tensor operator in the spins and will tend to average to zero. Small effects will remain due to unsaturated spins in those shells that are not closed in the sense of L–S coupling. We neglect this term.

(iii) The contact terms may be neglected if we assume that the nucleon–nucleon interaction is strongly repulsive at short distances.

(iv) These terms represent the interaction of the magnetic moments with the local magnetic field due to the motion of the other particles. In the Fermi-gas approximation the direct terms average to zero and the exchange terms are very small.

(v) Finally we have the spin–orbit terms for which we may make the standard approximations [Sc69a] for the direct term. Averaging over the particles with coordinate label i, we may write an equivalent one-body interaction

$$V^{\mathrm{SPIN-ORBIT}} = (\mu_0/Mc)\sum_j[\tfrac{1}{2}(1-\tau_z{}^j)(\mu_p-\tfrac{1}{2}) + \mu_n\tfrac{1}{2}(1+\tau_z{}^j)]\boldsymbol{\sigma}_j\cdot\mathbf{l}_j(r_j)^{-1}[dV_c(r_j)/dr_j], \tag{3.19}$$

where $V_c(r_j)$ is the Coulomb potential of the system evaluated at the position of the jth particle.

The commutator

$$V_{\mathrm{SPIN-ORBIT}}{}^{(-)} = [V^{\mathrm{SPIN-ORBIT}}, T_-] = (e\hbar/4M^2c^2)\sum_j(\mu_p-\mu_n-\tfrac{1}{2})r_j{}^{-1} \times [dV_c(r_j)/dr_j]\boldsymbol{\sigma}_j\cdot\mathbf{l}_j\tau_-{}^j \tag{3.20}$$

will be used in Sec. 5 where we consider the contribution of this term to the displacement energy.

3.2 Isospin Violation of the Nuclear Hamiltonian

The p–n mass difference and the isospin violation of the nuclear interaction make up the isospin-violating parts of the nuclear Hamiltonian. These terms are also of electromagnetic origin; however, they arise in a more indirect way and are not fully understood at present. We will treat them in a purely phenomenological way.

3.21 The Proton-Neutron Mass Difference

The Hamiltonian of the nucleus depends in a static and in a dynamic way on the mass difference between protons and neutrons. The static effect arises since the Hamiltonian includes a term which represents the total mass of all nucleons of the nucleus. Because of the proton–neutron mass difference, this term violates isospin. Its commutator with T_- is $(M_n-M_p)T_-$, independent of position and spin and therefore does not contribute to the escape amplitude but only to the displacement energy. We expand the kinetic energy term to first order in the p–n mass difference

$$H_{\mathrm{KIN}} = \sum_i (p_i{}^2/2M)[1-\tfrac{1}{2}(\Delta M/M)\tau_z{}^i] \tag{3.21}$$

[14] The neutron–proton mass difference is taken up in Sec. 3.21. Effects of finite size and vacuum polarization in modifying the Coulomb interaction have already been discussed and are not considered in Eq. (3.17)

with

$$M=\tfrac{1}{2}(M_n+M_p), \qquad \Delta M=M_n-M_p,$$
$$\Delta M/M=0.14\times10^{-2}.$$

By taking the commutator of Eq. (3.21) with T_-, we find

$$[H_{\rm KIN}, T_-]=\tfrac{1}{2}(\Delta M/M)\sum_i (p_i^2/2M)\tau_-^i. \quad (3.22)$$

3.22 Charge Dependence and Charge Asymmetry of the Nuclear Force

When discussing the isospin properties of nuclear forces one makes a distinction between *charge symmetry* and *charge independence*. One calls a force charge symmetric if there is no difference between the p–p and n–n interactions. A force is charge independent if the p–p and the n–n interactions are equal to the $T=1$, n–p interaction. For this state we write the interaction as

$$V^{\rm NUCL}(1,2)=V_{np}^{T=1}(1,2)+V^{\rm CA}(1,2)T_z + (V^{\rm CD}(1,2)T_z^2, \quad (3.23)$$

where

$$T_z=[\tau_z(1)+\tau_z(2)]/2,$$
$$V^{\rm CA}=[(V_{nn}-V_{pp})/2], \quad (3.24)$$

and

$$V^{\rm CD}=[(V_{pp}+V_{nn})/2-V_{np}^{T=1}]. \quad (3.25)$$

Then charge independence requires $V^{\rm CD}=V^{\rm CA}=0$, while for charge symmetry $V^{\rm CA}$ must be zero.

After having taken account of the effects of the p–n mass difference, the Coulomb potential, the vacuum polarization, the magnetic forces, there is little evidence for a violation of charge symmetry which implies $\alpha=0$. However, the charge dependence of nuclear forces is well established ($V^{CT}\neq0$). That is, the purely nuclear parts of the p–p force and the $T=1$, n–p force differ from each other. The major effects which lead to a charge dependence of the nuclear forces are [He66,69a]:

(i) The mass difference of the mesons exchanged between the nucleons, especially the mass difference between the charged and the neutral π meson.

(ii) Radiative corrections, especially to the pion–nucleon coupling constant.

(iii) Mixing of meson states of different isobaric spin but with the same spin and parity, e.g., the π^0 meson and the η meson.

We consider separately the charge dependent part, $V^{\rm CD}$, and the charge asymmetric part, $V^{\rm CA}$, of $V^{\rm NUCL}$

$$V_{\rm CD}{}^{-}=[V^{\rm CD}, T_-]=-\tfrac{1}{2}V^{\rm CD}(1,2) \times[\tau_z(1)\tau_-(2)+\tau_-(1)\tau_z(2)] \quad (3.26a)$$

and

$$V_{\rm CA}{}^{(-)}=[V^{\rm CA}, T_-]. \quad (3.26b)$$

An analysis of the scattering length and the effective range of the p–p and n–p scattering leads to the estimate [He66a],

$$|(V_{pp}-V_{np}{}^{T=1})/V_{pp}|\lesssim 2\%, \quad (3.27a)$$

the interaction between protons and neutrons in $T=1$ states being more attractive than the force between protons. Also

$$|(V_{nn}-V_{pp})/V_{pp}|\leq 1\%, \quad (3.27b)$$

with V_{nn} more attractive [He69a]. Since the nuclear forces depend strongly on the spin, the relative orbital angular momentum, and the total angular momentum, we also expect the forces, $V^{\rm CD}$ and $V^{\rm CA}$, to be complicated.

As we will see the charge dependent and charge asymmetric part of the nuclear force contributes only a small part to the energy of the analog resonance and the escape amplitude. However, these forces may dominate in cases where the Coulomb matrix element is small, e.g., when several nucleons change their orbits. This is the case in isospin forbidden decays or rearrangement amplitudes (Sec. 6).

3.3 Summary

As we have seen previously [Eq. (2.5)], the commutator $V^{(-)}=[H, T_-]$ plays a central role in the calculation of various matrix elements which appear in the theory of a analog states. In this chapter we have discussed various contributions to this commutator and may now write

$$V^{(-)}=V_c{}^{(-)}+V_{\rm CD}{}^{(-)}+V_{\rm CA}{}^{(-)}+V_{\rm MAG}{}^{(-)}+V_{\rm KIN}{}^{(-)}, \quad (3.28)$$

where

$$V_c{}^{(-)}=[V_c, T_-],$$
$$V_{\rm CD}{}^{(-)}=[V^{\rm CD}, T_-],$$
$$V_{\rm CA}{}^{(-)}=[V^{\rm CA}, T_-],$$
$$V_{\rm MAG}{}^{(-)}=[V^{\rm MAG}, T_-], \quad (3.29)$$

and

$$V_{\rm KIN}{}^{(-)}=[H_{\rm KIN}, T_-]. \quad (3.30)$$

The effects of proton finite size and vacuum polarization are now included in the definition of V_c.

It will sometimes be useful to define the operators which are adjoint to those appearing in Eq. (3.28),

$$V^{(+)}=[V^{(-)}]^\dagger=[T_+, H],$$
$$V_c{}^{(+)}=[V_c{}^{(-)}]^\dagger=[T_+, V_c], \quad (3.31)$$

etc.

4. THE NORM

Since the normalization constant $\langle\pi|T_+T_-|\pi\rangle$ introduced in the definition of the analog state $|A\rangle$ appears in various theoretical expressions, a separate,

though short, section is devoted to its evaluation. Some of the notation and techniques used in later sections will be introduced here.

We assume the parent state $|\pi\rangle$ to be normalized and to be an eigenfunction of T_z, although not necessarily an eigenstate of $\mathbf{T}^2$. Then by commuting T_+ and T_-, we obtain

$$\langle\pi|T_+T_-|\pi\rangle=2T+\langle\pi|T_-T_+|\pi\rangle, \quad (4.1)$$

where $2T=(N-Z)$. The second quantity in Eq. (4.1), the norm of the state $T_+|\pi\rangle$, is always positive and vanishes if and only if the parent state is an eigenfunction of $\mathbf{T}^2$ with $T_z=T$. One can estimate the correction term in Eq. (4.1) in *two* different ways.

(i) The parent state is expanded into states of good isospin

$$|\pi\rangle=(1-\epsilon^2)^{1/2}|T,T\rangle+\epsilon|T+1,T\rangle, \quad (4.2)$$

where ϵ^2 is the coefficient of the isospin impurity for this expansion. For simplicity we restrict ourselves to the admixture of states with isospin $T+1$. Inserting Eq. (4.2) into (4.1) we find

$$\langle\pi|T_+T_-|\pi\rangle=2T+(2T+2)\epsilon^2. \quad (4.3)$$

The parameter ϵ has been estimated using a collective model for the state $|T+1,T\rangle$. For this model it is found that [Bo67]

$$\epsilon^2=5.5\times10^{-7}Z^{8/3}/(T+1). \quad (4.4)$$

(ii) A more detailed approach proceeds through the introduction of creation operators for neutrons ($b_\alpha^\dagger$) and protons ($a_\alpha^\dagger$) and corresponding destruction operators, b_α and a_α. The operators T_+ and T_- may be expressed in terms of the b's and a's:

$$T_+=\sum_\alpha b_\alpha^\dagger a_\alpha, \qquad T_-=\sum_\alpha a_\alpha^\dagger b_\alpha, \quad (4.5)$$

where $\{\alpha\}$ denotes any complete set of single-particle functions. In general the expression

$$\langle\pi|T_-T_+|\pi\rangle=\sum_{\alpha,\beta}\langle\pi|a_\alpha^\dagger b_\alpha b_\beta^\dagger a_\beta|\pi\rangle \quad (4.6)$$

cannot be simplified further. However, we assume $|\pi\rangle$ to factorize into a function containing only protons and one which contains only neutrons. Then Eq. (4.6) is reducible to a product of one-body densities for protons and neutrons,

$$\langle\pi|T_-T_+|\pi\rangle=\sum_{\alpha,\beta}\langle\pi|a_\alpha^\dagger a_\beta|\pi\rangle\langle\pi|b_\alpha b_\beta^\dagger|\pi\rangle. \quad (4.7)$$

The factorization in Eq. (4.7) corresponds to the neglect of p–n correlations in the parent state $|\pi\rangle$. Equation (4.7) holds trivially, if $|\pi\rangle$ is a Slater determinant. The same factorization follows also from the assumption that in the sum over intermediate states $|n\rangle$

$$\langle\pi|T_-T_+|\pi\rangle=\sum_n\sum_{\alpha\beta}\langle\pi|a_\alpha^\dagger a_\beta|n\rangle\langle n|b_\alpha b_\beta^\dagger|\pi\rangle, \quad (4.8)$$

the parent state exhausts most of the sum.

We introduce the single-particle density matrices

$$\rho_{\alpha\beta}^p=\langle\pi|a_\alpha^\dagger a_\beta|\pi\rangle,$$

and

$$\rho_{\alpha\beta}^n=\langle\pi|b_\alpha^\dagger b_\beta|\pi\rangle. \quad (4.9)$$

Then Eq. (4.6) is

$$\langle\pi|T_-T_+|\pi\rangle=\sum_{\alpha\beta}\rho_{\alpha\beta}^p(\delta_{\alpha\beta}-\rho_{\beta\alpha}^n)=Z-\sum_{\alpha\beta}\rho_{\alpha\beta}^p\rho_{\beta\alpha}^n, \quad (4.10)$$

which may be written as[15]

$$\langle\pi|T_-T_+|\pi\rangle=\int d\mathbf{x}[\rho^p(\mathbf{x},\mathbf{x})-\int d\mathbf{y}\rho^p(\mathbf{x},\mathbf{y})\rho^n(\mathbf{y},\mathbf{x})]=\int \mathrm{I}(\mathbf{x})\,d\mathbf{x}, \quad (4.11)$$

where we have defined the isospin impurity function, $\mathrm{I}(\mathbf{x})$,

$$\mathrm{I}(\mathbf{x})=\rho^p(\mathbf{x},\mathbf{x})-\int\rho^p(\mathbf{x},\mathbf{y})\rho^n(\mathbf{y},\mathbf{x})\,d\mathbf{y} \quad (4.12)$$

in terms of the coordinate representation of the proton and neutron density matrices. We can see from Eq. (4.10) or Eq. (4.12) that if the product of the proton and neutron density matrices yields the proton density matrix, the parent state $|\pi\rangle$ has good isospin. Different models of isospin impurity will give different forms for $\mathrm{I}(\mathbf{x})$. Of course, we have

$$\int \mathrm{I}(\mathbf{x})\,d\mathbf{x}\geq 0, \quad (4.13)$$

since this integral represents the norm of the state $T_+|\pi\rangle$.

In the special case that $|\pi\rangle$ is a Slater determinant such that

$$\rho^p(\mathbf{x},\mathbf{y})=\sum_\alpha\psi_\alpha^{p*}(\mathbf{x})\psi_\alpha^p(\mathbf{y}) \quad (4.14)$$

and

$$\rho^n(\mathbf{x},\mathbf{y})=\sum_\beta\psi_\beta^{n*}(\mathbf{x})\psi_\beta^n(\mathbf{y}),$$

we have

$$\mathrm{I}(\mathbf{x})=\sum_\alpha\psi_\alpha^{p*}(\mathbf{x})\psi_\alpha^p(\mathbf{x})-\sum_{\alpha,\beta}\psi_\alpha^p(\mathbf{x})\times(\int\psi_\alpha^p(\mathbf{y})\psi_\beta^{n*}(\mathbf{y})d\mathbf{y})\psi_\beta^n(\mathbf{x}), \quad (4.15)$$

where the sum goes over the occupied states. Finally, we have

$$\langle\pi|T_-T_+|\pi\rangle=Z-\sum_{\alpha,\beta}|\int\psi_\alpha^{p*}(\mathbf{x})\psi_\beta^n(\mathbf{x})\,d\mathbf{x}|^2. \quad (4.16)$$

[15] If there are short-range neutron–proton correlations, we may use a nuclear correlation factor $[1+g^C(\mathbf{x}-\mathbf{y})]$ multiplying the second term of (4.11) to suitably generalize the isospin impurity function $\mathrm{I}(\mathbf{x})$.

We note that expression Eq. (4.16) vanishes if the occupied proton orbits are equal to the corresponding neutron occupied orbits. Equation (4.16) may also vanish when there is no one-to-one correspondence. If the occupied proton orbits can be fully expanded in the *occupied* neutron orbits, the right-hand side of Eq. (4.16) is zero, and the Slater determinant has good isospin. In other words, the detailed shape of the occupied neutron orbits is relatively unimportant. Isospin purity requires only that they form a complete set for the occupied protons orbitals. Therefore, an increasing number of excess neutrons leads to increasing isospin purity. The only approximation entering the treatment of the Model (ii) is the neglect of p–n correlations. Such correlations may change the isospin impurity of nuclear states. A recent investigation [Bo67] shows that collective p–n correlations tend to reduce the isospin impurity of nuclear states by an order of magnitude compared with a single-particle estimates [Sl65; Ma55,56].

5. DISPLACEMENT ENERGIES

The position E_R of the isobaric analog resonance is given by

$$E_R=\langle A \mid H \mid A\rangle + \mathrm{Re}\,(\langle A \mid H\{q/[E_R-H_{qq}+\tfrac{1}{2}(iI)]\}H \mid A\rangle + \langle A \mid \mathrm{H}_{AP}\mathrm{G}_P^{(+)}\mathrm{H}_{PA} \mid A\rangle). \quad (5.1)$$

The first term in Eq. (5.1) is the dominant one and the difference between it and the energy of the parent will be called the *displacement energy* (see Fig. 5.1)

$$E_d^{\mathrm{TOT}}=E_A-E_\pi=\langle A \mid H \mid A\rangle-\langle \pi \mid H \mid \pi\rangle = \mathrm{N}^{-1}\langle \pi \mid T_+[H, T_-] \mid \pi\rangle, \quad (5.2)$$

where the definitions [Eqs. (2.2)–(2.3)] have been used.

The displacement energy deduced from isobaric analog resonance experiments is useful for the study of the distribution of the $(N-Z)$ excess neutrons in nuclei because the bulk of the displacement energy arises from Coulomb matrix elements between the wave functions of the protons and excess neutrons and is sensitive to the excess neutron distribution [No67; Be68a,b; Au69a; No69a,b; Sc69a,b]. However, in order to draw conclusions about the charge and matter distribution in nuclei, it is necessary to understand all of the different effects that contribute to the displacement energy.

Experimentally, the position of the isobaric analog resonance is measured. Therefore, in order to obtain the displacement energy it is necessary to calculate the shift due to the coupling of the analog state to the compound and continuum states as exhibited in the last two terms of Eq. (5.1). The first shift is of the order of a few keV while the coupling to the continuum contributes between tens and hundreds of keV. These shifts are dependent upon the specific reaction theory of isobaric analog resonances and are treated separately in Sec. 7.

The main contribution to the displacement energy comes from the two-body Coulomb force. In the accurate calculation of this main term we have to consider the influence of the Pauli and nuclear correlations, vacuum polarization, and finite proton size. Configuration mixing and isospin impurity in the parent state are considered in Secs. 5.3 and 5.2.

The other isospin violating parts of the Hamiltonian, the magnetic interactions, the n–p mass difference, and the charge-dependent nuclear force, contribute about 100–200 keV to the displacement energy. We will discuss these effects as they contribute to the displacement energies in Sec. 5.4.

We will not review here all of the work on the Coulomb energy as such since this is slightly afield of our subject. But we will try to isolate all of the small correction terms which are necessary for an accurate calculation of the displacement energy.

5.1 The Coulomb Displacement Energy

The Coulomb force, written in second quantization and including finite-size effects and vacuum polarization is

$$V_c=\tfrac{1}{4}\sum_{\alpha\beta\gamma\delta}\langle\alpha\beta \mid v_c \mid \delta\gamma\rangle_A a_\alpha^\dagger a_\beta^\dagger a_\gamma a_\delta \quad (5.3)$$

with

$$v_c(r)=(e^2/r)[1+(2\alpha/3\pi)I(r)+g^F(r)], \quad (5.4)$$

as discussed in Sec. 3. The creation operators in Eq. (5.3) refer to protons. The representation of the single-particle states $\{\alpha\}$ is arbitrary and the subscript A means that antisymmetrization is taken into account, $\langle\alpha\beta \mid v_c \mid \delta\gamma\rangle_A=\langle\alpha\beta \mid v_c \mid \delta\gamma\rangle-\langle\alpha\beta \mid v_c \mid \gamma\delta\rangle$.

Equation (5.2) may be rewritten in terms of an expectation value of a double commutator, and an additional term

$$E_d^{\mathrm{TOT}}=E_d+\Delta E_d, \quad (5.5)$$

where

$$E_d=\mathrm{N}^{-1}\langle \pi \mid [T_+, [H, T_-]] \mid \pi\rangle, \quad (5.6)$$

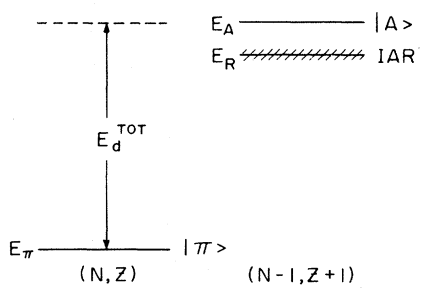

FIG. 5.1. Schematic representation of the relation of the displacement energy $E_d^{\mathrm{TOT}}=E_A-E_\pi$ and the observed energy of the isobaric analog resonance, E_R.

and

$$\Delta E_d = \mathrm{N}^{-1}\langle\pi \mid [H, T_-]T_+ \mid \pi\rangle. \quad (5.7)$$

The term ΔE_d vanishes in the case in which isospin is conserved, since in that case $T_+ \mid \pi\rangle = 0$. For states where isospin is approximately conserved this term is very small; we will return to the consideration of this term in Sec. 5.2. In this section we consider the first term, Eq. (5.6), and approximate the norm $\langle\pi \mid T_+T_- \mid \pi\rangle$ by $2T$.

Using the isospin lowering and raising operators T_- and T_+ in second quantized form, Eq. (4.5), we evaluate the single and double commutators and find

$$[V_c, T_-] = \tfrac{1}{2}\sum_{\alpha\beta\gamma\delta}\langle\alpha\beta \mid v_c \mid \delta\gamma\rangle_A a_\alpha^\dagger a_\beta^\dagger a_\gamma b_\delta \quad (5.8)$$

$$[T_+, [V_c, T_-]] = \sum_{\alpha\beta\gamma\delta}\langle\alpha\beta \mid v_c \mid \delta\gamma\rangle_A \times (b_\alpha^\dagger a_\beta^\dagger a_\gamma b_\delta - \tfrac{1}{2}a_\alpha^\dagger a_\beta^\dagger a_\gamma a_\delta). \quad (5.9)$$

Thus, the displacement energy depends on the two expectation values,

$$\langle\pi \mid b_\alpha^\dagger a_\beta^\dagger a_\gamma b_\delta \mid \pi\rangle \quad \text{and} \quad \langle\pi \mid a_\alpha^\dagger a_\beta^\dagger a_\gamma a_\delta \mid \pi\rangle.$$

If the wave function of the parent is well described by a Slater determinant with definite N and Z, these matrix elements factorize

$$\langle\pi \mid b_\alpha^\dagger a_\beta^\dagger a_\gamma b_\delta \mid \pi\rangle = \rho_{\alpha\delta}{}^n\rho_{\beta\gamma}{}^p$$

and

$$\langle\pi \mid a_\alpha^\dagger a_\beta^\dagger a_\gamma a_\delta \mid \pi\rangle = \rho_{\alpha\delta}{}^p\rho_{\beta\gamma}{}^p - \rho_{\alpha\delta}{}^p\rho_{\beta\delta}{}^p. \quad (5.10)$$

Thus Eq. (5.7) reads

$$E_d = (2T)^{-1}\sum_{\alpha\beta\gamma\delta}\langle\alpha\beta \mid v_c \mid \delta\gamma\rangle_A(\rho_{\alpha\delta}{}^n - \rho_{\alpha\delta}{}^p)\rho_{\beta\gamma}{}^p$$
$$= (2T)^{-1}\int\int d\mathbf{x}\, d\mathbf{y}\{[\rho^n(\mathbf{x}) - \rho^p(\mathbf{x})]v_c(|\mathbf{x}-\mathbf{y}|)\rho^p(\mathbf{y}) - \tfrac{1}{2}[\rho^n(\mathbf{x},\mathbf{y}) - \rho^p(\mathbf{x},\mathbf{y})]v_c(|\mathbf{x}-\mathbf{y}|)\rho^p(\mathbf{x},\mathbf{y})\}, \quad (5.11)$$

where $\rho(\mathbf{x}, \mathbf{y})$ is the density matrix in coordinate space, and $\rho(\mathbf{x}) \equiv \rho(\mathbf{x}, \mathbf{x})$. The second term in (5.11) is the exchange term, and the factor $\frac{1}{2}$ in this term arises from the assumption that the density matrix is independent of spin.

In general, proton–neutron correlations and proton–proton correlations will modify Eq. (5.11). Therefore, we introduce spin-dependent correlation functions $g_{pp}{}^{CS}(|\mathbf{x}-\mathbf{y}|)$ and $g_{np}{}^{CS}(|\mathbf{x}-\mathbf{y}|)$ describing the short-range proton–proton and $T=1$ neutron–proton correlations, and defer discussion of long-range correlations (i.e., configuration mixing) to Sec. 5.3. Then Eq. (5.11) may be written

$$E_d = (2T)^{-1}\int\int d\mathbf{x}\, d\mathbf{y} v_c(|\mathbf{x}-\mathbf{y}|)\sum_{S=0,1}(2S+1)/4 \times\{[1+g_{pn}{}^{CS}(|\mathbf{x}-\mathbf{y}|)] \times[\rho^n(\mathbf{x})\rho^p(\mathbf{y}) + (-1)^S\rho^n(\mathbf{x},\mathbf{y})\rho^p(\mathbf{x},\mathbf{y})] - [1+g_{pp}{}^{CS}(|\mathbf{x}-\mathbf{y}|)] \times[\rho^p(\mathbf{x})\rho^p(\mathbf{y}) + (-)^S\rho^p(\mathbf{x},\mathbf{y})\rho^p(\mathbf{x},\mathbf{y})]\} \quad (5.12)$$

where $g^{CS}(|\mathbf{x}-\mathbf{y}|)$ refers to the triplet and singlet part of the correlation function for $S=1$, 0 respectively. It has been assumed here that the density matrices are spin independent. In the more general case, not considered here, we have

$$\rho(\mathbf{x}, \mathbf{y}) = \rho_0(\mathbf{x}, \mathbf{y}) + \boldsymbol{\sigma}\cdot(\mathbf{x}\times\mathbf{y})\rho_v(\mathbf{x}, \mathbf{y}),$$

where $\boldsymbol{\sigma}$ is the Pauli spin operator. If we admit spin dependence of the density matrices, Eq. (5.12) takes on a more complicated structure which we do not present here. We note that the spin-dependent vector term only contributes to exchange integrals. In addition we expect the vector part ρ_v to be small since it only receives contributions from nonclosed shells in the sense of L–S coupling. We usually assume that

$$[g_{pn}{}^{CS}(|\mathbf{x}-\mathbf{y}|)\rho^n(\mathbf{x}) - g_{pp}{}^{CS}(|\mathbf{x}-\mathbf{y}|)\rho^p(\mathbf{x})] = g^{CS}(|\mathbf{x}-\mathbf{y}|)[\rho^n(\mathbf{x}) - \rho^p(\mathbf{x})]$$

which implies that the core part of the np and pp correlations are equal, and defines $g^{CS}(|\mathbf{x}-\mathbf{y}|)$ as the correlation of the excess neutrons with the core protons. Then Eq. (5.12) simplifies to

$$E_d = (2T)^{-1}\int d\mathbf{x}\, d\mathbf{y}\sum_S \tfrac{1}{4}(2S+1)(1+g^{CS}(|\mathbf{x}-\mathbf{y}|)) \times\{[\rho^n(\mathbf{x}) - \rho^p(\mathbf{y})]\rho^p(\mathbf{y}) + (-)^S \times[\rho^n(\mathbf{x},\mathbf{y}) - \rho^p(\mathbf{x},\mathbf{y})]\rho^p(\mathbf{x},\mathbf{y})\}v_c(|\mathbf{x}-\mathbf{y}|). \quad (5.13)$$

5.11 The Direct Part of the Coulomb Energy

The dominant term in Eq. (5.13) is

$$E_d{}^{\mathrm{COUL}} = (e^2/2T)\int\int d\mathbf{x}\, d\mathbf{y}[\rho^n(\mathbf{x}) - \rho^p(\mathbf{x})] \times(1/|\mathbf{x}-\mathbf{y}|)\rho^p(\mathbf{y}). \quad (5.14)$$

In order to evaluate this term, which contributes more than 90% to the displacement energy, we take the proton density as determined from other experiments and parameterize the function $[\rho^n(\mathbf{x}) - \rho^p(\mathbf{x})]$ which we call the excess neutron distribution. Elastic electron scattering from nuclei and muonic x-ray experiments probe the charge distribution in nuclei. The distributions resulting from these experiments are usually expressed in terms of two or three parameters [El67; Ho67a]. The two parameter form is of the Fermi type:

$$\rho^{\mathrm{charge}}(r) = \text{constant}/\{1 + \exp[4\ln 3(r-c)/t]\}. \quad (5.15)$$

Using a three-parameter charge distribution does not change the result by more than 100 keV.

The nuclear charge distribution determined from electron scattering or muonic atoms includes the effect of the proton finite size, i.e., in momentum space,

$$\rho^{\mathrm{charge}}(q^2) = \rho^p(q^2)G_p(q^2), \quad (5.16)$$

where $\rho^p(q^2)$ is the Fourier transform of $\rho^p(r)$, the dis-

tribution of point protons, and $G_p(q^2)$ is the form factor of the proton.[16] The charge density appearing in Eq. (5.14) is for point charges indicating that the finite-size effect has been removed from the experimental charge distribution using Eq. (5.16).

Now, the only unknown quantity in Eq. (5.14) is the excess neutron density $[\rho^n(\mathbf{x})-\rho^p(\mathbf{x})]$. By parameterizing $[\rho^n(\mathbf{x})-\rho^p(\mathbf{x})]$ and fitting the experimental displacement energy we obtain information about the excess neutron distribution. In naive calculations the excess neutron distribution is often represented by the wave functions of the excess neutrons, i.e.,

$$[\rho^n(\mathbf{x})-\rho^p(\mathbf{x})]=\sum_{\nu=Z+1}^{N}|\varphi_\nu(\mathbf{x})|^2, \quad (5.17)$$

where wave functions $\varphi_\nu(\mathbf{x})$ are obtained by solving a single-particle Schrödinger equation with a Saxon–Woods potential. The sum in Eq. (5.17) runs over the shell-model orbits occupied by the excess neutrons. The depth of the potential and the diffuseness is always chosen to fit the experimental binding energies of the excess neutrons. The only free parameter is the radius of the potential. Including all the corrections discussed below, the radius is chosen so that a fit is obtained to the experimental energy of the analog resonance. The change of the radius of the potential well is only a device for varying the extension of the neutron distribution, and, in general, the displacement energy will determine the relation between the parameters characterizing the differences in shapes of the proton and neutron distributions.

5.12 The Exchange Term

The next largest contribution is the exchange term defined by

$$E_d^{\mathrm{EXCH}}=-(2T)^{-1}\tfrac{1}{2}e^2\int\int d\mathbf{x}\,d\mathbf{y}$$
$$\times[\rho^n(\mathbf{x},\mathbf{y})-\rho^p(\mathbf{x},\mathbf{y})](1/|\mathbf{x}-\mathbf{y}|)\rho^p(\mathbf{x},\mathbf{y}). \quad (5.18)$$

Again, the single-particle model can be used to approximate the density matrix of the excess neutrons

$$\rho^n(\mathbf{x},\mathbf{y})-\rho^p(\mathbf{x},\mathbf{y})=\sum_{\nu=Z+1}^{N}\varphi_\nu(\mathbf{x})\varphi_\nu(\mathbf{y}), \quad (5.19)$$

where the sum runs over the orbits occupied by the excess neutrons. In a similar way we have to parameterize the proton density matrix $\rho^p(\mathbf{x},\mathbf{y})$, since electron scattering or muonic atom experiments only yield information concerning $\rho^p(\mathbf{x})$. The parameters of a proton well are chosen such that $\rho^p(\mathbf{x})$ agrees with experiment. The proton wave functions of this well are used to construct the proton density matrix, $\rho^p(\mathbf{x},\mathbf{y})$, and the exchange term, Eq. (5.18), is calculated.

The ratio of the exchange to direct terms is not very sensitive to the exact form of the proton wave function. Because of this feature we can accurately determine this ratio from infinite matter [Be36; Be68b]. We *define* a Pauli correlation function $g^P(\mathbf{x},\mathbf{y})$ by the use of the following equation

$$\tfrac{1}{2}\rho^p(\mathbf{x},\mathbf{y})[\rho^n(\mathbf{x},\mathbf{y})-\rho^p(\mathbf{x},\mathbf{y})]$$
$$\equiv\rho^p(\mathbf{x})[\rho^n(\mathbf{y})-\rho^p(\mathbf{y})]g^P(\mathbf{x},\mathbf{y}). \quad (5.20)$$

Thus Eq. (5.18) becomes

$$E_d^{\mathrm{EXCH}}=-(e^2/2T)\int d\mathbf{x}\,d\mathbf{y}[\rho^n(\mathbf{x})-\rho^p(\mathbf{x})]$$
$$\times(|\mathbf{x}-\mathbf{y}|)^{-1}\rho(\mathbf{y})g^P(\mathbf{x},\mathbf{y}). \quad (5.21)$$

In infinite matter the correlation function $g^P(\mathbf{x},\mathbf{y})$ is translationally invariant and is given by

$$g^P(|\mathbf{x}-\mathbf{y}|)=\frac{1}{2}\int_0^{k_F{}^p}d\mathbf{k}^p\int_{k_F{}^p}^{k_F{}^n}d\mathbf{k}^n$$
$$\times\exp[i(\mathbf{k}^n-\mathbf{k}^p)\cdot(\mathbf{x}-\mathbf{y})]\left(\int_0^{k_F{}^p}d\mathbf{k}^p\int_{k_F{}^p}^{k_F{}^n}d\mathbf{k}^n\right)^{-1} \quad (5.22)$$

Here, $k_F{}^n$ and $k_F{}^p$ are the Fermi momenta of the neutrons and protons respectively. The integration limits in the second integral reflect the fact that we integrate only over the *excess* neutrons. Integration over the angles of $\mathbf{k}^p$ and $\mathbf{k}^n$ is implied. If we introduce the notation $z=k_F{}^p|\mathbf{x}-\mathbf{y}|$ and $\lambda=k_F{}^n/k_F{}^p$, the integral in Eq. (5.22) is evaluated to be

$$g^P(|\mathbf{x}-\mathbf{y}|)=\tfrac{9}{2}(\lambda^3-1)^{-1}\int_0^1 j_0(yz)y^2\,dy\int_1^\lambda j_0(y'z)y'^2\,dy'$$
$$=\tfrac{9}{2}(\lambda^3-1)^{-1}z^{-2}j_1(z)[\lambda^2 j_1(\lambda z)-j_1(z)], \quad (5.23)$$

where the j_l are spherical Bessel functions. This function differs from the usual nucleon–nucleon correlation function [Bo69] since it only describes the Pauli

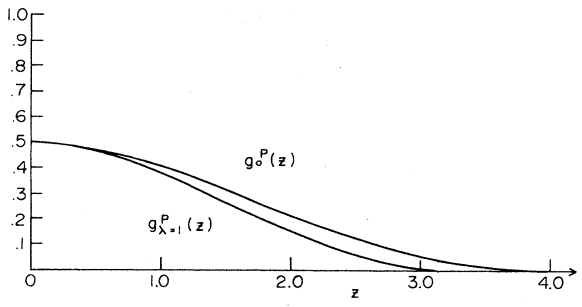

FIG. 5.2. A comparison of the correlation functions $g_0{}^P(z)=9j_1{}^2(z)/2z^2$ and $g_{\lambda=1}{}^P(z)=3j_0(z)j_1(z)/2z$.

[16] Strictly, the nuclear charge form factor as measured experimentally is $\rho(q^2)=\rho^p(q^2)G_p(q^2)+\rho^n(q^2)G_n(q^2)$, where ρ^p and ρ^n describe the distributions of point protons and point neutrons, respectively, and $G_p(q^2)$ and $G_n(q^2)$ are the charge form factors of protons and neutrons. Since $G_n(0)=0$, and $\rho^n(q^2)$ goes to zero rapidly with increasing q^2, the term with ρ^n may be neglected.

correlations between core nucleons and nucleons near the top of the Fermi sea. The usual average correlation function is obtained from the $\lambda=0$ limit of $g^P(x)$

$$g_0{}^P(z)\equiv g^P(z)_{\lambda\to 0}=(9/2z^2)[j_1(z)]^2. \quad (5.24)$$

A comparison of $g^P(z)$ for $\lambda=1$ and the usual proton–proton correlation function $g_0{}^P(z)$, is made in Fig. 5.2.

Assuming that the Pauli correlation function is translationally invariant (as in the case of nuclear matter) and using the fact that this function is of short range ($k_F\sim 1.4\text{F}^{-1}$), we may write

$$\begin{aligned}E_d{}^{\text{EXCH}}&\simeq -(e^2/2T)\int d\mathbf{s}\, d\mathbf{x}\\ &\quad\times[\rho^n(\mathbf{x})-\rho^p(\mathbf{x})]s^{-1}\rho^p(\mathbf{x}+\mathbf{s})g^P(s)\\ &\simeq -(e^2/2T)\int d\mathbf{x}[\rho^n(\mathbf{x})-\rho^p(\mathbf{x})]\rho^p(\mathbf{x})\\ &\quad\times 4\pi\int_0^\infty s^{-1}g^P(s)s^2\,ds, \quad (5.25)\end{aligned}$$

where we have dropped derivatives of $\rho^p(\mathbf{x})$. The first factor of (5.25) can be estimated by assuming that ρ^p and ρ^n have square shapes. The integral on s can be performed to yield

$$E_d{}^{\text{EXCH}}=-\frac{27}{16}\frac{e^2}{R}Z\frac{1}{(k_F{}^pR)^2}\left(\frac{\lambda^2+\lambda+2}{\lambda^2+\lambda+1}\right), \quad (5.26)$$

where R is the nuclear radius.

Using the fact that $\lambda=k_F{}^n/k_F{}^p=(N/Z)^{1/3}$ and expanding to first order in $(N-Z)/Z$ we have

$$E_d{}^{\text{EXCH}}\simeq -\frac{9}{4}\frac{Ze^2}{R}\frac{1}{(k_F{}^pR)^2}\left(1-\frac{N-Z}{12Z}\right). \quad (5.27)$$

Finally, we recognize that the integral on s in Eq. (5.25) must be cut off before the nuclear radius. Using the dimensionless cutoff value equal to $\sqrt{2}k_FR$ we have

$$\begin{aligned}E_d{}^{\text{EXCH}}&=-\frac{9}{4}\frac{Ze^2}{R}\frac{1}{(k_F{}^pR)^2}\left(1-\frac{N-Z}{12Z}\right)\\ &\quad\times\left(1-\frac{2}{A^{2/3}(k_F{}^pr_0)^2}\right)+\cdots\\ &\simeq -900\frac{Z}{A}\text{ keV}. \quad (5.28)\end{aligned}$$

This estimate agrees with the numerical result obtained using the single-particle model (see Sec. 5.4).

5.13 The Effect of the Finite Proton Size

We consider now the term in Eq. (5.13) which contains the effect of the finite size of the protons. Including the exchange contribution, we define

$$\begin{aligned}E_d{}^F&=(e^2/2T)\int\int d\mathbf{x}\, d\mathbf{s}[\rho^n(\mathbf{x})-\rho^p(\mathbf{x})]\\ &\quad\times s^{-1}g^F(s)\rho^p(\mathbf{x}+\mathbf{s})[1-g^P(s)]. \quad (5.29)\end{aligned}$$

Again using the short-range expansion, we may write Eq. (5.29) as:

$$\begin{aligned}E_d{}^F&=(e^2/2T)\int d\mathbf{x}[\rho^n(\mathbf{x})-\rho^p(\mathbf{x})]\rho^p(\mathbf{x})\\ &\quad\times\int d\mathbf{s}[g^F(s)/s][1-g^P(s)]. \quad (5.30)\end{aligned}$$

We may obtain a rough estimate of $E_d{}^F$ by expanding $g^P(s)$ to second order in $(k_F{}^ps)$ and taking the $\lambda=1$ limit

$$g^P(s)\simeq\tfrac{1}{2}-\tfrac{2}{15}(k_F{}^ps)^2. \quad (5.31)$$

We find in the nuclear matter limit,

$$\begin{aligned}E_d{}^F&=-(Ze^2/R)(r_p/R)^2[\tfrac{1}{2}+\tfrac{1}{6}(r_pk_F{}^p)^2]\\ &\simeq(-250Z/A)\text{ keV}. \quad (5.32a)\end{aligned}$$

In Eq. (5.32a), R is the nuclear radius and r_p (defined in Sec. 3.12) is equal to 0.83F. Detailed calculation of Eq. (5.30) for finite nuclei confirms an approximately constant value of $E_d{}^F\sim -100$ keV.

We may also estimate the effect of the finite charge distribution of the neutron using the neutron mean square radius. To this same order only the Coulomb interaction of the neutron with the proton point charge enters, and the result is

$$E_d{}^{F,\text{neutron}}=+\tfrac{1}{8}(N-Z)(e^2/R)(r_n/R)^2\leq 1\text{ keV}. \quad (5.32b)$$

5.14 Vacuum Polarization

As we saw in Sec. 3.13, the additional potential due to vacuum polarization is given by Eqs. (3.11)–(3.13). As noted there the logarithmic singularity for small r in the function $I(r)$ would be removed if we were to correct for finite proton size following the procedure used previously for the Coulomb interaction itself (Sec. 3.12).

To obtain an estimate of the vacuum polarization correction it is sufficient to use $I(r)$ evaluated for a mean value of the distance $r\simeq r_0=1.2$F. Then $\ln(\kappa r)\simeq 5.6$, and a factor of 2 change in r_0 changes $\ln(\kappa r)$ by only ± 0.7. (Note that $r\geq c$, where c is the hard-core radius). The correction corresponds to an increase of e^2 by about 0.6% when calculating the Coulomb displacement energy. Expressing this vacuum polarization correction in terms of Z and A we have

$$E_d{}^{\text{POL}}=8.5(Z/A^{1/3})\text{ keV}. \quad (5.32c)$$

5.15 Short-Range Correlations

The term in Eq. (5.13) arising from the short-range spin-independent correlations is[17]

$$\begin{aligned}E_d{}^C&=(e^2/2T)\int d\mathbf{x}\, d\mathbf{s}g^C(s)[\rho^n(\mathbf{x})-\rho^p(\mathbf{x})]s^{-1}\rho^p(\mathbf{x}+\mathbf{s})\\ &\quad\times[1+g^F(s)][1-g^P(s)]. \quad (5.33)\end{aligned}$$

[17] When $g^C(s)$ is spin dependent as in Eq. (5.13), we obtain the same form with $g^C(1-g^P)$ replaced by

$$g^C(1-g^P)\to\sum_S\tfrac{1}{4}(2S+1)g^{CS}(1+(-1)^S2g^P).$$

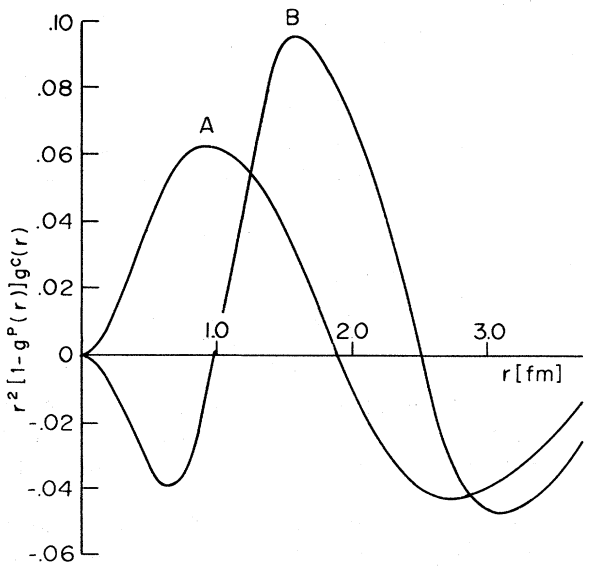

FIG. 5.3. The product of nuclear correlation $g^C(s)$ and the Pauli correlation function as taken from the work of Di Toro, Nunberg, and Riihimaki [Di70]. Curve A refers to the Tabakin potential, and curve B to the Kerman–Rouben–Riihimaki potential.

Making the short-range expansion, we find

$$E_d{}^C = \pm \frac{e^2}{2T} L^2 \int d\mathbf{x}[\rho^n(\mathbf{x}) - \rho^p(\mathbf{x})]\rho^p(\mathbf{x})$$

$$\simeq \pm \frac{3}{4\pi}\left(\frac{e^2}{r_0}\right)\frac{Z}{A}\left(\frac{L}{r_0}\right)^2, \qquad (5.34)$$

where

$$L^2 = |\int ds g^C(s) s^{-1}[1-g^P(s)][1+g^F(s)]|. \qquad (5.35)$$

The integrand of Eq. (5.35) is composed of the short-range nuclear correlation, the Pauli correlation function, the finite size correction, and a factor $1/s$ arising from the point Coulomb interaction. The sign and the value of the correlation correction, Eq. (5.34), depend sensitively on the form of the nuclear correlation function. This correlation function must satisfy the normalization condition (see Appendix 2),

$$\int ds g^C(s)[1-g^P(s)] = 0, \qquad (5.36)$$

which holds in the same short-range approximation used in the previous discussion. We see that the integrand of Eq. (5.36) will contain oscillations which influence the size of $E_d{}^C$.

The short-range correlation correction has been calculated [Di70] for two different nucleon-nucleon forces. The quantity $s^2[1-g^P(s)]g^C(s)$ as obtained by these authors for a semirealistic two term separable interaction [Ta64] and a modified realistic form [Ro69a,b] with a local tail is shown in Fig. (5.3). In Table 5.1 we present the results for $E_d{}^C$ obtained by these authors [Di70] with and without the proton finite-size correction. We see that the separable potential yields positive corrections as it exhibits attraction at short distances where the Coulomb interaction is strongest. For the more realistic interaction there is a short-range repulsion followed by an attractive region so that it is harder to guess the sign of the correlation correction. Indeed the sign of the result changes as one includes the finite size correction. Using the finite size results from Table 5.1 (KRR potential,) we may write Eq. (5.34) approximately as

$$E_d{}^C \simeq 60(Z/A) \text{ keV}. \qquad (5.37)$$

5.2 Isospin Mixing in the Parent State

In this section we are concerned with the effects of isospin mixing on the displacement energies. Some of the effects have already been included in the calculation of E_d using phenomenological charge densities. An additional effect is contained in the term ΔE_d, Eq. (5.7). This term vanishes in the case of no isospin mixing and is small otherwise. We first discuss the calculation of ΔE_d in a model which neglects correlations. This is reasonable as ΔE_d is a small correction term. We then go on to discuss ΔE_d using an expansion of the parent in states of good isospin.

In Sec. 5.23 we discuss a model which treats the *entire* contribution of isospin mixing to the displacement energy without separating these contributions to E_d and ΔE_d. Finally in Sec. 5.24 we consider some estimates for the shifts due to isospin mixing.

5.21 Evaluation of ΔE_d in a Single-Particle Model

Thus far we have only considered the quantity E_d given by Eq. (5.6). We now turn to a consideration of the term ΔE_d, Eq. (5.7), which vanishes if there is no isospin mixing and is otherwise small.

It is important to note that the whole effect of isospin mixing is not isolated in ΔE_d since we have used phenomenological densities in evaluating E_d. The isospin violation, as it affects the densities, has been included in E_d.

TABLE 5.1 Short-range correlation correction to the displacement energy [Di70].

	$E_d{}^C$(keV)		
	Ca^{48}	Sr^{88}	Pb^{208}
Tabakin Potential [Ta64]			
Point charge	71	79	...
Finite size	45	44	27
KRR potential [Ro69a,b]			
Point charge	−2	−13	...
Finite size	22	26	...

We recall the form taken by ΔE_d

$$\Delta E_d = \mathrm{N}^{-1}\langle \pi \mid [H, T_-]T_+ \mid \pi\rangle. \quad (5.7)$$

In second quantization we find

$$\Delta E_d = \mathrm{N}^{-1}\tfrac{1}{2}\sum_{\alpha\beta\gamma\delta\epsilon}\langle\alpha\beta \mid v_c \mid \delta\gamma\rangle_A \times\langle \pi \mid a_\alpha^\dagger a_\beta^\dagger a_\gamma b_\delta b_\epsilon^\dagger a_\epsilon \mid \pi\rangle. \quad (5.38)$$

Since this is a small term we evaluate this last matrix element neglecting correlations

$$\Delta E_d = \mathrm{N}^{-1}\sum_{\alpha\beta\gamma\delta\epsilon}(\delta_{\delta\epsilon}-\rho_{\epsilon\delta}{}^n)(\rho_{\beta\gamma}{}^p\rho_{\epsilon\alpha}{}^p-\rho_{\beta\epsilon}{}^p\rho_{\gamma\alpha}{}^p)\langle\alpha\beta \mid v_c \mid \delta\gamma\rangle \quad (5.39)$$

$$=\mathrm{N}^{-1}\sum_{\alpha\beta\gamma\delta}(\mathrm{I}_{\alpha\delta}\rho_{\beta\gamma}{}^p-\mathrm{I}_{\beta\delta}\rho_{\gamma\alpha}{}^p)\langle\alpha\beta \mid v_c \mid \delta\gamma\rangle, \quad (5.40)$$

where

$$\mathrm{I}_{\alpha\delta}=\rho_{\alpha\delta}{}^p-\sum_\epsilon \rho_{\delta\epsilon}{}^n\rho_{\epsilon\alpha}{}^p. \quad (5.41)$$

We may also write Eq. (5.40) in configuration space as

$$\Delta E_d = \mathrm{N}^{-1}\int\int \mathrm{I}(\mathbf{x})v_c(|\mathbf{x}-\mathbf{y}|)\rho^p(\mathbf{y})\,d\mathbf{x}\,d\mathbf{y}-\mathrm{N}^{-1} \times\int\int \mathrm{I}(\mathbf{x},\mathbf{y})v_c(|\mathbf{x}-\mathbf{y}|)\rho^p(\mathbf{x},\mathbf{y})\,d\mathbf{x}\,d\mathbf{y} \quad (5.42)$$

where[18]

$$\mathrm{I}(\mathbf{x},\mathbf{y})=\rho^p(\mathbf{x},\mathbf{y})-\int\rho^n(\mathbf{x},\mathbf{z})\rho^p(\mathbf{z},\mathbf{y})\,d\mathbf{z}, \quad (5.43)$$

and $\mathrm{I}(\mathbf{x})=\mathrm{I}(\mathbf{x},\mathbf{x})$. This latter function has been introduced previously in Sec. 4 as the isospin impurity function [Eq. (4.12)]. Various models for the proton and neutron densities allow us to calculate ΔE_d via Eq. (5.39) or (5.42).

5.22 *Alternative Approach for the Evaluation of* ΔE_d

We consider the parent state $\mid\pi\rangle$ to be expanded in states of good isospin

$$\mid\pi\rangle=\sum_{n=0}\epsilon_n \mid T+n, T\rangle, \quad (5.44)$$

the first term being the main term of the expansion. Substituting Eq. (5.44) in the expression for ΔE_d, we have

$$\Delta E_d = \mathrm{N}^{-1}\sum_{n=1}\langle\pi \mid [H, T_-] \mid T+n, T+1\rangle \times\epsilon_n[n(2T+n+1)]^{1/2} \simeq \mathrm{N}^{-1}\sum_{n=1}(E_\pi - E_{T+n,T+1})\langle\pi \mid T_- \mid T+n, T+1\rangle \times\epsilon_n[n(2T+n+1)]^{1/2}, \quad (5.45)$$

where we have assumed that H is approximately diagonal in the states of good isospin

$$H \mid T+n, T+1\rangle \simeq E_{T+n,T+1} \mid T+n, T+1\rangle. \quad (5.46)$$

[18] We consider the variables $\mathbf{x}$ and $\mathbf{y}$ to include the spin. When the densities are spin independent, the variables $\mathbf{x}$ and $\mathbf{y}$ can be taken as pure space variables if a factor 1/2 is inserted in the second term of (5.43).

Again, using Eq. (5.44), we obtain

$$\Delta E_d \simeq -\sum_{n=1}[n(2T+n+1)/\mathrm{N}]\epsilon_n{}^2\delta E_n, \quad (5.47a)$$

where

$$\delta E_n \equiv E_{T+n,T+1}-E_\pi \simeq E_{T+n,T+1}-E_{T,T}. \quad (5.47b)$$

If we assume that the main contribution to Eq. (5.47a) comes from the admixture of a single state with $T+1$ in Eq. (5.44) we have

$$\Delta E_d \simeq -\epsilon_1{}^2[(T+1)/T]\delta E_1. \quad (5.48)$$

In the models we consider (see Sec. 5.23) the quantity δE_1 will be positive. Approximations for this quantity and $\epsilon_1{}^2$ will also be given in Sec. 5.24.

5.23 *Total Contribution of the Isospin Violation to the Displacement Energy*

In the last two sections we have considered the calculation of ΔE_d which is a part of the displacement energy, $E_d{}^{\mathrm{TOT}}=E_d+\Delta E_d$. We note again that isospin violation also modifies the value of E_d. It is useful, therefore, to have a model in which the *total* contribution of isospin violation is considered rather than having its effect present in two different terms. We consider such a model in this section.

Assume that the parent state with isospin T and z component $T_z=T$ contains admixtures of states with isospin $T+1$ with total probability, ϵ^2

$$\mid\pi\rangle = \mid T, T\rangle(1-\epsilon^2)^{1/2}+ \mid T+1, T\rangle\epsilon \quad (5.49)$$

Inserting Eq. (5.49) into Eq. (5.2) and using the properties of T_+ and T_-, we have

$$E_d{}^{\mathrm{TOT}}=\frac{2T(1-\epsilon^2)E_d{}^{T,T}+2\epsilon^2(2T+1)E_d{}^{T+1,T}}{2T+\epsilon^2 2(T+1)} +\epsilon\left[\left(\frac{4(2T+1)}{T}\right)^{1/2}\langle T, T-1 \mid H \mid T+1, T-1\rangle - \frac{(3T+1)}{T}\langle T, T \mid H \mid T+1, T\rangle\right], \quad (5.50)$$

where we have introduced the displacement energy of a state with pure isospin (see Fig. 5.4)

$$E_d{}^{T,T_z}\equiv\langle T, T_z-1 \mid H \mid T, T_z-1\rangle-\langle T, T_z \mid H \mid T, T_z\rangle, \quad (5.51)$$

and have neglected some terms of higher order than ϵ^2. With the definition of δ

$$[(T-1)/(2T+1)]\delta=(E_d{}^{T+1,T}-E_d{}^{T,T}), \quad (5.52)$$

we obtain

$$E_d{}^{\mathrm{TOT}}=E_d{}^{T,T}+E_d{}^{T-IMP}, \quad (5.53)$$

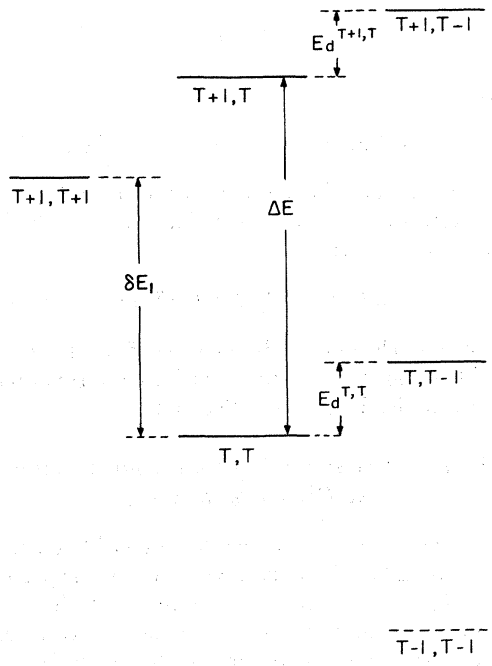

FIG. 5.4. A diagrammatic representation of the energy differences between multiplets of good isospin. The various quantities defined appear in Eqs. (5.47b), (5.51), and (5.55). The admixture of the state $(T+1, T)$ into the state (T, T) is assumed to be the main source of isospin impurity of the latter state.

where

$$E_d^{T-IMP}=\epsilon\{[4(2T+1)/T]^{1/2}\langle T, T-1 \mid H \mid T+1, T-1\rangle - [(3T+1)/T]\langle T, T \mid H \mid T+1, T\rangle\}+\epsilon^2\delta[(T-1)/T]. \quad (5.54)$$

The quantity $\delta(T-1)/(2T+1)$ of Eq. (5.52) represents the difference of the displacements of two states with pure isospin and is of the same order as the shifts due to the state dependence of the Coulomb energies, i.e., of the order of a few tens of keV or less.

In order to obtain E_d^{T-IMP}, the total contribution to the displacement energy from isospin impurity, we need to evaluate the first term in Eq. (5.54). To treat this term we decompose the interaction into spherical tensors in the isospin space. These consist of scalar, vector and tensor terms, the main contribution being from the Coulomb interaction. The most important term will be the isovector part $V_c^{(1)}$ of the Coulomb interaction, since this term contains the field effects affecting the matrix elements off-diagonal in isospin.

The amplitude ϵ, in first-order perturbation theory, is

$$\epsilon=-\langle T+1, T \mid V_c^{(1)} \mid T, T\rangle/\Delta E = -\{1/[(T+1)(2T+3)]^{1/2}\}\langle T+1 \| V_c^{(1)} \| T\rangle/\Delta E, \quad (5.55)$$

where use has been made of the Wigner–Eckart theorem, and ΔE is the excitation energy of the center-of-gravity of the $T+1$ excitations with respect to the ground state (see Fig. 5.4).

Again using the Wigner–Eckart theorem in Eq. (5.54) and using Eq. (5.55), we obtain

$$E_d^{T-IMP}=-\epsilon^2[(T-1)/T](\Delta E+\delta) \quad (5.56)$$

As we shall see in the next section ΔE is of the order of several tens of MeV so that δ may be neglected in Eq. (5.56).

Since the state $\mid T+1, T-1\rangle$, [see Fig. (5.4)], is part of the q space, it also contributes to the *compound mixing* discussed in Secs. 2 and 7. We find an energy shift,

$$E_d^{\mathrm{COMP}}=-\epsilon^2[1/T(2T+1)]\Delta E \quad (5.57)$$

which should be added to E_d^{TOT}.

Adding Eq. (5.56) (neglecting δ) and Eq. (5.57), we finally find,

$$\hat{E}_d^{\mathrm{TOT}}\equiv E_d^{\mathrm{TOT}}+E_d^{\mathrm{COMP}}=E_d^{T,T}+E_d^{T-IMP}+E_d^{\mathrm{COMP}} =E_d^{T,T}-\epsilon^2[(2T-1)/(2T+1)]\Delta E. \quad (5.58)$$

We recall the calculation of ΔE_d in the previous section resulting in Eq. (5.48), It can be shown that to a good approximation the same compound correction, Eq. (5.57), should be added so that we may also write $\hat{E}_d^{\mathrm{TOT}}$ of Eq. (5.58) as

$$\hat{E}_d^{\mathrm{TOT}}=E_d+\Delta E_d+E_d^{\mathrm{COMP}}, \quad (5.59)$$

where E_d^{COMP} is given by Eq. (5.57).

Now we may relate E_d and $E_d^{T,T}$ by comparing the two expressions for E_d^{TOT} using Eq. (5.48), and noting that $\Delta E=\delta E_1+E_d$ (see Fig. 5.4). Thus, we find that

$$E_d\simeq E_d^{T,T}+(2\epsilon^2/T)[\Delta E-\tfrac{1}{2}(T+1)E_d^{T,T}], \quad (5.60)$$

neglecting δ and higher order terms in ϵ^2.

Recall that $E_d^{T,T}$ was calculated for states of good isospin and E_d, Eq. (5.6), contained the effects of isospin impurity in modifying the densities. Therefore, the last term in Eq. (5.60) contains the isospin impurity correction to the displacement energy due to density modifications.

5.24 Estimates of Energy Shifts Caused by Isospin Violation

We now use the results of a model for isospin mixing in low-lying states of nuclei introduced by Bohr, Damgaard, and Mottelson [Bo67] to estimate ΔE and ϵ^2. In this model the isospin impurity in the $\mid T, T\rangle$ state is due to a single collective state, $\mid T, +1, T\rangle$ composed of strongly correlated particle–hole pairs with $T=1$. Treating the nucleus as a two-fluid system of protons and neutrons Bohr *et al.* are able to derive expressions for the amount of isospin impurity and for

the excitation energy:

$$\epsilon^2 = 5.5\times 10^{-7} Z^{8/3}/(T+1) \tag{5.61}$$

and

$$\Delta E = 170 A^{-1/3} \text{ MeV}. \tag{5.62}$$

Due to the correlations, ΔE is about twice as large as the energy expected from a single-particle model. Also the nondiagonal matrix element $\langle T \,||\, V_c^{(1)} \,||\, T+1\rangle$ is smaller in the calculations of Bohr *et al.* than it is in an independent-particle model. The isospin impurities in the collective model are therefore of order of magnitude smaller than in those that would be obtained from an elementary shell model.

Finally, using Eq. (5.48), with $\epsilon_1=\epsilon$, Eq. (5.61), Eq. (5.62), and $\delta E_1 \simeq (\Delta E - E_d^{T,T})$, we find[19]

$$\Delta E_d = -(Z^{8/3}/A^{1/3})(N-Z)^{-1}(0.19-1.5Z\times 10^{-3}) \text{ keV}. \tag{5.63}$$

This quantity is to be added to our calculated values of E_d. It amounts to a few tens of keV.

5.3 Configuration Mixing in the Parent State

Part of the correlations in the parent state have been taken into account explicitly by introducing a short-range correlation function $g^C(|\,\mathbf{x}-\mathbf{y}\,|)$. In the present section we consider configuration mixing in the parent state which may be looked upon as correlations of a long-range nature.

Since we have used the *empirical proton densities* in the calculation of the Coulomb displacement energies, we must carefully separate configuration mixing contributions which contribute to density modification from the true correlation terms. The situation is somewhat different for the neutron density as this quantity is not directly measurable. In this case, a model of the density must be employed and neutron *density* modifications due to configuration mixing may be considered as well as true correlation terms.

5.31 General Effects of Configuration Mixing

The effects of configuration mixing on the displacement energy may be studied in several ways. First let us assume that the parent state is expanded in various configurations $|\,\varphi_i\rangle$:

$$|\,\pi\rangle = \sum_i \alpha_i |\,\varphi_i\rangle. \tag{5.64}$$

Equations (5.2) and (5.64) may be combined as

$$E_d = \sum_i |\,\alpha_i\,|^2 E_d{}^i + \mathrm{N}^{-1} \sum_{i\neq j} \alpha_i\alpha_j \times \langle\varphi_i \,|\, [T_+, [H, T_-]] \,|\, \varphi_j\rangle = \sum_i |\,\alpha_i\,|^2 E_d{}^i + \sum_{i\neq j} \alpha_i\alpha_j E_d{}^{ij}, \tag{5.65}$$

where we have defined

$$E_d{}^{ij} = \mathrm{N}^{-1}\langle\varphi_i \,|\, [T_+, [H, T_-]] \,|\, \varphi_j\rangle. \tag{5.66}$$

Here $E_d{}^i \equiv E_d{}^{ii}$ is the displacement energy for the ith configuration,[20] and isospin impurity is neglected.

We may now calculate the contribution from the the displacement energy arising from the proton and excess neutron densities of the parent. The difference between the result of Eq. (5.65) and the calculation made in terms of the densities will represent the long-range correlation effect on the displacement energy. For simplicity we will consider only the direct term of Eq. (5.11).

We have for the proton and excess neutron densities

$$\rho^p(\mathbf{x}) = \sum_{i,j} \alpha_i\alpha_j \langle\varphi_i \,|\, a^\dagger(\mathbf{x}) a(\mathbf{x}) \,|\, \varphi_j\rangle = \sum_{i,j} \alpha_i\alpha_j \rho_{ij}{}^p(\mathbf{x}), \tag{5.67}$$

and

$$\rho^{\text{exc}}(\mathbf{x}) = \sum_{ij} \alpha_i\alpha_j [\rho_{ij}{}^n(\mathbf{x}) - \rho_{ij}{}^p(\mathbf{x})] = \sum_{ij} \alpha_i\alpha_j [\rho_{ij}{}^{\text{exc}}(\mathbf{x})]. \tag{5.68}$$

Thus, from Eq. (5.11), we have (neglecting exchange)

$$\begin{aligned} E_d \simeq \mathrm{N}^{-1} &\sum_{ijkl} \alpha_i\alpha_j\alpha_k\alpha_l \iint d\mathbf{x}\, d\mathbf{y} \\ &\times \rho_{ij}{}^{\text{exc}}(\mathbf{x}) v_c(|\,\mathbf{x}-\mathbf{y}\,|) \rho_{kl}{}^p(\mathbf{y}) \\ = \mathrm{N}^{-1} &\sum_i |\,\alpha_i\,|^4 \iint d\mathbf{x}\, d\mathbf{y} \rho_{ii}{}^{\text{exc}}(\mathbf{x}) v_c(|\,\mathbf{x}-\mathbf{y}\,|) \rho_{ii}{}^p(\mathbf{y}) \\ + \mathrm{N}^{-1} &\sum_{ijkl} (1-\delta_{ij}\delta_{jk}\delta_{kl}) \alpha_i\alpha_j\alpha_k\alpha_l \iint d\mathbf{x}\, d\mathbf{y} \\ &\times \rho_{ij}{}^{\text{exc}}(\mathbf{x}) v_c(|\,\mathbf{x}-\mathbf{y}\,|) \rho_{kl}{}^p(\mathbf{y}). \end{aligned} \tag{5.69}$$

In Eq. (5.69) we may use the relations

$$E_d{}^i \simeq \mathrm{N}^{-1} \iint d\mathbf{x}\, d\mathbf{y} \rho_{ii}{}^{\text{exc}}(\mathbf{x}) v_c(|\,\mathbf{x}-\mathbf{y}\,|) \rho_{ii}{}^p(\mathbf{y}) \tag{5.70}$$

and

$$\sum_i |\,\alpha_i\,|^4 E_d{}^i = \sum_i |\,\alpha_i\,|^2 (1 - \sum_{j\neq i} |\,\alpha_j\,|^2) E_d{}^i = \sum_i |\,\alpha_i\,|^2 E_d{}^i - \sum_{j\neq i} |\,\alpha_i\,|^2 |\,\alpha_j\,|^2 E_d{}^i.$$

Thus comparing Eq. (5.65) and Eq. (5.69) we find that the (long-range) correlation energy is

$$E_d{}^{\text{CORR}} = \sum_{ij} (1-\delta_{ij}) [\alpha_i\alpha_j E_d{}^{ij} + |\,\alpha_i\,|^2 |\,\alpha_j\,|^2 E_d{}^i] - \sum_{ijkl} (1-\delta_{ij}\delta_{jk}\delta_{kl}) \alpha_i\alpha_j\alpha_k\alpha_l E_d{}^{ijkl}, \tag{5.71}$$

where we have defined

$$E_d{}^{ijkl} = \mathrm{N}^{-1} \iint d\mathbf{x}\, d\mathbf{y} \rho_{ij}{}^{\text{exc}}(\mathbf{x}) v_c(|\,\mathbf{x}-\mathbf{y}\,|) \rho_{kl}{}^p(\mathbf{y})$$

[19] To obtain Eq. (5.63), we have used the rough approximation, $E_d{}^{T,T} \simeq 1.4Z/A^{1/3}$. Empirically determined expressions for $(E_R - E_\pi)$ may be found in [No69b].

[20] The various $E_d{}^i$ will usually not be very different. For example, if two configurations φ_1 and φ_2 differ by having n particles excited from orbit α to β, then $|\,E_d{}^1 - E_d{}^2\,| \simeq (n/2T)(\langle\beta\,|\,V_c\,|\,\beta\rangle - \langle\alpha\,|\,V_c\,|\,\alpha\rangle)$, where the matrix elements are single-particle matrix elements of the Coulomb field. Such differences are small, of the order of 10 to 100 keV, and relatively smaller in heavy nuclei where $2T$ is large.

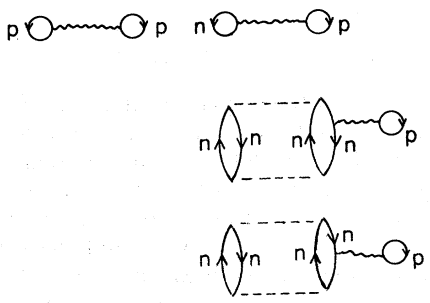

FIG. 5.5. Some contributions to the Coulomb displacement energy assuming only neutron–neutron correlations in the parent state. The dashed lines refer to the strong interaction and the wavy lines refer to the various Coulomb matrix elements appearing in Eq. (5.9).

These comments may be illuminated by diagrams representing the contractions appearing in the evaluation of the expectation value of the operator $[T_+, [V_c, T_-]]$, Eq. (5.9), in the parent state. We discuss a few examples:

(i) We assume here that the parent is a double-closed shell with two-particle two-hole neutron admixtures. The diagrams for this case are shown in Fig. (5.5). (Note that the operator $[T_+, [V_c, T_-]]$ does not contain any neutron–neutron interaction terms.) The wavy lines represent the matrix elements of the Coulomb interaction and the dashed lines the neutron–neutron strong interaction which is the source of the configuration admixture. The terms with *only* a wavy line represent the interaction of the excess neutrons with the proton distribution. The other two terms represent the modification of the neutron density due to the two-particle two-hole part of the wave function. The sum of all the diagrams, appropriately weighted, describes the interaction of the excess neutron density (modified because of the n–n interaction) with the proton density. There are no correlation terms in this case.

(ii) We turn to the case where there is a strong force giving rise to correlations between protons and neutrons. Some of the diagrams arising in the calculation of the displacement energy are shown in Fig. (5.6). The modification of the proton density is described by the diagrams of Fig. (5.6a) and the modification of the neutron density by Fig. (5.6b). Some of the correlation effects are included in the diagrams of Fig. (5.6c).

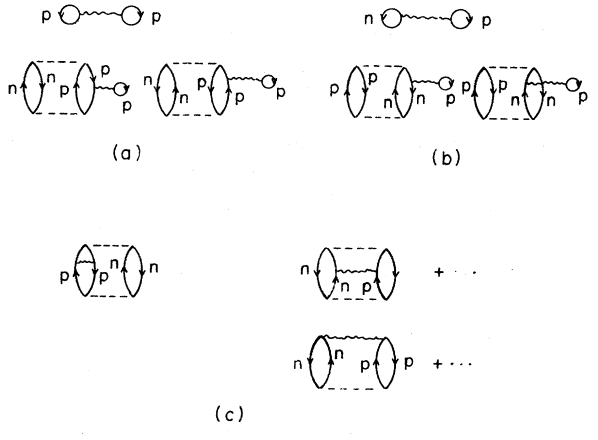

FIG. 5.6. Some of the diagrams which contribute to the evaluation of the Coulomb displacement energy for the case of a parent with proton–neutron correlations. The dashed lines refer to the strong interaction.

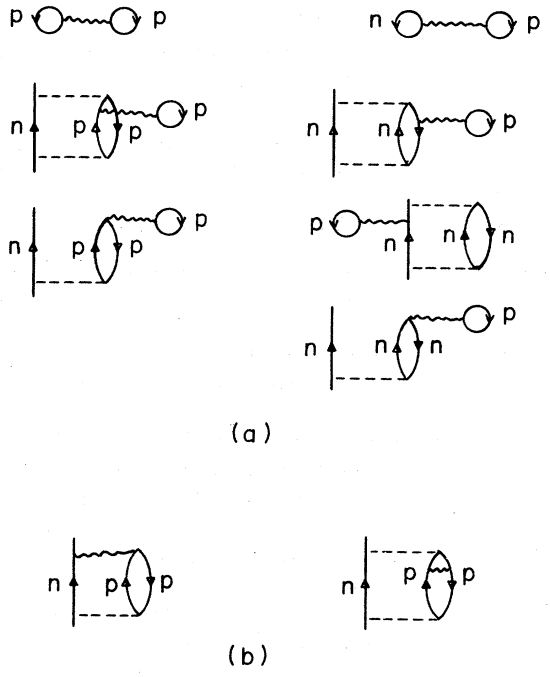

FIG. 5.7. Diagrams contributing to the Coulomb displacement energy for a parent state consisting of a neutron outside a core. The diagrams involving density modifications due to the strong interactions (dashed lines) are shown in (a), while correlation diagrams are shown in (b). See [Au69b].

(iii) Recently the mirror pair Ca^{41}–Sc^{41} has been discussed [Au69b]. In this case the admixture of a monopole $T=1$ core mode to the $f_{7/2}$ neutron wave function is possible via the strong interaction. The resulting parent state may be considered to have good isospin ($T=\frac{1}{2}$). The major effect on the displacement energies arises from the modification of the neutron and proton *densities* because of the $T=1$ admixture. This effect may be sizeable, of the order of several hundred kilovolts. The *correlation* effects are estimated to be much smaller. In Fig. (5.7a) we have indicated some diagrams involving densities and in Fig. (5.7b) some correlation diagrams are shown.

5.32 Estimates of Configuration Mixing Effects

We include here some estimates of the correction arising from the admixture of some two-particle one-hole states to states of a single particle. To this end we have calculated the quantity E_d^{ik} of Eq. (5.66), where configuration i is a single neutron of angular momentum j, and configuration k is a neutron of angular momentum j', ($j' \neq j$), coupled to a proton particle–hole state of angular momentum 2^+. The matrix element is of the form

$$E_d^{ik} = \mathrm{N}^{-1}\langle [0^+]\varphi_j^{(n)}; j \mid [T_+, [H, T_-]] \times \mid [\varphi_{j_1}^{(p)}\varphi_{j_2}^{(p)-1}]_{2^+}\varphi_{j'}^{(n)}; j\rangle. \quad (5.72)$$

We have considered orbitals appropriate to Sr^{89}, i.e., neutrons in the $d_{5/2}$, $s_{1/2}$, and $d_{3/2}$ states, and have limited ourselves to the contribution of the Coulomb force to E_d^{ik}. Some of the results for the matrix elements of Eq. (5.72) are shown in Table 5.2a. They are quite small; usually less than 3 keV.

TABLE 5.2 The quantity E_d^{ik} of Eq. (5.72) for single neutron states admixed with two-particle, one-hole states (a) or with particle-vibration modes (b). Configurations chosen are appropriate to the strontium region. Note that E_d^{ik} is related to the matrix element listed by a factor (1/N)—see Eq. (5.72).

Matrix element	E_d^{ik}(keV)
$\langle 0^+ s_{1/2} \mid V_c \mid (p_{3/2}^{-1}p_{1/2})_{2^+}d_{5/2}\rangle$	−0.3
$\langle 0^+ s_{1/2} \mid V_c \mid (p_{3/2}^{-1}p_{1/2})_{2^+}d_{3/2}\rangle$	−2.2
$\langle 0^+ s_{1/2} \mid V_c \mid (f_{5/2}^{-1}p_{1/2})_{2^+}d_{5/2}\rangle$	1.5
$\langle 0^+ s_{1/2} \mid V_c \mid (f_{5/2}^{-1}p_{1/2})_{2^+}d_{3/2}\rangle$	1.6
$\langle 0^+ d_{5/2} \mid V_c \mid (p_{3/2}^{-1}p_{1/2})_{2^+}s_{1/2}\rangle$	−1.2
$\langle 0^+ d_{5/2} \mid V_c \mid (p_{3/2}^{-1}p_{1/2})_{2^+}d_{3/2}\rangle$	−1.5
$\langle 0^+ d_{5/2} \mid V_c \mid (f_{5/2}^{-1}p_{1/2})_{2^+}s_{1/2}\rangle$	0.9
$\langle 0^+ d_{5/2} \mid V_c \mid (f_{5/2}^{-1}p_{1/2})_{2^+}d_{3/2}\rangle$	0.4
$\langle 0^+ d_{3/2} \mid V_c \mid (p_{3/2}^{-1}p_{1/2})_{2^+}s_{1/2}\rangle$	−0.5
$\langle 0^+ d_{3/2} \mid V_c \mid (p_{3/2}^{-1}p_{1/2})_{2^+}d_{5/2}\rangle$	−2.9
$\langle 0^+ d_{3/2} \mid V_c \mid (f_{5/2}^{-1}p_{1/2})_{2^+}s_{1/2}\rangle$	−1.0
$\langle 0^+ d_{3/2} \mid V_c \mid (f_{5/2}^{-1}p_{1/2})_{2^+}d_{5/2}\rangle$	−0.7
$\langle 0^+ d_{3/2} \mid V_c \mid (f_{5/2}^{-1}p_{1/2})_{2^+}d_{5/2}\rangle$	−0.7
$\langle 0^+ s_{1/2} \mid V_c \mid (2^+ \times d_{5/2})\rangle$	6.0
$\langle 0^+ s_{1/2} \mid V_c \mid (2^+ \times d_{3/2})\rangle$	4.8
$\langle 9^+ d_{5/2} \mid V_c \mid (2^+ \times s_{1/2})\rangle$	3.5
$\langle 0^+ d_{5/2} \mid V_c \mid (2^+ \times d_{3/2})\rangle$	2.4
$\langle 0^+ d_{3/2} \mid V_c \mid (2^+ \times s_{1/2})\rangle$	−3.4
$\langle 0^+ d_{3/2} \mid V_c \mid (2^+ \times d_{5/2})\rangle$	−3.0

We also consider the case of particle–vibration coupling. The matrix element to the particle–core state is proportional to the square root of the $B(E\lambda)$, where λ is the multipolarity of the collective core state. Table 5.2b contains the values of E_d^{ik} for Sr^{89} with $\lambda = 2$. The values are somewhat larger than for the two-particle one-hole case but are still small.

We conclude that correlations of this type make only very small corrections to the displacement energies. However, we have not considered the contribution of the isospin-violating nuclear force to E_d^{ik}. Although this force is as weak as the Coulomb force, it has a short range. Its nondiagonal matrix elements might be larger than the nondiagonal Coulomb matrix elements.

5.4 Other Isospin Violating Parts of the Hamiltonian

In this section we consider all the smaller isospin-violating terms of the Hamiltonian. Since these terms are small, it is sufficiently accurate to calculate their contributions to the displacement energy assuming pure isospin and neglecting correlations. In evaluating the displacement energy, we therefore only need to compute the double commutator term E_d in Eq. (5.6).

5.41 Electromagnetic Spin–Orbit Effects

We first consider the isospin-violating term arising from the electromagnetic spin–orbit interaction derived in Sec. 3. The commutator $V^{(-)}{}_{\text{SPIN ORBIT}}$ is a single-particle operator. For any single-particle operator K, the commutator with T_- is of the form,

$$K^{(-)} = [K, T_-] = \sum_i K_i t_-{}^i. \quad (5.73)$$

In second-quantized form we have

$$K^{(-)} = \sum_{\alpha,\beta} \langle \alpha \mid K \mid \beta\rangle a_\alpha{}^\dagger b_\beta. \quad (5.74)$$

Then we have

$$[T_+, [K, T_-]] = \sum_{\alpha,\beta} (b_\alpha{}^\dagger b_\beta - a_\alpha{}^\dagger a_\beta)\langle \alpha \mid K \mid \beta\rangle, \quad (5.75)$$

so that

$$E_d{}^K = \mathrm{N}^{-1}\langle \pi \mid [T_+, [K, T_-]] \mid \pi\rangle = \mathrm{N}^{-1}\sum_{\alpha\beta} (\rho_{\alpha\beta}{}^n - \rho_{\alpha\beta}{}^p)\langle \alpha \mid K \mid \beta\rangle.$$

In the approximation (5.17) where the excess neutron density is given in terms of the wave functions of the excess neutrons, we have

$$E_d{}^K = \mathrm{N}^{-1}\sum_{\alpha=Z+1}^{N} \langle \alpha \mid K \mid \alpha\rangle. \quad (5.76)$$

Here the summation is over the excess neutron states.

For the spin–orbit interaction, we have, from Eq. (3.20), (recall $\tau_- = 2t_-$),

$$K_j = (e\hbar/2M^2c^2)(\mu_p - \mu_n - \tfrac{1}{2})(1/r_j)(dV_c/dr_j)\boldsymbol{\sigma}_j \cdot \mathbf{l}_j. \quad (5.77)$$

Thus we obtain, with $N=2T$,

$$E_d^{SO}=\frac{(\mu_p-\mu_n-\frac{1}{2})}{2T}\frac{\hbar}{2M^2c^2}$$
$$\times\sum_{\alpha=Z+1}^{N}\langle\alpha\,|\,r^{-1}\frac{dV_c}{dr}\,|\,\alpha\rangle\langle j_\alpha\,|\,\boldsymbol{\sigma}\cdot\mathbf{l}\,|\,j_\alpha\rangle \quad (5.78)$$

where

$$\langle j_\alpha\,|\,\boldsymbol{\sigma}\cdot\mathbf{l}\,|\,j_\alpha\rangle=\hbar\begin{cases}l_\alpha & \text{for } j_\alpha=l_\alpha+\frac{1}{2}\\ -l_\alpha-1 & \text{for } j_\alpha=l_\alpha-\frac{1}{2}\end{cases}$$

The magnitude of E_d^{SO} is readily estimated by using for $V_c(r)$ the Coulomb potential of a sphere with radius R_c. In this case $(1/r)[dV(r)/dr]$ is a constant inside the nucleus, and since the nuclear wave functions vanish rapidly outside, a reasonable approximation is,

$$\langle\alpha\,|\,r^{-1}(dV_c/dr)\,|\,\alpha\rangle\simeq-Ze^2/R^3. \quad (5.79)$$

Then

$$E_d^{SO}=-(2T)^{-1}\frac{Ze^2}{R}\frac{(0.06)}{A^{2/3}}\sum_{\alpha=Z+1}^{N}\langle j_\alpha\,|\,\boldsymbol{\sigma}\cdot\mathbf{l}\,|\,j_\alpha\rangle\hbar^{-1}, \quad (5.80)$$

where the sum is again over the excess neutrons. The excess neutrons often occupy both spin–orbit states ($j=l\pm\frac{1}{2}$), so that the different matrix elements in Eq. (5.80) will substantially cancel. Even if the cancellation does not occur, the quantity E_d^{SO} is small, of the order of a few tens of keV.

Since the electromagnetic spin–orbit correction depends on the j and l value of the particular state it may produce considerable relative shifts in the isobaric analog spectrum as compared with the parent spectrum (see Sec. 5.7) [At69; Sc69a].

5.42 *The Proton–Neutron Mass Difference*

The proton–neutron mass difference also gives rise to a single-particle term, $V_{KIN}^{(-)}=[H_{KIN}, T_-]$, of the form of Eq. (5.73) with $K_i=(\Delta M/M)(p_i^2/2M)$. Using Eq. (5.76), we obtain the mass difference correction to the displacement energy, which is thus proportional to the average kinetic energy of the excess neutrons. The kinetic energy of a nucleon near the Fermi surface is essentially equal to the Fermi energy. Since this kinetic energy depends weakly on the mass number and the particular state of the nucleon, the mass difference correction is given by

$$E_d^{KIN}\simeq(\Delta M/M)\epsilon_F\simeq 40\text{–}50\text{ keV}. \quad (5.81)$$

5.43 *The Charge-Dependent and Charge-Asymmetric Nuclear Force*

In this section we discuss the contribution of the charge-dependent nuclear force to the displacement energies. Eq. (3.26) when written in the second quantization formalism becomes

$$V_{CD}^{(-)}=\tfrac{1}{2}\sum_{\alpha\beta\gamma\delta}\langle\alpha\beta\,|\,v^{CD}\,|\,\delta\gamma\rangle_A$$
$$\times(a_\alpha^\dagger a_\beta^\dagger a_\gamma b_\delta-b_\alpha^\dagger a_\beta^\dagger b_\gamma b_\delta). \quad (5.82a)$$

Similarly, we have

$$V_{CA}^{(-)}=-\tfrac{1}{2}\sum_{\alpha\beta\gamma\delta}\langle\alpha\beta\,|\,v^{CA}\,|\,\delta\gamma\rangle_A$$
$$\times(a_\alpha^\dagger a_\beta^\dagger b_\gamma a_\delta+b_\alpha^\dagger a_\beta^\dagger b_\gamma b_\delta). \quad (5.82b)$$

Also,

$$[T_+, V_{CD}^{(-)}]=\tfrac{1}{2}\sum_{\alpha\beta\gamma\delta}\langle\alpha\beta\,|\,v^{CD}\,|\,\delta\gamma\rangle_A$$
$$\times(4b_\alpha^\dagger a_\beta^\dagger a_\gamma b_s-a_\alpha^\dagger a_\beta^\dagger a_\gamma a_\delta-b_\alpha^\dagger b_\beta^\dagger b_\gamma b_\delta), \quad (5.83a)$$

$$[T_+, V_{CA}^{(-)}]=-\tfrac{1}{2}\sum_{\alpha\beta\gamma\delta}\langle\alpha\beta\,|\,v^{CA}\,|\,\delta\gamma\rangle_A$$
$$\times(b_\alpha^\dagger b_\beta^\dagger b_\gamma b_\delta-a_\alpha^\dagger a_\beta^\dagger a_\gamma a_\delta). \quad (5.83b)$$

We now calculate the expectation value of the double commutator, Eq. (5.6), assuming that the short-range correlation function in the parent state vanishes. We obtain

$$E_d^{CD}=-(2T)^{-1}\sum_{\alpha\beta\gamma\delta}\langle\alpha\beta\,|\,v^{CD}\,|\,\delta\gamma\rangle_A$$
$$\times(\rho_{\beta\gamma}{}^n-\rho_{\beta\gamma}{}^p)(\rho_{\alpha\delta}{}^n-\rho_{\alpha\delta}{}^p). \quad (5.84a)$$

$$E_d^{CA}=-(2T)^{-1}\sum_{\alpha\beta\gamma\delta}\langle\alpha\beta\,|\,v^{CA}\,|\,\delta\gamma\rangle_A$$
$$\times(\rho_{\beta\gamma}{}^n-\rho_{\beta\gamma}{}^p)(\rho_{\alpha\delta}{}^n+\rho_{\alpha\delta}{}^p) \quad (5.84b)$$

Again we may consider the approximation where [Eq. (5.17–5.19)] the parent state is a single Slater determinant, such that the proton orbits can be expanded in the neutron orbits. Then we find

$$E_d^{CD}=-(2T)^{-1}\sum_{\mu\nu}\langle\mu\nu\,|\,v^{CD}\,|\,\mu\nu\rangle_A \quad (5.85a)$$

$$E_d^{CA}=-(2T)^{-1}\sum_{\mu\lambda}\langle\mu\lambda\,|\,v^{CA}\,|\,\mu\lambda\rangle_A, \quad (5.85b)$$

where μ and ν run over the *excess* neutron states, and λ runs over *all* nucleon states. Formula (5.85a) represents the difference in the average $T=1$ interaction between a proton and a neutron occupying each of the $N-Z$ excess states with the remaining $N-Z-1$ neutrons. An analog state is a superposition of states where each of the excess neutrons have been converted into protons in the same orbital state. Since the p–n force is more attractive than the n–n force, Eq. (3.27), the forces v^{CD} lead to a *lowering* of the energy difference between the analog state and its parent. It is believed that v^{CA} has an effect in the opposite direction [He69a].

As before we may include short-range correlations and the Pauli effect by making the short-range approximation in evaluating the parent-state expectation value of the double commutator, Eq. (5.83). In this approximation, and using a local charge-dependent force, we

have

$$E_d^{\mathrm{CD}} = -(2T)^{-1}\int[\rho^n(\mathbf{x})-\rho^p(\mathbf{x})]^2\, d\mathbf{x} \sum_{S=0,1} \tfrac{1}{4}(2S+1) \times \int v_S^{\mathrm{CD}}(\mathbf{s})[1+(-1)^S 2g^P(s)][1+g^{CS}(\mathbf{s})]\, d\mathbf{s} \tag{5.86a}$$

$$E_d^{\mathrm{CA}} = -(2T)^{-1}\int\{[\rho^n(\mathbf{x})]^2-[\rho^p(\mathbf{x})]^2\}\, d\mathbf{x} \sum_{S=0,1} \tfrac{1}{4}(2S+1) \times \int v_S^{\mathrm{CA}}(\mathbf{s})[1+(-1)^S]g^P(\mathbf{s})[1+g^{CS}(\mathbf{s})]\, d\mathbf{s}, \tag{5.86b}$$

where we have included the possibility of spin dependence in v^{CD} and v^{CA} as well as in the average correlation functions. These are different from one another in that the first is an average correlation among the excess neutrons and all the nucleons. We recall that in the Coulomb case, Eq. (5.33), the correlation was between excess neutrons and protons. One can obtain an approximate linear relation among these three average correlations.

We can crudely estimate E_d^{CD} and E_d^{CA} using (5.85) or (5.86) by noticing that they can be expressed in terms of average fields associated with the excess neutrons, or all of the nucleons, arising from v^{CD} and v^{CA}. In the case of v^{CD} we scale to an average arising from all the nucleons by introducing the factor $(2T-1)/A$. Thus we have

$$E_d^{\mathrm{CD}} \simeq -[(2T-1)/A]\langle V^{\mathrm{CD}}\rangle \tag{5.87a}$$

$$E_d^{\mathrm{CA}} \simeq -\langle V^{\mathrm{CA}}\rangle \tag{5.87b}$$

We may relate V^{CD} and V^{CA} to the quantity $V^{T=1}$ which is the average field due to the $T=1$ nucleon–nucleon interaction (~ -25 MeV). Then we find

$$E_d^{\mathrm{CD}} \simeq [(2T-1)/A]\langle V^{T=1}\rangle \times (0.02) \simeq -500[(2T-1)/A]\,\mathrm{keV}, \tag{5.88a}$$

$$E_d^{\mathrm{CA}} \simeq -\langle V^{T=1}\rangle \times .01 \simeq 250\ \mathrm{keV}, \tag{5.88b}$$

where Eq. (3.27) has been used. This estimate of E_d^{CD} is crude, as v^{CD} is strongly state dependent, and the approximation of Eq. (3.27) refers only to low-energy (S-state) properties of the interaction. Furthermore the treatment of the excess neutrons as giving rise to an average field due to the charge-dependent interaction is inappropriate as such a field would also be strongly state dependent. In particular, the excess neutrons usually do not have saturated spin states. The spin-dependent part of the density matrix becomes relatively more important for the exchange matrix elements which are large in this case, as v^{CD} is of short range. This situation is unlike the case of the long-range, spin-independent Coulomb interaction where a similar analysis was successful. Actually, our estimate of E_d^{CA} is more precise in this respect because we *do* average on all of the nucleons.

For these reasons we find it necessary to make a more precise evaluation of the contribution of the charge-dependent forces. Some of the matrix elements appearing in Eq. (5.85) were evaluated in the j–j representation using harmonic oscillator wave functions with the Rouben force [Ro69a,b]. The ratios of the diagonal matrix elements of v^{CD} to the corresponding matrix elements of v_{pp} are found in the range of 2%–15% and the absolute values are of the order of 10–100 keV depending on the particular state. The strong spin dependence leads to positive as well as negative matrix elements.

A detailed calculation of the charge-dependent effect has been carried through by DiToro, Nunberg, and Riihimaki [Di70]. They have considered two versions of a nonlocal soft-core potential [Ro69a,b] and have calculated E_d^{CD} from Eq. (5.85) as well as the term of first order in *both* v^{CD} and v^{NUCL}. The latter term is a correlation correction to the calculation of E_d^{CD}. Their perturbation procedure for g^C appears to be convergent for one version of the soft-core potential in which the short-range nonlocal core is taken as charge independent. The results obtained for this potential are shown in Table 5.3. These results give the order of magnitude of the charge-dependent effects; however, other nucleon–nucleon potentials should be investigated so that the dependence of these effects on the shape of the potential can be determined.

Unlike the finite-size effect or the mass correction, which are constant over the periodic table, E_d^{CD} depends on the excess neutron orbits. Furthermore, since E_d^{CD} depends quadratically on the excess neutron density (Eq. 5.86), and is divided by the first power of $2T$, we expect the charge-dependent force to give a major contribution to the isotopic dependence of the displacement energy. Because of its strong l and spin dependence this force also strongly influences the state dependence of the displacement energy. The relative shifts of the different orbits due to v^{CD} are of the order of 5–10 keV.

Additional studies using different phenomenological potentials are necessary to evaluate the contributions of the charge dependent nuclear forces to the displacement energies.

TABLE 5.3 Contribution to the displacement energy due to a charge-dependent force [Di70]. The first row corresponds to Eq. (5.85), and the second row represents the correction due to nuclear correlations as calculated in perturbation theory.

	Ca^{48} (MeV)	Sr^{88} (MeV)
E_d^{CD} no correlations	−0.093	−0.095
δE_d^{CD} correlation effect	−0.050	−0.049
Total	−0.143	−0.144

TABLE 5.4 Summary of formulas for the displacement energy.

Term	Formula or designation	Numerical estimate
Direct Coulomb	$E_d^{\mathrm{COUL}}=(e^2/2T)\int d\mathbf{x}d\mathbf{y}\{[\rho^n(\mathbf{x})-\rho^p(\mathbf{x})]/\lvert\mathbf{x}-\mathbf{y}\rvert\}\rho^p(\mathbf{y})$	See Sec. 5.6
Exchange	$E_d^{\mathrm{EXCH}}=-(27/16)(e^2/R)[Z/(k_F{}^pR)^2]\times[(\lambda^2+\lambda+2)/(\lambda^2+\lambda+1)]$, $\lambda=(N/Z)^{1/3}$	$-900Z/A$ keV
Finite size	$E_d^F=-(Ze^2/R)(r_p/R)^2[\frac{1}{2}+\frac{1}{6}(r_pk_F{}^p)^2]$	~-100 keV
Vacuum polarization	$E_d^{\mathrm{POL}}=0.006E_d^{\mathrm{COUL}}$	$8.5Z/A^{1/3}$ keV
Short-range correlations	$E_d^C\simeq\pm(3/4\pi)(e^2/r_0)(Z/A)(L/r_0)^2$ (see Table 5.1)	$\sim 60Z/A$ keV (KKR potential)
Isospin violation (partial)	$\Delta E_d=-\epsilon^2[(T+1)/T]\delta E_1$	$-(Z^{8/3}/A^{1/3})(N-Z)^{-1}\times(0.19\text{–}1.5\times10^{-3}Z)$ keV
Spin–Orbit	$E_d^{SO}=-(2T)^{-1}(Ze^2/R)[(0.06)/A^{2/3}]\sum_{\alpha=Z+1}^{N}\times[(j_\alpha\mid\boldsymbol{\sigma}\cdot\mathbf{l}\mid j_\alpha)/\hbar]$	(Variable)
Neutron-proton mass difference	$E_d^{\mathrm{KIN}}\simeq(\Delta M/M)\epsilon_F$	$\sim$40–50 keV
Charge-dependent and charge-asymmetric nuclear force	E_d^{CD}[Di70] (see Table 5.3)	$-500[(2T-1)/A)]$keV
	E_d^{CA}	$\lesssim 250$ keV

5.5 Summary of Formulas

In Table 5.4 we have summarized the various contributions to the displacement energy as discussed in the previous sections. In most cases we have given simple approximations for each term obtained from Fermi gas estimates or from more detailed calculations. The effects of long-range correlations (configuration mixing) are not included in the table as these small corrections depend on the detailed features of the wave function (see Sec. 5.3). The dominant term is the direct Coulomb term which is sensitive to the model chosen for the excess neutron distribution. The simplest model for this distribution is considered in the next section.

5.6 Models for the Excess Neutron Distribution

As we have noted previously, information concerning the proton density is available from electron scattering experiments and from μ-mesic atoms. This is not the case for the excess neutron distribution and various models for this distribution may be considered.

Simple shell-model densities have been considered [Sc69a; Au69a]. It is possible to parameterize $\rho^p(\mathbf{x})-\rho^n(\mathbf{x})$ by single-particle wave functions generated by a Saxon–Woods potential well with a standard diffuseness

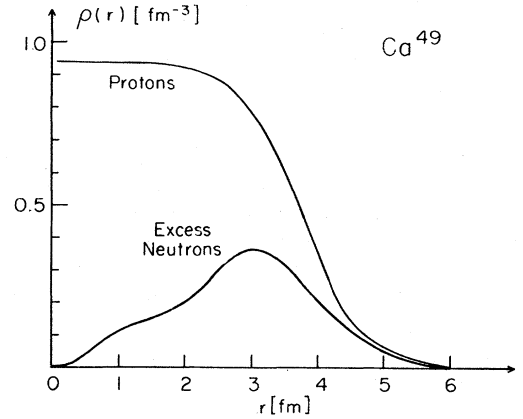

FIG. 5.8. Empirical charge distribution for calcium, and matter distribution of the excess neutrons as calculated with Saxon–Woods wave functions. (See text).

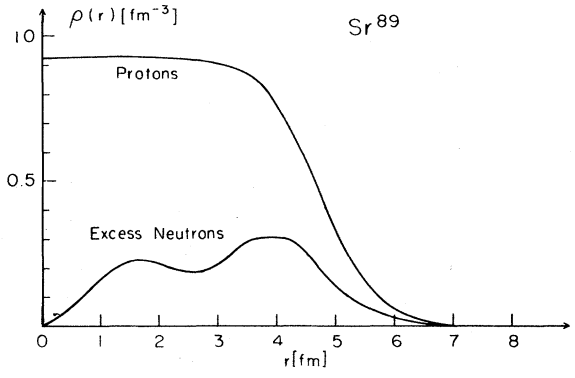

FIG. 5.9. Empirical charge distribution of strontium and matter density of the excess neutrons as calculated with Saxon–Woods wave functions (See text).

TABLE 5.5. The state dependence of the energy difference between isobaric analog resonance and parent states. The example chosen is Sr^{89}. All energies in keV are taken relative to the $d_{5/2}$ resonance at 5.00 MeV ($S=0.9$). The experimental values are taken from [Co68]. The continuum and compound shifts, $\delta\Delta^{COMT}$ and $\delta\Delta^{CONP}$, are discussed in Sec. 7.

Resonance	Experimental spectroscopic factors S	δE_d^{COUL}	δE_d^{CD}	δE_d^{SO}	δE_d^{KIN}	$\delta\Delta^{CONT}$	$\delta\Delta_A^{COMP}$	δE_d total Calc	δE_d total Expt
$s_{1/2}$(6 MeV)	0.90	+12	−4	−4	+0.3	28.	−2.	30	37
$d_{3/2}$(7 MeV)	0.45	+7	−12	−10	0.0	12.	−0.3	−3	16
$g_{7/2}$(7.7 MeV)	0.74	+1	···	−14	−0.3	−18.	+0.5	≤ -31	−34

parameter. The well depth may be adjusted in order to reproduce the experimental binding energies of the excess neutrons, and the radius of the well may be varied until calculated and experimental resonance energies agree. Within the uncertainties in the treatment of the charge-dependent and charge-asymmetric interactions, short-range correlations, compound and continuum shifts (see Sec. 7), and isospin impurities, this simple model indicates that the radii of the neutron and proton distributions are rather similar [Sc69a; Au69a]. In Figs. (5.8)–(5.11) are shown the distribions for protons and excess neutrons for various nuclei. The proton distributions are empirical (of Fermi type) with parameters extrapolated from [El67; Ho67a] and corrected for the proton finite size. The excess neutron distributions is calculated from the Saxon–Woods potential whose radius has been adjusted to fit the displacement energy with all its corrections.

It is of interest to consider the effects of special cases of configuration mixing on the determination of the excess neutron density. A step in this direction has been taken by Auerbach *et al.* [Au69b]. These authors suggest that the $T=1$ polarization of the core by the excess neutrons may lead to a sizeable effect. More studies of this type will be useful in helping to determine the size of the neutron distribution from information on displacement energies (see also Sec. 5.31).

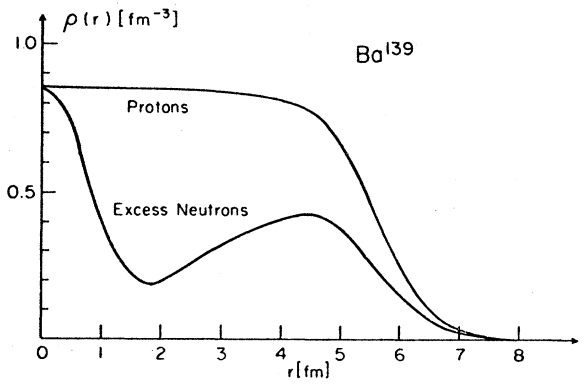

FIG. 5.10. Empirical charge distribution for barium, and matter density of the excess neutrons as calculated with Saxon–Woods wave functions. (See text).

5.7 State Dependence of the Displacement Energy

In most nuclei, one not only observes the isobaric analog resonance which corresponds to the ground state of the parent nucleus, but a whole sequence of resonances which can be related to the sequence of excited parent states. If the position of the resonances is measured very carefully, one finds that the energy differences between two resonances $E_R(A_1)-E_R(A_2)$ does not exactly coincide with the energy differences of the corresponding parent states $E_{\pi_1}-E_{\pi_2}$. For medium and heavy nuclei, the difference

$$\delta E_d=[E_R(A_1)-E_R(A_2)]-[E_{\pi_1}-E_{\pi_2}] \quad (5.89)$$

is of the order of a few tens of keV or less.

A priori, very little can be said about how the difference, Eq. (5.89), comes about and which effects dominate in the evaluation of the state dependence of the displacement energy. Therefore, a numerical study of the effects which determine the displacement energy has been made for several levels in ^{89}Sr. The results are shown in Table 5.5. While the Coulomb displacement energy, E_d^{COUL}, dominates the absolute values of the displacement energy, it plays a minor role in the state dependence. This result is probably a feature of the particular example, since all orbits, the $2d_{5/2}$, $3s_{1/2}$, $2d_{3/2}$, and the $1g_{7/2}$ belong to the same major shell and therefore are expected to have similar mean-square radii. According to Table 5.5, the continuum shift and the charge dependence of the nuclear forces contribute most to the state dependence of the displacement energy. While the continuum shift may be calculated rather accurately, the values for the charge-dependent forces have been calculated from a phenomenological potential [Ro69a,b]. These values should be regarded with caution since they depend strongly on the spin and orbital angular momentum dependence of this force. In the case of Sr^{89} the effects of state dependence are small and it is unlikely that we can extract useful information, such as the neutron distribution or charge radii of excited states, from the study of the state

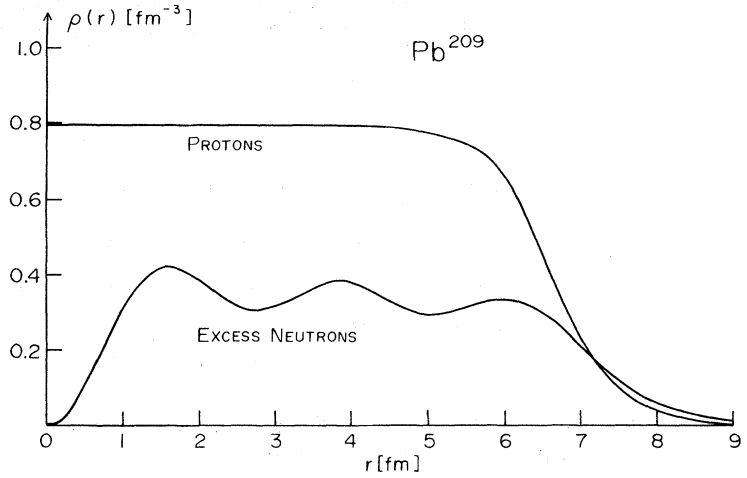

FIG. 5.11. Empirical charge distribution for lead, and the excess neutron matter density calculated with Saxon–Woods wave functions. (See text).

dependence. There are, however, cases where the state dependent effects are larger and their study may help in deducing certain nuclear structure information. As a typical example we may note the case of Ca^{41} and its analog Sc^{41}. The shift of the $p_{3/2}$ orbit relative to the $f_{7/2}$ indicates a large Thomas–Ehrman (or continuum) shift.

Another differential effect that might be useful in providing nuclear structure information or information concerning the importance of various isospin-breaking terms in the Hamiltonian is the *isotope shift* of the displacement energies; i.e., the change in the displacement energy resulting from the addition of neutrons to a nucleus with fixed Z.

Most of the terms collected in Table 5.4 show weak isotopic dependence. This also holds for the main term, E_d^{COUL}, which behaves essentially like $A^{-1/3}$. Some deviations of the isotope shift from the $A^{-1/3}$ behavior have been attributed to the dependence of the proton potential on the neutron excess [Pe66].

The isotope shift is not a subject of our study, and we do not intend to review this topic [Sh67]. It is worth pointing out, however, that in Table 5.4 there exists a term which has strong functional dependence on the number of neutrons, namely the term coming from charge-dependent nuclear force is proportional to $2T=N-Z$. It is possible therefore that in certain cases the main contributor to the isotope shift of the displacement energy (or its deviation from the $A^{-1/3}$ law) is the charge-dependent nuclear force. In order to make definite conclusions about the shifts caused by the charge-dependent nuclear force, it is necessary to obtain more information about this force. Because of its complicated nature, the contributions to the isotope shift may vary in magnitude and size depending on the particular regions of the periodic table. But there does remain the possibility that from the isotope shift of the displacement energy we may learn more about the matrix elements of the charge-dependent part of the nuclear force.

5.8 Summary

In this section we have discussed the calculation of the displacement energy, E_d^{TOT}, defined in Eq. (5.2). If supplemented by the shifts due to the analog-state coupling to the compound and continuum spaces, see Eq. (5.1), the knowledge of the displacement energy enables us to calculate the position of the analog resonance. In Sec. 5.1 the displacement energy was written as the sum of two terms, $E_d+\Delta E_d$, the latter vanishing if isospin is conserved. The leading term, E_d, is discussed in Sec. 5.1 and it is shown that the value of this term is sensitive to the distribution of protons (presumably known) and neutrons in the nucleus. The effects of short-range correlations, vacuum polarization, proton finite size, etc. are discussed and numerical estimates are given.

Section 5.2 contains a discussion of the term ΔE_d, resulting in the numerical estimate of Eq. (5.63). This section also contains an estimate of the *total* contribution to the displacement energy from the isospin impurity, $E^{T\text{-}IMP}$. [See Eqs. (5.53) and (5.56)].

The effects of configuration mixing (long-range correlations) are discussed in Sec. 5.3, and some estimates are given. Section 5.4 contains a discussion of the contribution to the displacement energy due to isospin-violating parts of the Hamiltonian other than the Coulomb interaction.

Most of our results are summarized in the Tables 5.1–5.5.

6. ESCAPE AMPLITUDES AND SPECTROSCOPIC FACTORS

In this section we discuss the calculation of the escape amplitudes defined in Sec. 2.32 and indicate how

the experimental determination of these amplitudes yields spectroscopic information.

6.1 Direct and Compound Escape Amplitudes

We recall that we had defined the escape amplitude Eq. (2.33) for the channel c as,[21]

$$\gamma_{A,c} = \exp(-i\delta_c)\langle\tilde{\Phi}_c^{(-)} \mid \mathrm{H}[E+\tfrac{1}{2}(iI)] \mid A\rangle = \exp(-i\delta_c)\langle A \mid \mathrm{H}[E+\tfrac{1}{2}(iI)] \mid \Phi_c^{(+)}\rangle, \quad (6.1)$$

where the effective interaction was given by

$$\mathrm{H}[E+\tfrac{1}{2}(iI)] = H + H\{q/[E-H_{qq}+\tfrac{1}{2}(iI)]\}H. \quad (6.2)$$

It is useful to discuss the contributions of the two terms of the effective interaction separately. We define a *direct escape amplitude*

$$\gamma_{A,c}^{\mathrm{DIR}} = \exp(-i\delta_c)\langle\tilde{\Phi}_c^{(-)} \mid H \mid A\rangle = \exp(-i\delta_c)\langle A \mid H \mid \Phi_c^{(+)}\rangle. \quad (6.3)$$

This amplitude describes the emission of a particle from the analog state directly into the continuum. The amplitude which describes the transition of a particle to the continuum via the q space is called the *compound escape amplitude*,

$$\gamma_{A,c}^{\mathrm{COMP}} = \exp(-i\delta_c)\langle\tilde{\Phi}_c^{(-)} \mid H \times\{q/[E-H_{qq}+\tfrac{1}{2}(iI)]\}H \mid A\rangle. \quad (6.4)$$

Thus we have

$$\gamma_{A,c} = \gamma_{A,c}^{\mathrm{DIR}} + \gamma_{A,c}^{\mathrm{COMP}}. \quad (6.5)$$

In most cases of interest we find $\gamma_{A,c}^{\mathrm{DIR}} \gg \gamma_{A,c}^{\mathrm{COMP}}$.

6.11 The Direct Escape Amplitude

The direct escape amplitude may be written in terms of a *direct analog state form factor*,

$$V_c^A(r) = \langle r, c \mid [H, T_-] \mid \pi\rangle/\mathrm{N}^{1/2}, \quad (6.6)$$

where we have again expressed the analog state in terms of its parent, $\mid \pi\rangle$. We find using Eqs. (2.13) and (2.29), that

$$\gamma_{A,c}^{\mathrm{DIR}} = \exp(-\eta_c)\sum_{c'}\int_0^\infty \varphi_{cc'}^{(0)}(r)\, V_{c'}^{A}(r) r^2\, dr, \quad (6.7)$$

or if we neglect direct interactions, the last expression takes the simpler form,

$$\gamma_{A,c}^{\mathrm{DIR}} = \exp(-\eta_c)\int_0^\infty \varphi_c^{(0)}(r)\, V_c^A(r) r^2\, dr. \quad (6.8)$$

[21] It should be kept in mind that c may refer either to an elastic or inelastic channel, and that $\gamma_{A,c}$ depends upon the energy. The main energy dependence is contained in the continuum state vector, $\langle\tilde{\Phi}_c^{(-)}\mid$, or $\mid\Phi_c^{(+)}\rangle$.

6.12 The Compound Escape Amplitude

The compound escape amplitude was defined in Eq. (6.4). We shall find that the compound amplitude is usually only a few percent of the direct amplitude (see Sec. 6.6).

If we introduce the *form factor for the compound state*,

$$V_c^q(r) = \langle r, c \mid H \mid q\rangle, \quad (6.9a)$$

and the *escape amplitude for the compound state*

$$\gamma_{q,c} = \exp(-\eta_c)\sum_{c'}\int_0^\infty \varphi_{cc'}^{(0)}(r)\, V_{c'}^{q}(r) r^2\, dr, \quad (6.9b)$$

and the matrix element describing the compound-analog coupling,

$$V_A^q = \langle q \mid H \mid A\rangle = \mathrm{N}^{-1/2}\{\langle q \mid [H, T_-] \mid \pi\rangle\}, \quad (6.10)$$

we may write

$$\gamma_{A,c}^{\mathrm{COMP}} = \sum_q \gamma_{q,c} V_A^q/[E-E_q+\tfrac{1}{2}(iI)]. \quad (6.11)$$

We have seen a statistical estimate for $\mid\gamma^{\mathrm{COMP}}\mid^2$ following Eq. (2.54).

As before, $\mid q\rangle$ are the continuum and discrete eigenfunctions of H_{qq}. In Eq. (6.10) we have indicated that the coupling of the analog state to the q space is expressible in terms of the isospin-violating parts of H. This reduction is not possible for the compound state form factors $V_c^q(r)$, and the calculation of the compound state escape amplitudes require a specification of the strong-interaction part of H.

Finally we may note the relation between the form factors introduced in this section and the analog state form factor of Eq. (2.35)

$$\mathrm{V}_c^A(r) = V_c^A(r) + \sum_q V_c^q(r) V_A^q/[E-E_q+\tfrac{1}{2}(iI)]. \quad (6.12)$$

We will return to a further discussion of the compound escape amplitude in Sec. 6.6.

6.2 The Direct Escape Amplitude, Spectroscopic Factors, and the Single-Particle Escape Amplitude

We have seen that the calculation of the direct escape amplitude involves the matrix elements of the isospin-violating parts of H through the commutator $[H, T_-]$ connecting the parent $\mid\pi\rangle$ to the continuum. This amplitude has its main contribution from the two-body Coulomb interaction contained in H, i.e.,

$$V_c^{(-)} = [H, T_-] = \tfrac{1}{2}\sum_{i\neq j}(e^2/r_{ij})[\tfrac{1}{2}\tau_-{}^i\tfrac{1}{2}(1-\tau_z{}^j)+\tfrac{1}{2}(1-\tau_z{}^i)\tfrac{1}{2}\tau_-{}^j]. \quad (6.13)$$

As noted previously, this expression is a charge-changing two-body interaction involving the transformation

of a neutron–proton pair into a proton–proton pair.[22] It is known that matrix elements of a long-range force such as the Coulomb force are small if two particles change their orbits. Given a particular continuum channel, the main contribution to $\gamma_{A,c}{}^{\mathrm{DIR}}$ is expected to arise from that portion of the parent state $|\pi\rangle$ that is simply related to that continuum channel. In this section we will show how we may use this aspect of the escape amplitude to obtain information about the structure of the parent state $|\pi\rangle$.

Using Eqs. (6.6) and (6.7) we may write the direct escape amplitude as

$$\gamma_{A,c}{}^{\mathrm{DIR}}=\frac{\exp(-\eta_c)}{\mathrm{N}^{1/2}}\sum_{c'}\int_0^\infty \varphi_{cc'}{}^{(0)}(r)\times\langle r,c'\,|\,[H,T_-]\,|\,\pi\rangle r^2\,dr. \quad (6.14)$$

Now we note that, in general, the commutator $[H,T_-]$ will contain a neutron destruction operator, and therefore this commutator may be put in the form

$$[H,T_-]=\sum_\alpha \mathrm{O}_\alpha b_\alpha. \quad (6.15)$$

For example, in the case of the Coulomb interaction we have

$$V_c{}^{(-)}=[V_c,T_-]=\tfrac{1}{2}\sum_{\alpha\rho\gamma\delta}\langle\gamma\delta\,|\,v_c\,|\,\alpha\rho\rangle_A a_\gamma{}^\dagger a_\delta{}^\dagger a_\rho b_\alpha \quad (6.16)$$

so that, in this case,

$$\mathrm{O}_\alpha=\tfrac{1}{2}\sum_{\gamma\delta\rho}\langle\gamma\delta\,|\,v_c\,|\,\alpha\rho\rangle_A a_\gamma{}^\dagger a_\delta{}^\dagger a_\rho. \quad (6.17)$$

It is now useful to make a decomposition of the state formed when destroying a neutron in the parent, $|\pi\rangle$. Thus we find

$$b_\alpha\,|\,\pi\rangle=\sum_\Lambda \varphi_{\Lambda,\alpha}{}^\pi\,|\,\Lambda\rangle, \quad (6.18)$$

where Λ is the complete set of target states. Note that if α denotes definite single-particle orbital, n, ($n\equiv\{n,l,j,m\}$), we may write

$$\bar{b}_{nljm}\equiv(-1)^{j+m}b_{nlj-m} \quad (6.19)$$

$$\varphi_{\Lambda,n}{}^\pi=\langle\Lambda IM\,|\,b_{nljm}\,|\,\pi J\mathrm{M}\rangle=(-1)^{j-m}C_{\mathrm{M}-mM}{}^{JjI}[\langle\Lambda I\,||\,\bar{b}_{nlj}\,||\,\pi J\rangle/(2I+1)^{1/2}]. \quad (6.20)$$

We also note that [Bo69; p. 86],

$$\langle\Lambda I\,||\,\bar{b}_{nlj}\,||\,\pi J\rangle=(-1)^{I+j-J}\langle\pi J\,||\,b_{nlj}{}^\dagger\,||\,\Lambda I\rangle. \quad (6.21)$$

We may define a spectroscopic factor

$$S_{\Lambda,n}{}^\pi=|\,\langle\Lambda I\,||\,\bar{b}_{nlj}\,||\,\pi J\rangle\,|^2/(2J+1)=|\,\langle\pi J\,||\,b_{nlj}{}^\dagger\,||\,\Lambda I\rangle\,|^2/(2J+1) \quad (6.22)$$

for the orbit n.[23]

In the case that α refers to the position (and spin) coordinate we may also introduce a "spectroscopic" wave function

$$b(\mathbf{r})=\sum_\Lambda \varphi_\Lambda{}^\pi(\mathbf{r})\,|\,\Lambda\rangle, \quad (6.18)$$

which is independent of the choice of any particular set of single-particle orbitals. Clearly, we have

$$\varphi_\Lambda{}^\pi(\mathbf{r})=\langle\Lambda\,|\,b(\mathbf{r})\,|\,\pi\rangle. \quad (6.19)$$

It will also be useful to divide the set $|\Lambda\rangle$ into two groups of states, those used to form the channel states $|r,c\rangle$ and the rest. The former states have been denoted by $|\lambda\rangle$ (see Sec. 2.2). It is also advantageous to use a less abbreviated notation for the channel states, $|r,c\rangle$. We denote these $|r,c(\lambda)\rangle$ in this section, exhibiting the label of the target state in the channel [see Eq. (A1.7)]. We also write $\gamma_{A,c(\lambda)}$ for $\gamma_{A,c}$ and $\varphi_{c(\lambda),c'(\lambda')}{}^{(0)}(r)$ for $\varphi_{c,c'}{}^{(0)}(r)$, in case the extended notation is helpful. With these modifications of notation we have

$$\gamma_{A,c(\lambda)}{}^{\mathrm{DIR}}=\frac{\exp(-\eta_c)}{\mathrm{N}^{1/2}}\sum_{c'(\lambda'),\Lambda}\int_0^\infty \varphi_{c(\lambda),c'(\lambda')}{}^{(0)}(r)\times\sum_n\langle r,c'(\lambda')\,|\,\mathrm{O}_n\,|\,\Lambda\rangle\langle\Lambda\,|\,b_n\,|\,\pi\rangle r^2\,dr. \quad (6.23)$$

Upon inspection we see that the various terms of (6.23) fall into two main classes and two subclasses:

I. Single-Particle Amplitudes ($\Lambda=\lambda'$)

The condition ($\Lambda=\lambda'$) implies that the form factor $\langle r,c'(\lambda')\,|\,\mathrm{O}_n\,|\,\lambda'\rangle$ will be large since it is a diagonal matrix element in the target space. It includes a single-particle transition from state n to the continuum; hence, the name "single-particle" for this case. We can divide these amplitudes into two classes.

(A) Diagonal in the channel coupling ($\lambda'=\lambda$). This amplitude is finite in the absence of channel coupling. Amplitudes of this class yield contributions to $\gamma_{A,c(\lambda)}{}^{\mathrm{DIR}}$ proportional to the spectroscopic amplitudes $(S_{\lambda,n}{}^\pi)^{1/2}$.

(B) Nondiagonal terms in the channel coupling ($\lambda'\neq\lambda$). This amplitude is zero if channel coupling is neglected, and is generally expected to be small.

---

[22] The contribution to the commutator from the isospin-violating terms in the strong interactions will also change a neutron–proton pair into a proton–proton pair. However, this latter contribution will also change a neutron–neutron pair into a neutron–proton pair and will thus contribute to the *neutron* width of the analog state.

[23] If Λ refers to the elastic channel, Eq. (6.20) specifies the same parentage that one considers in stripping experiments. Thus, when we determine the elastic channel spectroscopic factors we may compare our results with spectroscopic factors obtained from analysis of stripping experiments. In addition, analysis of inelastic scattering proceeding through analog resonances provides us with spectroscopic information which is not obtainable from stripping experiments.

II. Rearrangement Amplitudes ($\Lambda \neq \lambda'$)

The condition $\Lambda \neq \lambda'$ requires that at least two particles change their quantum numbers. Amplitudes of this type will generally be much smaller than single-particle amplitudes. Again we divide these into two classes.

(A) Diagonal in the channel coupling ($\lambda' \neq \lambda$). This amplitude is finite in the absence of channel coupling.

(B) Non-diagonal in the channel coupling ($\lambda' \neq \lambda$). This amplitude is zero if channel coupling is neglected. Rearrangement amplitudes of this class will be particularly small if the channel coupling is weak. If $\Lambda = \lambda$, we have a rearrangement amplitude which is non-diagonal in the channel coupling but yields contributions to $\gamma_{A,c(\lambda)}{}^{\mathrm{DIR}}$ proportional to the spectroscopic amplitude $(S_{\lambda,n}{}^{\pi})^{1/2}$.

In general, single-particle amplitudes will be shown to be much larger than rearrangement amplitudes. However, for any given parent state, the relative importance of single-particle escape or rearrangement escape depends upon the magnitude of the spectroscopic factors. In general, amplitudes diagonal in channel coupling will be larger than those which are nondiagonal. However, in the case of deformed nuclei, rearrangement amplitudes and channel coupling effects may become large and should not be neglected.

In Fig. 6.1 we have schematically indicated amplitudes of various classes described above. Of these, the simplest process is depicted in Fig. (6.1a). In this case a neutron in orbital n escapes directly to the proton continuum, this escape being mediated by the *charge-changing* field $V_c{}^{(-)}$ averaged over the proton orbits of the parent. We will now concentrate on these diagonal single-particle escapes and define a *single-particle escape amplitude.* This amplitude is defined as the coefficient of $(S_{\lambda n}{}^{\pi})^{1/2}$ in the direct amplitude, Eq. (6.23), for the special case $\Lambda = \lambda' = \lambda$. When the parent state is composed of a neutron in the orbit n, coupled to a state $|\lambda\rangle$, so that,

$$b_n |\pi\rangle = |\lambda\rangle \tag{6.24}$$

and $S_{\lambda,n}{}^{\pi} = 1$ the single-particle escape amplitude is exact. Thus, we define

$$(\gamma_{n,c(\lambda)})_{\mathrm{sp}} = \frac{\exp(-\eta_c)}{\mathrm{N}^{1/2}} \int_0^{\infty} \varphi_{c(\lambda)}{}^{(0)}(r) \times \langle r, c(\lambda) | \mathrm{O}_n | \lambda \rangle r^2 \, dr. \tag{6.25}$$

We also introduce a *single-particle form factor*

$$V_{n,c(\lambda)}(r) = \langle r, c(\lambda) | \mathrm{O}_n | \lambda \rangle / \mathrm{N}^{1/2}, \tag{6.26}$$

and write

$$(\gamma_{n,c(\lambda)})_{\mathrm{sp}} = \exp(-\eta_c) \int_0^{\infty} \varphi_{c(\lambda)}{}^{(0)}(r) V_{n,c(\lambda)}(r) r^2 \, dr. \tag{6.27}$$

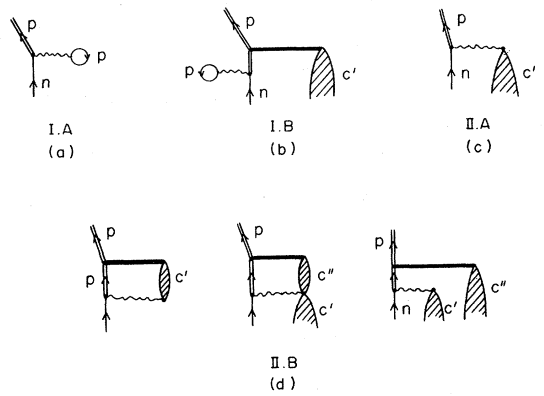

FIG. 6.1. Various escape amplitudes leading to the channel c. Double lines refer to continuum proton orbits; solid horizontal lines refer to direct-interaction coupling between channels and wavy lines to the charge-changing interaction $V_c{}^{(-)}$. The crossed "bubbles" indicate states of the target system other than that found in channel c.

This amplitude may be calculated for various simple models as discussed in the next section. In many cases, channel coupling amplitudes (Class IB), direct rearrangement amplitudes (Classes IIA and IIB), and the compound escape amplitude will be quite small, so that

$$\gamma_{A,c(\lambda)} = \gamma_{A,c(\lambda)}{}^{\mathrm{DIR}} + \gamma_{A,c(\lambda)}{}^{\mathrm{COMP}} \simeq \gamma_{A,c(\lambda)}{}^{\mathrm{DIR}} \simeq (S_{\lambda,n}{}^{\pi})^{1/2} (\gamma_{n,c(\lambda)})_{\mathrm{sp}}. \tag{6.28}$$

In this case a theoretical calculation of $(\gamma_{n,c(\lambda)})_{\mathrm{sp}}$ supplemented by an experimental measurement of $\gamma_{A,c(\lambda)}$ allows one to determine $S_{\lambda,n}{}^{\pi}$. This simple result clearly does not hold in more general cases. For example, if we continue to neglect rearrangement and compound amplitudes, but include direct channel coupling we have

$$\gamma_{A,c(\lambda)}{}^{\mathrm{DIR}} = \exp(-\eta_c) \sum_{c'(\lambda'),n} \int_0^{\infty} \varphi_{c(\lambda),c'(\lambda')}{}^{(0)}(r) \times V_{n,c'(\lambda')}(r) r^2 \, dr \langle \lambda' | b_n | \pi \rangle. \tag{6.29}$$

We will not discuss in detail any amplitudes involving channel coupling, i.e., only amplitudes of classes IA and IIA will be considered [(see Fig. (6.1a) and Fig. (6.1c)].

6.3 Calculation of the Single-Particle Escape Amplitude

In this section we are interested in calculating the single-particle escape amplitude $(\gamma_{n,c(\lambda)})_{\mathrm{sp}}$ defined in Eq. (6.25). This amplitude was given in Eq. (6.27) as an integral of the single-particle form factor $V_{n,c(\lambda)}(r)$ with the complex wave function $\varphi_{c(\lambda)}{}^{(0)}(r)$. As in the case of the Coulomb displacement energy, we will discuss the role of the various isospin-violating parts of H which contribute to this amplitude.

6.31 The Charge-Changing Coulomb Force $V_c^{(-)}$

The main contribution to $(\gamma_{n,c(\lambda)})_{sp}$ comes from the matrix elements of the charge-changing Coulomb force $V_c^{(-)}$ given in Eq. (6.16). We now consider the calculation of the single-particle form factor $V_{n,c(\lambda)}(r)$ [Eq. (6.26)] for this case. We have, using Eq. (6.17),

$$V_{n,c(\lambda)}(r)=N^{-1/2}\tfrac{1}{2}\sum_{\alpha\beta\gamma}\langle r, c(\lambda)|\, a_\alpha^\dagger a_\beta^\dagger a_\gamma\,|\lambda\rangle \times\langle\alpha\beta\,|\,v_c\,|\,n\gamma\rangle_A. \quad (6.30)$$

For simplicity we will assume that the state λ has zero angular momentum. Also, because of the fact that v_c is a long-range, spin-independent force, it is useful to work in configuration space, so that

$$V_{n,c(\lambda)}(r)=N^{-1/2}\tfrac{1}{2}\{\int\int d\mathbf{r}'\,d\mathbf{r}'' \times[\langle r, c(\lambda)|\, a^\dagger(\mathbf{r}')a^\dagger(\mathbf{r}'')a(\mathbf{r}'')|\,\lambda\rangle v_c(|\,\mathbf{r}'-\mathbf{r}''\,|)\varphi_n(\mathbf{r}') -\langle r, c(\lambda)|\, a^\dagger(\mathbf{r}')a^\dagger(\mathbf{r}'')a(\mathbf{r}')|\,\lambda\rangle v_c(|\,\mathbf{r}'-\mathbf{r}''\,|)\varphi_n(\mathbf{r}'')]\} \quad (6.31)$$

where $\varphi_n(r')$ is the neutron wave function for the orbit, n. Now we recall that the states $|\,r, c\rangle$ were related to the states $|\,r, c)$ by Eq. (A1.13) and further that the states $|\,r, c)$ are simply related [see Eq. (A1.2)] to the states[24]

$$|\,\mathbf{r},\lambda\rangle\equiv a^\dagger(\mathbf{r})|\,\lambda\rangle. \quad (6.32)$$

Thus we may discuss the form factor,

$$\tilde{V}_{n,\lambda}(\mathbf{r})=N^{-1/2}\tfrac{1}{2}\int\int d\mathbf{r}'\,d\mathbf{r}'' \times[\langle\lambda\,|\,a(\mathbf{r})a^\dagger(\mathbf{r}')a^\dagger(\mathbf{r}'')a(\mathbf{r}'')|\,\lambda\rangle v_c(|\,\mathbf{r}'-\mathbf{r}''\,|)\varphi_n(\mathbf{r}') -\langle\lambda\,|\,a(\mathbf{r})a^\dagger(\mathbf{r}')a^\dagger(\mathbf{r}'')a(\mathbf{r}')|\,\lambda\rangle v_c(|\,\mathbf{r}'-\mathbf{r}''\,|)\varphi_n(\mathbf{r}')]. \quad (6.33)$$

Now we use the Hartree–Fock factorization,

$$\langle\lambda\,|\,a(\mathbf{r})a^\dagger(\mathbf{r}')a^\dagger(\mathbf{r}'')a(\mathbf{r}'')|\,\lambda\rangle =[\delta(\mathbf{r}-\mathbf{r}')-\rho_\lambda(\mathbf{r}',\mathbf{r})]\rho_\lambda(\mathbf{r}'') -[\delta(\mathbf{r}-\mathbf{r}'')-\rho_\lambda(\mathbf{r}'',\mathbf{r})]\rho_\lambda(\mathbf{r}',\mathbf{r}''), \quad (6.34)$$

where the ρ_λ's are the density matrices for the state λ, i.e.,

$$\rho_\lambda(\mathbf{r}',\mathbf{r})=\langle\lambda\,|\,a^\dagger(\mathbf{r}')a(\mathbf{r})|\,\lambda\rangle, \qquad \rho_\lambda(\mathbf{r})=\langle\lambda\,|\,a^\dagger(\mathbf{r})a(\mathbf{r})|\,\lambda\rangle, \quad (6.35)$$

etc. Noting that the second term of Eq. (6.33) just doubles the first, we have

$$\tilde{V}_{n,\lambda}(\mathbf{r})=N^{-1/2}\{\int d\mathbf{r}'[\delta(\mathbf{r}-\mathbf{r}')-\rho_\lambda(\mathbf{r}',\mathbf{r})]V_c(\mathbf{r}')\varphi_n(\mathbf{r}') -\int\int d\mathbf{r}'\,d\mathbf{r}''[\delta(\mathbf{r}-\mathbf{r}'')-\rho_\lambda(\mathbf{r}'',\mathbf{r})] \times v_c(|\,\mathbf{r}'-\mathbf{r}''\,|)\rho_\lambda(\mathbf{r}',\mathbf{r}'')\varphi_n(\mathbf{r}'')\}, \quad (6.36)$$

with

$$V_c(\mathbf{r}')\equiv\int d\mathbf{r}''v_c(|\,\mathbf{r}'-\mathbf{r}''\,|)\rho_\lambda(\mathbf{r}''). \quad (6.37)$$

[24] We are suppressing the spin index, σ, and the angular momentum designation $\{I, M\}$ for the target state $|\,\lambda\rangle$.

Here $V_c(r')$ is just the average Coulomb field of the target state λ. Exchange processes are contained in the second term of Eq. (6.36). Again, we obtain a simple result if we use a Hartree–Fock description for the state $|\,\lambda\rangle$. In this approximation the $(1-\rho)$ terms are just projection operators for the orbitals unoccupied in $|\,\lambda\rangle$. If the continuum waves $\varphi_E^{(0)}(r)$ are constructed such that they are orthogonal to the occupied orbits, we find for the escape amplitude, Eq. (6.27),

$$(\gamma_{n,c})_{sp}=N^{-1/2}\exp(-\eta_c)\{\int\varphi_E^{(0)}(\mathbf{r})V_c(\mathbf{r})\varphi_n(\mathbf{r})\,d\mathbf{r} -\int\int\varphi_E^{(0)}(\mathbf{r})\rho(\mathbf{r},\mathbf{r}')v_c(|\,\mathbf{r}-\mathbf{r}'\,|)\varphi_n(\mathbf{r}')\,d\mathbf{r}\,d\mathbf{r}'\}. \quad (6.38)$$

Alternately we may write Eq. (6.38) as

$$(\gamma_{nlj})_{sp}=N^{-1/2}\exp(-\eta_{lj})\sum_\beta\langle\nu\beta\,|\,v_c\,|\,n\beta\rangle_A, \quad (6.39)$$

where ν refers to the labels of the continuum orbit, $\nu=\{E, l, j, m_j\}$, and n refers to the bound neutron orbit, $n=\{n, l, j, m_j\}$. The sum in Eq. (6.39) is over the quantum numbers of the occupied proton orbits, denoted by β.

We will call $(\gamma_{nlj})_{sp}$, defined in Eq. (6.39), the *elementary single-particle escape amplitude*. Note that $(\gamma_{nlj})_{sp}$ is the amplitude for the escape of a neutron [orbit $\varphi_{nlj}(r)$] to the continuum proton orbit, $\varphi_{E,lj}^{(0)}(r)$, in the case that the parent state consists of the neutron coupled to an $I=0$ core. We will discuss more complicated cases of angular momentum coupling in Sec. 6.4.

We have not discussed the details involved in obtaining the form factor $V_{n,c(\lambda)}(r)$ from $\tilde{V}_{n,\lambda}(\mathbf{r})$. The distinction between these form factors (other than rather straightforward questions of angular momentum coupling) involves the proper treatment of the Pauli principle. This feature of the theory may be expanded upon by using the formalism of Appendix 1. In the Hartree–Fock approximation we avoid these complications. We will continue to use the Hartree–Fock approximation and leave the question of (long-range) ground-state correlations and their effects on escape amplitudes for further study.

6.311 Direct and Exchange Terms. The direct and exchange contributions to $(\gamma_{nlj})_{sp}$ are depicted in Fig. (6.2). The direct part is given by

$$(\gamma_{nlj})_{sp}=[\exp(-N_{lj})/N^{1/2}] \times\int\varphi_{E,lj}^{(0)}(r)V_c(r)\varphi_{nlj}(r)r^2\,dr \quad (6.40)$$

with

$$V_c(r)=\int d\mathbf{r}'v_c(|\,\mathbf{r}-\mathbf{r}'\,|)\rho(\mathbf{r}'). \quad (6.41)$$

It is found that the exchange term is only a few percent of the direct term. The dominance of the direct term has the consequence of reducing the theoretical uncertainty in the calculation of γ_{sp} since this term depends on the charge density which may be determined from the analysis of electron scattering experiments or from the study of muonic atoms. The empirical density has been used in the calculation of the direct

TABLE 6.1. Comparison of $\gamma_{sp}{}^{DIR}$ calculated with projected and unprojected continuum wave functions. The parent nucleus is Sr^{89}. The amplitudes are in units of $[MeV]^{1/2}$.

Neutron orbit	$2d_{5/2}$	$3s_{1/2}$	$2d_{3/2}$
$(\gamma_{sp}{}^{DIR})$ (Projected)	$0.0452-0.004i$	$0.146-0.0123i$	$0.1128-0.0095i$
$(\gamma_{sp}{}^{DIR})$ (Unprojected)	$0.0338+0.003i$	$0.112+0.0018i$	$0.0874+0.0011i$

term, while the smaller exchange term has been calculated using proton orbitals, $\varphi_\beta(r)$, obtained from a Saxon–Woods potential. This potential is chosen such that the resulting $\varphi_\beta(r)$ reproduce the empirical charge density.

We again consider the specific case of a Sr^{88} target. In Fig. 6.3 we have exhibited the wave function for the $2d_{5/2}$ neutron in Sr^{89} and the direct and exchange contributions to the form factor $V_{2d_{5/2}}(r)$. As in the case of the Coulomb energy calculations, the exchange contribution is small. It contributes about 4% in the calculation of the escape amplitude.

The $d_{5/2}$ bound neutron orbit has also been obtained from a Saxon–Woods potential. The binding energy of this orbit is chosen to agree with the neutron separation energies for Sr^{89} and the radial extension of this orbit is compatible with the Coulomb displacement energy calculation. This phenomenological treatment of the neutron bound state leads to a small uncertainty in the value of $(\gamma_{nlj})_{sp}$.[25]

Finally we may comment on the continuum wave functions $\varphi_{E,lj}{}^{(0)}(r)$ which enter in the calculation of $(\gamma_{nlj})_{sp}$. Recall that these wave functions were modified due to the orthogonality requirement between the P and A spaces [see Eq. (2.8)]. We have investigated the effect of this projection on the calculation of the escape amplitude. Table 6.1 contains the results for a calculation of the $(\gamma_{nlj})_{sp}$ with projected and unprojected continuum wave functions. We see that the projection is an important feature of the calculation.[26]

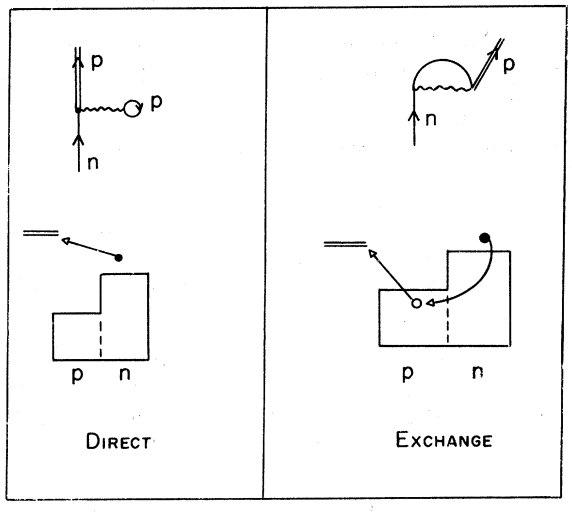

FIG. 6.2. Two schematic representations of the direct and exchange contributions to the elementary single-particle escape amplitude. The double line indicates the continuum proton orbit, and the wavy line the charge-changing Coulomb interaction.

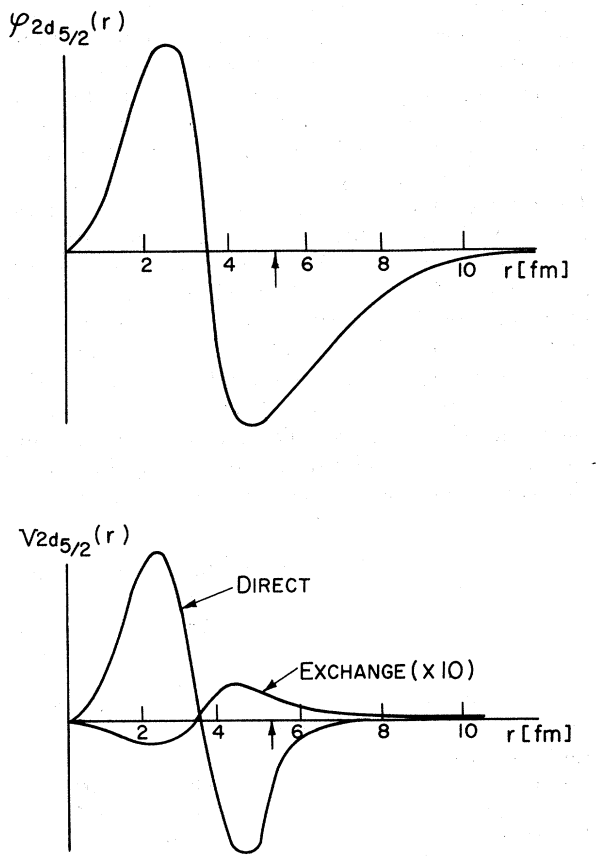

FIG. 6.3. The bound state $2d_{5/2}$ neutron wave function for $Sr^{8}{}_{6}$ and the direct and exchange contributions to the single-particle form factor. The nuclear radius is indicated by an arrow.

[25] If comparison is to be made for spectroscopic factors obtained from analog resonances and stripping processes, one should use the same neutron wave functions in each case to obtain meaningful comparisons.

[26] Expressions for single-particle escape amplitudes may also be obtained from the Lane equations either in terms of the symmetry potential, $U_1(r)$, or the quantity $[V_c(r)-\Delta]$, where $V_c(r)$ is the one-body Coulomb potential, and Δ is the displacement energy. In these expressions one requires the *unprojected* continuum wave. The appearance of Δ in the expression for the escape amplitude is related to the absence of an explicit projection procedure in the Lane equations.

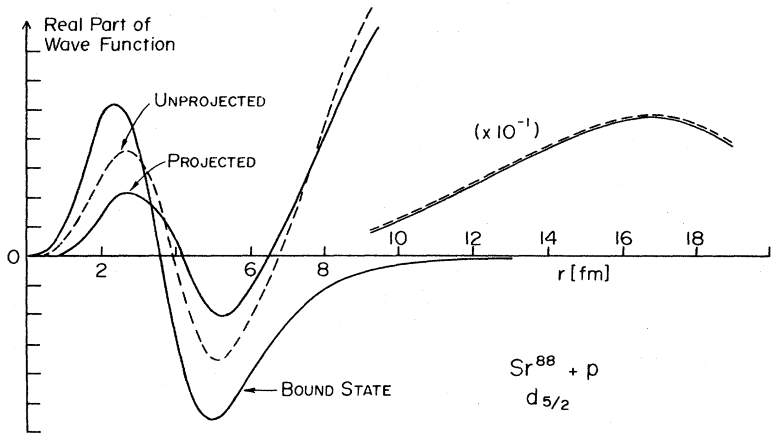

FIG. 6.4. The $2d_{5/2}$ bound state neutron wave function for Sr^{89} and the real part of the continuum wave function $\phi_{d\,5/2}^{(0)}(r)$ (not to scale). Both the projected and unprojected continuum wave functions are shown.

In Fig. 6.4 we have exhibited the bound $2d_{5/2}$ neutron wave function and the real part of the projected proton continuum wave function (not to scale). The Coulomb barrier and the projection causes the continuum wave function to be small in the nuclear interior. Further reduction of the continuum wave in the "nuclear interior" would probably result if account is taken of the Perey effect; however, this point has not been investigated. We have studied the relative importance of the "nuclear interior" to the evaluation of the integral appearing in Eq. (6.40). The form of the various terms of the integrand is important for values of r both inside and outside the nucleus and no further simplification of the calculation of the escape amplitude seems possible.

6.312 Finite Proton Size, Vacuum Polarization and Short-Range Correlations. The effects of finite proton size and vacuum polarization are readily included in the calculation of the escape amplitude by using $v_c(|x-y|)$ of Eq. (5.4) in Eq. (6.39). We saw that the effect of vacuum polarization could be reasonably taken into account by a small renormalization of the electron charge (see Sec. 5.14). Some of the finite size effects have been calculated and are shown in Table (6.2). These lead to about a 1–2 percent reduction in the escape amplitude.

As we have seen in Sec. 5.15, the effects of short-range correlations are small and dependent on the details of the strong interaction. We have not estimated the effect of short-range correlations on the escape widths but it is clear that this effect will provide only a small correction.

6.32 Other Isospin Violating Parts of the Hamiltonian

The contribution of the electromagnetic spin–orbit force and the proton–neutron mass difference to the

TABLE 6.2. Various contributions to the single-particle escape amplitude (as a percentage of the direct term).

	Ca^{41}	Sr^{89}		Ba^{139}		Pb^{209}	
Parent State	$p_{3/2}$ (2MeV)	$s_{1/2}$ (7MeV)	$d_{5/2}$ (7MeV)	$f_{7/2}$ (10MeV)	$p_{1/2}$ (10MeV)	$g_{9/2}$ (15MeV)	$s_{1/2}$ (15MeV)
Coulomb Force							
Direct	100	100	100	100	100	100	100
Exchange	−4.1	−2.8	−3.2	−2.5	−2.3	−1.7	−1.5
Finite size	−2.0	−1.3	−1.5	−1.2	−1.0	−1.6	0.7
Vacuum polarization	0.5	0.5	0.5	0.5	0.5	0.5	0.5
Nuclear Force							
v^{CD}	0.02	0.7		1.0		0.8	
v^{CA}	5.0	4.0		2.0		2.0	
Spin-orbit	−0.5	0.0	−0.6	−0.7	+0.4	−0.7	0.0
Dynamic $p-n$ mass difference	+1.2	0.9	1.0	+0.8	+0.7	+0.7	+0.6
Isospin Impurity	−0.04	−0.1	−0.1	−0.2	−0.2	−0.4	−0.4

escape amplitude is readily estimated. As these are single-particle operators, the operator O_α of Eq. (6.15) has a simple structure,

$$O_\alpha = \sum_\beta \langle \beta \mid \kappa \mid \alpha \rangle a_\beta^\dagger, \tag{6.42}$$

and the contribution to the single-particle escape amplitude is just (for κ local in coordinate space),

$$(\gamma_{nlj})_{\rm sp} = \frac{\exp(-\eta_{lj})}{N^{1/2}} \int_0^\infty \varphi_{E,lj}^{(0)}(r)\kappa(r)\varphi_{nlj}(r) r^2\, dr, \tag{6.43}$$

where $\varphi_{nlj}(r)$ is the bound neutron wave function discussed previously.

The specific forms for the operator κ are given in Secs. 5.41 and 5.42. The contributions to the escape amplitude of these single-particle terms are given in Table 6.2.

We now consider the contribution of the charge-dependent nuclear force to the single-particle escape width. We recall Eq. (5.82a)

$$V_{\rm CD}^{(-)} = \tfrac{1}{2} \sum_{\alpha\beta\gamma\delta} \langle \alpha\beta \mid v^{\rm CD} \mid \delta\gamma \rangle_A (a_\alpha^\dagger a_\beta^\dagger a_\gamma b_\delta - b_\alpha^\dagger a_\beta^\dagger b_\gamma b_\delta). \tag{5.82a}$$

From this expression we find

$$O_n^{\rm CD} = \tfrac{1}{2} \sum_{\alpha\beta\gamma} \langle \alpha\beta \mid v^{\rm CD} \mid n\gamma \rangle_A (a_\alpha^\dagger a_\beta^\dagger a_\gamma - b_\alpha^\dagger a_\beta^\dagger b_\gamma). \tag{6.44}$$

Therefore, the contribution to the single-particle escape amplitude from the charge-dependent nuclear interaction is

$$(\gamma_{nlj}^{\rm CD})_{\rm sp} = [\exp(-\eta_{lj})/N^{1/2}] \sum_{\beta\gamma} \langle \nu\beta \mid v^{\rm CD} \mid n\gamma \rangle_A \times (\rho_{\beta\gamma}^{\,p} - \rho_{\beta\gamma}^{\,n}), \tag{6.45}$$

where

$$\rho_{\beta\gamma}^{\,p} = \langle 0 \mid a_\beta^\dagger a_\gamma \mid 0 \rangle,$$
$$\rho_{\beta\gamma}^{\,n} = \langle 0 \mid b_\beta^\dagger b_\gamma \mid 0 \rangle. \tag{6.46}$$

In Eq. (6.45), ν stands for the quantum numbers of the continuum orbital, $\nu = \{E, lj\}$, and $n = \{nlj\}$ for the quantum numbers of the bound neutron wave function.

We will make a very rough estimate of $\gamma_{\rm sp}^{\rm CD}$. First we write

$$\gamma_{\rm sp}^{\rm CD} = [\exp(-\eta_{lj})/N^{1/2}][(Z-N)/A]\langle \nu \mid \bar{V}^{\rm CD} \mid n \rangle, \tag{6.47}$$

where $\bar{V}^{\rm CD}$ is the average isospin violating nuclear field. Now from the analysis of low energy nucleon-nucleon scattering we expect $\mid \bar{V}^{\rm CD} \mid = 0.02 \mid \bar{V}^{T=1} \mid$, an estimate we have used previously in Sec. 5. Further, if we assume $\bar{V}^{T=1} \simeq -25$ MeV, we can compare this to the matrix element of the average Coulomb field. These considerations lead to the approximation

$$\gamma_{\rm sp}^{\rm CD} \simeq \tfrac{1}{2}[(Z-N)/ZA^{2/3}][\exp(-\eta_{lj})/N^{1/2}]\langle \nu \mid V_c \mid n \rangle. \tag{6.48}$$

The usefulness of the last estimate lies in the fact that the escape amplitude is usually expressed as a matrix element of the one-body Coulomb potential taken between the neutron bound state and the proton continuum orbit. Thus we have

$$\gamma_{\rm sp}^{\rm CD} \simeq \tfrac{1}{2}[(Z-N)/ZA^{2/3}]\gamma_{\rm sp}. \tag{6.49}$$

Similarly, we have

$$\gamma_{\rm sp}^{\rm CA} \lesssim (A^{1/3}/4Z)\gamma_{\rm sp}. \tag{6.50}$$

We stress that this is a crude estimate, particularly if the charge dependent nuclear force is strongly dependent upon spin. However $\gamma_{\rm sp}^{\rm CD}$ and $\gamma_{\rm sp}^{\rm CA}$ are certainly more than a few percent of $\gamma_{\rm sp}$.

6.4 Application of the Elementary Single-Particle Escape Amplitude

In the last section we defined an *elementary single-particle escape amplitude*, $(\gamma_{nlj})_{\rm sp}$ (for class IA transitions). The *single-particle* elastic and inelastic escape amplitudes may be written in terms of this amplitude. We first present a general formula and then go on to some simple specific cases.

Starting from Eq. (6.23) we apply the condition for no channel coupling and no rearrangement ($\Lambda = \lambda = \lambda'$). Using the definitions, (6.15), (6.17), and (6.25) and taking account of the angular momentum algebra we obtain an expression for the *single-particle escape amplitude*,[27]

$$\gamma_{A,\{(l\frac{1}{2})jIJM,\lambda\}}^{\rm DIR,sp} = (2J+1)^{-1/2} \times \sum_n \langle \lambda I \mid\mid \bar{b}_{nlj} \mid\mid \pi J \rangle (\gamma_{nlj})_{\rm sp} \tag{6.51}$$

in terms of the elementary single-particle amplitude (6.39) and a reduced spectroscopic matrix element defined by

$$\langle \lambda IM \mid b_{nljm} \mid \pi JM \rangle = (-1)^{j-m} C_{M-m\,M}^{J\,jI} \times \langle \lambda I \mid\mid \bar{b}_{nlj} \mid\mid \pi J \rangle / (2I+1)^{1/2}. \tag{6.52}$$

We can calculate the reduced spectroscopic matrix element by expanding both the parent state and the target into configurations where the orbit nlj is singled out. Thus we have

$$\mid \pi JM \rangle = \sum_{kJ_kJ_0} \mid j^k(J_k) J_0 JM \rangle \alpha_{kJ_kJ_0}^{\pi}(nljJ), \tag{6.53}$$

[27] Here we have assumed that the average field in (6.39) is spherically symmetric so that ν and n have the same angular momentum quantum numbers. The generalization is straightforward.

and

$$|\lambda IM\rangle = \sum_{k,J_{k-1}J_0} |j_k^{-1}(J_{k-1})J_0 IM\rangle \beta_{kJ_{k-1}J_0}{}^{\lambda}(nljI), \tag{6.54}$$

where k and $k-1$ are the number of neutrons in the orbit nlj in a given configuration for the parent or the target, respectively. The quantum number J_0 stands for the occupation and quantum numbers of all the rest of the particles (neutrons *and* protons).

We then obtain the expression for the single-particle escape amplitude where a particle lj escapes in the channel $[(l\frac{1}{2})j(\lambda)IJ]$.[27] Thus we have

$$\gamma_{A,\{(l\frac{1}{2})j(\lambda)IJM\}}{}^{\mathrm{DIR,sp}} = \sum_{kJ_kJ_{k-1}J_0} (-1)^{J_0+j+J_k+I} \times [(2I+1)(2J_k+1)]^{1/2} \begin{Bmatrix} J_{k-1} & J_0 & I \\ J & j & J_k \end{Bmatrix} \times k^{1/2}[j^{k-1}(J_{k-1})jJ_k \,|\}j^kJ_k] \times \alpha_{kJ_kJ_0}{}^{\pi}(nljI)\beta_{kJ_{k-1}J_0}{}^{\lambda}(nljI)(\gamma_{nlj})_{\mathrm{sp}}, \tag{6.55}$$

where the quantity in square brackets is a standard [De63] fractional parentage coefficient.

The expression (6.55) shows us that, to the extent analog resonance widths are dominated by the *direct single-particle amplitude*, they are sensitive to the makeup of the parent and the target wave functions and can be used to test models for the amplitudes α and β. It is of course not always convenient to make the particular expansion we have performed here. For example, if pairing is an important feature it may be useful to make the usual quasiparticle transformation on b_{nlj} in the reduced matrix element of (6.51). If the nuclei are very deformed it is convenient to calculate (6.51) in the intrinsic frame [Ke70]. In the following subsections are presented some simple examples of the use of (6.55).

6.41 *Elastic Escape Amplitude for Single-Particle Parent*

The elastic channel single-particle amplitude is depicted in Fig. 6.2. There is no complication due to angular momentum coupling as the bound neutron orbit has the same (l, j) as the continuum proton orbit. We have $I=J_0=0$, $k=1$, $J_k=j$, $J_{k-1}=0$. The single-particle escape amplitude depends on the energy and the quantum numbers l and j and is equal to the elementary single-particle escape amplitude $(\gamma_{nlj})_{\mathrm{sp}}$ [see Eq. (6.39)].

6.42 *Inelastic Amplitudes to Particle-Hole Final States*

If (nlj) is one of the core orbits we obtain the escape amplitude to various particle–hole excitations. Any one of the core neutrons (nlj) can escape to become a continuum proton leaving behind a neutron hole in the (nlj) orbit. This process is depicted in Fig. 6.5 using the same scheme as that for Fig. 6.2.

For this case, the parent state is simple because the (nlj) orbit is completely filled. We find

$$|\pi j_1 m_1\rangle = |j^{2j+1}(0)j_1 j_1 m_1\rangle, \tag{6.56}$$

where we now label the extra odd particle as $j_1 m_1$. The single-particle escape amplitude will then only pick out of the target state that part which is a hole in the (nlj) orbit coupled to the extra odd particle

$$|\lambda IM\rangle = |j^{2j}(j)j_1 IM\rangle \beta_{jj_1}(jI) + \text{rest}. \tag{6.57}$$

The partial parentage coefficient for $k=2j+1$ is unity, and the six-j symbol is simple because $J_k=0$, $J_{k-1}=j$, $J_0=j_1$. The result is then

$$\gamma^{\mathrm{DIR,sp}} = [(2I+1)/(2j_1+1)]^{1/2}\beta_{jj_1}(jI)(\gamma_{nlj})_{\mathrm{sp}}. \tag{6.58}$$

Of course this result can be obtained more directly from the original expression. It is an example of a class of simpler forms treated in the next section.

6.43 *Cases with Simple Fractional Parentage*

There are some special cases where the fractional parentage coefficient is particularly simple:

1. A particle escapes from closed shell, i.e., $k=2j+1$, $J_k=0$, $J_{k-1}=j$, $J_0=J$. Then we have

$$\gamma^{\mathrm{DIR,sp}} = [(2I+1)/(2J+1)]^{1/2}\alpha_{0j}(jJ)\beta_{jJ}(jI)(\gamma_{nlj})_{\mathrm{sp}}. \tag{6.59}$$

2. A particle escapes from orbit with only one particle, i.e., $k=1$, $J_k=j$, $J_{k-1}=0$, $J_0=I$. Then we have

$$\gamma^{\mathrm{DIR,sp}} = (-1)^{I+j-J}\alpha_{jI}(jJ)\beta_{0I}(jI)(\gamma_{nlj})_{\mathrm{sp}}. \tag{6.60}$$

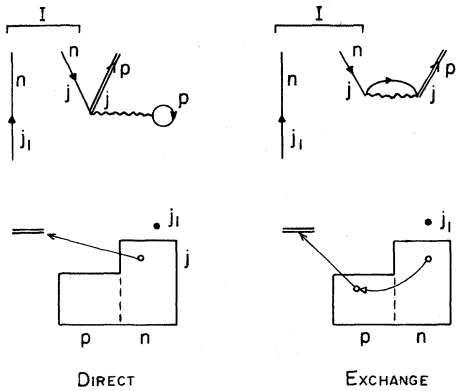

FIG. 6.5. Two schematic representations of the direct and exchange contributions to the escape amplitude leading to a neutron particle–hole state. The particle is in state j_1 and the core neutron which escapes has angular momentum j. The neutron particle–hole pair is indicated as coupled to a total angular momentum I.

3. A particle escapes from an orbit with two particles, i.e., $k=2$, $J_{k-1}=j$, $J_k=J_2$, and we have

$$\gamma^{\mathrm{DIR,sp}}=\sqrt{2}(-1)^{J_0+j+J_2+I}[(2I+1)(2J_2+1)]^{1/2} \times \begin{Bmatrix} j & J_0 & I \\ J & j & J_2 \end{Bmatrix} \alpha_{J_2J_0}(jJ)\beta_{jJ_0}(jI)(\gamma_{nlj})_{\mathrm{sp}}. \quad (6.61)$$

4. An escape when $k=2j$, $J_k=j$, $J_{k-1}=J_2$ where we have

$$\gamma^{\mathrm{DIR,sp}}=-(2j)^{1/2}(-1)^{J_0+I}[(2I+1)(2j+1)]^{1/2} \times \begin{Bmatrix} J_2 & J_0 & I \\ J & j & j \end{Bmatrix} \alpha\beta(\gamma_{nlj})_{\mathrm{sp}}. \quad (6.62)$$

A simplification in another direction is seen in the next section.

6.44 Valence Particle Escape

If the parent has a closed ($J_0=0$) core plus k valence neutrons in the (nlj) orbit and one of these escapes we get just the fractional parentage coefficient. Thus we have $J_k=J$, $J_{k-1}=I$ and

$$\gamma^{\mathrm{DIR,sp}}=k^{1/2}[j^{k-1}(I)jJ\,|\}j^kJ]\beta_{I0}(nljI)(\gamma_{nlj})_{\mathrm{sp}}. \quad (6.63)$$

When $k=2$ the fractional parentage coefficient is unity and we have

$$\gamma^{\mathrm{DIR,sp}}=\sqrt{2}(\gamma_{nlj})_{\mathrm{sp}}\beta(j), \quad (6.64)$$

where $\beta(j)$ is the amplitude in which the final state is pure single particle. This is a special case of Eq. (6.61).

6.45 Pairing Effects

Finally we consider Eq. (6.51) for the nuclei for which pairing is a good first approximation. It is easy to see from the usual quasiparticle transformation that

$$\langle\lambda I \,||\, b_{nlj} \,||\, \pi J\rangle = V_{nlj}\langle\lambda I \,||\, \alpha_{nlj} \,||\, \pi J\rangle + U_{nlj}\langle\lambda I \,||\, \alpha_{nlj}^{\dagger} \,||\, \pi J\rangle, \quad (6.65)$$

where α and $\alpha^{\dagger}$ are the quasiparticle annihilation and creation operators. We consider the simple cases where the parent and target states have zero, one, or two quasiparticles. These are proportional to either V or U. Thus we have

$$\gamma^{\mathrm{DIR,sp}}=V_{nlj}(\gamma_{nlj})_{\mathrm{sp}}, \qquad 1\ \mathrm{qp}\rightarrow 0\ \mathrm{qp} \quad (6.66a)$$

or

$$\gamma^{\mathrm{DIR,sp}}=U_{nlj}(\gamma_{nlj})_{\mathrm{sp}}, \qquad 0\ \mathrm{qp}\rightarrow 1\ \mathrm{qp} \quad (6.66b)$$

for the simplest cases which have no angular momentum coupling.

When two quasiparticles are involved we have statistical or phase factors

$$\gamma^{\mathrm{DIR,sp}}=(-1)^{I+j-J}V_{nlj}(\gamma_{nlj})_{\mathrm{sp}}, \qquad 2\ \mathrm{qp}\rightarrow 1\ \mathrm{qp} \quad (6.67a)$$

$$\gamma^{\mathrm{DIR,sp}}=[(2I+1)/(2J+1)]^{1/2}U_{nlj}(\gamma_{nlj})_{\mathrm{sp}}, \qquad 1\ \mathrm{qp}\rightarrow 2\ \mathrm{qp} \quad (6.67b)$$

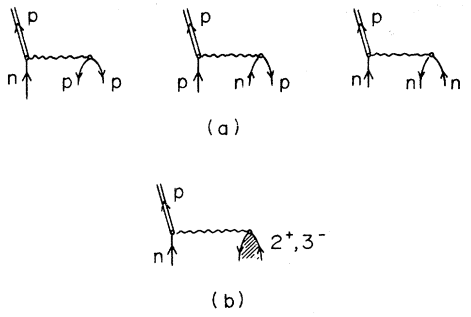

FIG. 6.6. (a) Diagrammatic representations of some rearrangement escape amplitudes. $V_c^{(-)}$ only contributes to the *first* of the three processes shown. (b) Rearrangement amplitude involving a neutron coupled to a vibration.

6.5 Calculation of the Rearrangement Escape Amplitude

We now turn to a discussion of the amplitudes of Class II. The contribution to the direct escape amplitude from this class is given by

$$\gamma_{A,c(\lambda)}{}^{\mathrm{DIR}}=\frac{\exp(-\eta_c)}{N^{1/2}}\sum_{c'(\lambda'),\,\Lambda\neq\lambda'}\int_0^{\infty}\varphi_{c(\lambda),c'(\lambda')}{}^{(0)}(r) \times\sum_n\langle r,c'(\lambda')|\,O_n\,|\,\Lambda\rangle r^2\,dr\langle\Lambda\,|\,b_n\,|\,\pi\rangle. \quad (6.68)$$

By construction, this amplitude describes processes in which at least two particles change their orbits. Amplitudes involving transitions of this type have been termed *rearrangement amplitudes*.

Consider again the simple model in which the target is a doubly closed shell core. In this case the states $|\,\Lambda\rangle$ may contain one-particle one-hole states, or vibrations. Thus a typical term contributing to the rearrangement part of $\gamma_{A,c}{}^{\mathrm{DIR}}$ comes from a term in the parent which consists of a particle coupled to a vibration.

For purposes of orientation some of these diagrams were calculated for the force $V_c^{(-)}$ and for orbitals appropriate to the parent Sr^{89}. The Sr^{88} core was taken to be doubly closed. The results are exhibited in Table 6.3. Relative to the magnitude of $(\gamma_{nlj})_{\mathrm{sp}}$ the diagrams of Fig. 6.6a are much less than 1%. If we consider the possibility of collective enhancement (Fig. 6.6b) we find that contribution to the amplitude is still only about 1% in Sr. In the latter case the experimental $B(E2)$ values were used to estimate the matrix elements between the core and the collective 2^+ state in the particle core model. For deformed nuclei these contributions

TABLE 6.3. Some rearrangement escape amplitudes for the parent Sr^{89}. The computation is made for the emission of an $s_{1/2}$ proton, and the results presented have been divided by the magnitude of the elementary single-particle escape amplitude. Only the contribution of $V_c^{(-)}$ is included.

Present State	$[\gamma^{\mathrm{DIR}}(\mathrm{Rearrangement})/\lvert\gamma_{sp}\rvert]\times 100$		
	Direct matrix element	Exchange matrix element	Total
$[(p_{1/2}p_{3/2}^{-1})_{2^+}d_{5/2}]_{1/2^+}$	$0.34-0.001i$	$0.30-0.03i$	$0.04+0.003i$
$[(p_{1/2}p_{3/2}^{-1})_{2^+}d_{3/2}]_{1/2^+}$	$0.25-0.002i$	$-0.06+0.005i$	$0.31-0.007i$
$[(p_{1/2}f_{5/2}^{-1})_{2^+}d_{5/2}]_{1/2^+}$	$-0.28-0.003i$	$-0.04-0.01i$	$-0.24-0.002i$
$[(p_{1/2}f_{5/2}^{-1})_{2^+}d_{3/2}]_{1/2^+}$	$-0.20-0.001i$	$-0.21-0.004i$	$0.01+0.003i$
$[(\mathrm{collective})_{2^+}d_{5/2}]_{1/2^+}$	$0.65+0.001i$		$0.65+0.001i$
$[(\mathrm{collective})_{2^+}d_{3/2}]_{1/2^+}$	$0.47+0.002i$		$0.47+0.002i$

will be larger as the 2^+ state is more collective than in the case of Sr.

The isospin violating terms of one-body character such as the spin–orbit term and the ΔM correction do not contribute to the rearrangement amplitudes. Contributions to $[H, T_-]$ from the two-body nuclear term have not been calculated. These two-body charge-changing forces are of short range and are expected to yield contributions to rearrangement amplitudes of the same order as $V_c^{(-)}$ or possibly somewhat larger. The inclusion of direct interactions (Class IIB) can also yield important contributions.

Finally we note that the rearrangement amplitudes of Table 6.3 may be used for an estimate of the inelastic escape amplitudes for a single-particle parent going to a final particle–hole state or to a final collective state in the absence of direct interaction effects. The result is very small, an amplitude of the order of $10^{-2}\gamma_{\mathrm{sp}}$ in the case of strontium.

6.6 Nonstatistical Contributions to the Compound Escape Amplitude

We recall that the compound escape amplitude was defined by Eq. (6.4) [see Eq. (6.11)], and a statistical estimate has been given following Eq. (2.54). The application of the random-phase argument used in the statistical estimate is limited by the possibility of having some states $\lvert q\rangle$ which have significant coupling to the analog state and the continuum channels. This situation has already been discussed in Sec. 2.43 where we introduced the concept of doorway states in the q space.

6.61 Configuration States

In this section we will discuss the contribution to the compound escape amplitude of the configuration states considered as doorway states.

We again consider a simple parent state which is a neutron coupled to a doubly closed core. For this discussion it is useful to introduce the following notation. Let $\lvert \mathrm{O}\rangle$ denote the core and $\lvert \mathrm{A}\rangle$ its analog. The analog state is then

$$\lvert A\rangle=(2T)^{-1/2}[\lvert \psi_p\mathrm{O}\rangle+\lvert \psi_n\mathrm{A}\rangle(2T-1)^{1/2}] \quad (6.69)$$

where ψ_n is a neutron orbit, and ψ_p represents a proton in the same orbit.[28] An interesting state with the same configurations is the so-called antianalog state defined by (Sec. 2.43)

$$\lvert \bar{A}\rangle=(2T)^{-1/2}[\lvert \psi_p\mathrm{O}\rangle(2T-1)^{1/2}-\lvert \psi_n\mathrm{A}\rangle]. \quad (6.70)$$

Applying the doorway analysis we have a contribution to $\gamma_{A,c}{}^{\mathrm{COMP}}$ due to the antianalog state (see Eqs. 2.52 and 2.31–35).

$$\gamma_{A,c}{}^{\mathrm{COMP}(\bar{A})}=\gamma_{\bar{A},c}\langle\bar{A}\mid H\mid A\rangle/\{E-E_{\bar{A}}+\tfrac{1}{2}[i\Gamma_{\bar{A}}(E)]\}, \quad (6.71)$$

where

$$E\simeq E_R\simeq E_A,$$

and

$$\gamma_{\bar{A},c}=\exp(-i\delta_c)\langle\bar{\Phi}_c^{(-)}\mid H\mid\bar{A}\rangle. \quad (6.72)$$

The matrix element $\langle\bar{A}\mid H\mid A\rangle$ can be expressed in terms of the commutator $V^{(-)}$ in the usual manner [Eq. (2.5)]. The dominant contribution arises from the Coulomb force which leads to

$$\langle\bar{A}\mid H\mid A\rangle=[(2T-1)^{1/2}/2T]\times[\langle\psi_n\mid V_c\mid\psi_n\rangle-\langle\psi_k\mid V_c\mid\psi_k\rangle_{\mathrm{AV}}], \quad (6.73)$$

where $V_c=V_c(r)$ is the one-body Coulomb potential and $\langle\psi_k\mid V_c\mid\psi_k\rangle_{\mathrm{AV}}$ is the average of the Coulomb matrix element over the *excess* neutron orbitals. In Eq. (6.72)

[28] For this model, we see that $\psi_p(r)$ is just the function $u_{A,c}(r)$ defined in Eq. (A.1.34) and used in Sec. 2.23.

we have neglected exchange and isospin-violating terms other than those arising from the Coulomb potential.[29]

The first factor in $\gamma_{A,c}{}^{\mathrm{COMP}}$, which is the coupling of the antianalog to the continuum, can be estimated by writing

$$|\bar{A}\rangle = |A\rangle(2T-1)^{1/2} - |\psi_n \mathrm{A}\rangle[(2T-2)/(2T)^{1/2}]. \tag{6.74}$$

Then we can see that

$$\gamma_{\bar{A},c} = [(2T-1)/2T]^{1/2} \exp(-\eta_c) \times \int \varphi_E^{(0)}(r)\{V_c(r) - (T-1)U_1(r)\}\psi_n(r) r^2\, dr, \tag{6.75}$$

where we have neglected exchange terms; $U_1(r)$ is the symmetry potential arising from the off-diagonal matrix element,[30] i.e.,

$$\langle \varphi^{(0)}\mathrm{O} \mid H \mid \psi_n \mathrm{A}\rangle \cong [(2T-1)^{1/2}/2] \times \int \varphi^{(0)}(r) U_1(r) \psi_n(r) r^2\, dr. \tag{6.76}$$

In terms of $U_1(r)$ we also have

$$E_A - E_{\bar{A}} = T\int |\psi_n|^2 |\, U_1(r) r^2\, dr - [2(T-1)/(2T-1)^{1/2}]\langle A \mid H \mid \bar{A}\rangle. \tag{6.77}$$

Finally we see that by applying Eq. (2.62) to the state $|\bar{A}\rangle$ we have

$$\Gamma_{\bar{A}} = 2\langle \bar{A} \mid W_E \mid \bar{A}\rangle. \tag{6.78}$$

If we require that the operator W is isospin conserving, the equation analogous to (6.76) leads to the approximate result

$$\Gamma_{\bar{A}} = 2 \operatorname{Im} \int |\psi_n(r)|^2 W_E(r) r^2\, dr, \tag{6.79}$$

where we have assumed that W is local. The real part of $W_E(r)$ leads to a small correction to $U_1(r)$ which is of course included in the usual phenomenological equations.

We can now write the total result for $\gamma_{A,c}$ in terms of the total form factor $\mathrm{V}_{A,c}(r)$ including the anti-analog, i.e.,

$$\mathrm{V}_{A,c}(r) \simeq (2T)^{-1/2}\psi_n(r) \times \{V_c(r) + [\langle \bar{A} \mid H \mid A\rangle(2T-1)^{1/2}/(E - E_{\bar{A}} + i\Gamma_{\bar{A}}/2)] \times [V_c(r) - (T-1)U_1(r)]\}. \tag{6.80}$$

The expression in curly brackets is a kind of "effective" Coulomb potential for escape (also for continuum mixing).

For the strontium example, the ψ_n denote the neutron orbits, $2d_{5/2}$, $3s_{1/2}$, and $2d_{3/2}$. The other excess neutron orbits, ψ_k, are the $1g_{9/2}$ and $2p_{1/2}$. In Table 6.4 we present the results of a calculation of $\exp(2i\phi_c)\Gamma_{A,c}$ which includes the effect of the antianalog. The optical model parameters of Auerbach *et al.* [Au66] were used. The escape width $\Gamma_{A,c}$ differs from the single-particle width Γ_{sp} by only one or two percent.

In addition to the antianalog we have also considered the influence of the other configuration state, in this case,

$$|\bar{A}_1\rangle = |\psi_n \bar{\mathrm{A}}\rangle, \tag{6.81}$$

where $|\bar{\mathrm{A}}\rangle$ is the antianalog of the target $|\mathrm{O}\rangle$. These configuration states can be considered as monopole excitations of the core without change in radial quantum number. While the matrix element $\langle \bar{A}_1 \mid H \mid A\rangle$ can again be reduced to a difference in single-particle Coulomb energies (here, between $g_{9/2}$ and $p_{1/2}$), the escape width has to be computed from a microscopic model. If we assume an effective isospin-dependent two-body interaction of the form

$$v_{12} = c\delta(\mathbf{r}_1 - \mathbf{r}_2)\mathbf{t}_1 \cdot \mathbf{t}_2, \tag{6.82}$$

we can determine the constant c from the "macroscopic" potential $U_1(r)$ given by

$$U_1(r) = c\sum_{k=1}^{2}(2j_k+1)|\psi_k|^2(2T)^{-1/2}. \tag{6.83}$$

In terms of the same constant, the potential for the decay of $|\bar{A}_1\rangle$ is

$$\bar{U}_1(r) = c[(2j_1+1)(2j_2+1)]^{1/2} \times [|\psi_1(r)|^2 - |\psi_2(r)|^2](2T)^{-1/2}. \tag{6.84}$$

Here $\psi_1(r)$ and $\psi_2(r)$ are neutron orbits, $g_{9/2}$ and $p_{1/2}$. As the strength of the isospin-dependent single-particle potential $U_1(r)$ is reasonably well determined by many experiments, we know the constant c in Eq. (6.82). Because of the form of Eq. (6.84) compared to Eq. (6.83) the escape width of $|\bar{A}_1\rangle$ is smaller than that of $|\bar{A}\rangle$. The contribution of $|\bar{A}_1\rangle$ is about 20% that of $|\bar{A}\rangle$ as seen in Table 6.4.

The strontium example seems to be atypical in that $\langle \bar{A}_1 \mid H \mid A\rangle$ is larger than $\langle \bar{A} \mid H \mid A\rangle$ by a factor of 2–3. In this case, a specific, coherent linear combination of $|\bar{A}\rangle$ and $|\bar{A}_1\rangle$ considered as a doorway may increase the value of $\gamma^{\mathrm{COMP}(\bar{A})}$. Even in this case of coherent mixing of $|A\rangle$ and $|\bar{A}_1\rangle$, $\gamma^{\mathrm{COMP}(\bar{A})}$ only contributes 2–4% to the escape width, $\Gamma_{A,c}$.

6.62 Giant-Isovector Monopole

We have illustrated the role of the configuration states as doorways in γ^{COMP}. These do not exhaust all of the monopole strength. It is certainly necessary to consider the $\tau = 1$, monopole collective excitation discussed in Sec. 5.24. In the microscopic description this is a coherent linear combination of $J = 0$, neutron-hole proton-particle states, where the particle has only its radial quantum number different from the hole [Bo67].

[29] There are cases where the Coulomb terms (6.72) happen to cancel more than usual. In those cases the nuclear charge-dependent forces must be included.

[30] We note the cancellation which occurs between the V_c and U_1 terms of this expression. This implies that the nuclear escape width of the antianalog is not large.

TABLE 6.4. Contributions of the anti-analog to the escape width of the analog state.

	$d_{5/2}$ at 4.98 MeV	$s_{1/2}$ at 5.95 MeV	$d_{3/2}$ at 6.95 MeV
$\Gamma_{sp}^{DIR}\exp(2i\phi_{sp}^{DIR})=2\pi(\gamma_{sp})^2$	$7.16+0.25i$	$76.10+4.9i$	$46.98+2.4i$ keV
$\lvert\gamma_{\bar{A},c}/\gamma_{sp}\rvert$	0.65	0.55	0.57
$\langle\bar{A}\mid H\mid A\rangle$	−91.4	−163.9	−112.7 keV
$E_A-E_{\bar{A}}+i\Gamma_{\bar{A}}/2$	$6838+1195i$	$6335+1100i$	$6825+1187i$ keV
$\Gamma_{A,c}\exp(2i\phi_c)=2\pi(\gamma_{A,c})^2$	$7.04+0.26i$	$73.96+5.0i$	$46.11+2.4i$ keV
$\lvert\gamma_{\bar{A}_1,c}/\gamma_{\bar{A},c}\rvert$	0.06	0.05	0.08
$\lvert\langle A\mid H\mid\bar{A}_1\rangle/\langle A\mid H\mid\bar{A}\rangle\rvert$	3.2	1.8	2.6

Just as in the case of the anti-analog we have a contribution

$$\gamma_{A,c}^{COMP(M)}=\gamma_{M,c}\langle M\mid H\mid A\rangle/[E_A-E_M+\tfrac{1}{2}(i\Gamma_M)], \tag{6.85}$$

where M refers to the collective giant monopole state. This state is actually split by symmetry effects in the same way as the giant dipole [Fa65], but it has *three* members with isospins $T+1$, T, and $T-1$ in the compound nucleus. These arise from the coupling of the $\tau=1$ monopole isovector with the isospin (T) of the (excess neutron) core. The matrix elements to the monopole can be estimated by calculating the sum of the squares of the matrix elements of the Coulomb field $V_c^{(-)}$ to the proton–particle neutron–hole states [Me70b]. Thus we have

$$\langle M\mid H\mid A\rangle=(2T)^{-1/2}\langle M\mid V_c^{(-)}\mid\pi\rangle \tag{6.86}$$

and

$$\langle M\mid H\mid A\rangle^2\simeq(2T)^{-1}\langle T1T_MT-1\mid TT,1-1\rangle^2\times\sum_{nlm}\langle nl\mid V_c\mid n+1l\rangle^2$$

$$\simeq 0.16\left(\frac{1.2}{r_0}\right)^6\left(\frac{2T-1}{2T+1}\right)\frac{Z^2}{2T}A^{-4/3}\times\sum_{nlm}(n+l+\tfrac{3}{2})(n+1)\,(\mathrm{MeV})^2, \tag{6.87}$$

where r_0 is the charge radius parameter in Fermis and we have used oscillator wave functions. The vector coupling coefficient is about 1 for $T_M=T-1$ and of order $(1/T)$ for the other modes, so that we need only carry the case of $T_M=T-1$ to a first approximation. What is more, the other two modes have higher energies because of the symmetry splitting and this further reduces their effect. This leads to the estimate

$$\langle M\mid H\mid A\rangle^2\sim 4(\mathrm{MeV})^2 \tag{6.88}$$

in nuclei with $A\gtrsim 90$. However the collective nature of the state must be taken into account more carefully because of the energy weighted sum rule. Since the state is pushed up about a factor of two from the particle–hole energy, the squared matrix element should be reduced by about the same factor. The hydrodynamic model [Bo67], which takes account of this effect, leads to a value

$$\langle M\mid H\mid A\rangle^2\simeq(2T)^{-1}\times[(2T-1)/(2T+1)](Z^2/100)\,(\mathrm{MeV})^2 \tag{6.89}$$

corresponding to the energy given by Eq. (5.62). For the $T_M=T-1$ mode this energy must be reduced by the symmetry splitting to obtain (E_M-E_A) in Eq. (6.85). An estimate for this energy difference is then

$$E_M-E_A\simeq(170/A^{1/3})-[110(T+1)/A]\ \mathrm{MeV}. \tag{6.90}$$

Because this energy difference is rather small (especially for the case of Pb^{208}), it is somewhat uncertain and the estimates are probably unreliable. This remark also applies to the matrix element. Nevertheless, we use these estimates for orientation purposes. They lead to

$$2\pi\mid\gamma_{A,c}^{COMP(M)}\mid^2=\Gamma_{M,c}/150, \tag{6.91}$$

$$\Gamma_{M,c}=2\pi\mid\gamma_{M,c}\mid^2 \tag{6.92}$$

for the case of Pb^{208}. We expect that $\Gamma_{M,c}$ will not be much larger than $(\Gamma_{A,c})_{sp}$ itself, so that the correction due to (6.91) will be small. This is so, even though $\Gamma_{M,c}$ is a nuclear escape, because the collective monopole contains only a small fraction of the channel c. In addition, the escape must be calculated at the energy E_A rather than E_M which brings in additional small Coulomb penetrability factors.

A more careful estimate could be carried through if we knew the monopole escape form factor $V_2(r)$. Then the total form factor (6.80) would have an additional contribution

$$\delta V_{A,c}^{M}=(2T)^{-1/2}\psi_n(r)\times\{\langle M\mid V_c^{(-)}\mid\pi\rangle/[E_A-E_M+\tfrac{1}{2}(i\Gamma_M)]\}V_2(r), \tag{6.93}$$

where,

$$\gamma_{M,c}=\int\varphi_E^{(0)}(r)\,V_2(r)\psi_n(r)r^2\,dr. \tag{6.94}$$

This same form factor enters into the discussion of (i) monopole mixing effects in the Coulomb energy (Sec. 5.31); (ii) absorption widths and shifts (Sec. 6), and (iii) various other nuclear characteristics such as the isotope shift, the optical model, etc. These modes will be taken up again in Sec. 7. The role of higher multipole doorways (for example the giant dipole plus particle) should also be considered [Fa66] including the effect of nuclear isospin violating terms.

6.7 Channel Coupling Contributions to the Escape Amplitude

In the weak-coupling limit, where the channel coupling may be treated in perturbation theory, we expect the influence of the other channels on the escape amplitude to be small, except in the case that $\gamma_{A,c}{}^{\mathrm{DIR}}$, calculated without channel coupling, is itself small. This special case occurs if the spectroscopic factor for the channel c is small.

We define

$$\gamma_{A,c}{}^{\mathrm{CHANNEL}}=\exp(-i\delta_c)\sum_{c'\neq c}\int\langle A\mid H\mid r,c'\rangle \times\varphi_{cc'}{}^{(+)}(r)r^2\,dr. \quad (6.95)$$

(Note that without the restriction, $c'\neq c$, the right side of Eq. (6.95) would just equal $\gamma_{A,c}{}^{\mathrm{DIR}}$.)

6.71 Distorted-Wave Born Approximation

In most cases we may treat the channel coupling in perturbation theory so that for $c'\neq c$, we have

$$\varphi_{cc'}{}^{(+)}(r)=\int_0^\infty\int_0^\infty G_{c'c'}{}^{(+)}(r,r')\langle r',c'\mid H\mid r'',c\rangle \times\varphi_{E,c}{}^{(+)}(r'')r'^2r''^2\,dr'\,dr'' \qquad (c'\neq c), \quad (6.96)$$

where $\varphi_{E,c}{}^{(+)}(r)$ is $\varphi_{cc}{}^{(+)}(r)$ with the energy dependence explicitly put in evidence. If we now write

$$G_{c'c'}{}^{(+)}(r,r')=\int[\varphi_{E',c'}{}^{(+)}(r)\varphi_{E',c'}{}^{(-)}(r')\,dE'/(E-E'-E_{c'}+i\epsilon)], \quad (6.97)$$

we find

$$\gamma_{A,c}{}^{\mathrm{CHANNEL}}=\sum_{c'\neq c}\int\frac{\exp(2\eta_{c'})\gamma_{A,c'}{}^{\mathrm{DIR}}T_{c'c}{}^{\mathrm{DWBA}}(E',E)}{E-E'-E_{c'}+i\epsilon}\,dE'. \quad (6.98)$$

In Eq. (6.97) and (6.98), $E_{c'}$ is the threshold for the inelastic channel, c'

$$T_{c'c}{}^{\mathrm{DWBA}}=\int_0^\infty\int_0^\infty\exp(-\eta_{c'})\varphi_{E',c'}{}^{(0)}(r')\langle r',c'\mid H\mid r'',c\rangle \times\varphi_{E,c}{}^{(0)}(r'')\exp(-\eta_c)r'^2r''^2\,dr'\,dr'', \quad (6.99)$$

and

$$\gamma_{A,c'}{}^{\mathrm{DIR}}=\exp(-\eta_{c'})\int_0^\infty\langle A\mid H\mid r,c'\rangle \times\varphi_{E',c'}{}^{(0)}(r)r^2\,dr \quad (6.100)$$

has the usual definition.

As noted above, $\gamma_{A,c'}{}^{\mathrm{DIR}}$ will be large for those states with large spectroscopic factors for particle emission to the channel c'. If we neglect the imaginary potential, the $\varphi^{(0)}(r)$ are real and therefore $\gamma^{\mathrm{CHANNEL}}$ has only *real* contributions from the closed channel ($E_{c'}<E$). For the open channels ($E>E_{c'}$) we find

$$\mathrm{Im}\,\gamma_{A,c}{}^{\mathrm{CHANNEL}}=-\pi\sum_{c'\neq c}T_{c'c}{}^{\mathrm{DWBA}}(E-E_{c'},E) \times\gamma_{A,c'}{}^{\mathrm{DIR}}(E-E_{c'}) \qquad (c'\text{ open}). \quad (6.101)$$

The calculation of the real part of $\gamma_{A,c}{}^{\mathrm{CHANNEL}}$ is somewhat more difficult. In general we write

$$\gamma_{A,c}{}^{\mathrm{DIR}}=(\gamma_{A,c}{}^{\mathrm{DIR}})_{NC}+\gamma_{A,c}{}^{\mathrm{CHANNEL}}, \quad (6.102)$$

where $(\gamma_{A,c}{}^{\mathrm{DIR}})_{NC}$ denotes the direct amplitude calculated without channel coupling.

6.72 Deformed Nuclei

For the case of strongly deformed nuclei, the channel coupling between states in the rotational band of the target is especially strong. For this case one would like to avoid the distorted-wave Born approximation. This can be done in a useful way by introducing the adiabatic approximation which neglects rotational energies [Ch57]. Then the escape amplitude can be seen to obey rotational intensity rules. For example, in the case of an even–even nucleus [Ke70], we have

$$\gamma_{A,\{(I_0^+)jIJM\}}=\begin{Bmatrix} j & I & J\\ K & 0 & K\end{Bmatrix}\gamma_{ljK}, \quad (6.103)$$

with

$$\begin{Bmatrix} j & I & J\\ K & 0 & K\end{Bmatrix}=[(2I+1)/(2J+1)]^{1/2}\sqrt{2}^{-1} \times[\langle jRJK\mid K0\rangle+(-1)^{j-J}\langle jRJ-K\mid -K0\rangle], \quad (6.104)$$

where the parent state can be any state of the rotational band (KJM) and the target state is any member of the $K=0$ band with angular momentum I. The intrinsic escape amplitude γ_{ljK} can be easily calculated if we neglect compound couplings and intrinsic rearrangement terms. We then have an *elementary intrinsic single-particle amplitude* which can be written as a three-dimensional integral (actually two dimensional due to axial symmetry),

$$\gamma_{ljK}{}^{\mathrm{sp}}=(2T)^{-1/2}\int d^3r A^{ljK}(\mathbf{r})V_c(\mathbf{r})\chi_K(\mathbf{r}), \quad (6.105)$$

where $\chi_K(\mathbf{r})$ is the Nilsson orbital with projection K, $V_c(\mathbf{r})$ is the deformed Coulomb field (we have neglected exchange) and $A^{ljK}(\mathbf{r})$ is the scattering solution in the intrinsic frame with incoming waves in the channel ljK. It is understood that the variable $\mathbf{r}$ includes spin. Equation (6.105) can be evaluated by expanding in the lj representation, in which case we obtain a double sum of single integrals. This includes a sum on Nilsson coefficients a_{ljK}. In the limit of small deformation, a single coefficient may suffice if we neglect the deformation of $V_c(\mathbf{r})$ and the intrinsic channel coupling. Then [Ca69] we have

$$\gamma_{ljK} \simeq a_{ljK}(\gamma_{lj}{}^{\mathrm{DIR}})_{\mathrm{sp}} \tag{6.106}$$

which is calculated in a spherical basis.

6.8 The Asymmetry Phase

In the many-channel case, the resonant part of the T matrix has the general form, Eq. (2.38),

$$T_{c'c}{}^{A} = \exp(i\delta_{c'})\gamma_{A,c'}\gamma_{A,c}\exp(i\delta_c)/[E-E_R+\tfrac{1}{2}(i\Gamma)], \tag{2.38}$$

where the escape amplitudes

$$\gamma_{A,c} = \exp(-i\delta_c)\langle A \mid H \mid \Phi_c{}^{(+)}\rangle$$

$$= \exp(-\eta_c)\sum_{c'}\int_0^\infty \varphi_{cc'}{}^{(0)}(r)\mathrm{V}_{c'}{}^{A}(r)r^2\,dr \tag{2.34}$$

are complex numbers. The phase of these amplitudes originates:

(i) from the imaginary part in the form factor $\mathrm{V}_{c'}{}^{A}(r)$ [see Eqs. (2.18) and (2.35)], and

(ii) from the use of imaginary optical potentials, and which make $\varphi_{cc'}{}^{(0)}$ complex, and

(iii) from the fact that the scattering functions, $\varphi_{cc'}{}^{(0)}$, are complex (even for a real optical potential) if there are several open channels and direct coupling is included in the calculation.

In the presence of direct channel coupling, these effects are especially difficult to disentangle. In any case the analysis of experimental data should be carried out by parameterizing the complex escape amplitudes $\gamma_{A,c}$ in Eq. (2.38) in terms of an asymmetry phase ϕ_c as defined by Eq. (2.42). The presence of ϕ_c leads to characteristic asymmetries in the cross sections (see Sec. 2.52). We now turn to a more detailed discussion of the asymmetry phase.

6.81 The Optical Asymmetry Phase

Recalling the separation of the escape amplitude into a direct part, $\gamma_{A,c}{}^{\mathrm{DIR}}$, and a compound part, $\gamma_{A,c}{}^{\mathrm{COMP}}$, we define the *optical phase* $\phi_c{}^{\mathrm{OPT}}$ by

$$\gamma_{A,c}{}^{\mathrm{DIR}} = \exp(i\phi_c{}^{\mathrm{OPT}})\,|\,\gamma_{A,c}{}^{\mathrm{DIR}}\,|. \tag{6.107}$$

The phase of the direct amplitude originates from the imaginary part of the optical potential and from the direct channel coupling [items (ii) and (iii), above].

It is also useful to define the difference between the phase of $\gamma_{A,c}$ and $\gamma_{A,c}{}^{\mathrm{DIR}}$. We call this difference $\delta\phi_c$ and write

$$\delta\phi_c = \phi_c - \phi_c{}^{\mathrm{OPT}}. \tag{6.108}$$

In most cases $\phi_c{}^{\mathrm{OPT}}$ is not large and we may note that $\delta\phi_c$ will also be small if $|\,\gamma_{A,c}{}^{\mathrm{COMP}}\,| \ll |\,\gamma_{A,c}{}^{\mathrm{DIR}}\,|$, which is true for most cases of interest. This implies that ϕ_c can have important contributions from both terms.

6.82 The Unitary Limit

We recall that the consideration of unitarity for the elastic S matrix, Eq. (2.41), in the form $|\,S(E)|^2 \leq 1$ for all E, led to the condition

$$\cos 2\phi_c \geq \exp(2\eta_c) - (\Gamma/\Gamma_{A,c})\sinh 2\eta_c, \tag{2.96}$$

which in the limit $\eta_c \to 0$, yields

$$\phi_c{}^2 \leq \eta_c[(\Gamma-\Gamma_{A,c})/\Gamma_{A,c}]. \tag{6.109}$$

Now one finds that $|\,S(E)|^2$ has a maximum at the energy

$$E_{\mathrm{MAX}} = E_R + \frac{[\Gamma\cos 2\phi_c - \Gamma_{A,c}\exp(2\eta_c)] + \{[\Gamma\cos 2\phi_c - \Gamma_{A,c}\exp(2\eta_c)]^2 + \Gamma^2\sin^2 2\phi_c\}^{1/2}}{2\sin 2\phi_c}. \tag{6.110}$$

As long as the phase ϕ_c lies in the interval $0 < \phi_c < \pi/2$ one finds $E_{\mathrm{MAX}} > E_R$. Since the p–n cross section is proportional to $[1-|\,S(E)|^2]$, the minimum of this cross section occurs at the energy E_{MAX}. Experimentally, one observes $E_{\mathrm{MAX}} > E_R$ and this is therefore in agreement with the general result for the calculated optical phases (Sec. 8), that they are positive and less than $\pi/2$.

6.83 Estimates of the Optical Asymmetry Phase

We recall the expression for the direct escape amplitude in the *absence of channel coupling*,

$$\gamma_{A,c}{}^{\mathrm{DIR}} = \exp(-\eta_c)\int_0^\infty \varphi_c{}^{(0)}(r)\,V_c{}^{A}(r)r^2\,dr. \tag{6.8}$$

Here the form factor is real, and the phase of the direct escape amplitude ϕ^{OPT} is due to the fact that the wave function $\varphi_c{}^{(0)}(r)$ is complex.

For isobaric analog resonances which occur well below the Coulomb barrier, the treatment of the imaginary part of the optical potential, iW, in Born approximation is indicated [Hü69]. Then to first order

TABLE 6.5. The different contributions to the asymmetry phase in radians. Direct channel coupling is neglected, and only the anti-analog state is considered for $\delta\phi$. The results are given for the analog states in Y^{89} (parent Sr^{89}).

State (energy)	ϕ^{OPT}	$\delta\phi$ [Eq.(6.112)] $\phi_{\bar{A}}{}^{R}$	$\phi_{\bar{A}}$	Total	ϕ	Unitarity limit (6.109)
$d_{5/2}$ (5.00 MeV)	+0.018	+0.0027	−0.0006	+0.002	0.020	0.03
$d_{5/2}$ (8.22 MeV)	+0.028	+0.0022	−0.0006	+0.0016	0.030	0.07
$s_{1/2}$ (5.99 MeV)	+0.031	+0.004	−0.001	0.003	0.034	0.05
$d_{3/2}$ (6.98 MeV)	0.025	+0.003	−0.001	0.002	0.027	0.045
$g_{7/2}$ (8.40 MeV)	0.020	+0.001	−0.0003	0.001	0.021	0.04

in W we find ($\tan\phi^{OPT}\sim\phi^{OPT}$)

$$\phi_c{}^{OPT}=\int_0^\infty\int_0^\infty \bar{G}_c{}^{(P)}(r,r')W(r')\bar{\varphi}_c{}^{(0)}(r')V_c{}^{A}(r)r^2r'^2\,dr\,dr'\Big/\left[\int_0^\infty \bar{\varphi}_c{}^{(0)}(r)V_c{}^{A}(r)r^2\,dr\right]. \tag{6.111}$$

In the equation $\bar{\varphi}_c{}^{(0)}(r)$ and the principle value Green's function, $\bar{G}_c{}^{(P)}(r,r')$, are evaluated with $W=0$; these are real quantities.

According to Eq. (6.111), the phase $\phi_c{}^{OPT}$ does not show a rapid energy dependence, since the penetration effects appearing in the wave function $\bar{\varphi}_c{}^{(0)}$ divide out. As an example, we show some optical phases in Table 6.5. One observes that $\phi_c{}^{OPT}$ is positive and small in all cases.

6.84 The Compound Phase

The contribution of the compound escape amplitude to the compound phase difference $\delta\phi_c$ [Eq. (6.108)] can be simply expressed in terms of the doorway quantities if

$$\gamma_{A,c}{}^{COMP}\ll\gamma_{A,c}{}^{DIR}$$

and all the phases are small. Then we have

$$\delta\phi_c=\sum_d \langle d\mid H\mid A\rangle/[(E_A-E_d)^2+\tfrac{1}{4}\Gamma_d{}^2]$$
$$\times(\Gamma_{d,c}/\Gamma_{A,c}{}^{DIR})^{1/2}(\phi_d+\phi_d{}^{R}-\phi^{OPT}) \tag{6.112}$$

with

$$2\pi\gamma_{d,c}{}^2=\Gamma_{d,c}\exp(2i\phi_d) \tag{6.113}$$

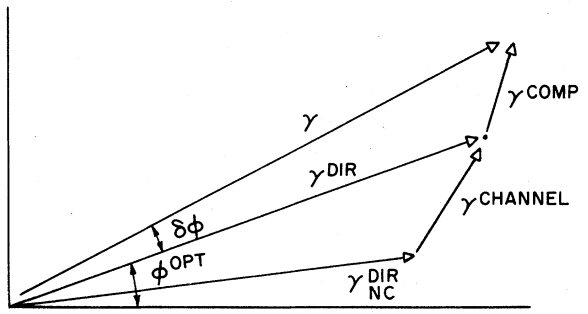

FIG. 6.7. The composition of the escape amplitudes considered as complex vectors. The phase of $\gamma_{A,c}{}^{DIR}$ is ϕ^{OPT}, and the phase of $\gamma_{A,c}$ is $\phi_c=\phi_c{}^{OPT}+\delta\phi_c$. [See Eqs. (6.95), (6.102), (6.107), and (6.108)].

and

$$\phi_d{}^{R}\simeq\Gamma_d/2(E_A-E_d).$$

In Table (6.5) we show the contribution to $\delta\phi_c$ for Sr^{89} arising from the antianalog state $|\bar{A}\rangle$. These contributions are very small. It is expected that contributions from the isovector monopole are larger.

Figure 6.7 summarizes the various amplitudes and their phases. Very few reliable experimental determinations of the asymmetry phase are available at present. Therefore it is not clear to us whether the optical phase accounts for most of the value of ϕ_c or whether the compound part contributes considerably. In general one can say that the ratio of the imaginary part to the real part is much larger for the compound part of the escape amplitude than for the direct part $\gamma_{A,c}{}^{DIR}$. Therefore, whenever $\gamma_{A,c}{}^{DIR}$ is particularly small, e.g., because of a small spectroscopic factor, the influence of the compound amplitude and direct channel coupling may be first seen in a modification of the asymmetry phase.

6.9 Forbidden Transitions

As we have seen from all of our previous discussion, the phenomenon of the isobaric analog resonance has its origin in isospin violations. The analog state energy shifts into the continuum and a particle escapes as a result of the average Coulomb field effects. Nevertheless, the normal escape amplitudes *do* have $\Delta T=0$ *as well as* $\Delta T=1$ parts because the isospin of the final configurations is not unique. The average Coulomb field, which mediates the escape, contributes to both these amplitudes. In this section we would like to discuss escapes which are weak due to the additional hindrance effect which arises when there *must* be a change in isospin during the transition. These are usually defined as *forbidden transitions*. There are three different kinds of forbidden escapes which are interesting to discuss.

(i) Neutron escape from a low-lying resonance. In this case the final nucleus always has dominant isospin

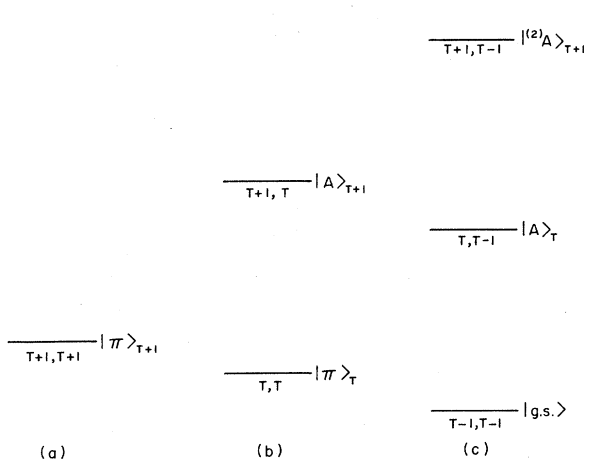

FIG. 6.8. Schematic representations of the multiplets containing the analog and the *double analog*. In (c) we indicate the ground state of a nucleus, an analog state and a *double analog*, denoted $|\,^{(2)}A\,\rangle_{T+1}$. In (b) we show the parent of the analog and a member of the multiplet containing the double analog. Finally in (a) we indicate the state of the double-analog multiplet with maximum T_z. In this figure we denote only the member of the multiplet with maximum T_z by the symbol π. As usual the state obtained by a single application of the operator T_- to a state $|\,\pi\,\rangle$ is written without a superscript, as $|\,A\,\rangle$.

of $(T'=T-\frac{3}{2})$ which cannot be obtained by coupling the neutron isospin $(1/2)$ to the analog state isospin (T). Neutron widths for such escapes in light nuclei have been seen in (γ, n) reactions [Be70] and with transfer reactions using He^3 beams [Ad69; Mc70].

(ii) Proton escape from a "double analog resonance". These arise from analog states which can be obtained by applying $(T_-)^2$ to a neutron rich parent with isospin $T+1$ (see Fig. 6.8). Except for the special case of $T+1=\frac{3}{2}$, the double analogs have an isospin which is *two* units greater than the ground state of the same nucleus. When the proton escapes to a low-lying state of the final nucleus with isospin $(T'=T-\frac{1}{2})$, we once more have a forbidden transition. Cases like this have been observed in light nuclei with $T=\frac{3}{2}$ and $T=2$ [Ad69; Ha69a; Mc69; Te69; Mc70].

(iii) Escape of composite particles with low isospin. When we consider the deuteron or alpha particle width of an analog resonance, we are always dealing with a forbidden transition because the isospin of the emitted particle is zero and the analog state has one unit of isospin more than the final nucleus. These have been seen in (d, p), (t, p), and (p, d) reactions [Ha67b; Ar68; Be68c; St68b] and in α decays following various transfer reactions in light nuclei. A survey is given in [Mc69].

6.91 Possible Mechanisms

We can see that possible mechanisms for all of these forbidden decays are already available in the general scheme of this section.

(*i*) *Direct Rearrangement* [*Sec.* 6.2]

The dominant mechanism for the allowed escape was the action of the averaged (single-particle) charge-changing field. This allows a neutron to escape as a proton [Fig. 6.2]. Clearly this mechanism cannot be used to emit a neutron or a composite particle. The matrix element which can lead to the emission of a neutron must come from the isospin-violating *nuclear* force which leads to a *two-body* charge-changing force, $V_N^{(-)}$. The effect of $V_N^{(-)}$ is to turn two neutrons into a neutron (which escapes) and a proton (which is bound). Note that this mechanism will not allow for deuteron escape because the final (np) deuteron is space and spin symmetric while the initial (nn) pair must be antisymmetric.

For the case of proton escape from a double analog, the two-body matrix element which enters is a *double* charge-changing force which turns two neutrons in the neutron rich parent [recall the role of $(T_-)^2$] into two protons. In general this leads to a small amplitude because it is not proportional to Z and in most cases *two* particles change orbit. This is so even though there are contributions to this amplitude from the Coulomb force as well as from the nuclear isospin-violating force. In fact, the two-body Coulomb matrix elements are much smaller than the nuclear ones because of the smooth nature of the *point-charge* Coulomb force. The finite-size effect in the Coulomb force will lead to an effect like that of a weak, charge-asymmetric nuclear force. Some calculations of the Coulomb matrix elements have been carried out [Ar69; Au71] and they lead to very small escape widths ($\sim$1 eV) compared to the experimental ones (50 eV$\rightarrow$2000 eV). As expected, the nuclear charge-asymmetry matrix elements give much larger numbers ($\sim$50 eV) but they are probably still too small [Au71; Mi71] to explain the magnitude of the experimental widths. The finite-size effect deserves further investigation.

(*ii*) *Compound Escape*

Forbidden transitions take place naturally through the compound escape mechanism because the dominant compound coupling matrix element always changes the isospin from T to $T-1$ [see Eqs. (6.12) and (6.6)]. For example, we may go through the configuration states or other $T-1$ compound modes. Nucleons can then escape by isospin-conserving nuclear mechanisms. For example, the configuration states can emit a neutron via an ordinary two-body nuclear matrix element. In the case of a double analog, the corresponding configuration states can emit a proton through a nuclear matrix element.

For the $T=\frac{3}{2}$ multiplets it has been found that this mechanism is large enough to account for the forbidden nucleon escapes [Au71]. Some of the strength associated with the monopole has been investigated in [Ar69] and shown to lead to a similar contribution;

however, collective effects in the monopole could reduce the result by an order of magnitude.

(iii) Channel Coupling

Forbidden escapes can occur very generally through the mechanism of channel coupling. We think of the following sequence. First an allowed proton escape occurs virtually, followed by an appropriate reaction amplitude for the virtual proton to produce the final state. This amplitude can be a (p, d) or (p, α) amplitude to produce a deutron or α particle, or a (p, n) or (p, p') reaction amplitude for the other forbidden reactions. The general expressions for this kind of mechnaism have been given in Sec. 6.7. They have been used [Pi69] for estimating deuteron widths with some success.

6.10 Summary

In this section we have studied the escape amplitude, $\gamma_{A,c}$, writing it as a sum of a *direct* and a *compound* term. In Sec. 6.2 we classified the various transitions that contribute to the direct amplitude, $\gamma_{A,c}{}^{\mathrm{DIR}}$, introducing single-particle and rearrangement amplitudes. (It is shown that the single-particle amplitudes are much larger than the rearrangement amplitudes, unless the relevant spectroscpic factors are particularly small).

Particularly important is the *elementary single-particle escape amplitude*, $(\gamma_{nlj})_{\mathrm{sp}}$ of Eq. (6.39). Of central importance for spectroscopic studies is the approximate relation,

$$\gamma_{A,c}{}^{\mathrm{DIR}} \simeq (S_{\lambda,n}{}^{\pi})^{1/2}(\gamma_{nlj})_{\mathrm{sp}}.$$

The calculation of $\gamma_{A,c}{}^{\mathrm{DIR}}$ for parent states expanded in elementary configurations is taken up in Sec. 6.4. It is related there to $(\gamma_{nlj})_{\mathrm{sp}}$ the elementary single-particle amplitude, for various elastic and inelastic transitions [see Eq. (6.51)]. The discussion of spectroscpic factors continues in Sec. 8.

Some further discussion of the rearrangement amplitudes is given in Sec. 6.5, and some results for these amplitudes are given in Table 6.3. The compound escape amplitude is discussed in Sec. 6.6, and the importance of the giant isovector monopole is stressed (see Sec. 6.62).

Some comments on channel coupling are made in Sec. 6.7, and the asymmetry phase is discussed in Sec. 6.8. Forbidden transitions are the topic of Sec. 6.9.

7. COMPOUND AND CONTINUUM WIDTHS AND ENERGY SHIFTS

In this section we are concerned with those effects which determine the position and width of the isobaric analog resonance. In Sec. 2 the general formula for these quantities was derived, Eqs. (2.27–2.28),

$$E_R - i(\Gamma/2) = \langle A \mid H \mid A \rangle + \langle A \mid \mathrm{H}G_P{}^{(+)}\mathrm{H} \mid A \rangle. \quad (7.1)$$

In Eq. (7.1), $\mathrm{H} = H + W$, with W given by Eq. (2.49). The larger term in Eq. (7.1), $\langle A \mid H \mid A \rangle$, appeared in the definition of the displacement energy, $E_d{}^{\mathrm{TOT}} = \langle A \mid H \mid A \rangle - E_\pi$, and was extensively discussed in Sec. 5. The other terms in Eq. (7.1) may be classified as follows. We define the *compound mixing* as

$$\langle A \mid W \mid A \rangle = \Delta^{\mathrm{COMP}} - i\Gamma^{\mathrm{COMP}}/2$$
$$= \sum_q \{ \langle A \mid H \mid q \rangle \langle q \mid H \mid A \rangle / [E - E_q + \tfrac{1}{2}(iI)] \}, \quad (7.2)$$

and the *continuum mixing* as

$$\Delta^{\mathrm{CONT}} - i\Gamma^{\mathrm{CONT}}/2 = \langle A \mid \mathrm{H}G_P{}^{(+)}\mathrm{H} \mid A \rangle. \quad (7.3)$$

The *total shift* and *total width* are then

$$\Delta = \Delta^{\mathrm{COMP}} + \Delta^{\mathrm{CONT}}, \quad (7.4)$$

and

$$\Gamma = \Gamma^{\mathrm{COMP}} + \Gamma^{\mathrm{CONT}}. \quad (7.5)$$

There is some similarity between what we call "compound mixing" and Robson's "internal mixing", [Ro65a], and also between the "continuum mixing" and his "external mixing". In R-matrix theory, the matching radius, which is somewhat larger than the nuclear radius, divides the *configuration space* into an internal region and an external one. In the shell-model theory of nuclear reactions [Ma69a] and in the formalism used here, the distinction is not made in configuration space but in *Hilbert space*. One distinguishes compound states $\{q\}$ and continuum states $\{P\}$. The states of $\{q\}$ in the energy region of interest (near the analog resonance) are essentially non-zero only in the "internal region" of R-matrix theory. Furthermore, in the case of analog resonances, the proton scattering states are well below the Coulomb barrier and hardly penetrate the internal region. Therefore a correspondence exists between compound and internal mixing on one hand and between continuum and external mixing on the other. There is some ambiguity in the separation into the two subspaces q and P. Although the important open channels should always be found in P and the compound states always in q, closed channels may be put either in q or in P. This ambiguity does not have any effect on the *sum* of the contributions from compound and continuum mixing which is the only observable quantity. In general, we will also have in P those channels which are closed at the particular energy we are considering but which have a threshold not too far away and are therefore of importance.

In some situations it is convenient to separate out components from the P space which are essentially bound, such as true bound states or single-particle resonances of $h(rr')$. These bound state components must then be added to the q space and this modifies the definition of "compound" and "continuum".

This procedure is especially useful if these components are important in forming specially correlated states. We have already seen this in the case of the antianalog [Sec. 6.6] which involves the component $u_{A,c}(r)$, projected from the analog state itself.

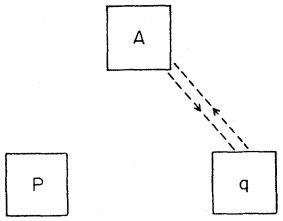

FIG. 7.1. Diagrammatic representation of the compound mixing.

Another important example of such a correlated state may be the giant isovector monopole collective mode constructed from neutron-hole proton-particle states in the parent. These have been discussed in Secs. 5.24 and 6.62. If the monopole strength is concentrated in a collective state at high excitation energy it may be necessary to project these components from the P space and include them in the compound space as special doorways.

7.1 The Compound Mixing

The compound mixing, Eq. (7.2), may be represented as in Fig. (7.1). The coupling of the analog state and the compound states takes place through the isospin-violating parts of H, so that Eq. (7.2) may be written

$$\Delta^{\mathrm{COMP}}-i\Gamma^{\mathrm{COMP}}/2=\mathrm{N}^{-1}$$
$$\times\sum_q\{\langle\pi\mid V^{(+)}\mid q\rangle\langle q\mid V^{(-)}\mid\pi\rangle/[E-E_q+\tfrac{1}{2}(iI)]\}, \tag{7.6}$$

where $V^{(-)}=[H, T_-]$, etc.

7.11 Sum Rules

Various methods may be used to estimate the size of Δ^{COMP} and Γ^{COMP}. For example one may write

$$\langle A\mid W\mid A\rangle=\mathrm{N}^{-1}$$
$$\times\{\langle\pi\mid V^{(+)}qV^{(-)}\mid\pi\rangle/[E-\bar{E}+\tfrac{1}{2}(i\bar{\Gamma})]\}, \tag{7.7}$$

where $\bar{E}-i\bar{\Gamma}/2$ is a suitable complex average energy defined such that closure is possible for the sum appearing in Eq. (7.6). When using closure in Eq. (7.6) special care has to be taken, since the closure $\langle\pi\mid V^{(+)}V^{(-)}\mid\pi\rangle$ would not only contain the effect of all states in q but also those in P and A. The P space has a complexity similar to the parent state and large *single-particle* matrix elements connect $\mid\pi\rangle$ with P. The states $\mid q\rangle$ (with few exceptions) are much more complex and *two-body* matrix elements connect $\mid\pi\rangle$ and $\mid q\rangle$.

If most of the matrix element strength arises from the monopole collective mode it may actually be sensible to include P and q together in a single space orthogonal to A. Then the total mixing is actually contained in the compound term. This can be done independent of how the breakup is made for the escape amplitudes.

As usual in this kind of problem, the average energy $\bar{E}-\frac{1}{2}i\bar{\Gamma}$ is difficult to estimate and usually one obtains a rough upper limit on the desired quantities. The method of sum rules has been used by Wigner [Wi66] and recently by Mekjian [Me70a] to evaluate the compound mixing.

7.12 Doorways

An alternative approach to the calculation of Eq. (7.6) is possible through the use of a shell-model description of the states $\mid q\rangle$ and $\mid\pi\rangle$. Special attention has to be paid to the requirement that the states $\mid q\rangle$ are eigenstates of the model Hamiltonian and that they are orthogonal to the analog state. Preferentially the states $\mid q\rangle$ would be obtained by diagonalizing suitable classes of states like $3p-2h$, $4p-3h$, etc. A first step in using the shell-model approach has been made by Beres [Be68d]. However, this approach seems unnecessarily complicated because we only require statistical information about the major part of the q space.

Probably, fairly reliable estimates of the compound mixing may be made if one uses the method of "doorway states" discussed in Sec. (2.4). One assumes that among the compound states $\mid q\rangle$, which are very complicated, there exist certain states, $\mid d\rangle$, which couple strongly to the parent state, $\mid\pi\rangle$ (see Fig. 7.2). In this approximation, one has

$$\Delta^{\mathrm{COMP}}-i\Gamma^{\mathrm{COMP}}/2=\mathrm{N}^{-1}$$
$$\times\sum_d\{\langle\pi\mid V^{(+)}\mid d\rangle\langle d\mid V^{(-)}\mid\pi\rangle/[E-E_{\mathrm{d}}+\tfrac{1}{2}(i\Gamma_{\mathrm{d}})]\}, \tag{7.8}$$

where the doorway-state approximation leads to the width Γ_{d} in the denominator of Eq. (7.8). The position E_{d} and the width Γ_{d} of the doorway states can sometimes be observed experimentally in reactions leading to the formation of $\mid d\rangle$ as a final or as a compound state. However, Γ_{d} is a function of the energy. In the expression (7.8), $\Gamma_{\mathrm{d}}(E)$ should be taken near $E=E_R$ and not at the doorway energy E_{d}. In general E will be rather different from E_R and therefore the observed width $\Gamma_{\mathrm{d}}(E)$ and the one needed for the evaluation of Eq. (7.3) may be rather different. However, as long as $\Gamma_{\mathrm{d}}(E_R)$ is comparable in magnitude to $\mid E_{\mathrm{d}}-E_R\mid$, the

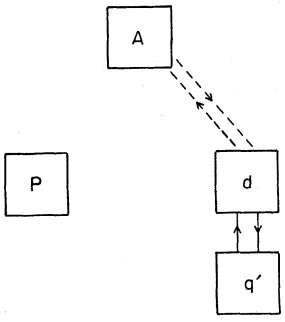

FIG. 7.2. Diagrammatic representation of the compound mixing using the doorway hypothesis.

TABLE 7.1. The magnitude of the compound mixing, Eq. (7.9), arising from the anti-analog, the circuit term in Eq. (7.16), and the continuum mixing proper, Eq. (7.21), are shown. The example chosen is Zr^{91} at $E=5$ MeV with the channel indicated in Column 1 assumed to be open. All quantities are in keV.

	Compound mixing		Circuit term		Continuum mixing proper		
	$\Delta^{\mathrm{COMP}}(E)$	$\Gamma^{\mathrm{COMP}}(E)$	$\Delta^{\mathrm{CIR}}(E)$	$\Gamma^{\mathrm{CIR}}(E)$	$\tilde{\Delta}^{\mathrm{CONT}}(E)$	$\tilde{\Gamma}^{\mathrm{CONT}}(E)$	$\tilde{\Gamma}^{\mathrm{ABS}}(E)$
$s_{1/2}$	1.4	0.6	2.8	−0.6	−62.7	40.6	7.6
$d_{3/2}$	0.6	0.2	1.6	+1.6	−40.7	14.5	4.6
$d_{5/2}$	<0.1	<0.1	0.5	<0.1	−34.6	9.2	5.45
$g_{7/2}$	<0.1	<0.1	−0.5	<0.1	−14.0	2.1	1.97

compound width

$$\Gamma^{\mathrm{COMP}}=\mathrm{N}^{-1}\sum_{\mathrm{d}}\Gamma_{\mathrm{d}}\times\{\langle\pi\mid V^{(+)}\mid d\rangle\langle d\mid V^{(-)}\mid\pi\rangle/[(E_R-E_{\mathrm{d}})^2+(\tfrac{1}{2}\Gamma_{\mathrm{d}})^2]\} \tag{7.9}$$

is rather insensitive to Γ_{d}. Each term in the sum Eq. (7.9) has a very broad maximum as a function of Γ_{d} at the value $\Gamma_{\mathrm{d}}=2\mid E_R-E_{\mathrm{d}}\mid$. Using this maximal value for Γ_{d}, Eq. (7.9) reduces to

$$\Gamma^{\mathrm{COMP}}\leq\mathrm{N}^{-1}\times\sum_{\mathrm{d}}[\langle\pi\mid V^{(+)}\mid d\rangle\langle d\mid V^{(-)}\mid\pi\rangle/\mid E_R-E_{\mathrm{d}}\mid]. \tag{7.10}$$

If the doorway states $\mid d\rangle$ have strong single-particle components, their spreading widths are of the order of several MeV, and Eq. (7.10) should be a good approximation. The problem in the doorway-state approach consists in finding the right doorway states, i.e., those which exhaust most of the strength of the interaction of $\mid\pi\rangle$ with $\mid q\rangle$. In their study of the compound mixing in Sr^{89}, de Toledo Piza *et al.* [Pi66] found the important doorway states to be the anti-analog state, the other configuration states, and the giant-dipole resonance. The doorway-state technique has also been used to estimate the compound mixing from isospin-violating nuclear forces [Me69]. These contributions have all given rather small values for the upper limit, $\Gamma^{\mathrm{COMP}}\simeq 1-5$ keV. Some values for Δ^{COMP} and Γ^{COMP} obtained from including only the anti-analog state as an important doorway are given in Table 7.1. The results presented in this table are for parent states of single-particle character.

However it is likely that a very important contribution arises from the giant-monopole doorway referred to above. The construction of this doorway requires important components of the P space because these P-space states are of the character of proton–particle, neutron–hole states in the parent. Therefore it probably *is* the best strategy to include everything orthogonal to A in the discussion of the monopole. In this case the estimate of the complex energy, Eq. (7.1), is completely given by the $(T-1)$ monopole $\mid M\rangle$, i.e.,

$$\Delta-i(\Gamma/2)\simeq(2T)^{-1}\times\{\langle\pi\mid V^{(+)}\mid M\rangle\langle M\mid V^{(-)}\mid\pi\rangle/[E_A-E_M+\tfrac{1}{2}(i\Gamma_M)]\}. \tag{7.11}$$

Using Eq. (6.87) and (6.90) we have

$$\Delta-i\frac{\Gamma}{2}\simeq\left(\frac{2T-1}{2T+1}\right)\times\frac{150(z^2/A)}{\{-(170/A^{1/3})+i\Gamma_M(E_A)/2\}+[110(T+1)/A]}\ \mathrm{keV}, \tag{7.12}$$

where we have used the approximate form

$$(2T)^{-1}\sum_{nlm}(n+l+\tfrac{3}{2})(n+1)\sim 3.5A^{1/3} \tag{7.13}$$

which is good when T is large.

Using the fact that $\Gamma_M\ll 2(E_M-E_A)$ we have

$$\Delta\simeq-\left(\frac{2T-1}{2T+1}\right)\frac{150(Z^2/A)}{\{(170/A^{1/3})-[110(T+1)/A]\}}\ \mathrm{keV} \tag{7.14}$$

and

$$\Gamma\simeq\left(\frac{2T-1}{2T+1}\right)\Gamma_M(E_A)\times\frac{150(Z^2/A)}{\{(170/A^{1/3})-[110(T+1)/\mathrm{A}]\}^2}\ \mathrm{keV}. \tag{7.15}$$

It is expected that $\Gamma_M(E_A)$ is approximately constant throughout the periodic table just as in the case of the gaint-dipole resonance. However $\Gamma_M(E_A)$ will tend to increase because the analog is moving closer to E_M as we go through the perodic table. For example, in Sr^{88}, $\Delta\simeq-80$ keV, $\Gamma\simeq 2.7\Gamma_M(E_A)$ keV, and in Pb^{208}, we have $\Delta\simeq-300$ keV and $\Gamma\simeq 16\Gamma_M(E_A)$ keV, where $\Gamma_M(E_A)$ is in MeV. It is difficult to be sure of the values of $\Gamma_M(E_A)$, but if a reasonable value of 4 MeV is taken for Sr^{88} we have $\Gamma\sim 10$ keV. To obtain the correct total width for Pb^{208} we would need a value of $\Gamma_M(E_A)\sim$ 12 MeV which seems somewhat large. The hydrodynamic estimate [Bo67] for the matrix element would

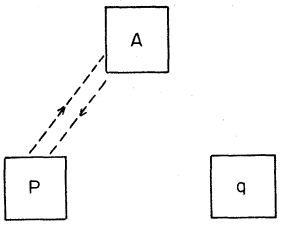

FIG. 7.3. Diagrammatic representation of the continuum mixing proper.

reduce these results further (possibly by a factor of 2) so that it is probably necessary to take some explicit continuum effects into account. This is especially true for the odd nuclei where the properties depend on the state of the last particle.

7.2 The Continuum Mixing

Even though there is not a unique choice as to which part of the space (orthogonal to A) is most profitably included in the continuum (P space), the general structure of the continuum mixing is similar. The formal expressions of this section do not depend on this choice; however, the physical approximations which can be made do depend on the separation. For example, if the monopole is dominant, this implies strong channel coupling between the various ($J=0$) proton–particle neutron–hole channels. If this channel coupling is neglected, the continuum mixing leads to very large shifts and widths (Sec. 8). Explicit channel coupling can be sometimes avoided by projecting from the P space that part which is involved in the coupling and transferring it into the q space. The remainder of the P space would then exhibit weak channel coupling. An example of this procedure is to include only the elastic channel in the P space when dealing with odd isotopes.

This procedure assumes that the dominant contribution to the total width from the inelastic channels, in an odd nucleus, is that calculated in Sec. (7.12) for the monopole. Then the rest of the total width comes from the continuum mixing of the last particle.

In general, the continuum mixing defined in Eq. (7.3) is somewhat complicated as it contains the interaction of the analog state with the scattering states as well as the modification of the analog state due to the compound states. In coordinate space, the effect of the compound nucleus is included in the complex analog state form factor, Eq. (2.35), so that

$$\Delta^{\mathrm{CONT}}-i(\Gamma^{\mathrm{CONT}}/2)=\sum_{cc'}\int r^2\,dr\int r'^2\,dr' \times \mathrm{V}_c^{A}(r)\,\mathrm{G}_{cc'}{}^{(+)}(r,r')\,\mathrm{V}_{c'}^{A}(r') \quad (7.16)$$

where

$$\mathrm{V}_c^{A}(r)=V_c^{A}(r)+V_c^{A,\mathrm{COMP}}(r). \quad (7.17)$$

Equation (7.17) in conjunction with Eq. (6.12) defines the *compound form factor*. Using this definition, we may decompose the continuum mixing into three parts which are independent of, linear in, and quadratic in $V_c^{A,\mathrm{COMP}}(r)$, respectively. The three terms are represented in Figs. 7.3–7.5. We will call these terms, the *continuum mixing proper*, $\tilde{\Delta}^{\mathrm{CONT}}-i\tilde{\Gamma}^{\mathrm{CONT}}/2$, the *continuum circuit mixing*, $\Delta^{\mathrm{CIR}}-i\Gamma^{\mathrm{CIR}}/2$, and the *continuum round-trip mixing*, $\Delta^{\mathrm{RT}}-i\Gamma^{\mathrm{RT}}/2$. These terms are presented in order of descending importance.

To estimate the size of the second two terms we may again use the doorway hypotenesis for the q space. The doorway escape form factors and the direct analog form factors are not very different in magnitude [Eqs. (6.80) and (6.93)]. Therefore, each of the successive terms in Eq. (7.16) is smaller than the previous by the ratio

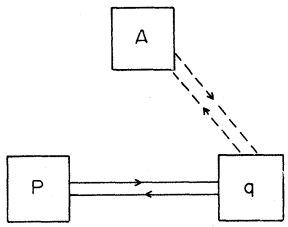

FIG. 7.5. Diagrammatic representation of the round-trip continuum mixing. The solid lines indicate coupling through the strong interaction.

$\langle A \mid H \mid d\rangle/(E_A-E_d+i\Gamma_d/2)$, which may take values between about one-tenth to one-one hundredth. Since the circuit term is already rather small (see Table 7.1) we need not discuss the round-trip term.

7.21 *The Continuum Mixing Proper and Absorption Width*

We define the *continuum mixing proper* by

$$\tilde{\Delta}^{\mathrm{CONT}}-i\tilde{\Gamma}^{\mathrm{CONT}}/2=\langle A \mid H(E^{+}-\mathrm{H}_{PP})^{-1}H \mid A\rangle \equiv \sum_{cc'}\int r^2\,dr\int r'^2\,dr' \times V_c^{A}(r)\,\mathrm{G}_{cc'}{}^{(+)}(rr')\,V_{c'}^{A}(r'). \quad (7.18)$$

It is useful to divide $\tilde{\Gamma}^{\mathrm{CONT}}$ into two parts

$$\tilde{\Gamma}^{\mathrm{CONT}}=\tilde{\Gamma}^{\mathrm{ABS}}+\sum_{c}\Gamma_{A,c}{}^{\mathrm{DIR}}, \quad (7.19)$$

where $\Gamma_{A,c}{}^{\mathrm{DIR}}$ is the direct escape width for channel c defined in analogy to Eq. (2.42),

$$\exp(2i\phi_c^{\mathrm{OPT}})\,\Gamma_{A,c}{}^{\mathrm{DIR}}=2\pi(\gamma_{A,c}{}^{\mathrm{DIR}})^2. \quad (7.20)$$

In Eq. (7.20) use has also been made of the *optical phase* defined in Eq. (6.107). The sum in Eq. (7.19) is

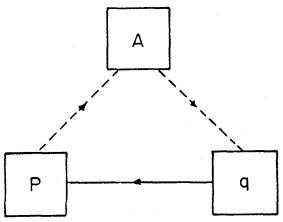

FIG. 7.4. Diagrammatic representation of the circuit continuum mixing. The solid line indicates coupling through the strong interaction.

over the open channels, elastic or inelastic, which one decides to include in the P space. The quantity $\Gamma^{\rm ABS}$, as defined, goes to zero with the imaginary part of the optical potential. This quantity represents the effect of the compound nucleus on the continuum width and describes absorption into channels which have not been explicitly included in the P space. Expressions for $\Gamma^{\rm ABS}$ and the sum of the direct escape widths may be obtained by separating the Green's function of Eq. (7.18) into a principal value part (PV) and an "on-shell" part. This represents a separation into real and imaginary parts of the Green's function only in special circumstances since the presence of an imaginary term in the optical potential will cause the principal value integrals to be complex. In this manner one finds

$$\tilde{\Gamma}^{\rm ABS}=\sum_c \Gamma_{A,c}^{\rm DIR}[\exp(2\eta_c)\cos 2\phi_c^{\rm OPT}-1]$$
$$-2\,\mathrm{Im}\sum_{cc'}\Big[\mathrm{PV}\int_0^\infty\int_0^\infty V_c^A(r)$$
$$\times G_{cc'}^{(+)}(r,r')V_{c'}^A(r')r^2r'^2\,dr\,dr'\Big]. \quad (7.21)$$

If we again neglect channel coupling, the double channel sum in Eq. (7.21) reduces to a single sum and in this case we have

$$\tilde{\Gamma}^{\rm ABS}=\sum_c \tilde{\Gamma}_{A,c}^{\rm ABS}. \quad (7.22)$$

In an entirely similar fashion one may also write

$$\tilde{\Delta}^{\rm CONT}=\sum_c \tilde{\Delta}_c^{\rm CONT}, \quad (7.23)$$

and

$$\tilde{\Gamma}^{\rm CONT}=\sum_c \tilde{\Gamma}_c^{\rm CONT}, \quad (7.24)$$

with the obvious definitions for $\tilde{\Delta}_c^{\rm CONT}$ and $\tilde{\Gamma}_c^{\rm CONT}$. It is also worth noting that the expression for the continuum mixing, Eq. (7.13)), has the same form as Eq. (7.18) except that H is replaced by H.

7.22 *Independent Single-Particle Channels vs Channel Coupling*

In almost all cases of interest many channels are open and a detailed description of the inelastic processes requires a knowledge of the structure of the residual nucleus in its excited states.

We may attempt to understand how the inelastic channels contribute to the continuum mixing by using a simple model. We start with the even–even *parent* and assume the channel processes involve the escape of a neutron without rearrangement. This escape leaves the system in a neutron–hole state of angular momentum j. We make the simplifying assumption that the hole strength is concentrated at the shell model position. In this simple-model the contributions of the channels to the continuum widths, shifts and absorption are readily calculated in terms of single-particle parameters defined by

$$\tilde{\Gamma}_{lj}^{\rm CONT}=\tilde{\Gamma}_{lj}^{\rm ABS}+\Gamma_{lj}^{\rm sp}. \quad (7.25a)$$

The *single-particle escape width* is defined as

$$\exp(2i\phi_{lj}^{\rm OPT})\,\Gamma_{lj}^{\rm sp}=2\pi(\gamma_{lj})^2_{\rm sp}, \quad (7.25b)$$

with a *single-particle absorption width*

$$\tilde{\Gamma}_{lj}^{\rm ABS}=\Gamma_{lj}^{\rm sp}[\exp(2\eta_{lj})\cos 2\phi_{lj}^{\rm OPT}-1]$$
$$-2\,\mathrm{Im}\Big[\mathrm{PV}\int_0^\infty\int_0^\infty V_{nlj}(r)\,G_{lj}^{(+)}(r,r')$$
$$\times V_{nlj}(r')r^2r'^2dr\,dr'\Big], \quad (7.26)$$

and a *single-particle continuum shift*

$$\tilde{\Delta}_{lj}^{\rm CONT}=\tfrac{1}{2}\Gamma_{lj}^{\rm sp}\exp(2\eta_{lj})\sin 2\phi_{lj}^{\rm OPT}$$
$$+\,\mathrm{Re}\Big[\mathrm{PV}\int_0^\infty\int_0^\infty V_{nlj}(r)\,G_{lj}^{(+)}(r,r')$$
$$\times V_{nlj}(r')r^2r'^2\,dr\,dr'\Big]. \quad (7.27)$$

Here $V_{nlj}(r)$ is the single-particle form factor, Eq. (6.26), and $G_{lj}^{(+)}(r,r')$ is the P space Green's function calculated in the absence of direct-channel coupling.

In this case, the total continuum shift is

$$\tilde{\Delta}^{\rm CONT}(E_R)=\sum_{l'j'}(2j'+1)\,\tilde{\Delta}_{l'j'}^{\rm CONT}(E^{l'j'}), \quad (7.28)$$

and the total absorption width is

$$\tilde{\Gamma}^{\rm ABS}(E_R)=\sum_{l'j'}(2j'+1)\,\tilde{\Gamma}_{l'j'}^{\rm ABS}(E^{l'j'}). \quad (7.29)$$

Here $E^{l'j'}$ is the escape energy for the hole state $(l'\,j')$ in the target,

$$E^{l'j'}=E_R-E_h^{l'j'}, \quad (7.30)$$

and $E_h^{l'j'}$ is the excitation energy of the hole state.

We shall see in Sec. 8 that this sum (7.29) gives a very large value for the total width of analog resonances in closed-shell nuclei. We have already remarked in Sec. 7.11 that the probable solution to this lies in the fact that there may be large channel coupling between these neutron-hole channels leading to collective states like the giant monopole.[31] As mentioned previously, it may be a better first approximation to place the collective mode in the q space. However, for the case of parent nuclei with a few valence neutrons it is probably more appropriate to carry the channels corresponding to valence neutron escape in the form of continuum mixing effects. This is in fact the basis of the calculations for escape amplitudes in Sec. 6. There the coupling of the

[31] This would show up as a giant resonance in the $J=0$ channel and should be measurable in the proper experiments. For example, this mode would show up as a resonance near 35 MeV in the excitation function of the $(p,\ e^+e^-)$ process on Pb^{207}. The monopole transition producing the (e^+e^-) pair would go to the analog state of Pb^{208} in the compound Bi^{208} with an energy $(E_M-E_A)\simeq 20$ MeV.

valence neutrons to the "core" monopole was included in the compound escape.

Thus we expect the expressions for single-particle continuum mixing effects Eqs. (7.25) to (7.29) to be useful with the appropriate restrictions on the summations $(l'j')$. In an odd neutron parent we might include only the term from the *single* odd neutron, which would then appear without the factor $(2j'+1)$. In Table 7.1 we have given some values for the single-particle valence orbits in Zr^{91}, including the small effects of the circuit correction due to the anti-analog only.

We note at this point that the evaluation of the single-particle quantities in this model requires the knowledge of the optical model parameters in the energy region, $0<E\leq E_R$. There is a further difficulty in that the phenomenological optical model parameters are usually obtained for the case in which the P space contains only the elastic proton channel. Our approximations therefore lead to a significant uncertainty in the specification of the optical model parameters, particularly for the imaginary part of the potential. An additional uncertainty arises from the coupling of the valence particles with the neutron holes which renders the channel energy for the simple model somewhat uncertain.

8. APPLICATION TO VARIOUS REGIONS OF THE PERIODIC TABLE AND EXTRACTION OF SPECTROSCOPIC FACTORS

8.1 Introduction

In this section we will discuss some applications of the theory given in the previous sections. In Sec. 5 we have discussed the effects which determine the displacement energy and have seen how knowledge of this quantity enables us to obtain information concerning the distribution of excess neutrons. Here we will present examples of calculations of other resonance parameters: the escape widths, absorption widths, continuum shifts, asymmetry phases, etc. We will compare the calculated and experimental quantities and extract spectroscopic factors for some states. The spectroscopic factors will be compared to those obtained from stripping or pickup reactions. These are not intended to be the ultimate calculations, but should be understood as an exploration of the scheme itself and as an examination of the sensitivity to various parameters.

The extraction of spectroscopic factors requires accurate values of the single-particle escape widths. In a number of papers, the escape widths defined in other approximations have been considered and the reliability of the extraction of spectroscopic factors from isobaric analog experiments has been investigated [Za67; Bu68, 70; Ha68a, b; Th68; Ha69b]. The situation is not quite clear and single-particle escape widths as calculated according to the different prescriptions differ considerably [Ha69b]. (Most authors stress the role of the optical potential as a major source of uncertainty in the extraction of spectroscopic factors). Before presenting results for this quantity it is valuable to note the various approximations used in our calculations.

The results presented in this chapter include those for the *single-particle escape width*, $\Gamma_{lj}^{\rm sp}$, defined by Eq. (7.25b) in terms of the single-particle escape amplitude extensively discussed in Sec. 6. We neglect all isospin-violating forces other than the Coulomb force and we also neglect direct channel coupling. Thus $(\gamma_{lj})_{\rm sp}$ is given by Eq. (6.38) or Eq. (6.39) and includes direct and exchange contributions. The direct contribution to Eq. (6.39) is the dominant one and is expressed by the simple one-dimensional integral of Eq. (6.40)

$$(\gamma_{nlj})_{\rm sp}=\frac{\exp(-\eta_{lj})}{(2T)^{1/2}}\int_0^\infty \varphi_{E,lj}^{(0)}(r)\,V_c(r)\,\varphi_{nlj}(r)\,r^2\,dr. \tag{6.40}$$

In the evaluation of this expression, the one-body Coulomb field, $V_c(r)$, is determined from the empirical charge density of the target nucleus. The continuum wave, $\varphi_{E,lj}^{(0)}(r)$, is determined from an empirical local optical potential.[32] The bound neutron wave function, $\varphi_{nlj}(r)$, is obtained from the Saxon-Woods potential, the depth of the potential being chosen to reproduce the binding energy of the orbit. The radius of the neutron potential well is fixed by using information obtained from the study of displacement energies.

Spectroscopic factors are obtained from the relation

$$S_{lj}=\Gamma_{lj}^{\rm expt}/\Gamma_{lj}^{\rm sp}, \tag{8.1}$$

where the single-particle widths are calculated with the approximations discussed above and include both direct and exchange Coulomb contributions. Various improvements on this calculation could be made. For example, corrections due to proton finite size and vacuum polarization may be included. Also, the various isospin-violating terms considered in the calculation of the displacement energy contribute to the escape widths. These corrections were calculated in some cases and the results presented in Table 6.2. As we have seen, they are always small.

We may also note that for the results presented in this section, we neglect the compound contribution to the escape amplitude. As noted before, these contributions may be important for those states having particularly small spectroscopic factors. The modification of the escape width and spectroscopic factors due to the inclusion of the compound amplitude arising from the coupling of the analog state to special doorway states was discussed in Sec. 6.6 and some results given in Table 6.4.

[32] The continuum optical wave function is made orthogonal to the neutron bound states using the procedure discussed in detail in Appendix 1 and summarized in Sec. 2. It should also be orthogonal to the proton occupied states. This latter point was checked and the corresponding corrections were very small.

In general, we may say that the uncertainties introduced by the use of the empirical optical model and the neglect of direct channel coupling[33] are probably greater than those arising from the neglect of compound amplitudes and from isospin-violating forces other than the Coulomb interaction. We note, however, that the strong channel coupling to the monopole components has usually been included in the compound term, and this is probably the largest effect there (Sec. 6.6).

In addition to the single-particle escape widths, we have also included in this section numerical results for the other quantities defined in Sec. 7.2. These include the optical phase, $\phi_{lj}^{\rm OPT}$, [Eq. (7.25b)], the single-particle continuum shift $\tilde{\Delta}_{lj}^{\rm CONT}$, [Eq. (7.27)], and the single-particle absorption width $\tilde{\Gamma}_{lj}^{\rm ABS}$, [Eq. (7.26)]. In the evaluation of the principal value integrals we have again only considered the contributions to the form factors from the Coulomb force. We must be careful to include in the single-particle form factors, $V_{nlj}(r)$, the density matrix factors, $(1-\rho)$, which appeared in Eq. (6.36). If these factors are neglected we obtain some spurious contributions to the principal value integral due to propagation in *occupied* bound orbitals. In the simplest approximation[34] we therefore write for the single-particle form factors

$$V_{nlj}(r)=(2T)^{-1/2}\int_0^\infty\left[\frac{\delta(r-r')}{rr'}-\sum_{n'}\varphi_{n'lj}(r)\varphi_{n'lj}(r')\right]\times V_c(r')\varphi_{nlj}(r')r'^2\,dr'(1-\alpha_{\rm exch}),\quad(8.2)$$

where the sum on n' is over the *occupied* bound proton orbits. In Eq. (8.2) the small exchange contribution to the form factor has been included approximately by a coefficient, $\alpha_{\rm exch}$, which is the ratio of the exchange term to direct term as found in the calculation made for the escape widths. The form factors of Eq. (8.2) are used in the evaluation of $\tilde{\Delta}_{lj}^{\rm CONT}$ and $\tilde{\Gamma}_{lj}^{\rm CONT}$. In practice one obtains $\tilde{\Gamma}_{lj}^{\rm ABS}$ from $\tilde{\Gamma}_{lj}^{\rm CONT}$ by subtracting $\Gamma_{lj}^{\rm sp}$ [Eq. (7.25a)].

Some results are given for nuclei with $N=50$, $N=82$, and $N=126$. The information is contained in a set of figures (Figs. 8.2–8.33); these figures may be used for neighboring nuclei[35] by correcting the factors Z^2 and $(2T)^{-1}$ and considering Coulomb barrier effects.

After a brief section concerning the comparison of the energy-dependent resonance parameters contained in the theoretical expressions to the experimental (constant) ones, we discuss in some detail the regions with $N=126$, $N=82$, and $N=50$.

[33] Recent calculations indicate that the neglect of channel coupling to quadrupole vibrations is a very good approximation for vibrational nuclei such as strontium [Co70].

[34] The expression in square brackets in Eq. (8.2) represents the density matrix factor $(1-\rho)$ in the approximation that the target state is a single Slater determinant. In this case we have the well known relation $\rho^2=\rho$, so that $(1-\rho)^2=(1-\rho)$. This allows us to use $(1-\rho)$ in Eq. (8.2) instead of the factor $(1-\rho)^{1/2}$ which appears in the exact expression.

[35] Of course we must also keep track of the dependence of these quantities on the radius of the single-particle potentials used for $\varphi_{nlj}(r)$ and $\varphi_{Elj}^{(0)}$.

8.2 Energy Dependence of the Resonance Parameters

In the general reaction theory presented here, the T matrix is given in terms of energy dependent parameters. For example, for elastic scattering we have from Eq. (2.40),

$$T_{00}^{A}=\frac{\exp[2i\delta(E)]}{2\pi}\,\frac{\exp[2i\phi_0(E)]\Gamma_0(E)}{E-E_R(E)+\frac{1}{2}[i\Gamma(E)]}.\quad(8.3)$$

Now, experiments are usually analyzed using a T matrix of the same form as Eq. (8.3) but with constant resonance parameters. In this section we wish to relate the experimentally obtained resonance parameters to the energy-dependent ones we have used in formulating our theory. To do this we make a linear approximation [Bu70]

$$\begin{aligned}\Gamma_0(E)&=\Gamma_0(E_R)+\epsilon\Gamma_0'(E_R),\\ \phi_0(E)&=\phi_0(E_R)+\epsilon\phi'(E_R),\\ E_R(E)&=E_R(E_R)+\epsilon E'(E_R),\\ \Gamma(E)&=\Gamma(E_R)+\epsilon\Gamma'(E_R),\qquad \epsilon=(E-E_R),\end{aligned}\quad(8.4)$$

where the prime indicates the derivative with respect to energy. We will assume that the energy dependence of $\delta(E)$ and $T^{\rm OPT}(E)$ is taken into account in the experimental fitting procedure. Thus the T matrix used in the fit to experimental data would have the form

$$T_{00}^{\rm expt}=T_{00}^{\rm OPT}(E)+\{\exp[2i\delta(E)]/2\pi\}\times\{\exp(2i\phi_0)\,\Gamma_0/[E-E_R+\tfrac{1}{2}(i\Gamma)]\},\quad(8.5)$$

where ϕ_0, Γ_0, E_R, and Γ are constants.[36] To lowest order in the primed quantities, we find the following relations between the parameters of Eqs. (8.3) and (8.5):

$$\Gamma\simeq\Gamma(E_R)[1+E_R'(E_R)],\quad(8.6)$$

$$E_R\simeq E_R(E_R)-\Gamma(E_R)\,\Gamma'(E_R)/4,\quad(8.7)$$

$$\phi_0\simeq\phi_0(E_R)-\tfrac{1}{4}[\Gamma'(E_R)]-\tfrac{1}{4}[\Gamma(E_R)][\Gamma_0'(E_R)/\Gamma_0(E_R)],\quad(8.8)$$

and

$$\Gamma_0\simeq\Gamma_0(E_R)[1+\phi'(E_R)\,\Gamma(E_R)+E_R'(E_R)].\quad(8.9)$$

As an example, we estimate the corrections for the $g_{9/2}$ resonance in $Pb^{208}(p,p)Pb^{208}$. We have

$$\begin{aligned}\Gamma_0'(E_R)&\simeq 4\times10^{-3}\\ \Gamma'(E_R)&\simeq 10^{-2}\\ E_R'(E_R)&\simeq 2.5\times10^{-2}\\ \phi'(E_R)&\simeq 0.05[\text{MeV}^{-1}].\end{aligned}\quad(8.10)$$

[36] When one converts the energy-dependent Breit–Wigner term, Eq. (8.3), into an energy-independent one like Eq. (8.5), there appears a term which is constant in energy. Although it depends on the resonance parameters, it is usually lumped into the background T matrix, $T_{00}^{\rm OPT}$, computed by an optical potential.

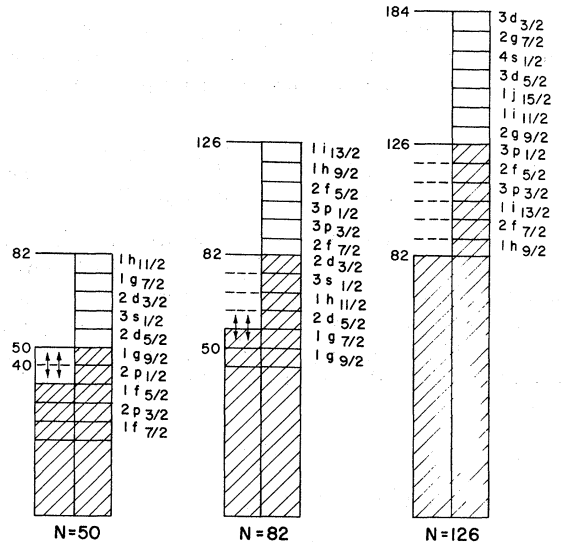

FIG. 8.1. Proton and neutron orbits in the regions, $N=50$, $N=82$, and $N=126$. The shaded areas denote the filled orbits.

The corrections are

$$\Gamma_0 \simeq (1+0.02)\,\Gamma_0(E_R),$$
$$\Gamma \simeq (1+0.03)\,\Gamma(E_R),$$
$$E_R \simeq E_R(E_R) - 0.4[\text{keV}],$$
$$\phi_0 \simeq \phi_0(E_R) - 0.01, \qquad (8.11)$$

which are all small.

8.3 Isobaric Analog Resonances in the Lead Region

We have already emphasized that the elastic and inelastic scattering of protons has become a powerful tool in studying the nuclear structure of the parent state. An important advantage of the isobaric analog studies over other reactions (such as stripping or pick-up) is the possibility of determining the parentage relations between the parent state and various target states.[37] This feature of the IAR experiments has been widely exploited in the lead region. From the experimental results and the knowledge of the parent state wave function, it has been possible to study and sometimes construct the wavefunctions of the various target states [An66; Br66; Ka66; Mo67a; Za67; Bo68; Gr68; Le68; Ri68; St68a, b; Za68; Fi69; Ma69b; Ri69; St69].

In order to perform such delicate analyses it is necessary to know the theoretical parameters determining the isobaric analog resonance, in particular, the single-particle escape width. In the present section, we exhibit the parameters characterizing the analog resonances in the lead region. We then make use of the calculated parameters to show how spectroscopic information is extracted from the experimental data.

8.31 *The Structure of the Lead Region*

The nuclei in the lead region may be described with respect to Pb^{208}. This nucleus is a good example of a doubly closed shell. The 44 excess neutrons occupy the following single-particle states: $1h_{9/2}$, $2f_{7/2}$, $1i_{13/2}$, $3p_{3/2}$, $2f_{5/2}$, and $3p_{1/2}$ (see Fig. 8.1). The low-lying excited states of Pb^{208} are of $1p$-$1h$ nature.

The low-lying states in Pb^{209} form a "good" single-particle spectrum. The positive parity states $2g_{9/2}$, $1i_{11/2}$, $3d_{5/2}$, $4s_{1/2}$, $2g_{7/2}$, and $3d_{3/2}$ have spectroscopic factors close to one. The exception is the $1j_{15/2}$ state, the only one with negative parity, for which S is significantly smaller than 1, about 0.5 or 0.6 [Au 69c, Ig 69b]. The single-particle $j_{15/2}$ state is most probably mixed with particle-plus-core states obtained by coupling a positive parity single-particle state to the $I=3^-$ vibrational state. At energies above 5 MeV one expects to see the single-particle states of the next shell ($N>184$) of negative parity, namely the $1k_{17/2}$, $2h_{9/2}$, etc. This single-particle strength is probably significantly spread because of the dense spectrum of compound states appearing at these energies.

The low-lying spectrum of Pb^{207} is of single-hole nature [Mu62]. Except for the $i_{13/2}$ state, all the holes are of negative parity. Other low-lying states of positive parity include a doublet, $J=7/2^+$ and $J=5/2^+$, at about 2.6 MeV. These two states have been described in terms of a $p_{1/2}$ hole coupled to the 3^- (2.76 MeV) vibrational state in Pb^{208} [Ha67a]. At somewhat higher energies many other states are observed. Most of them are of more complicated nature, such as $2h$-$1p$ or $3h$-$2p$ etc. Some of these may be described in simpler terms as particles coupled to vibrational states. Among these there are states which have large components $|\,Pb^{206}{}_{gs}\otimes j\rangle$ where j stands for the single-particle states $g_{9/2}$, $d_{5/2}$, etc. of the $126<N\leq 184$ shell. The spectroscopic factors obtained in (d, p) or (p, p) experiments for these levels are considerably smaller than one. The spreading of the single-particle strength is due to the proximity of other $2h$-$1p$ states, in particular the particle-plus-core states such as $|\,2^+\otimes j\rangle$ [Au68a].

8.32 *Analog Experiments in the Lead Region*

The elastic scattering Pb^{208} (p, p) Pb^{208} clearly shows seven single-particle isobaric analog resonances whose parents are states in Pb^{209}. From these experiments the escape width, Γ_{lj}, and total width, Γ, have been extracted [see Table 8.1]. The extraction of these parameters from experiment is usually difficult in this region because of the large total width of the resonances as compared with their spacings, and because the

[37] In reactions such as stripping or pickup, only the parentage of the ground state of the target and the parent system are studied.

TABLE 8.1. Escape widths and spectroscopic factors for the particle and hole states in Pb^{208}. The analog resonances are observed at proton energies E_R and have an escape width Γ_{lj}. The single-particle values, Γ_{lj}^{sp}, are read from the graphs, Figs. 8.2 and 8.3. The calculated spectroscopic factors, $S_{pp}=\Gamma_{lj}/\Gamma_{lj}^{sp}$, are compared with those from (d, p) and (t, d) reactions.

lj	E_R[MeV][a]	Γ_{lj} [keV][b]	Γ_{lj}^{sp} [keV]	S_{pp}	S_{dp} [c]	S_{dp} [d]	S_{td} [e]
				Particles			
$d_{3/2}$	17.48	46±15	64	0.72±0.25	1.1	0.99	0.83
$g_{7/2}$	17.43	36±15	33	1.1±0.5	1.0	1.04	0.90
$s_{1/2}$	16.96	48	74	0.65	1.0	0.97	0.86
$d_{5/2}$	16.50	58±10	62	0.94±0.15	1.0	1.06	0.86
$j_{15/2}$	16.34	(1)	1.2	(0.8)	1.2	1.38	0.60
$i_{11/2}$	15.72	2±1.6	0.8	2.5±2	1.2	1.52	1.05
$g_{9/2}$	14.92	19.6±0.8	20.5	0.96±0.04	0.9	0.88	0.93
lj	E_R [MeV][f]	Γ_{lj} [keV][h]	Γ_{lj} [keV][i]	Γ_{lj} [f]	Γ_{lj}^{sp}	S_{pp} [j]	S_{dt} [k]
				Holes			
$p_{1/2}$	11.49	33	25±4	28.0±1.4	27	1.04±0.05	1.06
$f_{5/2}$	10.92	3	≤3	4.2±0.5	4.7	0.90±0.11	1.10
$p_{3/2}$	10.59	11	10±3	15.8±0.9	16.5	0.96±0.06	0.91
$i_{13/2}$	9.74[g]	...	...	...	<0.001	...	0.98
$f_{7/2}$	9.15	...	...	0.6±0.1	0.53	1.1±0.2	0.76
$h_{9/2}$	8.06[g]	...	...	...	<0.001	...	1.0

[a] [Wh68].
[b] [Za68], [Ma69b], [Fi69].
[c] [Au69c] this reference gives averaged values from [Cr68], [Mu62], and [Mu67].
[d] From subCoulomb stripping [Do67].
[e] [Ig69b].
[f] [Br68].
[g] Extrapolated values using [Mu67].
[h] [An66].
[i] [Le68].
[j] Calculated with the Γ_{lj} from [Br68].
[k] [Mu67].

precise determination of the parameters necessitates the analysis of the interference with the background. For these reasons, very good statistics are needed and the experimentally determined Γ_{lj} have large uncertainties.

The isobaric analog resonances in Bi^{209} have partial widths for emitting a proton with the quantum numbers of the excess core neutrons leading to particle–hole states in Pb^{208}. This process is indicated in Fig. 6.5. Each single-particle analog will decay to all those particle–hole states in Pb^{208} possessing configurations which contain that particle. This process was discussed in Sec. 6.42, and Eq. (6.58) provides the relation between the amplitude for the escape to the particle–hole final state and the single-particle escape amplitudes for the core neutrons. In a series of *inelastic* proton scattering experiments, the excitation function to the different excited states of Pb^{208} (target) have been measured. The target states which are expected to have large components $[(j, p_{1/2}^{-1})_I$, $(j, p_{3/2}^{-1})_I$ or $(j, f_{5/2}^{-1})_I]$ indeed show prominant resonance behavior in their excitation functions. Penetrabilities of the outgoing protons, in some cases, are too small to observe the corresponding hole configurations (e.g., $h_{9/2}^{-1}$, $i_{13/2}^{-1}$). Some of the experiments were thoroughly analyzed and an attempt has been made to determine the wave function of the core states [Bo68; Wh68; Ri69].

Another possibility for studying the excited states in Pb^{208} is to find *their* analogs by means of elastic and inelastic scattering on Pb^{207}. For example, in the elastic channel one studies the $(p_{1/2}^{-1}, j)$ configurations in Bi^{208}. (The case of odd-neutron targets has been discussed in Sec. 6.43.) This possibiity has been exploited by a few experimental groups [e.g., Le68]. Some of the inelastic channels are of two-hole one-particle nature because of the escape of one of the core neutrons. These include target states which can be described as one hole coupled to a particle-hole vibration. Again, because of the penetrability, only escape of the $3p_{1/2}$, $2f_{5/2}$, $3p_{3/2}$ particles was observed.

In addition, if the particle–hole states in the parent are mixed (for example, the 3^- vibration), we can have inelastic scattering to the single-hole states by emission of $g_{9/2}$, $j_{15/2}$, and $i_{11/2}$ particles. The isobaric analog resonances have proved to be especially useful in establishing the validity of the particle-plus-core model. The (p, p') experiments in the $N=50$ and $N=82$ region have revealed that certain states in even–odd nuclei may be described in terms of a weak coupling of particle to a core state. The experiments in the lead region are even more striking in this respect. In particular, excitation functions of the collective octupole state $I=3^-$ in Pb^{208}, Pb^{206}, and Pb^{204} all show a very similar spectrum corresponding to a weak-coupling model based on this state. The particle–core coupling model has also been used for states built upon the quadrupole vibrational state ($I=2^+$) in Pb^{206}. A general result emerging from the isobaric analog studies is that the first $I=2^+$ vibrational state is most responsible for

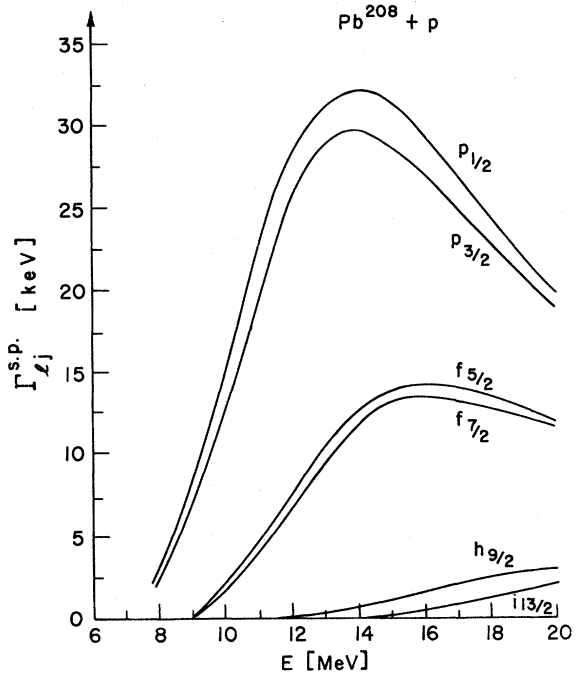

FIG. 8.2. The single-particle escape widths for the neutron (hole) orbits of lead. The optical potential used is that of Becchetti [Be69].

the fragmentation of the low-energy single-particle strength [St68a; St69].

8.33 Calculation of Resonance Parameters

In order to determine the structure of the nuclear states from the study of isobaric analog resonances it is essential to have precise theoretical values of various quantities which parameterize the T matrix. In particular, in order to determine the amplitudes of various configurations, it is necessary to know the single-particle escape width [defined in Eq. (7.25b)]. As we have seen, (Sec. 8.1), this quantity depends on the choice of the neutron bound-state wave function and the optical potential used to determine the continuum wave. The neutron wave functions are calculated in a Saxon–Woods potential whose radius is determined from the study of the Coulomb displacement energies. In the case of the optical potential, it would be desirable to have a potential appropriate to the nucleus being studied and determined at the appropriate energies. In most cases such a potential is not available and in the calculations reported here we have used the potential of Becchetti and Greenlees [Be69]. This potential is obtained by fitting a wide range of nuclei, $40 \leq A \leq 210$, in the energy region $10 \leq E \leq 40$ MeV. It is characterized by an energy dependent strength

$$V_R = 54.0 - 0.32E + 0.4Z/A^{1/3} + 24.0(N-Z)/A,$$

with radius and diffuseness parameters of $r_R = 1.17$ and $a_R = 0.75$. The imaginary part is of volume plus surface type. The strength of the volumn term is $W_R = 0.22E - 2.7$ or 0, whichever is greater. For the surface term we have $W_{SF} = 11.8 - 0.25E + 12.0(N-Z)/A$ or zero, whichever is greater. The potential also has a spin–orbit term of the usual form.

We emphasize that this potential is an average one and it does not provide an exact fit to the off-resonance data in Pb^{209}. This deficiency introduces significant uncertainties in the calculation of some of the parameters, particularly those which are sensitive to the imaginary part of the potential. (The latter is only poorly determined in the usual optical model analysis.)

8.331 The Single-Particle Excape Width. The *single-particle escape widths* have been calculated for most of the neutron orbits in lead. The escape widths for the hole orbits are presented in Fig. 8.2 and those for the particle orbits in Fig. 8.3. The results are presented as a function of the escape energy, E. The widths exhibit a characteristic behavior, increasing with energy as the Coulomb and centrifugal barriers are penetrated and decreasing after that point. The figures may be used to obtain escape widths for both elastic and inelastic decays. For example, if we consider the lowest isobaric analog resonance in Bi^{209} (the $g_{9/2}$ resonance at about 15 MeV), then Fig. 8.3 will provide the single-particle

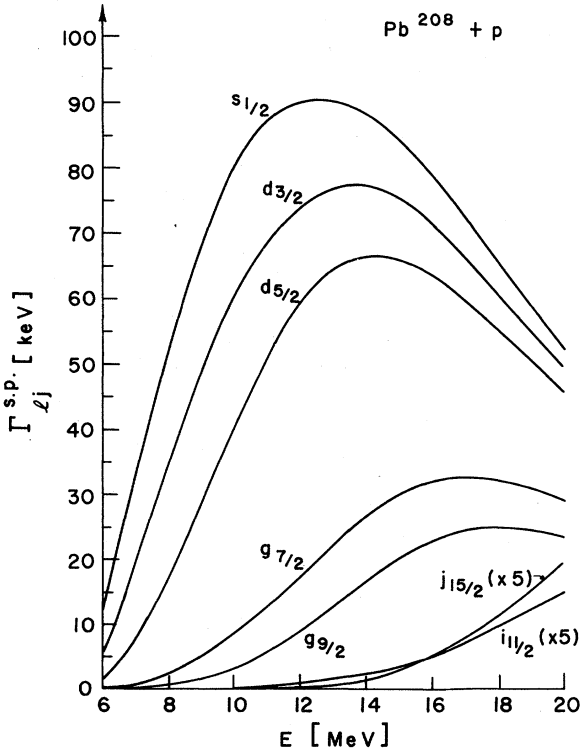

FIG. 8.3. The single-particle escape widths for the neutron (particle) orbits of lead. {Potential: [Be69]}.

widths (modified by appropriate coupling factors) for the decay to excited $1p$–$1h$ states in Pb^{208} up to about 9 MeV excitation.

8.332 The Continuum Absorption Width. The *single-particle width* was defined in Eq. (7.26) and has been calculated for the particle and hole orbits in lead. The results are shown in Fig. (8.4) and Fig. (8.5). The measurable quantity is the total width given by Eq. (7.1). This quantity is composed of the compound width and the continuum width, as in Eq. (7.5).

We have noted that the particular separation into continuum and compound parts depends on the importance of the monopole mode. We have seen in Sec. 7.2 that it is probably only useful to use the single-particle continuum absorption width for a few extra particles or holes relative to the closed shell at Pb^{208}. The total width is then approximated by that for Pb^{208} plus (or minus) the continuum contribution from the particles (or holes).

8.333 The Continuum Shift. The continuum shift, Δ^{CONT}, was defined in Eq. (7.3). Of course the same remarks apply here as for the width. We present the *single-particle continuum shift*, defined in Eq. (7.27), for the hole and particle orbits in lead [Fig. (8.6) and Fig. (8.7)].

As a function of energy, the single-particle continuum shifts exhibit similar behavior in all the regions studied. The shifts are negative well below the Coulomb barrier and become positive at higher energies. The zeros of $\tilde{\Delta}_{lj}^{\text{CONT}}$ correspond roughly to the maxima in the single-particle escape widths and are shifted to higher energies with increasing l.

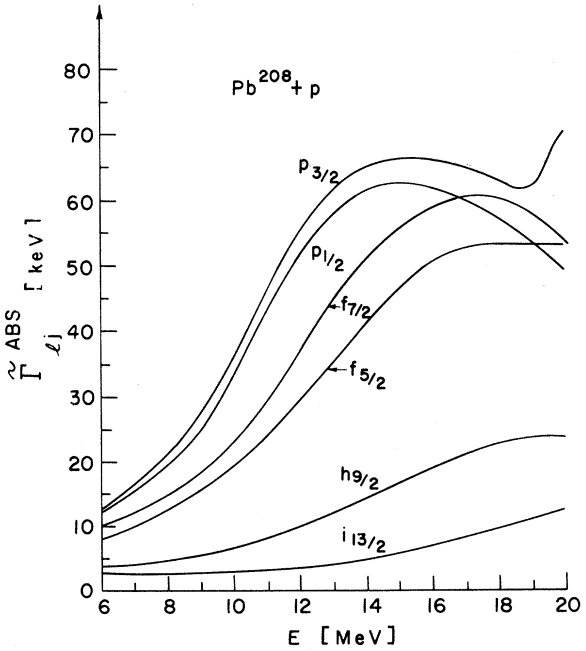

FIG. 8.4. The single-particle absorption widths for the neutron (hole) orbits of lead. {Potential: [Be69]}.

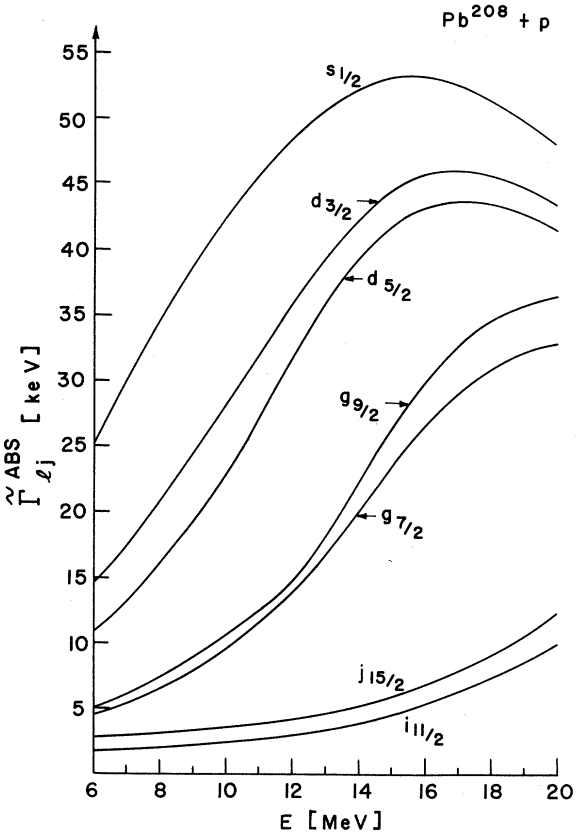

FIG. 8.5. The single-particle absorption widths for the neutron (particle) orbits of lead. {Potential: [Be69]}.

Superficially, $\tilde{\Gamma}_{lj}^{\text{CONT}}$ and $\tilde{\Delta}_{lj}^{\text{CONT}}$ exhibit resonance behavior with a large width. This seems to be roughly at the right energy for the next shell of proton single-particle orbits, although there are large shifts. However, inspection of the behavior of the phase shift and the proton wave function inside the nucleus does not show any simply interpretable resonance behavior. This is probably a result of the combined effects of the Coulomb barrier penetration and the large imaginary potential.

8.334 The Optical Phase, Scattering Phase Shift, and Absorption Parameter. In addition to the parameters discussed thus far in this section, we have also calculated the optical phase defined in Eq. (6.107). It is in most cases the dominant part of the asymmetry phase ϕ. The optical phase is directly related to the magnitude of the imaginary part of the optical potential and uncertainties in this imaginary part reflect themselves in uncertainties in ϕ^{OPT}. Results for the optical phase are given in Figs. (8.8) and (8.9) for lead.

The scattering phase shift, $\delta_{lj}+i\eta_{lj}$, defined in Eq. (2.30), has also been calculated. The results are

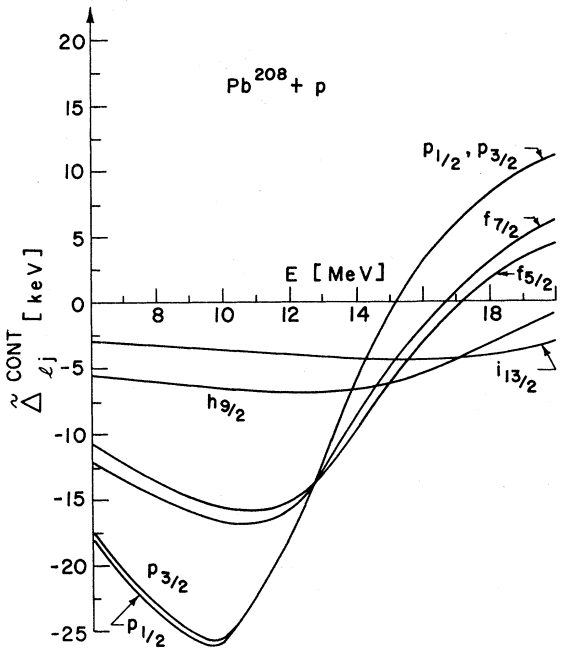

FIG. 8.6. The single-particle continuum shift for the neutron (hole) orbits of lead. {Potential: [Be69]}.

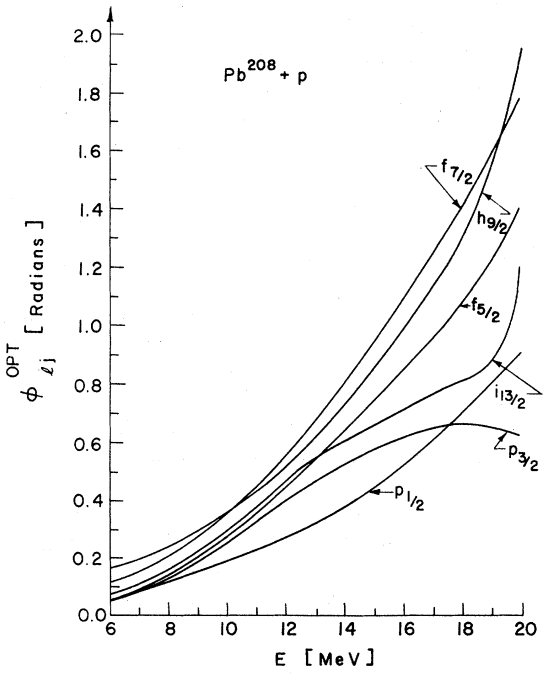

FIG. 8.8. The optical phase for the neutron (hole) orbits of lead. {Potential: [Be69]}.

presented for the nuclear phase, $\delta_{lj}^{NUCL}=\delta_{lj}-\sigma_l$, where the Coulomb phase, σ_l, has been subtracted from δ_{lj} to define δ_{lj}^{NUCL}. Figures (8.10) and (8.11) exhibit this quantity for lead.

Finally, the imaginary part of the phase shift due to the optical scattering, η_{lj}, has been obtained. The

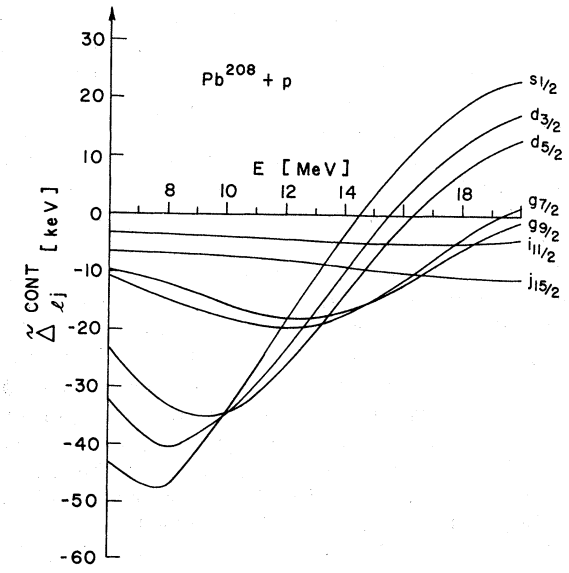

FIG. 8.7. The single-particle continuum shift for the neutron (particle) orbits of lead. {Potential: [Be69]}.

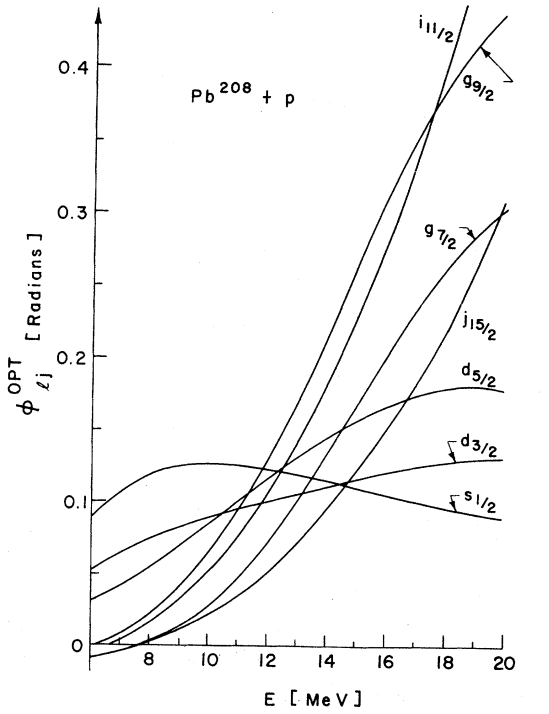

FIG. 8.9. The optical phase for the neutron (particle) orbits of lead. {Potential: Be69]}.

results are presented for the quantity $[1-\exp(-2\eta_{lj})]$ in Figs. (8.12) and (8.13) for lead. As in the case of $\Gamma_{lj}^{\mathrm{ABS}}$ and ϕ_{lj}^{OPT}, the values of η_{lj} are uncertain due to significant uncertainties in the determination of the imaginary part of the optical potential.

8.34 Comparison of the Calculated Parameters with Experiments

In spite of the very large number of isobaric analog experiments performed in the lead region, the number of resonant parameters determined from the experiment is rather limited. The large total width as compared with the resonance spacings does not always allow for unambiguous determination of parameters such as the escape widths and total widths.

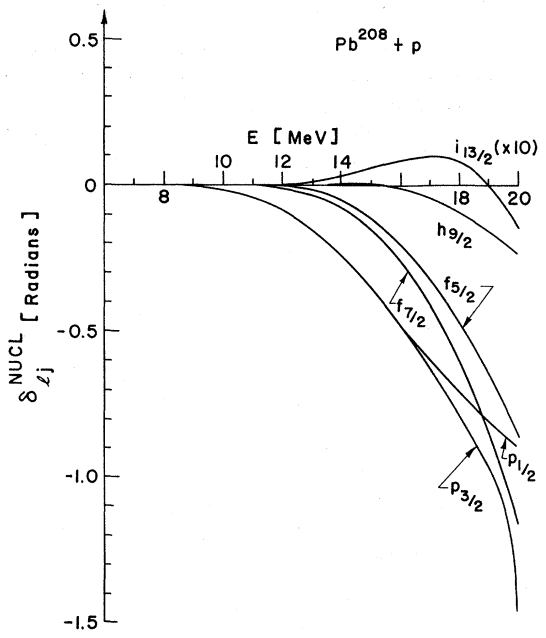

FIG. 8.10. The nuclear optical phase shift, $\delta_{lj}^{\mathrm{NUCL}} \equiv \delta_{lj} - \sigma_l$, for the neutron (hole) orbits of lead. {Potential: [Be69]}.

8.341 Escape Widths and Spectroscopic Factors. Parameters known with quite reasonable accuracy are the escape widths of the $p_{3/2}$, $f_{5/2}$, $p_{1/2}$, and $f_{7/2}$ orbits in Pb^{208} at certain energies. The measurements of the different experimental groups are very consistent and the values obtained are nearly the same. The experiments consist in elastic and inelastic proton scattering on Pb^{207}. The resonances excited are the analogs of the ground and excited states of Pb^{208}. Looking at the analog of the ground state of Pb^{208} and its elastic and inelastic decays to the low-lying states of Pb^{207}, the single-particle escape widths are deduced. The assumption made is that the ground state of Pb^{208} is a good closed shell and that the low-lying states of Pb^{207} are pure single-hole states. This assumption is very consistent with other experiments and theoretical investigations. The experimental results are given in Table 8.1 and compared with our calculations. The spectroscpic factors which are calculated using the theoretical single-particle widths are in all cases compatible with a spectroscpic factor of unity. This is also found to be the case in the (d, t) reaction [Mu67]. Since the errors are of the order of 10% (except for $f_{7/2}$), the agreement is quite satisfactory. In Table 8.2 several ratios of escape widths for the decay of the analog of the Pb^{208} ground state are listed. The experimental values have rather small errors, and for some of the ratios the theoretical values lie definitely outside the experimental errors. Part of this disagreement may be due to the spectroscopic factors not being unity. However, there is some disagreement (outside the error) between the measurements of [Br68] and [Ig69a].

TABLE 8.2. A comparison of various ratios of escape widths for the decay of the analog of the Pb^{208} ground state. The experimental values are taken from [Ig69a]. The calculated values assume factors proportional to $(2j+1)$ as in Sec. 6.43.

Ratio	Experiment	Theory
$\Gamma_{f\,5/2}/\Gamma_{p\,1/2}$	0.36±0.04	0.52
$\Gamma_{p\,3/2}/\Gamma_{p\,1/2}$	1.14±0.07	1.22
$(\Gamma_{f\,5/2}+\Gamma_{p\,3/2})/\Gamma_{p\,1/2}$	1.50±0.08	1.74
$\Gamma_{f\,5/2}/\Gamma_{p\,3/2}$	0.3±0.04	0.43
$\Gamma_{f\,7/2}/\Gamma_{p\,1/2}$	$\leq$0.08	0.08

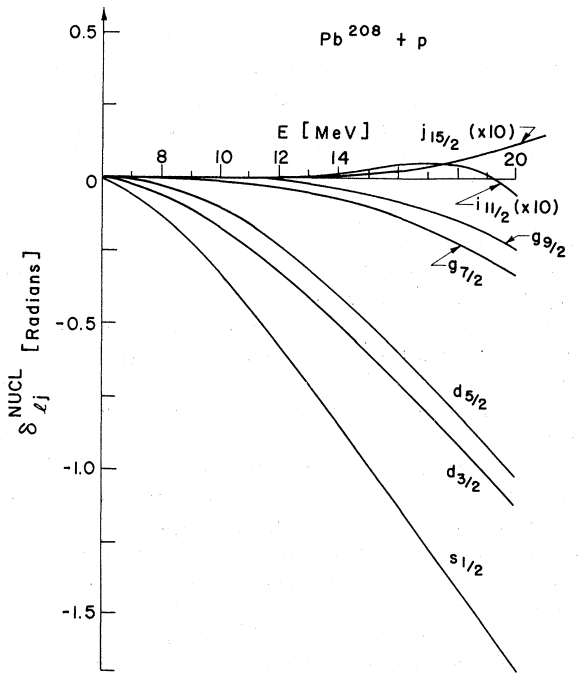

FIG. 8.11. The nuclear optical phase shift, $\delta_{lj}^{\mathrm{NUCL}} \equiv \delta_{lj} - \sigma_l$, for the neutron (particle) orbits of lead. {Potential: [Be69]}.

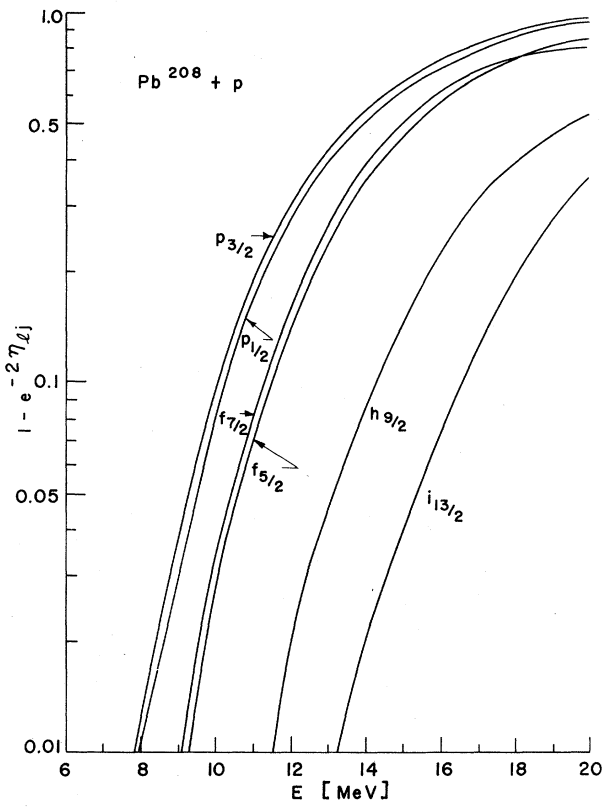

FIG. 8.12. The absorption parameter for the neutron (hole) orbits of lead presented in the form $[1-\exp(-2\eta_{lj})]$. {Potential: [Be69]}.

The escape widths for the particle orbits have been measured in the elastic scattering of protons on Pb^{208}. Here the experimental situation is much less favorable and the values obtained for the escape widths have large errors. This is especially true of the almost degenerate $d_{3/2}$ and $g_{7/2}$ resonances at energy of about 17.5 MeV. For these reasons a comparison of the data with the theoretical results is not conclusive. Nevertheless, the experimental and theoretical spectroscopic factors in Table 8.1 are not inconsistent. The experimentally well established value for the $g_{9/2}$ resonance agrees very well with the calculation. More experimental work is required in order to make a more meaningful comparison.

Within the assigned errors, and within the errors in the spectroscopic factors as determined from the (d, p) and (t, d) reactions, the spectroscopic factors from analog experiments are compatible with unity as well as with the results of other experiments.

8.342 Partial Absorption Widths. The total width of an isobaric analog resonance can be measured rather accurately, especially by considering inelastic reactions proceeding through the resonance. The total widths for the resonances in Bi^{209} are given in the second column of Table 8.3. The third column gives the experimentally determined escape widths for the elastic channel.

Now we may use experimental knowledge of the total width of the analog resonance in Bi^{208}, whose parent is the ground state of Pb^{208} [$\Gamma(Pb^{208}\ \text{gs}) = 230 \pm 10$ keV [Br68]], to extract partial absorption widths for the various particle orbits.[38] According to the discussion in Secs. 7.22 and 8.332 we use the expression

$$\Gamma(Pb^{209}; lj) = \Gamma_{lj}^{sp} + \tilde{\Gamma}_{lj}^{ABS} + \Gamma(Pb^{208}; \text{gs}), \quad (8.12)$$

where (lj) refers to the valence nucleon. In Eq. (8.12) we have identified the *core contribution* to the total widths of the Bi^{209} state (parent: Pb^{209}) with the total width of the Bi^{208} state (parent: Pb^{208}, ground state). Thus the partial absorption widths as extracted from the experimental data, are

$$\tilde{\Gamma}_{lj}^{ABS} = \Gamma(Pb^{209}; lj) - \Gamma_{lj}^{sp} - \Gamma(Pb^{208}; \text{gs}). \quad (8.13)$$

In these equations we are assuming that the spectroscopic factors are unity, so that escape widths and the partial absorption widths are identified with the corresponding single-particle quantities. The partial absorption widths obtained in this simple way are

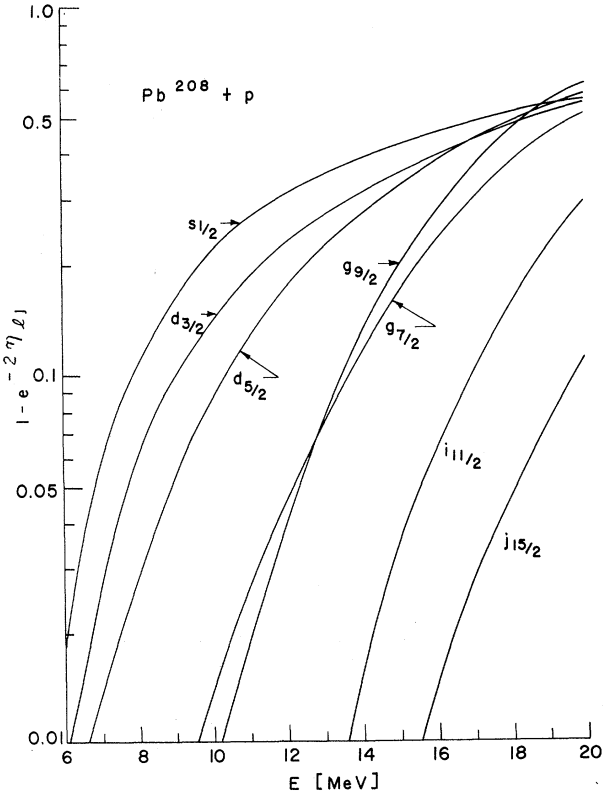

FIG. 8.13. The absorption parameter for the neutron (particle) orbits of lead presented in the form $[1-\exp(-2\eta_{lj})]$. {Potential: [Be69]}.

[38] In this section we will label the total widths, Γ, by the parent of the analog state giving rise to the resonance.

compared in Table 8.3 with the theoretical single-particle absorption widths. Within the rather large experimental uncertainties there is rough agreement between theoretical and experimental values for the partial absorption widths. Since the absorption width is essentially proportional to the imaginary part of the optical potential, the magnitude of the imaginary potential used [Be69] seems reasonable (to within factors of 2 or 3) at the energies at which the theoretical $\tilde{\Gamma}_{lj}^{\mathrm{ABS}}$ have been determined, about 15–20 MeV.

8.343 Total Widths. We now turn to a discussion of the total width of the analog state in Bi^{208} (parent: Pb^{208}, gs). Now the total width, as well as the escape widths associated with the various excess neutron orbits, are known experimentally. Therefore we may determine the *total absorption width* by subtracting from the total width the sum of the experimentally determined escape widths taken with their appropriate statistical weights.

In order to show that the channel coupling between the proton–particle, neutron–hole channels is really important we have calculated the total absorption width by summing the single-particle terms for *all* the excess neutron holes [see formula Eq. (7.29)]. We refer to this as the *independent channel calculation.* The result of the calculation is presented in Table 8.4. The calculated total absorption width, $\Gamma_{\mathrm{calc}}^{\mathrm{ABS}}=659$ keV, exceeds the one extracted from the experimental data ($\Gamma_{\mathrm{expt}}^{\mathrm{ABS}}\simeq 80\pm 20$ keV) by about a factor of 8. We also recall that this calculation of Γ^{ABS} involved rather specific assumptions, especially in the assignment of the energy arguments for the escape widths of the excess neutron orbits [see Eq. (7.30)]. Clearly, our choice of the inelastic channel energies introduces some uncertainty in the calculation of Γ^{ABS}. The actual one-particle one-hole strength is spread over a certain energy interval. However, in order to reduce the calculated width, Γ^{ABS}, by even a factor of 2 it is necessary to place a considerable amount of $1p$–$1h$ strength at very high excitation energies. Such spread of strength is rather inconsistent with various measurements. Theoretical calculations also indicate that the spread of the $1p$–$1h$ strength is not large enough to make it possible to reduce the absorption width significantly.

TABLE 8.3. Comparison of experimental and calculated values for the partial absorption width $\Gamma_{lj}^{\mathrm{ABS}}$ for the analog states in Bi^{209}. The experimental values for $\tilde{\Gamma}_{lj}^{\mathrm{ABS}}$ are obtained from

$$\tilde{\Gamma}_{lj}^{\mathrm{ABS}}=\Gamma-\Gamma_{lj}-\Gamma(\mathrm{Pb}^{208};\ \mathrm{gs}),$$

where Γ is the observed total width for each analog level (lj) and $\Gamma(Pb^{208}\ \mathrm{gs})=230+10$ [Br68] is the observed width of the lowest analog resonance in Bi^{208}. (All widths in keV).

	Experiment				Calc
lj	E_R[MeV] [a]	Γ [a]	Γ_{lj} [b]	$\tilde{\Gamma}_{lj}^{\mathrm{ABS}}$	$\tilde{\Gamma}_{lj}^{\mathrm{ABS}}$
$d_{3/2}$	17.48	280±20	46±15	<30	46
$g_{7/2}$	17.43	290±20	36±15	25±25	30
$s_{1/2}$	16.96	320±15	48±15	40±25	53
$d_{5/2}$	16.50	310±15	58±10	20±15	28
$j_{15/2}$	16.34	200±25	~0	<25	7
$i_{11/2}$	15.72	220±20	2±1.6	<25	5
$g_{9/2}$	14.92	250±10	19.6±0.8	<15	23

[a] [Wh68].
[b] See Table 8.1.

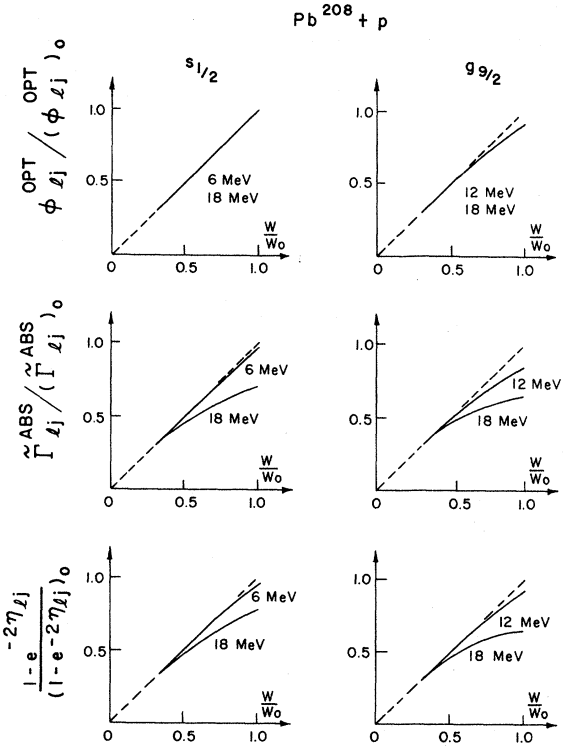

FIG. 8.14. The dependence of the optical phase, single-particle absorption width, and the absorption parameter on the strength of the imaginary part of the optical potential, W. The zero subscripts refer to the values obtained for the optical potential of Becchetti [Be69].

It is possible to reduce the independent channel absorption width by changing of the imaginary part of the optical potential. We have already mentioned that the optical potential used here is an average one, chosen to reproduce only the general features of the scattering data for a wide range of nuclei and energies. This particular calculation of Γ^{ABS} is sensitive to W and requires an accurate knowledge of the optical potential, particularly at low energies.

We have investigated the dependence of the parameters $\tilde{\Gamma}_{lj}^{\mathrm{ABS}}$, ϕ_{lj}^{OPT}, and $[1-\exp(-2\eta_{lj})]$ on the strength of the imaginary part of the optical potential. The results are shown in Fig. (8.14). There the quantities with subscript zero refer to the values calculated with the imaginary part of the optical potential as given by Becchetti [Be69]. The shape and the energy dependence of the Becchetti potential were kept fixed and only the strength of the imaginary part was varied

TABLE 8.4. Independent channel calculation of the total absorption width for the ground state resonance in Bi^{208}. The proton escape widths Γ_{lj} are taken from experiment (Table 8.1). The values for the calculated partial absorption widths are read from Fig. 8.4. Since the experimental total width of the Pb^{208} resonance is $\Gamma=230\pm10$ keV [Br68], the total experimental absorption width is $\Gamma^{ABS}=\Gamma-\Sigma g\Gamma_{lj}=80\pm20$, which has to be compared with a calculated value of 659 keV. All widths appearing in the Table are in keV.

Holes lj	E_R [MeV]	Γ_{lj}	$\tilde{\Gamma}_{lj}^{ABS}$	Statistical weight, g	$g\cdot\Gamma_{lj}$	$g\cdot\tilde{\Gamma}_{lj}^{ABS}$
$p_{1/2}$	11.49	28.0±1.4	50	2	56±2.8	100
$f_{5/2}$	10.92	4.2±0.5	24	6	25.2±3	144
$p_{3/2}$	10.59	15.8±0.9	42	4	63.2±4	168
$i_{13/2}$	9.74	<0.001	2.5	14	···	35
$f_{7/2}$	8.15	0.6±0.1	19	8	4.8±1	152
$h_{9/2}$	8.06	<0.001	6	10	···	60
Sum					149±6	659

from Becchetti's value (W_0). The results represented in the figure are for the $s_{1/2}$ and $g_{9/2}$ analogs of Pb^{209} parents evaluated with continuum (escape) energies of 6, 12, and 18 MeV. The calculated parameters depend approximately linearly on the strength of the imaginary potential.

By reducing the strength of the optical potential, it is possible to achieve agreement between the calculated and experimental total widths. On the other hand, the reduction of the imaginary potential required to do this is excessive.[39] We are thus led to prefer the calculation of Sec. 7.12 based on the monopole mode in spite of our lack of information on its position and width.

8.4 Analog Resonances in the Region of the Closed Neutron Shell $N=82$

8.41 Introduction

There are a number of stable nuclei which have $N=82$ and proton numbers from $Z=54$ to 62: $_{54}Xe_{82}^{136}$, $_{56}Ba_{82}^{138}$, $_{58}Ce_{82}^{140}$, $_{60}Nd_{82}^{142}$, and $_{62}Sm_{82}^{144}$. All these nuclei have been used as targets in isobaric analog experiments to form the analog states of the $N=83$ parents. The energy spacings and angular momenta of these resonances remain basically the same for all the above mentioned nuclei from $Z=54$ to $Z=62$ (cf. [Mo69b] or Table 8.5), At around 10-MeV proton energy a

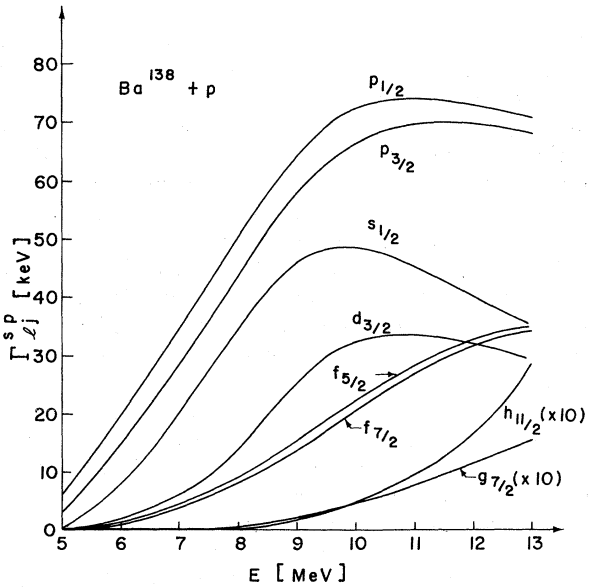

FIG. 8.15. The single-particle escape widths for the neutron orbits of barium. {Potential: [Wi67]}.

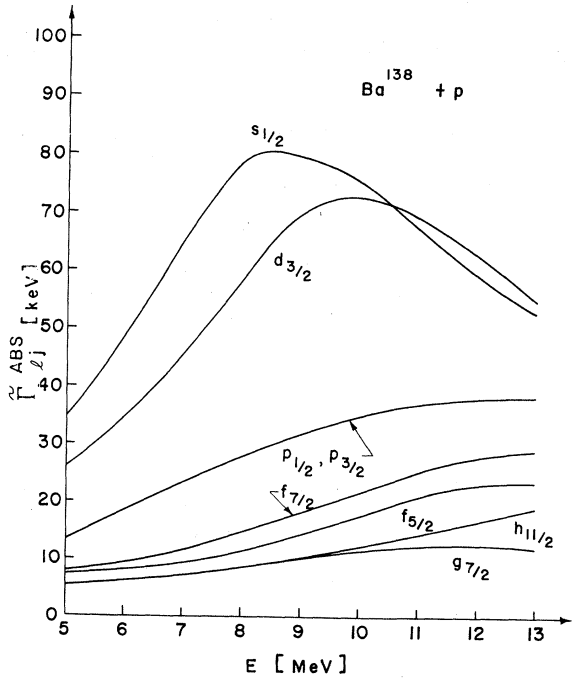

FIG. 8.16. The single-particle absorption widths for the neutron orbits of barium. {Potential: [Wi67]}.

[39] In contrast, the escape width depends on W mainly through the factor $e^{-2\eta}$. At the energies considered, this factor is close to unity, and reduction of η by a factor of 2 will change Γ_{lj}^{sp} by only a few percent.

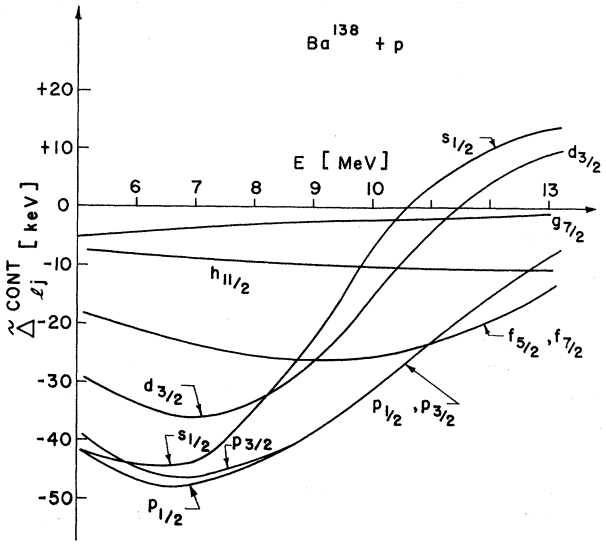

FIG. 8.17. The single-particle continuum shifts for the neutron orbits of barium. {Potential: [Wi67]}.

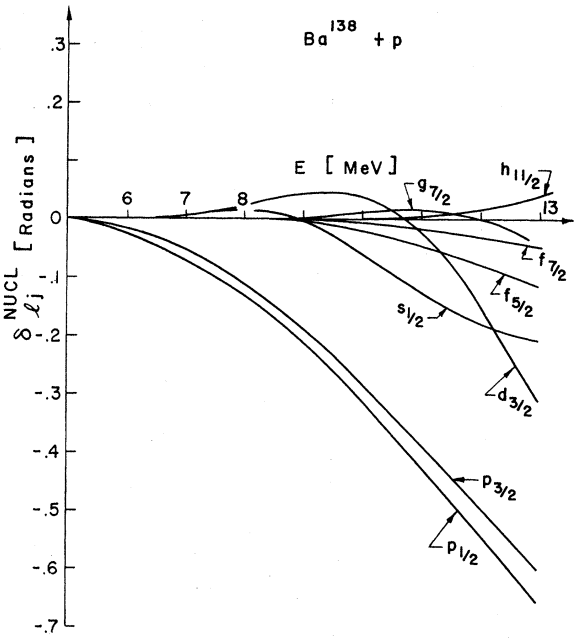

FIG. 8.19. The nuclear optical phase shift, $\delta_{lj}^{NUCL} \equiv \delta_{lj} - \sigma_l$, for the neutron orbits of barium. {Potential: [Wi67]}.

series of resonances appear, whose quantum numbers have been determined by polarization measurements where doubtful [Ve67,68]. These are given as $f_{7/2}$, $p_{3/2}$, $p_{1/2}$, and $f_{5/2}$. This sequence is expected from the single-particle shell model (see Fig. 8.1). Unlike the case of lead, the spectroscopic factors of the levels with $N=83$ are considerably smaller than 1 (cf. Table 8.5).

All the analog resonances decay strongly to the first excited 2^+ state of the target nucleus (which appears in all the $N=82$ targets at about 1.3–1.6 MeV excitation

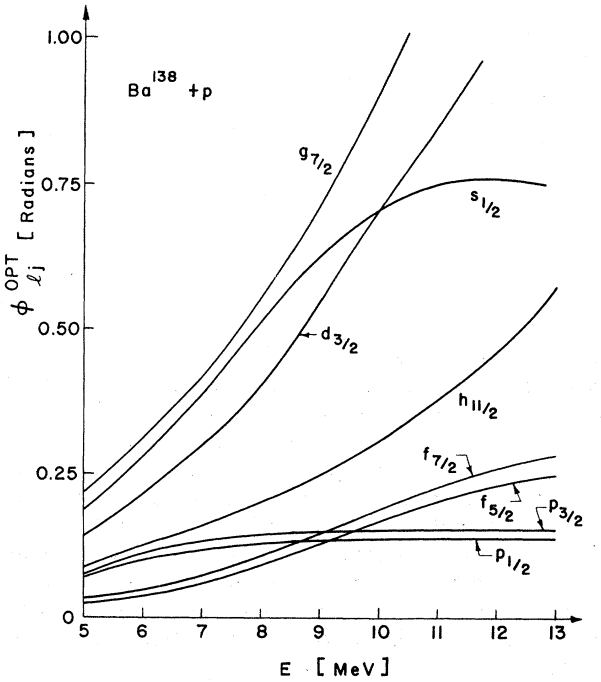

FIG. 8.18. The optical phase for the neutron orbits of barium. {Potential: [Wi67]}.

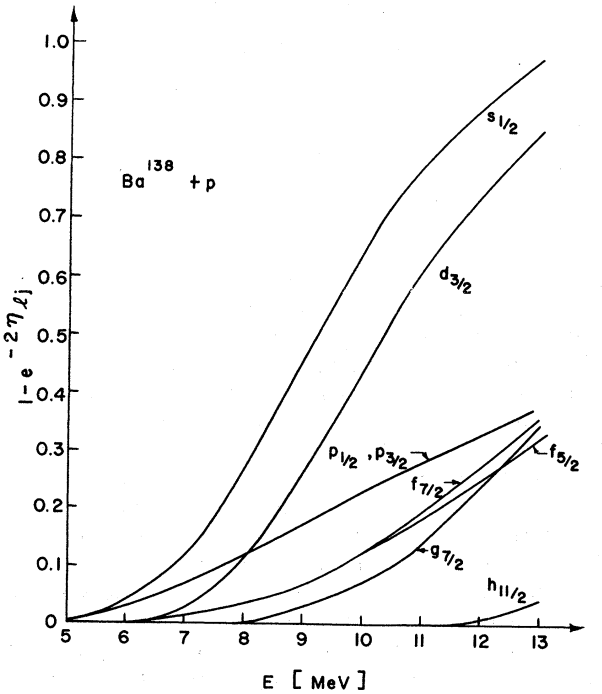

FIG. 8.20. The absorption parameter for the orbits of barium presented in the form $[1-\exp(-2\eta_{lj})]$. {Potential: [Wi67]}.

TABLE 8.5. Comparison of experimental and calculated values for the escape width Γ_{lj} and the asymmetry phase ϕ for the analog resonances in proton scattering on nuclei with $N=82$. All widths in keV. All angles in radians.

lj	E_R (MeV)	Γ_{lj} (keV)	Γ_{lj}^{sp} (keV)	S_{pp}		S_{dp}			ϕ_{rad}^{expt}	ϕ_{rad}^{OPT}
				$Xe^{136}+p$						
$f_{7/2}$	10.19	20.3[a]	21	0.97		0.68[b]				0.20
$p_{3/2}$	10.79	26.3	61	0.43		0.49				0.15
$p_{1/2}$	11.17	19.4	63	0.31		0.34				0.14
$f_{5/2}$	11.50	9.9	28	0.35		0.24				0.22
$f_{5/2}$	11.72	6.1	30	0.20		0.16				0.23
				$Ba^{138}+p$						
$f_{7/2}$	10.02	15.5[c] 17.0[d]	21	0.74	0.81	0.76[e]	0.52[f]	0.70[g]	0.16[h]	0.19
$p_{3/2}$	10.65	27.8 26.0	69	0.40	0.38	0.49	0.24	0.32	0.35	0.14
$p_{1/2}$	11.11	24.5 22.5	74	0.33	0.30	0.40	0.22	0.27	0.22	0.13
$f_{5/2}$	11.46	16 9.2	31	0.52	0.30	0.24	0.17	0.20	0.09	0.21
$f_{5/2}$	11.73	... 13.0	32	...	0.40	0.24	0.11	0.14	...	0.23
				$Ce^{140}+p$						
$f_{7/2}$	9.75	12[i]	18	0.67		0.89[e]			0.10[h]	0.18
$p_{3/2}$	10.40	22	75	0.29		0.42			0.30	0.14
$p_{1/2}$	10.88	20	81	0.25		0.38			0.29	0.13
$f_{5/2}$	11.25	7	30	0.23		0.30			0.32	0.21
$f_{5/2}$	11.49	7	32	0.22		0.38			...	0.22
				$Nd^{142}+p$						
$f_{7/2}$	9.50	10.5[j]	17	0.62		0.83[e]		0.66[k]	0.10[h]	0.17
$p_{3/2}$	10.23	23.5	81	0.29		0.40		0.40	0.22	0.14
$p_{1/2}$	10.80	23.	89	0.26		0.25		0.37	0.24	0.13
$f_{5/2}$	11.05	5.9	29	0.20		0.24		0.21	0.26	0.20
				$Sm^{144}+p$						
$f_{7/2}$	9.30	7[l]	16	0.44		0.58[m]		0.61[h]	0.0[h]	0.16
$p_{3/2}$	10.19	22	80	0.28		0.34		0.39	0.21	0.14
$(p_{1/2})$	10.93	10. (?)	98	0.10(?)		...		0.48	...	0.13
$(f_{5/2})$	10.97	4	34	0.12		0.11		0.06	...	0.20

[a] [Mo69b].
[b] [Mo68].
[c] [Se70].
[d] [Wi70].
[e] [Wi67].
[f] [Eh70] calculation with no cutoff.
[g] [Eh70] calculation with cutoff.
[h] [Ha68b].
[i] [Wu69].
[j] [Cl68] and [Gr70].
[k] [Ch67].
[l] [Ma66a].
[m] [Jo66].

energy), and therefore it is probable that the neutron single-particle states have a considerable admixture of states of a particle coupled to this collective 2^+ state. Above the 2^+ state a rather dense spectrum is observed in the decay of the analogs, and its structure has been only partly unravelled. It has been proposed [Wu69] that one interpret the strength in these final states as arising from neutron particle–hole configurations coupled to the vibration. Formally, we represent this structure as $b_\beta \mid \pi\rangle$ where $\mid \pi\rangle$ is an exact eigenstate of an $N=83$ nucleus, including admixtures of the 2^+ state, for example. Using this picture, it has been possible to extract some information about the location and the escape widths of the hole states. Their sequence is $d_{3/2}$, $s_{1/2}$, $h_{11/2}$, $d_{5/2}$, and $g_{7/2}$. Because of penetration effects one expects to observe only the $d_{3/2}^{-1}$ and $s_{1/2}^{-1}$ strength.

8.42 Escape Widths

The single particle quantities for the barium region are presented in Figs. (8.15-8.20). Table 8.5 presents a comparison between spectroscopic factors as determined from isobaric analog resonances and stripping experiments. (A similar comparison for the nuclei discussed here has been made by [Ha68a,b]). The spectroscopic factors as determined from the stripping experiments differ considerably [Eh70], partly because of the use of different optical potentials and partly because different form factors have been assumed for the single-particle orbits. Therefore, we do not expect the comparison to be meaningful with an accuracy of better than 10%–20%.

For our calculations, the Saxon–Woods potential in

which the neutron single-particle wave function is generated has a radius of $R=1.15A^{1/3}$F. The optical potential is that of [Wi67], i.e., in the notation of Becchetti [Be69],

$$\begin{aligned} &V_R=62.4-0.4E\ [\text{MeV}],\\ &R_R=1.25A^{1/3}\text{F} \qquad a_R=0.67\text{F}\\ &V_{SO}=5.0\ [\text{MeV}], \qquad R_{SO}=R_R,\\ &a_{SO}=a_R, \qquad W_V=0,\\ &W_{SF}=10.0\ [\text{MeV}],\\ &R_i=1.21A^{1/3}\text{F} \qquad a_i=0.69\text{F} \end{aligned} \tag{8.14}$$

This potential has been obtained by fitting various proton scattering experiments in this region. The imaginary part is appropriate for an energy around $E_R\simeq 10$ MeV; an energy dependence has not been determined for the imaginary part.

Although the trends of the (d, p) spectroscopic factors (S_{dp}) are well reproduced, the agreement of the absolute values is only fair. In general S_{pp} is smaller than S_{dp} by as much as 10%–30%. The uncertainty in the experimental value of Γ_{lj} is usually not available. However, estimates of an error of 10%–15% for the $f_{7/2}$ and $p_{3/2}$ resonance in $Sm^{144}+p$, and an error of 20%–30% for the other two resonances are available [Ma66]. Since the error in S_{dp} is also not known, it is hard to estimate the degree of discrepancy. However, there may be a systematic discrepancy due to the smaller radius of the potential in which the neutron wave function has been generated. [e.g. we use $r_0=1.15$F while the authors of [Wi67] use $r_0=1.23$F]. Since we use the additional Coulomb energy information, which favors a smaller value of r_0, our value for the spectroscopic factor may be more correct. However, the values for the escape widths for the neutron holes, Table 8.6, are also not reproduced too well. They are very sensitive to the optical potential, and to the assigned energy, $\bar{E}$, of the particle-hole final state. A change in $\bar{E}$ by 0.5 MeV changes Γ_{lj}^{sp} by a factor of 2.

8.43 The Asymmetry Phase

The asymmetry phase ϕ is a quantity which cannot be very accurately extracted from proton elastic scattering data. The quantity which is the only observable in the experiment is the phase $\alpha(\theta)$, the relative phase between the resonance term and the background scattering amplitude. We may write the background scattering amplitude as $f_B(\theta)=|f_B(\theta)|\,e^{i\phi(\theta)}$. This amplitude is a superposition of many partial waves and therefore its phase $\phi(\theta)$ will generally vary with angle. Therefore the observed phase difference, $\alpha(\theta)$, may be written

$$\alpha(\theta)=\phi(\theta)-2(\delta_{lj}^{\text{NUCL}}+\sigma_l)-2\phi_{lj}. \tag{8.15}$$

Usually one calculates $\phi(\theta)$ from an optical potential; if the potential is chosen properly, the difference $\alpha(\theta)-\phi(\theta)$ should be independent of the scattering angle. Then one subtracts from $\alpha(\theta)-\phi(\theta)$ the optical potential scattering phase shift $2(\delta_{lj}^{\text{NUCL}}+\sigma_l)$ (which includes the Coulomb phase shift σ_l) and obtains the asymmetry phase. Such an analysis has been performed by [Ha68b], and the results are shown in Table 8.5. We have also included the results for ϕ^{OPT} taken from Fig. 8.18. We have not calculated the effects of channel coupling or compound effects [Sec. 6.8] because they are expected to be small. The error attributed to the values ϕ^{expt} is of the order of 0.2 rad. One sees that theoretical and experimental values certainly agree within this error. However, this does not provide a very stringent test. It only indicates that the absorptive part of the optical potential has the right order of magnitude.

TABLE 8.6. Single-particle widths for neutron holes in Ce^{140}. The experimental values have been obtained by studying the decay of the $f_{7/2}$ and $p_{3/2}$ resonances in proton scattering from Ce^{140}.

	$\bar{E}$ (MeV)	Expt (keV)	Calc (keV)
$2\,\Gamma_{s\,1/2}{}^{sp}+4\,\Gamma_{d\,3/2}{}^{sp}$	5.95	8.5[a]	17.6
$\Gamma_{d\,3/2}{}^{sp}$	6.0	0.4[b]	0.9
$\Gamma_{s\,1/2}{}^{sp}$	6.0	3.5[c]	7

[a] [Wu69].
[b] [He69b].
[c] Calculated from (a) and (b).

8.44 The Total Width

The independent channel calculation for the total absorption width has also been carried through for one resonance in Ba, and, just as in the Pb region, one observes a discrepancy of a factor of 7. The total width of the $f_{7/2}$ resonance in $Ba^{138}+p$ is $\Gamma=69$ keV [Se70]. The elastic width is 16.5 keV and the sum of the inelastic widths is 12.8 keV [Mo67b], which gives $\Gamma^{\text{ABS}}\simeq 42$ keV. The sum of the $\tilde{\Gamma}_{lj}^{\text{ABS}}$ leads to a value of 290 keV. We have already discussed the reasons for this discrepancy, and indicated the correct procedure.

8.5 Isobaric Analog Resonances in the Region of the Closed Neutron Shell $N=50$

8.51 Introduction

The situation in the region of $N=50$ is similar to that in the $N=82$ region. A number of nuclei with $N=50$ can serve as targets: $_{38}Sr_{50}{}^{88}$, $_{40}Zr_{50}{}^{90}$, $_{42}Mo_{50}{}^{92}$. Extensive studies of isobaric analog resonances have been made using Sr^{88} and Zr^{90} as targets [Co68a, b; Li68; Sc69c; Wi69]. The observed spectra of the isobaric analog resonances are rather similar. The expected sequence of single-particle levels is $d_{5/2}$, $s_{1/2}$, $d_{3/2}$, $g_{7/2}$. Of these only the $d_{3/2}$ strength is considerably fragmented over a number of levels, while the other orbits are relatively pure (see the spectroscopic factors in Tables 8.7 and 8.8).

TABLE 8.7. Escape width, single-particle escape width, and spectroscopic factors for analog resonances in $Sr^{88}(p, p)$ Sr^{88}. All widths are in keV. The large spectroscopic factor for the $g_{7/2}$ orbit (>1) probably arises from the choice of a rather small radius for the neutron potential well (see Table 8.9). The same remark applies to Table 8.8. For comparison, a theoretical calculation of the spectroscopic factors is shown in the last column.

E_R [MeV][a]	lj [b]	Γ_{lj} [a]	Γ_{lj} [b]	Γ_{lj}^{sp} [c]	Γ_{lj}^{sp} [d]	S_{pp} [e]		S_{dp} [f]	S_{theory} [g]
5.00	$d_{5/2}$	8	4	5	5	1.6	0.8	0.79	0.91
5.99	$s_{1/2}$	46	...	52	48	0.9	...	0.90	0.93
6.91	$d_{5/2}$	11	5	27	24	0.4	0.2	0.09	0.05
6.98	$d_{3/2}$	23	28	38	35	0.60	0.75	0.45	0.40
7.42	$d_{3/2}$	18	22	43	39	0.42	0.51	0.34	0.40
7.70	$g_{7/2}$	4.0	4	3.0	2.7	1.3	1.3	0.74	0.80
8.10	$d_{3/2}$	5.6	7	51	46	0.11	0.14	0.08	0.11
8.22	$d_{5/2}$	3.0	1.5	42	36	0.07	0.04	0.043	0.001
Sum rule: ΣS_{pp}				$d_{5/2}$			1.04	0.92	0.97
				$d_{3/2}$		1.13	1.40	0.87	0.91

[a] [Co68a].
[b] [Wi69].
[c] Read from Fig. 8.21 for Potential (II).
[d] Read from Fig. 8.21 for Potential (I).
[e] $S_{pp}=\Gamma_{lj}/\Gamma_{lj}^{sp}$ with Γ_{lj} from [Co68a] and from [Wi69], respectively. Γ_{lj}^{sp} is calculated with Potential (II).
[f] [Co68b].
[g] [Hu69].

TABLE 8.8. Escape widths, single-particle escape widths, and spectroscopic factors for analog resonances in $Zr^{90}(p, p)Zr^{90}$. The values of Γ_{lj}^{sp} are calculated for Potential II—see text. (All widths are in keV).

E_R (MeV)	lj	Γ_{lj} [a]	Γ_{lj} [b]	Γ_{lj}^{sp}	S_{pp} [d]	S_{dp} [e]	S_{theory} [f]
4.67	$d_{5/2}$	...	4.0±0.5[c]	3.5	1.1±0.1	0.89	0.98
6.22	$d_{3/2}$	≤ 1	...	25	≤ 0.04	0.03	0.004
6.78	$d_{3/2}$	15	18	38	0.40(0.48)	0.45	0.81
6.99	$g_{7/2}$	2.5	...	1.7	1.4	0.52	0.88
7.27	$s_{1/2}$	17±3	...	70	0.24	0.24	0.005
7.63	$d_{3/2}$	10	2	45	0.22(0.04)	0.08	0.006
7.82	$d_{3/2}$	8	8	46	0.18(0.18)	0.11	0.15
8.04	$d_{3/2}$	8	6	50	0.16(0.12)	0.15	0.02
8.41	$d_{3/2}$	≤ 5	5	54	$\leq 0.1(0.1)$		...
Sum rule ΣS_{pp} for $d_{3/2}$					$<1.1(0.92)$	0.82	0.98

[a] [Li68].
[b] [Wi69].
[c] [Sc69c].
[d] Calculated with Γ_{lj} from [Li68]; those using Γ_{lj} from [Wi69] are given in brackets.
[e] [Co63].
[f] [Ra64] Spectroscopic factors obtained from a shell-model calculation.

TABLE 8.9. The dependence of the resonance parameters on the shape of the wave function of the parent state ($Sr^{88}+p$ at 7 MeV). The single-particle wave function of the extra neutron has been changed by changing the radius ($R=r_0A^{1/3}$) of the well. The well depth has been adjusted to obtain the experimental single-particle binding energy for the neutron orbit. The nuclear phase shift ($\delta+i\eta$) depends on r_0 through the fact that the bound neutron orbit is projected from the scattering solution as discussed in Sec. 2.23.

State	r_0 (fm)	Γ_{lj}^{sp} (keV)	ϕ_{lj}^{OPT} (rad)	$\tilde{\Delta}_{lj}^{CONT}$ (keV)	$\tilde{\Gamma}_{lj}^{ABS}$ (keV)	δ_{lj}^{NUCL} (rad)	$1-\exp(-2\eta_{lj})$
$s_{1/2}$	1.15	77.3	0.031	−49.8	10.0	−0.261	0.034
	1.25	75.7	0.034	−44.4	9.3	−0.293	0.038
$d_{5/2}$	1.15	25.6	0.043	−38.4	7.85	−0.0181	0.019
	1.25	27.7	0.037	−37.9	6.46	−0.0355	0.019
$g_{7/2}$	1.15	1.16	0.027	−14.7	2.74	+0.0024	0.0014
	1.25	1.65	0.017	−16.5	2.40	+0.0013	0.0014

In the quantitative analysis of the experimentally observed excitation functions a new feature appears in this region. In the case of lead and barium, the energy of the isobaric analog resonances is already so high that many neutron channels are open, and, therefore, compound nuclear levels will predominantly decay via neutron emission (which is favored by the absence of a Coulomb barrier). In $Zr^{90}(p, p)Zr^{90}$ the lowest $d_{5/2}$ resonance is below the first neutron channel and the compound contribution to the elastic scattering cannot be neglected [Sc69c].

8.52 Escape Widths

The single-particle quantities for the strontium region are presented in Figs. (8.21–8.26). Although the

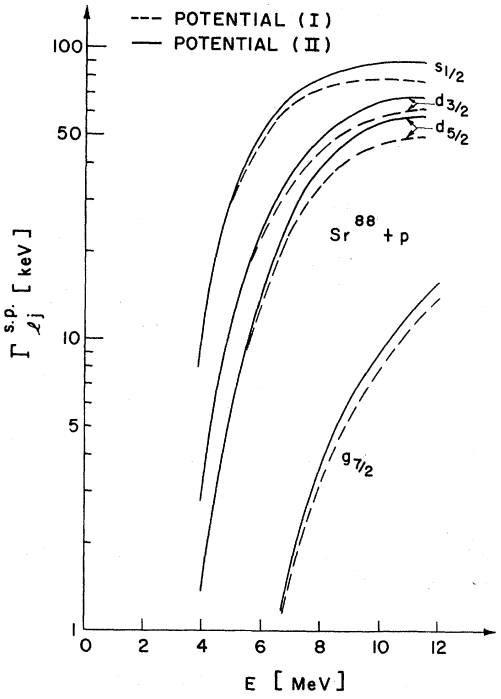

FIG. 8.21. The single-particle escape widths for the orbits of strontium. (Potentials: (I) [Be69], (II) [El69]).

isobaric analog resonances are well separated in most cases, the analysis of different excitation functions leads to rather different values for the escape widths, often differing by a factor of 2 or more. This situation leads to a large uncertainty in some of the calculated spectroscopic factors.

For the case of strontium, we considered two different optical potentials and calculated all resonance parameters with both potentials. Potential (I) is that of Becchetti [Be69] while Potential (II) has been obtained from a fit to proton scattering from strontium and also provides a fit to the polarization data [El69].

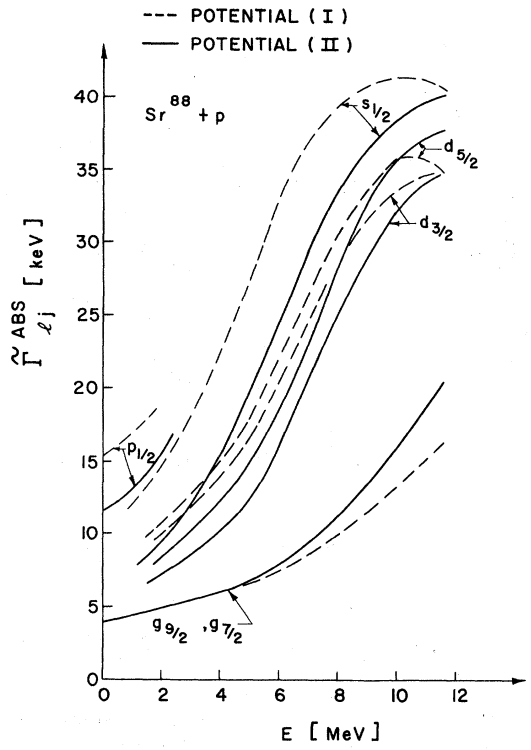

FIG. 8.22. The single-particle absorption widths for the neutron orbits of strontium. {Potentials: (I) [Be69], (II) [El69]}.

The parameters of Potential (II) are

$V_R = 55.0 - 0.3E$ [MeV],

$R_R = 1.287A^{1/3}$F, $\quad a_R = 0.666$F

$V_{SO} = 6.5$ [MeV], $\quad R_{SO} = 1.05A^{1/3}$F, $\quad a_{s0} = a_R$,

$W_V = 0$, $\quad W_{SF} = 12.0$ MeV,

$R_i = 1.301A^{1/3}$F, $\quad a_i = 0.512$F.

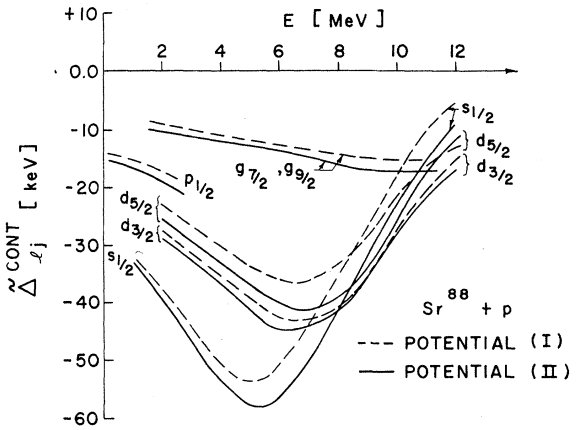

FIG. 8.23. The single-particle continuum shift for the neutron orbits of strontium. {Potentials: (I) [Be69], (II) [El69]}.

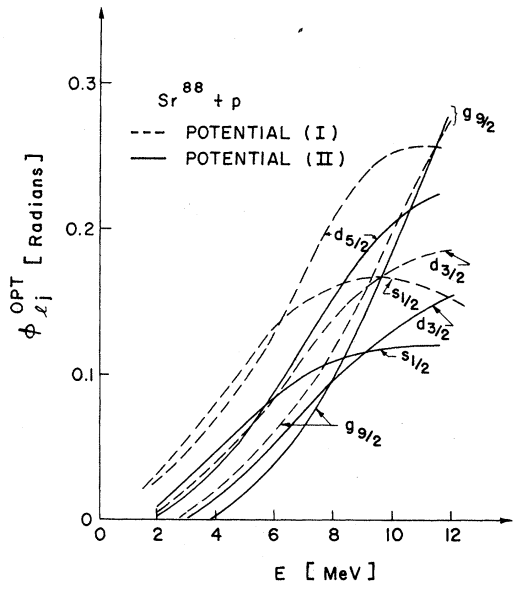

FIG. 8.24. The optical phase for the neutron orbits of strontium. {Potentials: (I) [Be69], (II) [El69]}.

The differences in the escape widths are small for the two potentials for those energies well below the Coulomb barrier, but become larger with increasing energy. This deviation mainly arises from the difference in the factors $e^{-2\eta}$ which multiply the transition matrix element. The main difference between potentials (I) and (II) appears to be in the imaginary potential, and therefore those quantities most sensitive to this quantity, such as Γ_{lj}^{ABS}, ϕ_{lj}^{OPT}, η_{lj}, show the greater differences.

Within the deviations of the experimental values for the escape widths, and considering an estimated error of ~20% for the spectroscopic factors extracted from the stripping analysis, there exists no obvious contradiction (except for the $g_{7/2}$ resonance) between analog spectroscopic factors and those of the stripping theory.

The deviations for the $g_{7/2}$ resonance, both in $Sr^{88}(p, p)$ Sr^{88} and $Zr^{90}(p, p)Zr^{90}$ seem to be significant. Because of the strong centrifugal barrier, $l=4$, the escape width is very sensitive to the details of both the proton continuum wave functions and the neutron form factor. The effect of changing the size of the neutron wave functions has been studied and some of the results are given in Table 8.9. As may be seen there, the $g_{7/2}$ escape width is by far the most sensitive to the details of the neutron wave function.

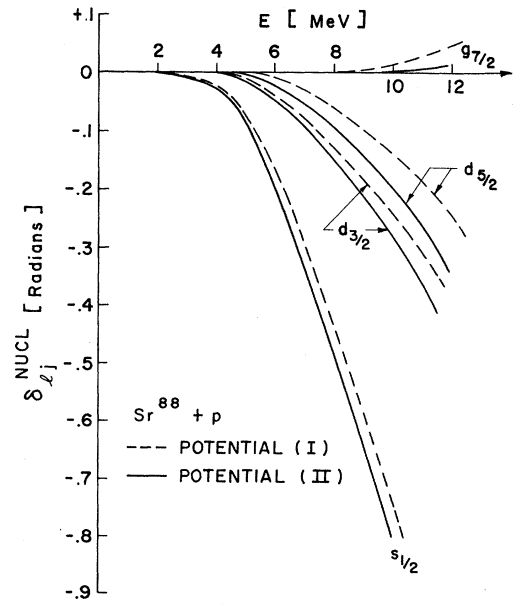

FIG. 8.25. The nuclear optical phase shift, $\delta_{jl}^{NUCL} \equiv \delta_{lj} - \sigma_l$, for the neutron orbits of strontium. {Potentials: (I) [Be69], (II) [El69]}.

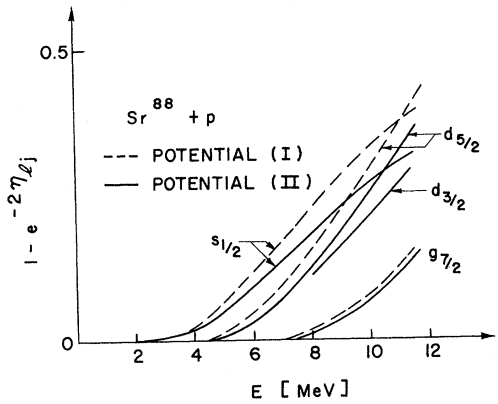

FIG. 8.26. The absorption parameter for the neutron orbits of strontium presented in the form $[1-\exp(-2\eta_{lj})]$. {Potentials: (I) [Be69], (II) [El69]}.

8.53 *The Optical Asymmetry Phase*

The optical asymmetry phase is sensitive to the strength of the imaginary part of the optical potential. In Table (8.10) we have compared the optical phase, corrected for energy dependence of the resonance parameters (see Sec. 8.2), with the experimental value for the asymmetry phase. This comparison neglects any contributions to the asymmetry phase from direct-channel coupling or from the compound escape amplitudes. As may be seen from the table, the results of this comparison show no significant disagreement between theory and the phases extracted from the experimental data for the states with large spectroscopic factors. It is expected that all of the small effects such as rearrangement, channel coupling, and compound escape are important for the other states. This is probably the reason for the disagreement in sign.

TABLE 8.10. Comparison of experimental asymmetry phase and the calculated optical phase for $Zr^{90}(p, p)Zr^{90}$. The experimental numbers are taken from [Sc69c] for the $d_{5/2}$ resonance and from [Wi69] for the other resonances.

E_R (MeV)	lj	ϕ^{expt}	$\phi^{\text{OPT}}(E_R)$		$-\frac{1}{4}\Gamma'$	$-\frac{1}{4}\Gamma(\Gamma_0'/\Gamma_0)$	ϕ^{OPT} [Eq. 8.8]	
4.67	$d_{5/2}$	0.125	0.06[a]	0.09[b]	−0.002	−0.005	+0.05[a]	+0.08[b]
6.81	$d_{3/2}$	0.1	0.07	0.1	−0.01	−0.015	0.05	0.08
7.67	$d_{3/2}$	0	0.09	0.115	−0.01	−0.05	0.07	0.1
7.85	$d_{3/2}$	−0.2	0.09	0.115	−0.01	−0.02	0.06	0.08
8.09	$d_{3/2}$	−0.2	0.1	0.12	−0.01	−0.025	0.07	0.09
8.47	$d_{3/2}$	−0.25	0.105	0.125	−0.01	−0.025	0.07	0.09

[a] Calculated with Potential (II). [b] Calculated with Potential (I).

8.6 Conclusions

In the previous parts of this section, a comparison has been made between experimental and calculated resonance parameters. This comparison is not complete:

(i) We have not attempted to collect and present all the experimental data which are available at present.

(ii) We have not re-analyzed all experimental curves in order to obtain a set of resonance parameters which are determined by the same method. Such analyses would be valuable in order to determine the uncertainties in the parameters; these uncertainties seem to be rather large.

(iii) For our calculations we have not attempted to find the best optical potentials, but have used those available in the literature which seemed appropriate for the region under investigation. Because of our poor knowledge of the optical potential, the theoretical resonance parameters have rather large uncertainties.

We summarize some of our conclusions with respect to the various parameters:

(i) The single-particle escape width:

We estimate that the uncertainty in the optical potentials leads to an uncertainty of the order of 10% or more in the escape widths and therefore in the spectroscopic factors, even at energies below the Coulomb barrier.[40] Above the Coulomb barrier the energy dependence of the escape width is strongly influenced by the factor $e^{-2\eta}$, hence by the imaginary potential whose strength is only poorly known. There is a further uncertaintly due to the monopole shielding effect arising from the compound escape, Eq. (6.93), since the parameters of the monopole are all but unknown experimentally.

(ii) The asymmetry phase and the partial absorption width:

The partial absorption width for the elastic channel and the asymmetry phase depend on the imaginary potential only at the energy of the resonance. These quantities should be predicted with reasonable confidence except for questions concerning the energy dependence of the imaginary part of the optical potential. Unfortunately, the asymmetry phase and the partial absorption width are obtained only with rather large uncertainties, as is the magnitude of the imaginary potential. Within these uncertainties, the calculation provides a representation of the data that is not grossly in error.

(iii) The total width and shift:

We conclude that the total width and shift should *not* be calculated in the independent channel approximation. The best estimates would seem to be those of Sec. 7, where it is seen that the giant monopole is the dominant feature. It is possible that large changes in what we believe the imaginary part of the optical potential to be would change this conclusion somewhat.

[40] The analysis of stripping at energies below the Coulomb barrier is fairly insensitive to the optical potential since the short range of the interaction between the deuteron and the stripped neutron ensures that the process happens well outside the nuclear center. For isobaric analog resonances, the interaction $V_c^{(-)}$ has a long range, and therefore the matrix element for the escape width receives about equal contributions from the "inside" and "outside" of the nuclear volume.

ACKNOWLEDGMENTS

We would like to thank Jerry Miller and Michael Strayer for helping in the preparation of the manuscript, and Antonio de Toledo Piza for helpful discussions. Two of us (Naftali Auerbach and Arthur K. Kerman) would like to thank Professor G. E. Brown for his hospitality at the State University of New York at Stony Brook during the fall of 1970.

APPENDIX 1. THE CONTINUUM SPACE AND THE OPTICAL MODEL

In this appendix we wish to indicate how the projection operator for the continuum space may be constructed. In this connection we shall review the theory of the optical model. The modifications of the continuum-space wave functions and projection operator necessary for the theory of analog resonances are also discussed.

A1.1 The Continuum Space Projection Operator

Our aim in this subsection is to construct a set of states which form a basis for the continuum space and which have orthonormality properties such that we may define the projection operator in terms of these states. We begin with a definition of channels for the scattering problem and introduce certain channel

vectors. An integral operator is then constructed which allows for the transformation of the original set of channel vectors to a new set which has the desired orthornormality properties. The formalism as presented allows for any number of channels in the continuum space. We note that some of the channels defined to be in this space may be closed at the energy of interest for the scattering problem. This feature does not modify the analysis.

Let us turn to the definition of the channels and introduce some useful operators.

Let $a^\dagger(\mathbf{r},\sigma)$ be the creation operator for a *proton* at point r with spin projection σ. If $a(\mathbf{r},\sigma)$ is the corresponding destruction operator we have, as usual

$$\{a^\dagger(\mathbf{r},\sigma), a(\mathbf{r}',\sigma')\}=\delta(\mathbf{r}-\mathbf{r}')\delta_{\sigma\sigma'},$$
$$\{a^\dagger(\mathbf{r},\sigma), a^\dagger(\mathbf{r}',\sigma')\}=0,$$
$$\{a^\dagger(\mathbf{r},\sigma), a(\mathbf{r}',\sigma')\}=0. \quad \text{(A1.1)}$$

We introduce the operator $a_{(l\frac{1}{2})jm_j}{}^+(r)$ via the following relations

$$a^\dagger(\mathbf{r},\sigma)=\sum_{ljmj} a_{(l\frac{1}{2})jm_j}{}^\dagger(r)\,\mathrm{Y}_{ljm_j}{}^\dagger(\hat{r},\sigma), \quad \text{(A1.2)}$$

or

$$a_{(l\frac{1}{2})jm_j}{}^\dagger(r)=\sum_\sigma \int \mathrm{Y}_{(l\frac{1}{2})jm_j}(\hat{r},\sigma)\,a^\dagger(\mathbf{r},\sigma)\,d\Omega_{\hat{r}} \quad \text{(A1.3)}$$

where

$$\mathrm{Y}_{ljm_j}(\hat{r},\sigma)=\sum_{ml\sigma'} C_{ml\sigma'm_j}{}^{l\frac{1}{2}jm_j}\,Y_{lm_l}(\hat{r})\,\chi_{\frac{1}{2}\sigma'}(\sigma). \quad \text{(A1.4)}$$

Here $Y_{lm_l}(\hat{r})$ is a spherical harmonic, and $\chi(\sigma)$ is a spinor. The commutation relations of these operators are

$$\{a_{(l\frac{1}{2})jm_j}{}^\dagger(r),\, a_{(l'\frac{1}{2})jm_{j'}}(r')\}=[\delta(r-r')/rr']\delta_{ll'}\delta_{jj'}\delta_{m_jm_{j'}}$$
$$\{a_{(l\frac{1}{2})jm_j}(r),\, a_{(l'\frac{1}{2})j'm_{j'}}(r')\}=0, \text{ etc.} \quad \text{(A1.5)}$$

We denote the states of the target as $|\lambda, IM\rangle$, where $\lambda=0$ denotes the ground state, $\lambda=1$ the first excited state, etc. The target state has angular momentum I and projection M. We may add to a target state a particle with orbital angular momentum l, total angular momentum j, and projection m_j. If we require that this particle be created at a *distance* r from the origin of the coordinate system, we define

$$|r,(l\tfrac{1}{2})jm_jIM,\lambda\rangle=a_{(l\frac{1}{2})jm_j}{}^+(r)\,|\lambda,IM\rangle. \quad \text{(A1.6)}$$

It is also useful to couple j and I to a total channel angular momentum J and projection M. We define,

$$|r,[(l\tfrac{1}{2})jI]\mathrm{JM},\lambda\rangle=\sum_{m_jM} C_{m_jM\mathrm{M}}{}^{jI\mathrm{J}}\,a_{(l\frac{1}{2})jm_j}{}^\dagger(r)\,|\lambda,IM\rangle. \quad \text{(A1.7)}$$

The indices $[(l\frac{1}{2}j)I]\mathrm{JM},\lambda$ will be denoted by the channel label c, so that our channel states are designated $|r,c)$ in an abbreviated notation.

The orthonormality properties of the states $|r,c)$ are such that they are not appropriate for the definition of a continuum space projection operator. We now proceed to the definition of a new set of fundamental channel states $|r,c\rangle$ which have more desirable orthonormality properties.

For the following discussion, let c denote the channels (open or closed) to be included in the continuum space. The orthonormality relation for the channel states $|r,c\rangle$ involves a channel density matrix, $\rho_{cc'}(r,r')$, such that

$$(r,c\,|\,r',c')=\delta[(r-r')/rr']\delta_{cc'}-\rho_{cc'}(r,r'). \quad \text{(A1.8)}$$

The construction of the projection operator requires the eigenfunctions of this channel density matrix. One assumes that the solutions of the eigenvalue problem

$$\sum_{c'}\int_0^\infty \rho_{cc'}(r,r')\,u_{c'}{}^{(\eta)}(r')\,r'^2\,dr'=\eta u_c{}^{(\eta)}(r), \quad \text{(A1.9)}$$

$$\sum_c \int_0^\infty u_c{}^{(\eta)*}(r)\,u_c{}^{(\eta')}(r)\,r^2\,dr=\delta_{\eta\eta'} \quad \text{(A1.10)}$$

are available. The completeness relation for the eigenfunctions is

$$\sum_\eta u_c{}^{(\eta)}(r)\,u_{c'}{}^{(\eta)}(r')=\delta_{cc'}\delta[(r-r')/rr'], \quad \text{(A1.11)}$$

where the sum runs over all η and includes all degenerate eigenfunctions. The solution $u_c{}^{(\eta)}(r)$ can be used along with (A1.8) to show that $\eta\leq 1$ (see for example [Ke66; Fr67,68]). From these solutions we construct the matrix

$$F_{cc'}(r,r')=\sum_{\eta\neq 1}[u_c{}^{(\eta)}(r)\,u_{c'}{}^{(\eta)}(r')/(1-\eta)^{1/2}], \quad \text{(A1.12)}$$

where the sum is over all the eigenvectors with $\eta\neq 1$.

The operator $F_{cc'}(r,r')$ may be used to introduce new channel vectors which have the desired orthonormality properties. The channel vectors are

$$|r,c\rangle=\sum_{c'}\int_0^\infty |r',c')\,F_{c'c}(r',r)\,r'^2\,dr', \quad \text{(A1.13)}$$

and satisfy the normalization condition

$$\langle r,c\,|\,r',c'\rangle=[\delta(r-r')/rr']\delta_{cc'}-\sum_{\eta=1} u_c{}^{(\eta)}(r)\,u_{c'}{}^{(\eta)}(r'). \quad \text{(A1.14)}$$

In terms of the vectors $|r,c\rangle$ the projection operator for the continuum space is

$$\mathrm{P}=\sum_c\int_0^\infty |r,c\rangle r^2\,dr\langle r,c|, \quad \text{(A1.15)}$$

where the summation is over the channels defined to be in this space. It is readily seen that P satsifies the projection operator relations, $\mathrm{P}^2=\mathrm{P}$, $\mathrm{P}^\dagger=\mathrm{P}$. The projection operator for the closed channels and those open channels not included in P is

$$\mathrm{Q}=1-\mathrm{P}. \quad \text{(A1.16)}$$

In the next section we use the operators P and Q to discuss the scattering problem and define a many-channel optical model Hamiltonian.

A1.2 The Optical Model

In this section we wish to review the formal theory of the optical model. If we use the projection operators of the previous section, the Schrödinger equation

$$H\,|\,\Psi\rangle=E\,|\,\Psi\rangle \tag{A1.17}$$

may be written,

$$\begin{aligned}(E-H_{\mathrm{PP}})\mathrm{P}\,|\,\Psi\rangle&=H_{\mathrm{PQ}}\mathrm{Q}\,|\,\Psi\rangle,\\ (E-H_{\mathrm{QQ}})\mathrm{Q}\,|\,\Psi\rangle&=H_{\mathrm{QP}}\mathrm{P}\,|\,\Psi\rangle,\end{aligned} \tag{A1.18}$$

where

$$\begin{aligned}|\,\Psi\rangle&=\mathrm{P}\,|\,\Psi\rangle+\mathrm{Q}\,|\,\Psi\rangle,\\ H_{\mathrm{QQ}}&\equiv\mathrm{Q}H\mathrm{Q},\qquad H_{\mathrm{PQ}}\equiv\mathrm{P}H\mathrm{Q}.\end{aligned} \tag{A1.19}$$

Using the formal solution

$$\mathrm{Q}\,|\,\Psi\rangle=[1/(E^{(+)}-H_{\mathrm{QQ}})]H_{\mathrm{QP}}\mathrm{P}\,|\,\Psi\rangle, \tag{A1.20}$$

where $E^{(+)}=E+i\epsilon$ we may write an equation determining the scattering in the P space:

$$(E-H_{\mathrm{PP}}-H_{\mathrm{PQ}}[1/(E^{(+)}-H)_{\mathrm{QQ}}]H_{\mathrm{QP}})\mathrm{P}\,|\,\Psi\rangle=0. \tag{A1.21}$$

We wish to reduce the complicated many-body equation, (A1.21) to a matrix equation in a single variable. This may be done with the aid of the channel vectors $|\,r,c\rangle$ defined in the previous section. We write

$$\mathrm{P}\,|\,\Psi_c^{(+)}\rangle=\sum_{c'}\int_0^\infty|\,r,c'\rangle\Psi_{cc'}^{(+)}(r)r^2\,dr, \tag{A1.22}$$

where the boundary conditions are such that one has incoming waves *only* in the channel c. We also define the operator,

$$h_{cc'}(r,r')=\langle r,c\,|\,\{H_{\mathrm{PP}}+H_{\mathrm{PQ}}[1/(E^{(+)}-H_{\mathrm{QQ}})]H_{\mathrm{QP}}\}\,|\,r',c'\rangle. \tag{A1.23}$$

If we impose the subsidiary condition

$$\sum_{c'}\int_0^\infty u_{c'}^{(\eta)}(r)\Psi_{cc'}^{(+)}(r)r^2\,dr=0 \tag{A1.24}$$

for $\eta=1$, we obtain[41]

$$E\Psi_{cc''}^{(+)}(r)=\sum_{c'}\int_0^\infty h_{c''c'}(r,r')\Psi_{cc'}^{(+)}(r')r'^2\,dr'. \tag{A1.25}$$

In the case in which the P space contains only the elastic channel, this equation reads

$$E\Psi^{(+)}(r)=\int_0^\infty h(r,r')\Psi^{(+)}(r')r'^2\,dr', \tag{A1.26}$$

and the wave function $\Psi^{(+)}(r)$ contains all the information necessary to describe the elastic scattering.

As we have not introduced an energy averaging procedure, the P-space scattering will contain many resonances due to the influence of the Q space modes. An energy averaged T matrix may be obtained via the introduction of the operator

$$h_{cc'}{}^{\mathrm{OPT}}(r,r')=\langle r,c\,|\,\{H_{\mathrm{PP}}+H_{\mathrm{PQ}}[E-H_{\mathrm{QQ}}+\tfrac{1}{2}(iI)]^{-1}H_{\mathrm{QP}}\}\,|\,r',c'\rangle. \tag{A1.27}$$

One therefore requires the solution of

$$E\psi_{cc''}{}^{(+)}(r)=\sum_{c'}\int_0^\infty h_{c''c'}{}^{\mathrm{OPT}}(r,r')\psi_{cc'}{}^{(+)}(r')r'^2\,dr' \tag{A1.28}$$

or

$$E\psi^{(+)}(r)=\int_0^\infty h^{\mathrm{OPT}}(r,r')\psi^{(+)}(r')r'^2\,dr' \tag{A1.29}$$

in the single-channel case. Further, if one approximates $h^{\mathrm{OPT}}(r,r')$ by a local optical-model Hamiltonian

$$h^{\mathrm{OPT}}(r,r')=[\delta(r-r')/rr']h^{\mathrm{OPT}}(r), \tag{A1.30}$$

one has

$$h^{\mathrm{OPT}}(r)\psi^{(+)}(r)=E\psi^{(+)}(r). \tag{A1.31}$$

The P-space vectors may now be written

$$\mathrm{P}\,|\,\Psi_c{}^{(+)}\rangle=\sum_{c'}\int_0^\infty|\,r,c'\rangle\psi_{cc'}{}^{(+)}(r)r^2\,dr, \tag{A1.32}$$

where again the index c specifies the boundary conditions for Eq. (A1.28).

There have been very extensive studies of phenomenological optical models (mostly local). Since the determination of $h^{\mathrm{OPT}}(r,r')$ from first principles is a formidable task, we will use the phenomenological optical potentials to determine the continuum wave functions for our study of analog states. However, the requirement of orthogonality between the continuum and analog spaces requires that we modify the solution of Eq. (A1.28) or Eq. (A1.31). This modification is discussed in the next subsection.

A1.3 Modification of the Continuum Space Wave Functions

As we have discussed in Sec. 2, the reaction theory for analog resonances requires the introduction of *three* projection operators P, A, and q. The analog states, $|\,A_i\rangle$ are constructed via the application of the charge raising operator to a set of parent states, $|\,\pi_i\rangle$. The analog state projection operator is defined as a projection operator onto the space spanned by the analog states. For simplicity, let us assume for the moment that the continuum space is defined as including only the elastic channel. In general, a parent state $|\,\pi\rangle$ will contain a component which may be described as a neutron coupled to the ground state of the target system. The application of the charge raising operator to the parent state will define an analog state, part of whose wave function will contain a *proton* in a *neutron orbit* coupled to the ground state of the target. This part of the analog state will give rise to a nonorthogonality between the analog space and the continuum

[41] If $\Psi_{cc'}{}^{(+)}(r)$ is obtained as the solution of (A1.25) the condition (A1.24) is automatically satisfied.

space. This difficulty may be avoided by explicitly removing the nonorthogonal component from the continuum space.

Recall that we had defined the projection operator

$$\mathrm{P}=\sum_c \int_0^\infty |\, r, c\rangle r^2\, dr \langle r, c\,| \qquad \text{(A1.15)}$$

We now introduce the projection operator[42]

$$P=\mathrm{P}-[\mathrm{P}\,|\,A\rangle\langle A\,|\,\mathrm{P}/\langle A\,|\,\mathrm{P}\,|\,A\rangle]$$
$$=\mathrm{P}-\frac{1}{\mathrm{p}_A}\sum_{cc'}\int_0^\infty |\, r, c\rangle u_{A,c}(r) r^2\, dr$$
$$\times\int_0^\infty u_{A,c'}(r')\langle r', c'\,|\, r'^2\, dr', \qquad \text{(A1.33)}$$

where

$$u_{A,c}(r)\equiv\langle r, c\,|\,A\rangle=\mathrm{N}^{-1/2}\langle r, c\,|\,T_-\,|\,\pi\rangle, \qquad \text{(A1.34)}$$

and

$$\mathrm{p}_A=\langle A\,|\,\mathrm{P}\,|\,A\rangle$$
$$=\sum_c\int_0^\infty u_{A,c}^2(r) r^2\, dr. \qquad \text{(A1.35)}$$

The space defined by the new operator P is orthogonal to the analog space.

In analogy to the procedures of Sec. A1.2 we introduce the P-space wave function $\varphi_{cc'}^{(+)}(r)$ through the definition

$$P\,|\,\Phi_c^{(+)}\rangle=\sum_{c'}\int_0^\infty |\, r, c'\rangle\varphi_{cc'}^{(+)}(r) r^2\, dr. \qquad \text{(A1.36)}$$

We also need the projected optical Hamiltonian

$$[h_P^{\mathrm{OPT}}(r, r')]_{cc'}=\langle r, c\,|\,\{H_{PP}$$
$$+H_{Pq}[q/(E-H_{qq}+iI/2)]H_{qP}\}\,|\,r'c'\rangle. \qquad \text{(A1.37)}$$

The functions $\varphi_{cc'}^{(+)}(r)$ are determined by the equation

$$\sum_{c''}\int_0^\infty [h_P^{\mathrm{OPT}}(r, r')]_{c'c''}\varphi_{cc''}^{(+)}(r') r'^2\, dr'=E\varphi_{cc'}^{(+)}(r), \qquad \text{(A1.38)}$$

and will satisfy the orthogonality condition,

$$\sum_{c'}\int_0^\infty u_{A,c'}(r)\varphi_{cc'}^{(+)}(r) r^2\, dr=0. \qquad \text{(A1.39)}$$

The latter relation is the coordinate space version of

$$\langle A\,|\,P\,|\,\Phi_c^{(+)}\rangle=0. \qquad \text{(A1.40)}$$

It is useful to exhibit the terms arising from the projection procedure in a more explicit form. To this end we define

$$[\tilde{h}^{\mathrm{OPT}}(r, r')]_{cc'}=\langle r, c\,|\,\{H_{\mathrm{PP}}$$
$$+H_{\mathrm{P}q}\frac{q}{E-H_{qq}+iI/2}H_{q\mathrm{P}}\}\,|\,r, c\rangle \qquad \text{(A1.41)}$$

which differs from $h^{\mathrm{OPT}}(r, r')$ introduced in (A1.27) because the q space does not contain the analog states, while the Q-space does. Using (A1.33) to compare (A1.37) with (A1.41), we find the relation

$$h_P^{\mathrm{OPT}}=\left(1-\frac{|\,u_A\rangle\langle u_A\,|}{\mathrm{p}_A}\right)\tilde{h}^{\mathrm{OPT}}\left(1-\frac{|\,u_A\rangle\langle u_A\,|}{\mathrm{p}_A}\right). \qquad \text{(A1.42)}$$

In (A1.42) we have introduced a matrix notation for the coordinates r, r' and the channel indices c and c'. In this notation we may rewrite (A1.38) and (A1.39):

$$h_P^{\mathrm{OPT}}\,|\,\varphi_c^{(+)}\rangle=E\,|\,\varphi_c^{(+)}\rangle, \qquad \text{(A1.43)}$$
$$\langle u_A\,|\,\varphi_c^{(+)}\rangle=0 \qquad \text{(A1.44)}$$

If we use (A1.42), Eq. (A1.38) becomes

$$(E-\tilde{h}^{\mathrm{OPT}})\,|\,\varphi_c^{(+)}\rangle=-\,|\,u_A\rangle\mathrm{p}_A^{-1}\langle u_A\,|\tilde{h}^{\mathrm{OPT}}\,|\,\varphi_c^{(+)}\rangle. \qquad \text{(A1.45)}$$

Equation (A1.45) is readily solved in terms of the Green's function for h^{OPT}, and the wave functions $|\,\psi_c^{(+)}\rangle$ defined as follows,

$$(E-\tilde{h}^{\mathrm{OPT}})G^{(+)}=1, \qquad \text{(A1.46)}$$
$$(E-\tilde{h}^{\mathrm{OPT}})\,|\,\psi_c^{(+)}\rangle=0. \qquad \text{(A1.47)}$$

We easily find

$$|\,\varphi_c^{(+)}\rangle=|\,\psi_c^{(+)}\rangle$$
$$-G^{(+)}(|\,u_A\rangle\langle u_A\,|\,\psi_c^{(+)}\rangle/\langle u_A\,|\,G^{(+)}\,|\,u_A\rangle). \qquad \text{(A1.48)}$$

Note that the solution (A1.48) is independent of the constant $\mathrm{n}_A=\langle A\,|\,\mathrm{P}\,|\,A\rangle$. We also define the Green's function for h_P^{OPT},

$$(E-h_P^{\mathrm{OPT}})G_P^{(+)}=1. \qquad \text{(A1.49)}$$

We find,

$$G_P^{(+)}=G^{(+)}-G^{(+)}\,|\,u_A\rangle(\langle u_A\,|\,G^{(+)}\,|\,u_A\rangle)^{-1}\langle u_A\,|\,G^{(+)}. \qquad \text{(A1.50)}$$

In principle there is some difference between h^{OPT} (A1.27) and $\tilde{h}^{\mathrm{OPT}}$ (A1.38). Phenomenological studies may be said to provide information concerning h^{OPT} since the analog states are not separated from other compound modes in any conventional optical model analysis. We will neglect the very small difference between these operators and assume that we have sufficient information to parameterize $\tilde{h}^{\mathrm{OPT}}$ and obtain the solution of Eq. (A1.47).

For the work discussed here we have neglected direct coupling and identified the functions $u_{A,c}(r)$ with neutron bound state wave functions obtained from a single particle potential. The Green's function, Eq. (A1.46), was obtained for the optical Hamiltonian and the wave functions $\varphi^{(+)}(r)$ of Eq. (A1.48) were constructed. With the neglect of direct coupling these wave functions depend only on the energy and the quantum

[42] In Sec. 2.23 we have written the general expression for the case of many analog states $|\,A_i\rangle$.

numbers l and j. In this case one has

$$\varphi_{lj}^{(+)}(r)=\psi_{lj}^{(+)}(r) - \int_0^\infty G_{lj}^{(+)}(r,r')u_{nlj}(r')r'^2\,dr' \int_0^\infty u_{nlj}(r)\psi_{lj}^{(+)}(r)r^2\,dr \Big/ \int_0^\infty\int_0^\infty u_{nlj}(r)G^{(+)}(r,r')u_{nlj}(r')r^2r'^2\,dr\,dr', \quad \text{(A1.51)}$$

where $u_{nlj}(r)$ is the bound *neutron* wave function.

Although the above discussion displays an explicit and general form of the solution to the orthogonality problem, it may be advantageous for computational purposes to note the following method. After solving the homogeneous equation (A1.47), we also solve the inhomogeneous equation

$$(E-\tilde{h}^{\rm OPT})|f_c\rangle=-|u_A\rangle. \quad \text{(A1.52)}$$

Then the wave function $|\varphi_c^{(+)}\rangle$ is given by

$$|\varphi_c^{(+)}\rangle=\lambda[|\psi_c^{(+)}\rangle-|f_c\rangle(\langle u_A|\psi_c^{(+)}\rangle/\langle u_A|f_c\rangle)], \quad \text{(A1.53)}$$

where the constant λ is determined by requiring that $|\varphi_c^{(+)}\rangle$ have the usual asymptotic normalization.

APPENDIX 2. NORMALIZATION CONDITIONS FOR THE SHORT-RANGE CORRELATION FUNCTION

In Eq. (5.36) we indicated that the short-range correlation function satisfied the relation

$$\int d\mathbf{s}g^C(s)[1-g^P(s)]=0. \quad \text{(A2.1)}$$

In this section we present a short derivation of this result.

Consider $|0\rangle$ to represent a state of Z protons. Then if $a^+(\mathbf{x})$ is a proton creation operator, we have, including the short-range nuclear correlation function

$$\langle 0|a^\dagger(\mathbf{y})a^\dagger(\mathbf{x})a(\mathbf{x})a(\mathbf{y})|0\rangle \simeq[\rho^P(\mathbf{x})\rho^P(\mathbf{y})-\rho^P(\mathbf{xy})\rho^P(\mathbf{x},\mathbf{y})][1+g^C(\mathbf{x}-\mathbf{y})] \quad \text{(A2.2)}$$

Integrating the left-hand side of Eq. (A2.2) over $\mathbf{x}$ and $\mathbf{y}$ leads to the factor $Z(Z-1)$. If the density matrix $\rho^p(\mathbf{x},\mathbf{y})$ is well approximated through a Slater determinant, we have $\rho^2=\rho$ so that the term independent of g^C on the right hand side leads to the same result, $Z(Z-1)$. Therefore we have

$$\int\int d\mathbf{x}\,d\mathbf{y}(\rho^p(\mathbf{x})\rho^p(\mathbf{y})-\rho^p(\mathbf{x},\mathbf{y})\rho^p(\mathbf{xy}))g^C(|\mathbf{x}-\mathbf{y}|)=0. \quad \text{(A2.3)}$$

Approximating the exchange term by the usual Pauli factor we have

$$\int\int d\mathbf{x}\,d\mathbf{y}\rho^p(\mathbf{x})\rho^p(\mathbf{y})[1-g^p(|\mathbf{x}-\mathbf{y}|)]g^C(|\mathbf{x}-\mathbf{y}|)=0. \quad \text{(A2.4)}$$

In the short-range approximation, we have

$$0=\int\int d\mathbf{x}\,d\mathbf{y}\rho^p(\mathbf{x})\rho^p(\mathbf{y})[1-g^P(|\mathbf{x}-\mathbf{y}|)]g^C(|\mathbf{x}-\mathbf{y}|) \simeq\int d\mathbf{x}\rho^p(\mathbf{x})\rho^p(\mathbf{x})\int d\mathbf{s}[1-g^P(s)]g^C(s), \quad \text{(A2.5)}$$

so that Eq. (A2.1) follows.

REFERENCES

[Ad66] J. L. Adams, W. J. Thompson, and D. Robson, Nucl. Phys. **89,** 33 (1966).

[Ad69] E. G. Adelberger, C. L. Cooke, C. H. Davids, and A. B. McDonald, Phys. Rev. Letters **22,** 352 (1969).

[An61] J. D. Anderson and C. Wong, Phys. Rev. Letters **7,** 250 (1961).

[An62a] ——, and C. Wong, Phys. Rev. Letters **8,** 442 (1962).

[An62b] ——, C. Wong, and J. W. McClure, Phys. Rev. **126,** 2170 (1962).

[An66] B. L. Andersen, J. P. Bondorf, and B. S. Madsen, Phys. Letters **22,** 651 (1966).

[Ar68] D. D. Armstrong and E. M. Bernstein, Phys. Rev. Letters **20,** 936 (1968).

[Ar69] A. Arima and S. Yoshida, in *Nuclear Isospin*, edited by J. D. Anderson, S. D. Bloom, J. Cerny, and W. W. True (Academic, New York, 1969) p. 73.

[At68] J. Atkinson, L. G. Mann, K. G. Tirsell, and S. D. Bloom, Nucl. Phys. **A114,** 143 (1968).

[At69] ——, and S. D. Bloom, in *Nuclear Isospin*, edited by J. D. Anderson, S. D. Bloom, J. Cerny, and W. W. True (Academic, New York, 1969) p. 799.

[Au66] E. H. Auerbach, C. B. Dover, A. K. Kerman, R. H. Lemmer, and E. H. Schwarcz, Phys. Rev. Letters **17,** 1184 (1966).

[Au68a] N. Auerbach and N. Stein, Phys. Letters **27B,** 122 (1968).

[Au68b] ——, Phys. Letters **27B,** 127 (1968).

[Au69a] ——, J. Hüfner, A. K. Kerman, and C. M. Shakin, Phys. Rev. Letters **23,** 484 (1969).

[Au69b] E. H. Auerbach, S. Kahana, and J. Weneser, Phys. Rev. Letters **23,** 1253 (1969).

[Au69c] N. Auerbach and N. Stein, Phys. Letters **28B,** 628 (1969).

[Au71] ——, and A. Lev, Phys. Letters **34B,** 13 (1971).

[Ba55] W. A. Barker and F. N. Glover, Phys. Rev. **99,** 317 (1955).

[Ba59] B. F. Bayman, A. S. Reiner, and R. K. Sheline, Phys. Rev. **115,** 1627 (1959).

[Be36] H. A. Bethe and R. F. Bacher, Rev. Mod. Phys. **8,** 82 (1936).

[Be38] ——, Phys. Rev. **54,** 436 (1938).

[Be68a] ——, and P. J. Siemens, Phys. Letters **27B,** 549 (1968).

[Be68b] ——, Phys. Rev. **167,** 879 (1968).

[Be68c] E. M. Bernstein and D. D. Armstrong, Phys. Letters **26B,** 365 (1968).

[Be68d] W. P. Beres and M. Divadennam, Phys. Rev. Letters **20,** 938 (1968) and Errata, *ibid.*, p. 1135.

[Be69] F. D. Becchetti, Jr. and G. W. Greenlees, Phys. Rev. **182,** 1190 (1969).

[Be70] B. Berman *et al.*, unpublished.

[Bl64] S. D. Bloom, Nuovo Cimento **32,** 1023 (1964).

[Bo66] J. P. Bondorf, H. Lütken, and S. Jägare, Phys. Letters **21,** 185 (1966).

[Bo67] A. Bohr, J. Damgaard, and B. R. Mottelson, in *Nuclear Structure*, edited by Hossain *et al.* (North Holland Publ. Co., Amsterdam, 1967).

[Bo68] J. P. Bondorf, P. v. Brentano, and P. Richard, Phys. Letters **27B,** 5 (1968).

[Bo69] A. Bohr and B. R. Mottelson, *Nuclear Structure,* (Benjamin, New York, 1969) Vol. I, p. 152.

[Br65] P. v. Brentano, N. Marquardt, J. P. Wurm, and S. A. A. Zaidi, Phys. Letters **17,** 124 (1965).

[Br66] D. J. Bredin, O. Hansen, G. Lenz, and G. M. Temmer, Phys. Letters **21,** 677 (1966).

[Br68] P. v. Brentano, H. J. Glöckner, E. Grosse, and C. F. Moore, Jahresbericht, Max-Planck-Institut, Heidelberg (1968).

[Bu68] G. W. Bund, Ph.D. Thesis, University of Washington, 1968, unpublished.

[Bu70] ——, and J. S. Blair, Nucl. Phys. **A144,** 384 (1970).

[Ca69] Y. Cassaignou, P. Foissel, C. Levy, W. Mittig, and L. Papineau, *Proceedings of the International Conference on Properties of Nuclear States,* edited by M. Harvey *et al.* (University of Montreal, Montreal, Canada, 1969) p. 14.

[Ch56] E. E. Chambers and R. Hofstadter, Phys. Rev. **103,** 1454 (1956).

[Ch57] D. R. Chase, Phys. Rev. **106,** 516 (1957).

[Ch67] P. R. Christensen, B. Herskind, R. R. Borchers, and L. Westgaard, Nucl. Phys. **A102,** 481 (1967).

[Cl67] G. Clausnitzer, R. Fleischman, G. Graw, D. Proetel, and J. P. Wurm, Nucl. Phys. **A106,** 99 (1967).

[Cl70] Francis E. Close and Hugh Osborn, Phys. Rev. **D2,** 2127 (1970).

[Co63] B. L. Cohen and O. V. Chubinsky, Phys. Rev. **131,** 2184 (1963).

[Co66] E. R. Cosman, H. A. Enge, and A. Sperduto, Phys. Letters **22,** 195 (1966).

[Co68a] ——, J. M. Joyce, and S. M. Shafroth, Nucl. Phys. **A108,** 519 (1968).

[Co68b] ——, H. A. Enge, and A. Sperduto, Phys. Rev. **165,** 1175 (1968).

[Co69] ——, R. Kalish, D. D. Armstrong, and H. C. Britt, *Nuclear Isospin,* edited by J. D. Anderson, S. D. Bloom, J. Cerny, and W. W. True (Academic, New York, 1969) p. 635.

[Co70] E. R. Cosman, A. K. Kerman, and J. Spenser, Phys. Rev. **C3,** 1179 (1971).

[Cr68] G. M. Crawley, B. V. N. Rao, and D. L. Powell, Nucl. Phys. **A112,** 223 (1968).

[De63] A. de Shalit and I. Talmi, *Nuclear Shell Theory* (Academic, New York, 1963).

[Di70] M. DiToro, P. Nunberg, and E. J. Riihimaki, Phys. Rev. **C2,** 13 (1970).

[Do67] M. Dost, W. R. Hering, and W. R. Smith, Nucl. Phys. **A93,** 357 (1967).

[Du57] L. Durand III, Phys. Rev. **108,** 1597 (1957).

[Ed57] A. R. Edmonds, *Angular Momentum in Quantum Mechanics* (Princeton University Press, Princeton, N.J., 1957).

[Eh70] D. v. Ehrenstein, G. C. Morrison, J. A. Nolen, Jr., and N. Williams, Phys. Rev. **C1,** 2066 (1970).

[El67] L. R. B. Elton, in Landoldt-Börnstein, *Nuclear Physics and Technology* (Springer-Verlag, Heidelberg, 1967) Vol. 2.

[El69] J. L. Ellis and W. Haeberli, *Nuclear Isospin,* edited by J. D. Anderson, S. D. Bloom, J. Cerny, and W. W. True (Academic, New York, 1969) p. 585.

[Fa65] S. Fallieros, B. Goulard, and R. H. Venter, Phys. Letters **19,** 388 (1965).

[Fa66] ——, A. K. Kerman, A. F. R. de Toledo Piza, and R. Venter, Nucl. Phys. **89,** 369 (1966).

[Fa71] ——, and G. E. Brown, Ann. Phys. (N.Y.) **66,** 293 (1971).

[Fe58] H. Feshbach, Ann. Phys. **5,** 357 (1958).

[Fe60] ——, in *Nuclear Spectroscopy,* edited by F. Ajzenberg-Selove (Academic, New York, 1960) Part B, p. 625.

[Fe62] ——, Ann. Phys. (N.Y.) **19,** 287 (1962).

[Fe67] ——, A. K. Kerman, and R. H. Lemmer, Ann. Phys. (N.Y.) **41,** 230 (1967).

[Fi69] S. Fiarman and N. Marquardt, Zeit. Physik **221,** 494 (1969).

[Fo54] L. L. Foldy and E. Eriksen, Phys. Rev. **95,** 1048 (1954).

[Fo55] ——, and E. Eriksen, Phys. Rev. **98,** 775 (1955).

[Fo64] J. D. Fox, C. F. Moore, and D. Robson, Phys. Rev. Letters **12,** 198 (1964).

[Fr67] W. A. Friedman, Ann. Phys. (N.Y.) **45,** 265 (1967).

[Fr68] W. A. Friedman and H. Feshbach, in *Spectroscopic and Group Theoretical Methods in Physics* (North-Holland Publ. Co., Amsterdam, 1968).

[Gi66] V. Gillet, A. M. Green, and E. A. Sanderson, Nucl. Phys. **88,** 321 (1966).

[Gl68] N. K. Glenndenning, in *International School of Physics, "Enrico Fermi,"* edited by M. Jean (Academic, New York, 1968) Course XL.

[Go67] M. Goitein, J. R. Dunning, and R. Wilson, Phys. Rev. Letters **18,** 1018 (1967).

[Gr68] E. Grosse, Ph.D. thesis, Heidelberg, 1968, unpublished.

[Gr70] E. Grosse, K. Melchoir, H. Seitz, P. v. Brentano, J. P. Wurm, and S. A. A. Zaidi, Nucl. Phys. **A142,** 345 (1970).

[Ha52] W. Hauser and H. Feshbach, Phys. Rev. **87,** 366 (1952).

[Ha67a] J. C. Hafele, Phys. Rev. **159,** 996 (1967).

[Ha67b] E. W. Hamburger, Phys. Rev. Letters **19,** 36 (1967).

[Ha68a] H. L. Harney, Nucl. Phys. **A119,** 591 (1968).

[Ha68b] ——, C. A. Wiedner, and J. P. Wurm, Phys. Letters **26B,** 204 (1968).

[Ha69a] S. S. Hanna, in *Nuclear Isospin,* edited by J. D. Anderson, S. D. Bloom, J. Cerny, and W. W. True (Academic, New York, 1969).

[Ha69b] H. L. Harney and H. A. Weidenmüller, Nucl. Phys. **A139,** 241 (1969).

[He32] W. Heisenberg, Z. Phys. **77,** 1 (1932).

[He60] L. Heller, Phys. Rev. **120,** 627 (1960).

[He66] E. M. Henley, in *Isobaric Spin in Nuclear Physics,* edited by J. D. Fox and D. Robson (Academic, New York, 1966) p. 3.

[He69a] E. M. Henley, in *Isospin in Nuclear Physics,* edited by D. H. Wilkinson (North-Holland Publ. Co., Amsterdam, 1969).

[He69b] A. Heusler, H. L. Harney, and J. P. Wurm, Nucl. Phys. **A136,** 286 (1969).

[He70] A. Heusler, unpublished.

[Ho67a] R. Hofstadter and H. R. Collard, in Landoldt-Börnstein, Group I, *Nuclear Physics and Technology* (Springer-Verlag, Heidelberg, 1967) Vol. 2.

[Ho67b] P. E. Hodgson, Ann. Rev. Nucl. Science **17,** 1 (1967).

[Hü69] J. Hüfner and C. M. Shakin, Ann. Phys. **52,** 486 (1969).

[Hu69] T. A. Hughes, Phys. Rev. **181,** 1586 (1969).

[Ig69a] G. I. Igo, C. A. Whitten, J. L. Perrenoud, J. W. Verba, T. J. Woods, J. C. Young, and L. Welch, Phys. Rev. Letters **22,** 724 (1969).

[Ig69b] G. I. Igo, P. D. Barnes, E. R. Flynn, and D. D. Armstrong, Phys. Rev. **177,** 1831 (1969).

[Jo66] R. K. Jolly and C. F. Moore, Phys. Rev. **145,** 918 (1966).

[Ka66] C. D. Kavaloski, J. S. Lilley, P. Richard, and N. Stein, Phys. Rev. Letters **16,** 807 (1966).

[Ke61] A. K. Kerman, Los Alamos Laboratory Report, LAMS–2740, unpublished.

[Ke66] ——, in *Lectures in Theoretical Physics,* (Colorado U.P., 1966) Vol. VIII–C.

[Ke68] ——, and A. F. R. de Toledo Piza, Ann. Phys. **48,** 173 (1968).

[Ke69] ——, in *Nuclear Isospin,* edited by J. D. Anderson, S. D. Bloom, J. Cerny, and W. W. True (Academic, New York, 1969).

[Ke71] A. K. Kerman and A. F. R. de Toledo Piza, Ann. Phys. (N.Y.) **66,** 351 (1971).

[La62a] A. M. Lane, Phys. Rev. Letters **8,** 171 (1962).

[La62b] ——, and J. M. Soper, Nucl. Phys. **37,** 506 (1962).

[La62c] ——, and J. M. Soper, Nucl. Phys. **37,** 663 (1962).

[La62d] ——, Nucl. Phys. **35,** 676 (1962).

[Le68] G. H. Lenz and G. M. Temmer, Nucl. Phys. **A112,** 625 (1968).

[Li68] K. P. Lieb, J. J. Kent, and C. F. Moore, Phys. Rev. **175,** 1482 (1968).

[Ma55] W. M. MacDonald, Phys. Rev. **100,** 51 (1955).

[Ma56] W. M. MacDonald, Phys. Rev. **101,** 271 (1956).

[Ma60] W. M. MacDonald, in *Nuclear Spectroscopy*, edited by F. Ajzenberg-Selove (Academic, New York, 1960) Part B.

[Ma66a] K. Marouchian, P. v. Brentano, J. P. Wurm, and S. A. A. Zaidi, Z. Naturf. **21a,** 929 (1966).

[Ma66b] N. Marquardt Diplomarbeit, Max-Planck-Institut Heidelberg (1966), unpublished.

[Ma66c] C. Mahaux and H. A. Weidenmüller, Nucl. Phys. **A89,** 33 (1966).

[Ma67] ——, and H. A. Weidenmüller, Nucl. Phys. **A94,** 1 (1967).

[Ma69a] ——, and H. A. Weidenmüller, *Shell-Model Approach to Nuclear Reactions* (North-Holland Publ. Co., Amsterdam, 1969).

[Ma69b] N. Marquardt, Ph.D. Thesis, Heidelberg (1969), unpublished.

[Mc69] R. L. McGrath, in *Nuclear Isospin*, edited by J. D. Anderson, S. D. Bloom, J. Cerny, and W. W. True (Academic, New York, 1969).

[Mc70] A. B. McDonald, E. G. Adelberger, H. B. Mak, D. Ashery, A. P. Shukla, C. L. Cocke, and C. H. Davids, Phys. Rev. Letters **31B,** 119 (1970).

[Me67] A. Z. Mekjian and W. M. MacDonald, Phys. Rev. **160,** 730 (1967).

[Me68] ——, and W. M. MacDonald, Nucl. Phys. **A121,** 385 (1968).

[Me69] ——, in *Nuclear Isospin*, edited by J. D. Anderson, S. D. Bloom, J. Cerny, and W. W. True (Academic, New York, 1969).

[Me70a] ——, Nucl. Phys. **146,** 288 (1970).

[Me70b] ——, Phys. Rev. Letters **25,** 888 (1970).

[Mi71] G. A. Miller, private communication.

[Mo67a] C. G. Moore, J. G. Kulleck, P. v. Brentano, and F. Rickey, Phys. Rev. **164,** 1559 (1967).

[Mo67b] G. C. Morrison, N. Williams, J. A. Nolen, and D. v. Ehrenstein, Phys. Rev. Letters **19,** 592 (1967).

[Mo68] P. A. Moore, P. J. Riley, C. M. Jones, M. D. Mancusi, and J. L. Foster, Phys. Rev. **175,** 1516 (1968).

[Mo69a] P. A. Moore, P. J. Riley, C. J. Jones, M. D. Mancusi, and J. L. Foster, Jr., Phys. Rev. Letters **22,** 356 (1969); Phys. Rev. **180,** 1213 (1969).

[Mo69b] G. C. Morrison, in *Nuclear Isospin*, edited by J. D. Anderson, S. D. Bloom, J. Cerny, and W. W. True (Academic, New York, 1969), p. 435.

[Mu62] P. Mukherjee and B. L. Cohen, Phys. Rev. **127,** 1284 (1962).

[Mu67] G. Muehllehner, A. S. Poltorak, W. C. Parkinson, and R. H. Bassel, Phys. Rev. **159,** 1039 (1967).

[No67] J. A. Nolen, J. P. Schiffer, N. Williams, and D. v. Ehrenstein, Phys. Rev. Letters **18,** 1140 (1967).

[No68] J. A. Nolen, J. P. Schiffer, and N. Williams, Phys. Letters **27B,** 1 (1968).

[No69a] ——, and J. P. Schiffer, Phys. Letters **29B,** 396 (1969).

[No69b] ——, and J. P. Schiffer, Ann. Rev. Nucl. Sci. **19,** 471 (1969).

[Pe62] F. G. Perey and B. Buck, Nucl. Phys. **32,** 353 (1962).

[Pe63] ——, Phys. Rev. **131,** 745 (1963).

[Pe66] ——, and J. P. Schiffer, Phys. Rev. Letters **17,** 324 (1966).

[Pi66] A. F. R. de Toledo Piza, A. K. Kerman, S. Fallieros and R. H. Venter, Nucl. Phys. **89,** 369 (1966).

[Pi67] A. F. R. de Toledo Piza and A. K. Kerman, Ann. Phys. (N.Y.) **43,** 363 (1967).

[Pi69] A. F. R. de Toledo Piza, *Proceedings of the International Conference on Properties of Nuclear States*, edited by M. Harvey *et al.*, (University of Montreal, Montreal, Canada 1969) p. 14.

[Ra64] S. Ramavataram, Phys. Rev. **B135,** 1288 (1964).

[Ra65] J. Rapaport and W. W. Buechner, Phys. Letters **18,** 299 (1965).

[Ri67] P. Richard, W. G. Weitkamp, W. Wharton, H. Wieman, and P. v. Brentano, Phys. Letters **26B,** 8 (1967).

[Ri68] ——, N. Stein, C. D. Kavaloski, and J. S. Lilley, Phys. Rev. **171,** 1308 (1968).

[Ri69] ——, P. v. Brentano, H. Weiman, W. Wharton, W. G. Weitkamp, W. W. McDonald, and D. Spalding, Phys. Rev. **183,** 1007 (1969).

[Ro65a] D. Robson, Phys. Rev. **B137,** 535 (1965).

[Ro65b] L. Rosen, J. G. Beery, A. S. Goldhaber, and E. H. Auerbach, Ann. Phys. (N.Y.) **34,** 96 (1965).

[Ro69a] B. Rouben, Ph.D. Thesis, M.I.T. (1969).

[Ro69b] ——, and E. Riihimaki, to be published.

[Sa67] G. R. Satchler, Nucl. Phys. **92,** 273 (1967).

[Sa69] ——, in *Isospin in Nuclear Physics*, edited by D. H. Wilkinson, North-Holland Publ. Co., Amsterdam, 1969).

[Sc50] J. Schwinger, Phys. Rev. **78,** 135 (1950).

[Sc69a] J. P. Schiffer, in *Nuclear Isospin*, edited by J. D. Anderson, S. D. Bloom, J. Cerny, and W. W. True (Academic, New York, 1969) p. 733.

[Sc69b] ——, J. A. Nolen, Jr., and N. Williams, Phys. Letters **29B,** 399 (1969).

[Sc69c] H. L. Scott, C. P. Swann, and F. Rauch, Nucl. Phys. **A134,** 667 (1969).

[Se70] H. Seitz, D. Rieck, P. v. Brentano, J. P. Wurm, and S. A. A. Zaidi, Nucl. Phys. **A140,** 673 (1970).

[Sh67] R. Sherr, Phys. Letters **24B,** 321 (1967).

[Sl65] L. A. Sliv and Yu. I. Kharitonov, Phys. Letters **16,** 176 (1965).

[St68a] N. Stein, C. A. Whitten, Jr., and D. A. Bromley, Phys. Rev. Letters **20,** 113 (1968).

[St68b] N. Stein, J. P. Coffin, C. A. Whitten, Jr., and D. A. Bromley, Phys. Rev. Letters **21,** 1456 (1968).

[St69] N. Stein, in *Nuclear Isospin*, edited by J. D. Anderson, S. D. Bloom, J. Cerny, and W. W. True, (Academic, New York, 1969) p. 481.

[Ta64] F. Tabakin, Ann. Phys. (N.Y.) **30,** 51 (1964).

[Ta65] T. Tamura, Rev. Mod. Phys. **37,** 679 (1965).

[Ta69] T. Tamura, Phys. Rev. **185,** 1256 (1969).

[Te68a] B. Teitelman and G. M. Temmer, Phys. Letters **26B,** 371 (1968).

[Te68b] G. M. Temmer, B. Teitchman, R. Van Bree, and H. Ogata, *Proc. Intern. Conf. on Nucl. Structure* (Physical Society of Japan, 1968) p. 229.

[Te69] G. M. Temmer, in *Isospin in Nuclear Physics*, edited by D. H. Wilkinson (North-Holland Publ. Co., Amsterdam, 1969).

[Th26] L. H. Thomas, Nature **117,** 514 (1926).

[Th27] ——, Phil. Mag. **3,** 1 (1927).

[Th68] W. J. Thompson, J. L. Adams, and D. Robson, Phys. Rev. **173,** 975 (1968).

[Ve67] L. Veeser, J. Ellis, and W. Haeberli, Phys. Rev. Letters **18,** 1063 (1967).

[Ve68] L. Veeser and W. Haeberli, Nucl. Phys. **A115,** 172 (1968).

[We66] H. A. Weidenmüller, Nucl. Phys. **85,** 241 (1966).

[We67a] ——, Nucl. Phys. **A99,** 289 (1967).

[We67b] ——, Nucl. Phys. **A99,** 269 (1967).

[We69] ——, in *Nuclear Isospin*, edited by J. D. Anderson, S. D. Bloom, J. Cerny, and W. W. True (Academic, New York, 1969).

[Wh68] W. R. Wharton, P. v. Brentano, W. K. Dawson, and P. Richard, Phys. Rev. **176,** 1424 (1968).

[Wi37] E. P. Wigner, Phys. Rev. **51,** 106 (1937).

[Wi66] ——, in *Isobaric Spin in Nuclear Physics*, edited by J. D. Fox and D. Robson (Academic, New York, 1966).

[Wi67] C. A. Wiedner, A. Heusler, J. Solf, and J. P. Wurm, Nucl. Phys. **A103,** 433 (1967).

[Wi69] K. Wienhard, G. Clausnitzer, G. Graw, and R. Fleischman, Zeit. Physik **228,** 129 (1969).

[Wi70] N. Williams, G. C. Morrison, J. A. Nolen, Jr., Z. Vager, and D. v. Ehrenstein, Phys. Rev. **C2,** 1539 (1970).

[Wu69] J. P. Wurm, A. Heusler, and P. v. Brentano, Nucl. Phys. **A128,** 433 (1969).

[Za65] S. A. A. Zaidi, P. v. Brentano, D. Rieck, and J. P. Wurm, Phys. Letters **19,** 45 (1965).

[Za67] ——, and S. Darmodjo, Phys. Rev. Letters **19,** 1446 (1967).

[Za68] ——, J. L. Parish, J. G. Kulleck, C. F. Moore, and P. v. Brentano, Phys. Rev. **165,** 1312 (1968).

[Za69] ——, and P. Dyer, Phys. Rev. **185,** 1332 (1969).